PRECIPITATION POLYMERIZATION AND PARTITIONING IN SUPERCRITICAL FLUIDS

Vol. 1

by

SANAT K. KUMAR

Bachelor of Technology, Indian Institute of Technology, Madras
(1981)
Master of Science, Massachusetts Institute of Technology
(1984)

SUBMITTED TO THE DEPARTMENT OF CHEMICAL ENGINEERING
IN PARTIAL FULFILLMENT OF THE REQUIREMENTS
FOR THE DEGREE OF

DOCTOR OF SCIENCE

at the

MASSACHUSETTS INSTITUTE OF TECHNOLOGY
(December 1986)

Signature of author _____
Department of Chemical Engineering
December 15, 1986

Certified by _____
Professor Robert C. Reid
Thesis Supervisor

_____
Professor Ulrich W. Suter
Thesis Supervisor

Accepted by _____
Professor William M. Deen, Chairman
Departmental Committee on Graduate Students

Vol. 1

To the memory of my Mother.
To my Father, Suji and Raman.

Steeped in ignorance, men engage themselves in activities and pursuits and considering themselves men of understanding and learning, stagger along aimlessly like blind men led by the blind, going round and round in the cycle of births.

The Upanishads

PRECIPITATION POLYMERIZATION AND PARTITIONING IN SUPERCRITICAL FLUIDS

by

SANAT KRISHNAMOORTI KUMAR

Submitted to the Department of Chemical Engineering
on December 15, 1986 in partial fulfillment of the requirements
for the degree of Doctor of Science in Chemical Engineering

ABSTRACT

Precipitation polymerizations of styrene were conducted in the presence of supercritical ethane with AIBN as a free-radical initiator. The feasibility of this synthesis scheme to produce polystyrenes of a low average molecular weight and a relatively narrow molecular weight distribution was explored in this work.

The partitioning of polystyrene chains into supercritical fluids (primarily ethane, and also CO_2 and a ethane-propane mixture) were measured to characterize the distribution of the different styrene oligomers between a coacervate-phase and an SCF-phase, as functions of pressure (8.5 MPa $\leq$ P $\leq$ 34.5 MPa), temperature (313K $\leq$ T $\leq$ 333K) and polymer chain length (3 $\leq X_1 \leq$ 40). In all cases studied, the ability of supercritical ethane to fractionate polystyrene chains could be varied continuously from a gas-like to a liquid-like character, with relatively small changes in operating conditions. It was also shown that the polystyrene phase in contact with ethane behaves as an ideal solution.

A statistical-mechanics based lattice equation of state was developed to correlate the data on the solubility of polystyrene chains into SCF. This model can quantitatively reproduce all the experimental trends for the polystyrene-ethane system, across changes in state variables, with one apparently constant binary interaction parameter, δ_{12}.

SCF precipitation polymerizations of styrene were then conducted in ethane under a variety of pressures (12 MPa $\leq$ P $\leq$ 25 MPa), temperatures (333K $\leq$ T $\leq$ 343K) and monomer concentrations (3.33 wt% $\leq$ [M] $\leq$ 6.66 wt%) to demonstrate that this synthesis scheme can be used to synthesize polystyrenes of low average molecular weights (*ca.* 1000 g mole^{-1}), and

molecular weight distributions narrower than could be obtained with the use of liquid solvents. Also, polystyrenes of different chain lengths, above a certain minimum molecular weight, partitioned between the ethane-phase and the precipitate-phase following the same partitioning law measured in the solubility experiments. In examining the sensitivity of the precipitate phase compositions to changes in pressure and monomer concentrations it was observed that the molecular weight distributions of the product polymer move to higher average values with increases in each of these variables, illustrating the approach to liquid-like behaviour of the SCF solvent.

Data obtained from the reaction experiments have been quantitatively correlated with a transient model developed in this work. Use of this model, along with activated state theories, illustrates the fact that the use of supercritical ethane allows us to affect selectively the kinetic rates of certain steps in the mechanism, thus permitting us to produce polystyrenes of relatively small molecular weight and polydispersity.

Thesis Supervisors: Professor Robert C. Reid
Professor Ulrich W. Suter

Titles: Professor of Chemical Engineering (Emeritus)
Bayer Associate Professor of Chemical Engineering

ACKNOWLEDGEMENTS

Over the last five years I have had the pleasure to work with Bob Reid. He has been a friend and teacher, and I would like to take this occasion to express my heartfelt gratitude to him.

Ueli Suter has been very patient with me while I learnt the rudiments of polymer science. I would like to thank him for providing me an opportunity to redeem myself professionally, and for his continuing support in my attempt to secure a job.

Pablo Debenedetti has been my friend and collaborator over the last few years. While we may not be at the same place in the next few years, I hope that we continue to be in contact with each other.

Thanasis Panagiotopoulos badgered me in the summer of 1984 to come back to MIT and do a PhD, almost against my better judgement. He and Richard Willson have helped me both academically and personally, and it is my pleasure to have them as my friends.

I would like to express my gratitude to Murali Viswanathan and Rohit Ramaswamy for being my friends, and, also, for teaching me in their own ways the value of patience.

Jesse Baskir and Pete Ludovice have been lots of fun to be with and I would like to thank them for their forbearance towards my idiosyncratic ways. I also would like to acknowledge the help that Kathy Brownell has given me in ever so many ways.

I would like to acknowledge the support of my thesis committee, Professors Stephanopoulos, Merrill and Botsaris. Also, my special thanks to Prof Virk.

Sanjay Chhabria worked with me in the summer, and the high quality of his data helped in giving my thesis more credibility.

I would like to acknowledge financial support from the National Science Foundation under grant number CBT85-09945.

TABLE OF CONTENTS

LIST OF FIGURES

LIST OF TABLES

CHAPTER 0

SUMMARY

0.1 INTRODUCTION

0.1.1 Motivation

Supercritical fluid extraction (SCFE) is a unit operation in which a supercritical fluid (SCF), a substance above its critical temperature and pressure, is used as an extractant to solubilize preferentially specific components from a mixture of low vapour pressure compounds (McHugh and Krukonis, 1986 and all references therein). SCF are attractive media for extraction since their density (and hence solvent power) can be varied from gas-like to liquid-like with relatively small changes in state variables.

Most of the work done in the past with SCF relates to their use as extraction media. A germane example is the fractionation of polymers with SCF solvents (Paulaitis et al., 1983). In this work it has been shown that a polydisperse polymer sample (polystyrene in this case) may be fractionated on the basis of molecular weight with the use of supercritical CO_2. The resultant products, both in the extract and the raffinate phases, are of narrower molecular weight distributions than the unextracted polymer. The point being emphasised here is that most of the prior art concerns itself with the application of SCFE in equilibrium processes, with little emphasis being placed on the possible use of SCF in other contexts of a process flowsheet.

A potentially interesting, alternate application of SCF combines concepts of solubility and reaction in a "SCF Precipitation Polymerization". Precipitation polymerization reactions, which have normally been conducted

in liquid solvents, involve the use of a liquid that behaves as a solvent for the monomer, but as a non-solvent for the corresponding polymer. The polymerization is initiated and occurs homogeneously in a single-phase until polymer chains grow past a point where they are essentially insoluble in the liquid-phase. At this time, chains insoluble in the solution precipitate to form a second, polymer-rich phase. Reaction may continue to occur in the coacervate-phase since some of the precipitated polymer may be unterminated. This phenomenon, called the Tromsdorff effect, may be slowed down in the coacervate phase by the proper adjustment of operating conditions, thus allowing for the synthesis of polymers of narrow molecular weight distributions (Bamford et al., 1980). In liquid solvents, however, frequently the precipitated polymer is present in the form a swollen gel since it is plasticized by the presence of large quantities of solvent (and monomer). The reaction rate in this phase could thus be very high (Jenkins, 1967) and the final product obtained would then be of a broad molecular weight distribution [with polydispersities, M_w/M_n ~5-10].

The potential use of SCF solvents in the context of precipitation polymerization stems from the following reasons:

(i) The adjustable solvation power of SCF allows for the variation of the threshold molecular mass for polymer precipitation. The molecular mass of the product polymer may then be varied by adjusting the pressure, temperature or the composition of the SCF phase.

(ii) Since SCF are expected to be poor solvents, it is anticipated that the problem of the broadening of the product molecular mass distributions due to reactions in the precipitate will be alleviated by their use.

(iii) Subsequent to the reaction, the monomer dissolved in the precipitated polymer can be recovered with relatively modest changes in the operating conditions. This is in sharp contrast to classical liquid-phase precipitation polymerizations wherein the recovery of the unreacted monomer is a highly energy intensive process (Gutowski et al., 1983).

0.1.2 Problem Definition

It is the aim of this work to examine and understand the phenomena occurring in a SCF precipitation polymerization, and contrast them to corresponding effects in a liquid-phase reaction system. The free-radical polymerization of styrene initiated with AIBN was the system chosen. Ethane was the primary SCF solvent, but CO_2 and a mixture of ethane and propane were also used.

a. Experimental and Theoretical Aspects: The specific aspects of this problem which were examined in this work are discussed below.

- Data on the solubility of polymers in SCF were measured, and correlated with an appropriate model, to characterize the distribution of different chain length species between an SCF-phase and a coacervate-phase.
- SCF precipitation polymerizations were then conducted to demonstrate the viability of this synthesis scheme. Also, in these experiments, the compositions of SCF and precipitate polymers were measured to formulate an applicable kinetic mechanism and deduce the values of relevant kinetic parameters.

0.1.3 Experimental Background

a. Solubility of Polymers in Conventional and SCF solvents: Most of the current literature indicates qualitatively that an SCF solvent may be used to fractionate polymers on the basis of molecular weight [Paulaitis et al., (1983); McHugh and Krukonis (1986)]. However, no quantitative data are available that illustrate the fractionating ability of SCF in the vicinity of their critical points.

The fractionation of polymers on the basis of molecular mass with liquids or very high pressure gases, however, is a subject that has received considerable attention in the past few decades (Flory, 1953; Schulz and Jirgensons,1940). It has been demonstrated for the fractionation of polymers with liquid-like solvents, that to a first approximation a mass-based

partition coefficient for each i-mer, K_i^{old}, between the two equilibrium phases (denoted by ' and '' respectively) depends only on the polymer chain length (r_i) in an exponential fashion,

$$\ell n(K_i^{old}) = \ell n(w_i''/w_i') = -\sigma r_i + \ell n\xi \qquad (2.6)$$

where ξ is a constant. σ, also termed as the "separation factor", determines the sensitivity of K_i^{old} on molecular mass, and is a function of temperature, pressure and concentration. Until recently however, analysis techniques of sufficient accuracy did not exist to separate and analyze polymer molecular mass distributions on an individual mer by mer basis. Thus, most data reported in the literature for fractionation of polymers by liquid solvents are in the form of number or mass averaged molecular weight data, with no data being presented on individual mers.

The solubility and fractionation of polymers (specifically polyethylene) in very high-pressure ethylene (of the order of 200 MPa) has been reported by Spahl and Luft (1982). Work in the area of solubility of polymers in supercritical gases has also been performed (Schröder and Arndt, 1976a and 1976b), but the authors only reported trends in solubility with changes in operating variables, without reporting absolute values.

b. Precipitation Polymerizations in Liquid Solvents: The time evolution of a precipitation polymerization is as follows: the polymerization of the monomer is initiated either by a chemical initiator or by other means (Flory,1953) and occurs initially in a single, homogenous phase. For the case of a free radical polymerization, the initiator (I), undergoes spontaneous thermal dissociation to form free radicals $(R^{\bullet})^1$,

$$I \xrightarrow{k_i} 2R^{\bullet} \qquad (2.9)$$

The polymerization continues in a single phase solution through addition

---

[1] In all subsequent notation, the bullet, (•), will always be used to represent a free electron that is present on a free-radical.

of monomer molecules (M), to free-radicals in a propagation step,

$$RM_x^{\bullet} + M \xrightarrow{k_p} RM_{x+1}^{\bullet} \qquad (2.12)$$

where $RM_x^{\bullet}$ represents a free radical of chain length x (≥ 0) monomeric units. The propagation reaction is normally terminated either by addition or disproportionation of two active, free-radical chains to form dead polymer chains.

$$RM_x^{\bullet} + RM_y^{\bullet} \longrightarrow P_{x+y+2} \qquad \text{(Addition)} \qquad (2.13a)$$

$$\xrightarrow{k_t} P_{x+1} + P_{y+1} \qquad \text{(Disproportionation)} \qquad (2.13b)$$

In a precipitation polymerization, these reactions proceed in a single phase until a threshold concentration of an n-mer is reached, when it precipitates. The determination of the precipitation threshold is one of the least understood aspects in this mechanism since it may be affected by system-specific parameters. Barrett and Thomas (1975) present a review of the variety of theoretical techniques used to model the nucleation process.

The precipitated polymer still possesses some active chain ends which may react further with more monomer in a propagation step [Eq(2.12)]. Significant reaction in the coacervate would broaden the molecular mass distribution. However, if the polymer were still to be a glass, then no significant reaction would occur in the precipitate.

0.2. SOLUBILITY OF POLYMERS IN SUPERCRITICAL FLUIDS

0.2.1 A Statistical-Mechanics based Lattice Equation of State

During the last decade equations of state (EOS) have been used increasingly to correlate and model the complex phase behaviour of molecular mixtures under a variety of conditions. Cubic EOS (for example van der Waals, 1873; Peng and Robinson,1976) are examples of the more popular models that have been employed. However, these EOS cannot be used to model polymer-SCF systems since they were derived for the case of mixtures of small, spherical molecules.

Lattice theories are a popular genre of models which have been employed in the correlation of polymer-SCF systems. The earliest attempts to represent polymer-solvent systems were made by Flory (1941) and Huggins (1941) who developed an activity coefficient model through the use of a mean-field analysis of molecules placed on a three-dimensional lattice. Most later developments in this field are attempts to alleviate the shortcomings inherent in these pioneering attempts [for example Flory, 1970; Panayiotou and Vera, 1982]. Since most of these theories are inadequate for the accurate representation of polymer-SCF equilibria we developed a lattice EOS based on statistical-mechanics to model systems of interest.

The EOS was developed on the assumption that three-dimensional space is divided *a-priori* into a cubic lattice, of cell size v_H and coordination number z. To account for the disparity of sizes in the molecules of the mixture, it was hypothesised that different molecular species occupied different numbers of lattice sites, r_i. Also, to account for volumetric constraints some sites on the lattice were empty. The canonical partition function for this ensemble was formulated and an EOS for a pure component obtained,

$$\frac{\tilde{P}}{\tilde{T}} = \ell n\left[\frac{\tilde{v}}{\tilde{v} - 1}\right] + \frac{z}{2}\ell n\left[\frac{\tilde{v} + (q_1/r_1) - 1}{\tilde{v}}\right] - \frac{\vartheta^2}{\tilde{T}} \qquad (3.15a)$$

where ϑ is the surface area fraction of sites in the lattice that are occupied by molecular segments. (zq_1) is the number of external contacts per molecule, P the pressure, T the temperature and v the specific volume. The tilde ($\tilde{}$) denotes reduced variables, which are defined by the equations

$$\tilde{P} = (P/P^*), \quad \tilde{T} = (T/T^*), \quad \tilde{v} = (v/v^*) \qquad (0.1)$$

P^* and T^*, the quantities used in reducing P and T to non-dimensional variables, are related by the equation

$$(z/2)\epsilon_{11} = P^* v_H = RT^* \qquad (3.14)$$

where ϵ_{11} is the interaction energy between segments of molecules. In the EOS for each pure component there are two unknown parameters, ϵ_{11} and v^*, the reducing parameter for vclume.

For pure components below their critical points, the technique of Joffe et al., (1970) was employed to obtain ϵ_{11} and v^*, while for substances above their critical points, the pure component parameters were obtained by fitting the EOS (Eq.3.15a) to isothermal P-v data.

Parameters for polystyrene above its glass transition temperature (~380K) are available in the literature (Panayiotou and Vera, 1982). These parameters were employed in our modelling in the temperature range of interest, with the following two assumptions:

(i) In the presence of solvents the glass transition temperature of a polymer is reduced. We assumed that polystyrene at the experimental conditions is in a thermodynamic equilibrium state.

(ii) ϵ_{11} and v^* (in units of $m^3\ kg^{-1}$) were chosen to be independent of chain length.

These assumptions were made since no specific data on thermodynamic properties for oligomers of any chain length are available.

Extension of this model to binary and multicomponent mixtures can be readily made if mixing and combining rules can be formulated. The coordination number (z) and the lattice size (v_H) are assumed constant, independent of composition. A linear mixing rule of the type

$$B_M = \sum B_i \; y_i \tag{0.2}$$

is used for the mixture parameters v^*, q and r. In Eq.(0.2), B represents some generalized property, while y_i is the *mole fraction* of component i in the relevant phase. The mixing rule for the energy parameter (ϵ) is,

$$\epsilon_M = \sum \sum \bar{\vartheta}_i \; \bar{\vartheta}_j \; \epsilon_{ij} \; \Gamma_{ij} \tag{3.46}$$

where ϑ_i is the surface area fraction of the segments of i molecules and Γ_{ij} is a factor that corrects for the non-random distribution of segments of j molecules about the segments of i molecules. (This factor is obtained by the solution of the quasi-chemical equations [Guggenheim, 1954].) In Eq.(3.46), we need a combining rule for the mixture parameter ϵ_{ij},

$$\begin{aligned} \epsilon_{ij} &= \epsilon_{ii} && (i=j) \\ &= 0.5\ (\epsilon_{ii}+\epsilon_{jj})\times(1-\delta_{ij}) && (i\neq j) \end{aligned} \tag{3.52}$$

where δ_{ij} represents a single adjustable parameter per binary.

We have examined the fitting ability of the lattice EOS to eight different binary systems covering a range of pressures and phase behaviour, and show that the capability of the EOS to correlate phase equilibria for mixtures of "small" molecules is comparable to traditionally employed techniques (for example the single parameter Peng-Robinson EOS). As examples, in Figures 3.3 and 3.6 we show fits obtained from the lattice EOS to two systems employing a *temperature independent* value of the binary interaction

parameter, δ_{12}: ethanol-water, a low-pressure non-ideal system, and acetone-CO_2, a medium-pressure phase equilibrium system with a SCF component. While we do not present comparisons to conventionally used techniques here, the point to be emphasised is the utility of the lattice EOS, developed mainly for the correlation of mixtures of molecules of disparate sizes, in modelling mixtures of small molecules.

0.2.2 Experimental and Correlation Results

a. Experimental Setup: The experimental apparatus employed for the measurement of solubilities of polymer chains in SCF is a flow-through apparatus shown schematically in Figure 4.1. The main feature of the setup is a stainless steel extraction column into which the polymer to be extracted is loaded. SCF is passed through the extractor and exits in equilibrium with the polymer. This "loaded" SCF is subsequently flashed to atmospheric pressure, where all dissolved polymer precipitates and is collected in

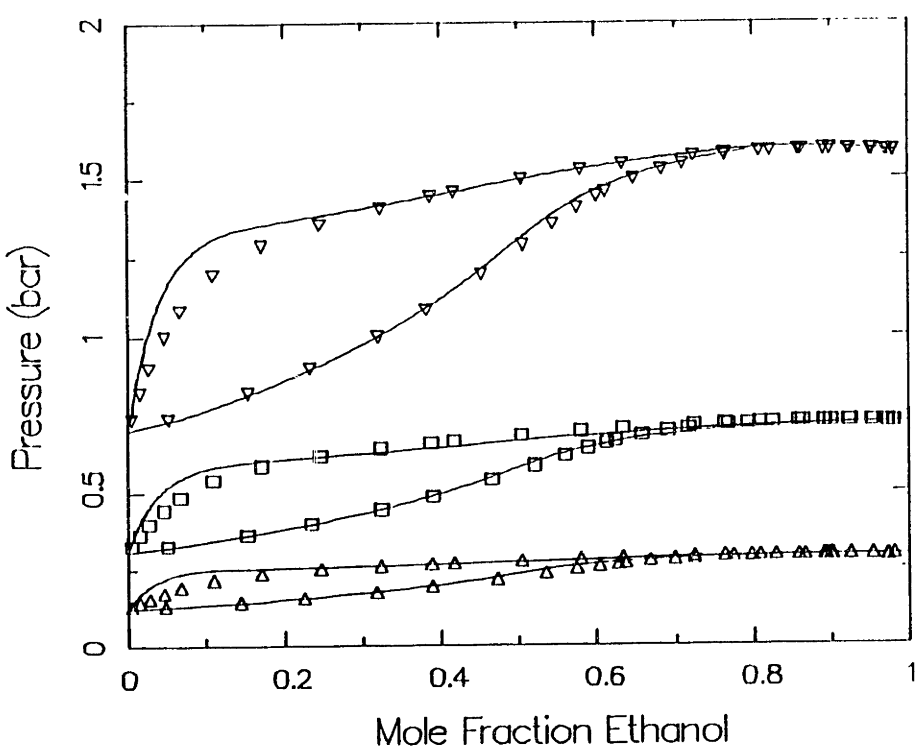

Figure 3.3: Comparison of the experimental data of Pemberton and Mash (1978) for the ethanol-water binary at (△) 323K, (□) 343K and (▽) 363K with (———) lattice model predictions with δ_{ij}=0.085.

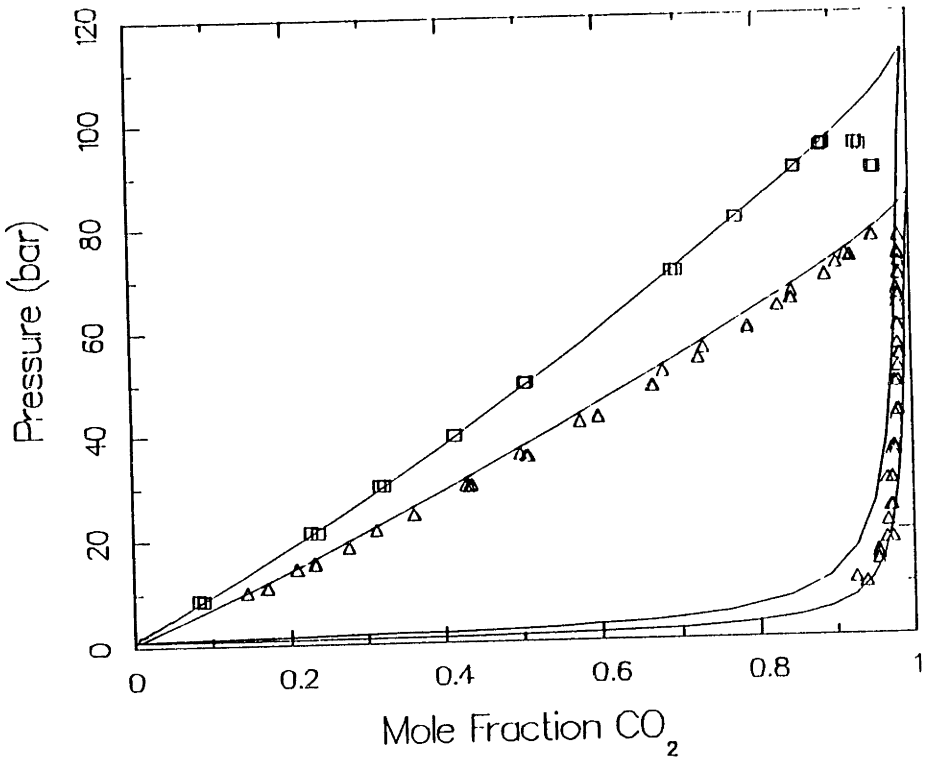

Figure 3.6: Comparison of the experimental data for the acetone-CO_2 binary (Panagiotopoulos, 1986) at (△) 313K and (□) 333K with (——) lattice model predictions with $\delta_{ij}=0.0$.

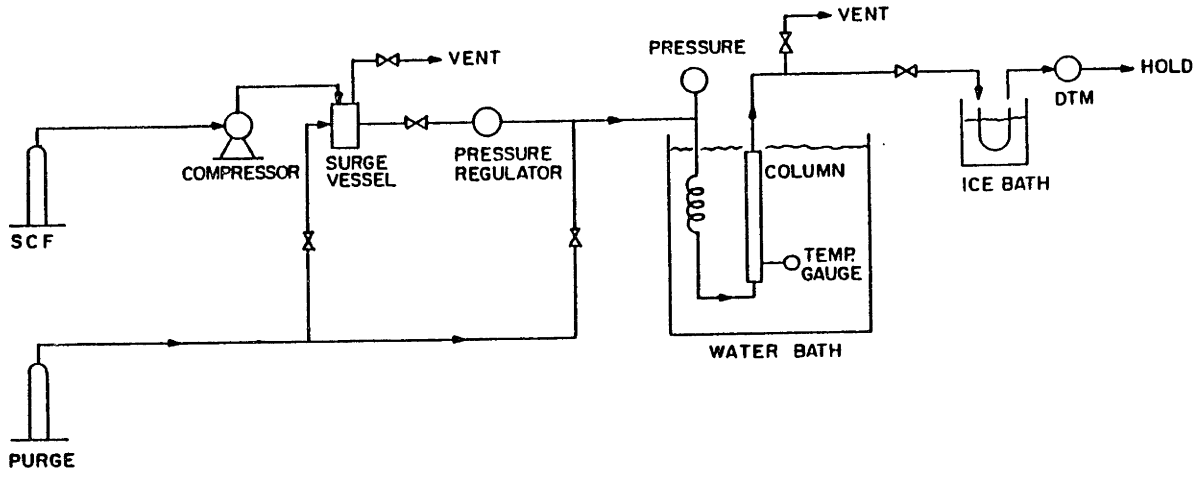

Figure 4.1: A Schematic representation of the solubility apparatus.

cold U-tubes. The unextracted and extracted polymer samples are then analyzed by size exclusion chromatography (SEC) for total mass injected and molecular weight distribution. Integrated gas flow rates are measured with a dry-test meter. The solubilities of different chain polymers in SCF are then completely determined.

b. Results and Discussion: In Figure 4.5 , we present a plot of the equilibrium solubility of polystyrene of average molecular weight 2060 g $mole^{-1}$ in n-heptane. The plotted ordinate is a mass based partition coefficient that is defined as,

$$K_i = w_i^v / w_i^s \tag{4.1}$$

where w_i^v is the mass concentration of the i^{th} mer in the solvent phase (in units of kg i-mer/kg solvent) while w_i^s is the mass fraction of the same i^{th} mer in the solid, polymer phase (in units of kg mer/kg solvent-free solid). This is in contrast to Eq.(2.6) where the mass fraction of the chain

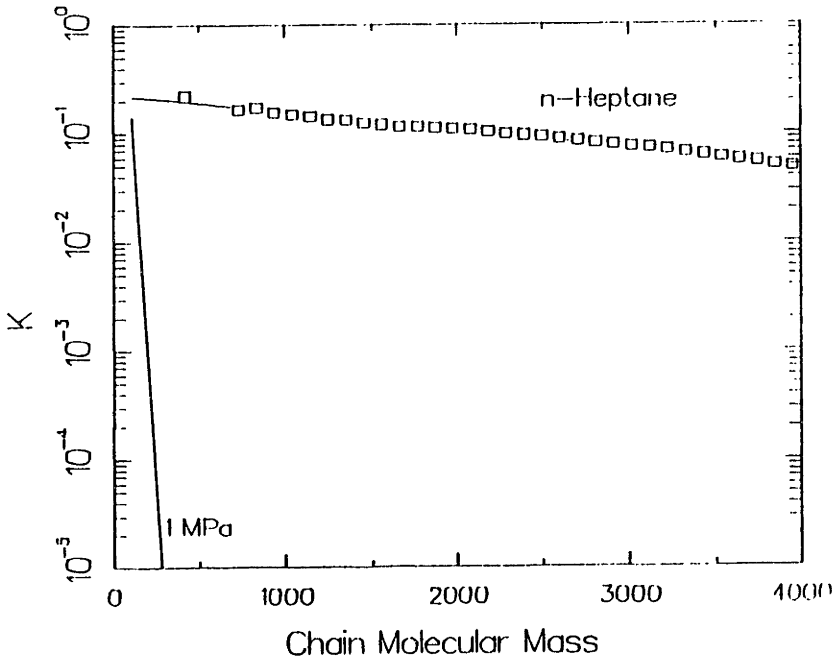

Figure 4.5: Comparison of the partitioning behaviour of n-heptane (298K) and ethane (at 1 MPa and 333K) for polystyrene oligomers between a polymer-rich phase and a solvent-rich phase. (□) are experimental data and the line through the points is a best-fit straight line. Ethane results are simulated from the ideal gas law.

in both phases (with the solvent) is used to calculate the separation factor. The point being stressed here, is the observed log-linear dependence of the partition coefficient of a polymer chain, on its molecular weight. This relationship has already been summarized in Eq.(2.6) as a general result that has been reported in the literature. However, the data presented here are for individual chain lengths, while in the past only average molecular weights have been reported. Results in Figure 4.5 show that for the system examined the equation

$$\log_{10}(K_i) = A(T) + B(T)\ X_i \qquad (4.3)$$

is strictly valid on a individual i-mer basis. Here X_i is the chain length of the relevant oligomer, and A(T) and B(T) are temperature dependent constants.

In Figure 4.5 we also show the fractionation expected if an ideal gas (ethane, in this case) at a pressure of 1 MPa and 333K were used as a solvent. With the use of a gaseous solvent pronounced fractionation is obtained. However, the loading of the polymer chains in the gas phase is low. Liquid solvents, on the other hand, offer poor fractionation as suggested by the small absolute value of the slope of the line log K vs. molecular mass, but afford higher loadings. The two lines shown in this figure represent the two extreme cases of fractionation that can be achieved through the use of conventional solvents. Since the solvent-power of these solvents cannot be altered easily, these also represent the fractionation that is normally achievable with conventional solvents.

In Figure 4.3, partition coefficients of polystyrene chains, between a polymer-phase and an ethane-phase (at 333K and 25 MPa), is shown as a function of chain molecular weight. Data obtained were from raw polymers of $M_n \sim$ 800 and 2060 g mole^{-1}, respectively.[2] It is seen that the measured

---

[2] In this context, note that measured solubility data on the low molecular mass chains in the 2060 g mole^{-1} polystyrene have not been reported since these are diffusion controlled measurements and do not represent equilibrium solubilities.

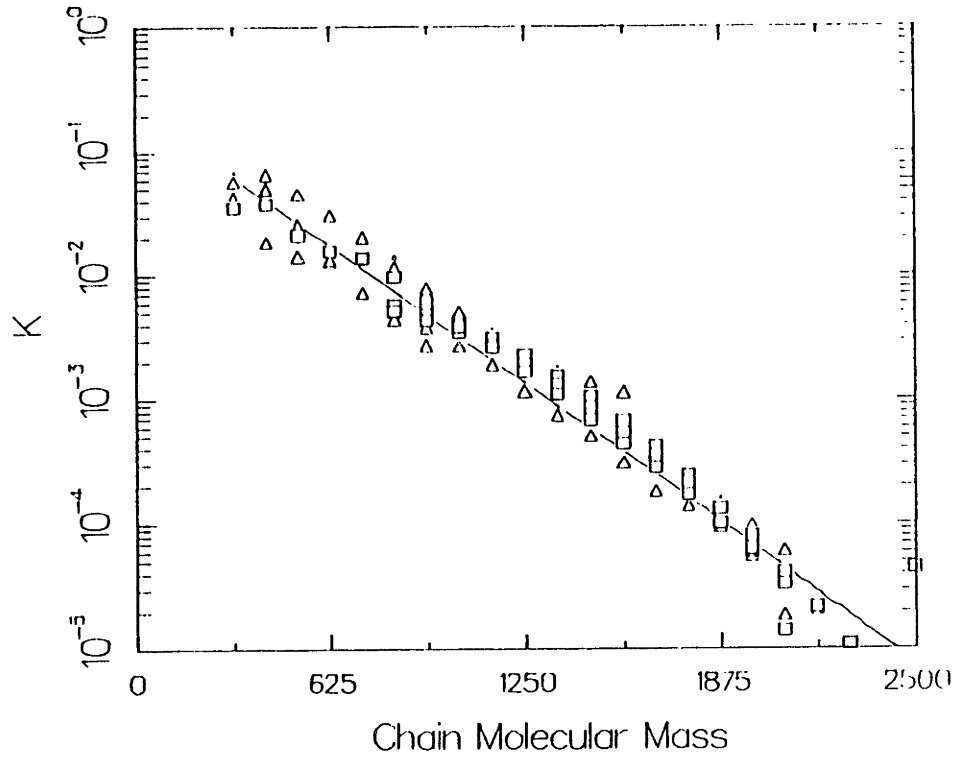

Figure 4.3: Experimental data for the partition coefficients of different styrene oligomers between a polymer-rich phase and an ethane-rich phase at 25 MPa and 333K. (□) is data obtained with a polymer of average molecular mass of 2060, and (△) from a polymer of molecular mass 800.

values of K_i for the various oligomers from both the samples fall on the same line. This has important connotations. First, it demonstrates that the partition coefficient of any chain from the polymer-rich phase to the supercritical phase is *independent* of the composition of the parent polymer. Figure 4.3, therefore, suggests that the observed linearity represents a general, universal behaviour for the solubility of polystyrene chains in supercritical ethane at these operating conditions. In addition, the composition-independence in Figure 4.3 implies that the equilibrium solubility of a polymer chain into an SCF phase occurs as if the condensed phase were an ideal solution. In essence, therefore, we are dealing with a linear combination of independent quasi-binaries of SCF with the individual chain length polymers. We shall use this deduction as a starting point in our modelling.

In Figure 4.6, we present averaged data for partition coefficients as a function of chain molecular mass at several pressures between 8.5 and 34 MPa

at 333K. Again, these include data from both the 800 and 2060 g mole^{-1} raw polymer samples. The partition coefficient data from Figure 4.5 (n-heptane, and ethane at 1 MPa) are also shown for comparison. The lines in Figure 4.6 were obtained by fitting the experimental data to the equation,

$$\log_{10}(K_i) = C_0 - (\text{Degree of Polymerization})_i \times C_1 \qquad (4.4)$$

It is seen that, at all pressures we have a log-linear dependence for K_i on the molecular mass of the polymer chain. At the lowest pressure (8.5 MPa) the partition coefficient line is steep, indicating a pronounced fractionation. As one proceeds to higher pressures, the ethane density increases (and so does its solvent power) and the loading of the SCF phase with chains of higher mass increases. However, the fractionation obtained becomes less pronounced. In summary, the fractionation ability of supercritical ethane at 333K varies continuously from gas-like to liquid-like as one progressively increases its density.

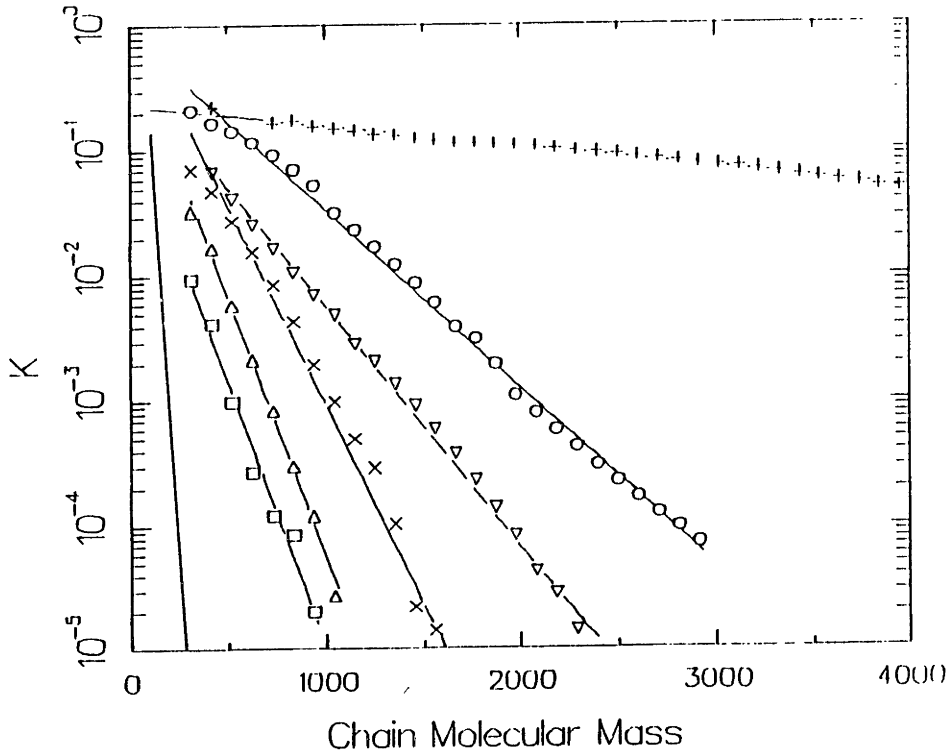

Figure 4.6: Experimental data for the solubility of polystyrene in various solvents. [The lines are best-fits.] (+) are data for partition coefficients in n-heptane at 298K. All other data are at 333K with ethane as solvent. (□) at 8.5 MPa, (△) 10 MPa, (×) 15 MPa, (▽) 25 MPa and (○) 34 MPa. The line with no points is ethane at 1 MPa.

Experimental data presented in Figure 4.6 were correlated with the Statistical-Mechanics based Lattice Model EOS; results are presented in Figure 4.7. A single interaction parameter, δ_{ij} (=0.018), independent of chain length and pressure was employed. The model results are in good agreement with the experimental data at all pressures, and chain lengths beyond molecular weights of 1200 g $mole^{-1}$. The reason for the disagreement between the model and experiment below this molecular mass is speculated to be due to two factors. First, we assume that segments of all chains interact with the same energy per contact area, ϵ_{11}. Clearly, this assumption breaks down for shorter chains when end effects become important. Also, the results shown are valid only as long as there are two phases in equilibrium; at pressures greater than 9.0 MPa at 333K, however, pure styrene monomer is completely soluble in ethane. Results predicted with a two-phase, quasi-binary model are, therefore, unreliable for the smallest oligomers.

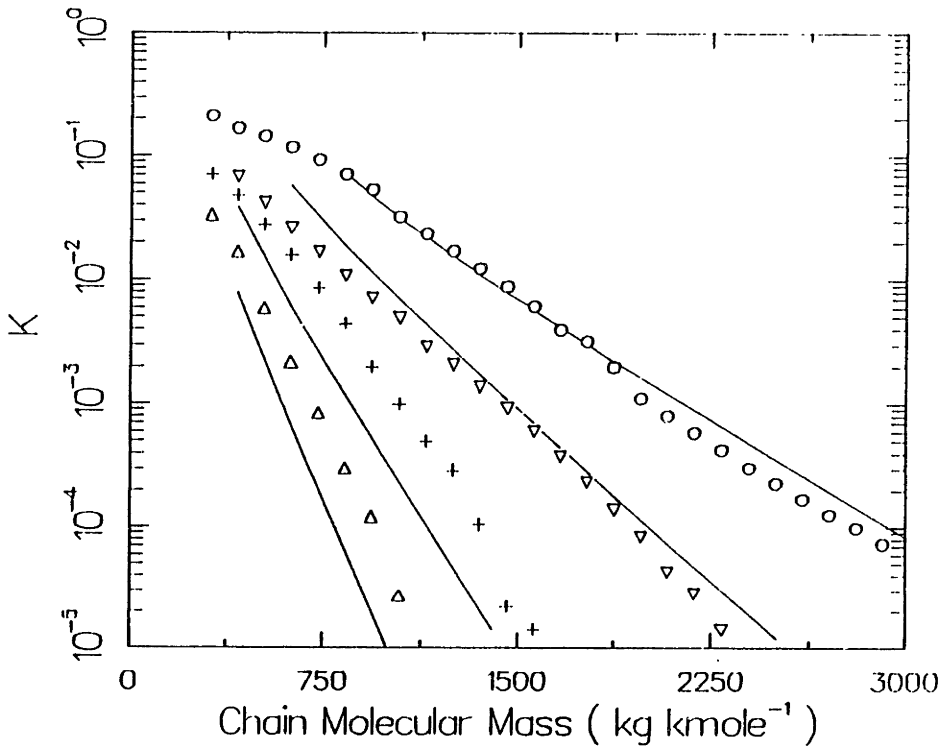

Figure 4.7: Comparison of the lattice model predictions with δ_{12}=0.018 (———), with experimental partition coefficient data for the polystyrene-ethane system at 333K and (Δ) 10 MPa, (+) 15 MPa, (∇) 25 MPa and (O) 34 MPa.

Partition coefficient curves for different temperatures at one pressure (25 MPa in this case) were examined to understand the effect of the variation of another state variable, temperature, on the fractionation ability of supercritical ethane. In Figure 4.12, the K_i values for polystyrene chains are plotted against chain molecular mass at three different temperatures (313, 323 and 333K respectively). The point demonstrated by this diagram is that the partition coefficient curves for this system are not as sensitive to temperature changes as they are to variations in pressure. This could be due to the fact that, at these conditions, ethane has an essentially liquid-like density (~300 kg m^{-3}) which is not very sensitive to relatively small changes in temperature.

The lattice model EOS was again used to fit the experimental data (see Figure 4.12). It was found that the same value of δ_{ij} (0.018) that was used at

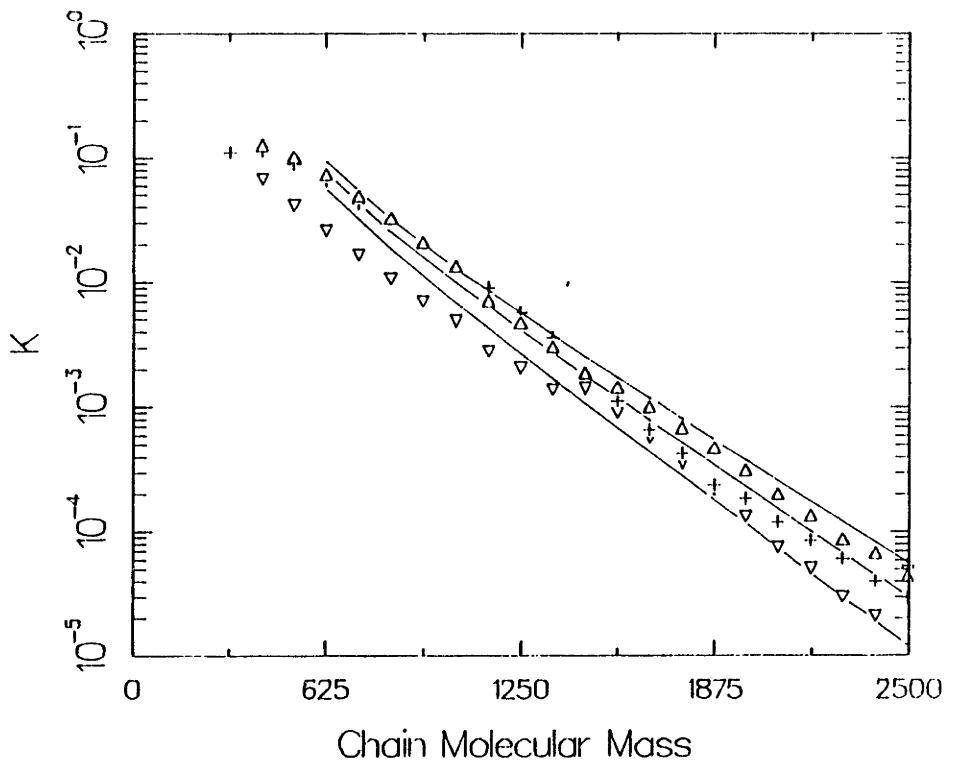

Figure 4.12: Comparison of lattice model predictions [δ_{12}= 0.018, (——)] with experimental partition coefficient data for the polystyrene-ethane system at 25MPa and (Δ) 313K, (+) 323K and (∇) 333K.

333K could be used over the temperature range of interest. The lattice model thus allows for the quantitative reproduction of experimental data for the polystyrene-ethane system, across variations in chain length, pressure and temperature with <u>one</u> apparently constant value of the interaction parameter, δ_{ij}. The utility of the lattice model in the modelling of such systems is emphasised by its capability, in principle, of predicting quantitative trends by fitting it to a single datum point for the system of interest.

The effect of the variation of solvent quality on the partition coefficient curves was also examined (Figure 4.14). Ethane and two other solvents were used to this end: CO_2, one of the popular supercritical solvents was examined at 25 MPa and 333K. A mixture of ethane and propane (*ca.* 87:13 by mole) was also employed. Since propane is a liquid under the experimental conditions, it is expected to behave in a manner similar to <u>n</u>-heptane. A mixture of ethane and propane was also used to examine if the fractionation

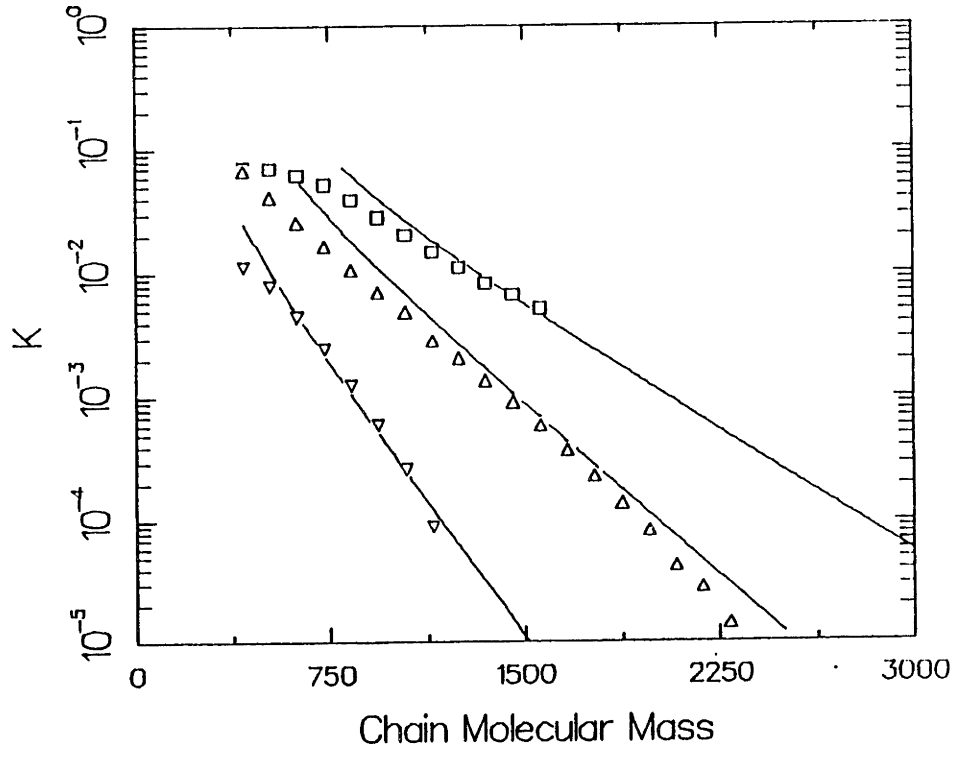

Figure 4.14: Comparison of lattice model fits (———) to experimental data for the fractionation of polystyrene chains with: (△) ethane (δ_{12}=0.018), (▽) CO_2 (δ_{12}=0.08) and (□) ethane + 13% propane (δ_{12}=0.03).

obtained with this system corresponded in some fashion to an interpolated behaviour between ethane and a liquid solvent.

Carbon dioxide is seen to be the worst solvent at these conditions. One reason for this could be attributed to the fact that at 25 MPa, CO_2 is at a lower reduced pressure (and hence lower reduced density). However a comparison of ethane and CO_2 at the same reduced pressure shows that CO_2 is still a poorer solvent than ethane. The mixture of ethane and propane, however, is a better solvent (and consequently a poorer fractionating medium) than pure ethane. This leads us to the important conclusion that a better solvent can be obtained simply by adding a small quantity of a higher member of the same homologous series to a relatively poor solvent. Alternately, the effect on the partition coefficient behaviour due to changes in pressure (as demonstrated with ethane and polystyrene in Figure 4.6) can be duplicated by changing the solvent.

The experimental data in Figure 4.14 have been modelled by the lattice EOS. Again quantitative fits were obtained with the use of a single adjustable parameter per polymer-SCF systems.

c. Summary: Regions of the partition coefficient diagram that could not be accessed with the use of conventional solvents can be reached with relative ease with the use of SCF. Experimental data on the fractionation ability of SCF for the polystyrene-ethane system show that the partitioning ability of ethane can be modified from gas-like to liquid-like with relatively small changes in pressure. However, temperature does not play as important a role in the range examined. The effect of changing pressure on the behaviour of the partition coefficient curves can be duplicated easily either by the use of other solvents or by adding relatively small quantities of liquid additives to the SCF.

Experimental data on these systems can be quantitatively reproduced with a lattice model EOS with the use of a single adjustable parameter per binary that apparently is independent of pressure, chain length (beyond a molecular mass of 1200 g $mole^{-1}$) and temperature.

Experimental data and modelling results for the polystyrene-SCF system suggest that the observed log-linear dependence of the partition coefficient on the chain molecular mass is a general trend for this polymer system. If we examine the lattice model in the context of a two-phase, quasi-binary n-mer-SCF equilibrium system, we may generalize the polystyrene results to the case of any polymer-SCF system outside the immediate vicinity of the region of the sharpest change in properties of the SCF (ca. $|T-T_c|/T_c <$ 0.05 and $|\rho-\rho_c|/\rho_c < 0.05$), i.e.,

$$\ell n(w_i^v/w_i^s) = \xi_0(T,P) + \xi_1(T,P)\ X_i \qquad (4.8)$$

Under the assumption of independent quasi-binaries, therefore, the trends displayed by the partition coefficient on chain molecular mass appear to represent a general behaviour for the solubility of polymers into SCF.

0.3 PRECIPITATION POLYMERIZATIONS IN SUPERCRITICAL FLUIDS

0.3.1 A Transient Model

The time evolution of a precipitation polymerization reaction in an SCF can be thought of as occurring in three distinct phases:

- Initially the reaction mixture composed of a known quantity of SCF, monomer and initiator is in a *single-phase, homogenous* solution, and reactions as represented in Eqs (2.9)-(2.13) are assumed to occur.
- As the reaction proceeds in time, the concentrations of polymer chains (in principle, both terminated and unterminated) increase, and at some point they nucleate to form a second, solid phase.
- At all times subsequent to this precipitation step, polymers of all chain-lengths equilibrate across the two phases, following a partition law which has been determined from experiments. Reaction continues to occur in the SCF phase; it is assumed that no reaction occurs in the precipitate-phase.

The modelling of a single-phase polymerization involving initiation,

propagation and termination by disproportionation[3], following Eq(2.9)-(2.13), is available in the existing literature [Flory, 1953; Odian, 1985]. The general rate equations governing this reaction sequence can be written following Flory (1953) as,

$$\frac{d[I]}{dt} = -k_i[I] \tag{6.10}$$

$$\frac{d[R^\bullet]}{dt} = k_i[I] - k_p[M][R^\bullet] - k_t[R^\bullet]\times\sum[RM_x^\bullet] \tag{6.11}$$

$$\frac{d[RM_x^\bullet]}{dt} = k_p[M][RM_{x-1}^\bullet] - k_p[M][RM_x^\bullet] - k_t[RM_x^\bullet]\times\sum[RM_x^\bullet] \quad (x>0) \tag{6.12}$$

$$\frac{d[P_{x+1}]}{dt} = k_t[RM_x^\bullet]\times\sum[RM_x^\bullet] \tag{6.13}$$

It must be recognized in this context that to maintain the mass balance we need to formulate an equation that will ensure the conservation of mass for the monomer.

$$[M] = [M]_0 - \sum x[RM_x^\bullet] - \sum x[P_x] \tag{6.14}$$

where $[M]_0$ is the initial monomer concentration, and [M] represents the monomer concentration at any instant of time.

The second part of the modelling involves the mathematical representation of the nucleation, and subsequent phase separation. In the course of this work, a simple theory of nucleation was employed. This involved the location of the first chain length that reached its binodal concentration in the gas-phase. This "first" chain length polymer can be determined from the

---

[3] In this formulation we neglect the termination by addition step [Eq(2.13a)].

partition law,

$$\ell n(K_i) = \ell n(w_i^v/w_i^s) = C_0 - C_1 \, Xi \qquad (4.4)$$

by setting w_i^s equal to unity. This "theory of nucleation" is appropriate only in the context of determining the overall SCF-phase and precipitate-phase compositions at long times. If more detailed information such as particle sizes, or volume to surface area ratios of the particles formed are desired, a more exact theory of nucleation must be employed (Nielsen, 1964; Barrett and Thomas, 1975).

Following precipitation the differential equation set Eq.(6.10)-(6.13) will now have to be reformulated to allow for the presence of a solid phase in equilibrium with the reacting SCF-phase. As an example we write here the mass balance equation for the initiator,

$$([I]_{t+\Delta t}-[I]_t)(MW)_I/\rho_{SCF} = -k_i [I]_t \, \Delta t(MW)_I/\rho_{SCF} - (MW)_I((m_s[I])_{t+\Delta t} - (m_s[I])_t)/K_2\rho_{SCF} \qquad (6.16)$$

In this equation, ρ_{SCF} is the density of the SCF (in kg m^{-3}) and $(MW)_I$ is the molecular weight of the initiator. K_2, is the partition coefficient of the initiator between the gas-phase and the precipitate-phase and m_s is the *mass of precipitate per unit mass of the SCF phase*. The left hand side of Eq (6.16) represents the net accumulation of the initiator in the SCF phase (in units of kg initiator/kg SCF) between times t and t+Δt. The first term on the right hand side is the destruction of initiator to form free-radicals in the same time period, and is analogous to the appropriate term in Eq (6.10). The second term then represents the loss of initiator into the precipitate phase. The differential equation for the concentration of the initiator in the SCF-phase can be obtained on dividing Eq (6.16) by Δt, and taking the limit $\Delta t \longrightarrow 0$.

$$\left(1+\frac{m_s}{K_2}\right)\frac{d[I]}{dt} = -k_i[I] - \frac{[I]}{K_2}\frac{dm_s}{dt} \qquad (6.17)$$

In a similar fashion we can now develop the governing differential equations for all species represented in Eqs(6.11)-(6.14). To complete this formulation, the mass balance equation for the monomer is,

$$[M] = [M]_0 - \sum x[RM_x^\bullet] - \sum x[P_x] - m_s[M]/K_1 - \sum x[\lambda_x]m_s/K_x \qquad (6.21a)$$

$$= ([M]_0 - \sum x[\lambda_x](1+m_s/K_x))/(1+m_s/K_1) \qquad (6.21b)$$

where $[\lambda_i]$ is the concentration in the gas-phase of *all* species of chain-length i (i.e., both terminated and unterminated chains) and $(MW)_i$ is the molecular mass of the appropriate species. The only unknowns in Eqs.(6.17), (6.21) are m_s and dm_s/dt. m_s can be tracked simply by closing the mass balances for each mer at every instant of time. The calculation of dm_s/dt, however is not straightforward. Analytical expressions for dm_s/dt can be obtained by realizing that the weight fractions of all the polymer chains in the solid phase must sum to unity.

$$\frac{dm_s}{dt} = \frac{k_p[M]\sum(MW)_i([RM_{i-2}^\bullet] - [RM_{i-1}^\bullet])(K_1-K_i-m_s)/(m_s+K_i)}{\sum[\lambda_i](MW)_iK_1/(m_s+K_i)K_i + [M]/K_1} \qquad (6.26)$$

Here the summation in the numerator goes from 2 to infinity. The mathematical formulation for the polymerization subsequent to precipitation is now complete.

A Digression: Reaction rate constants in SCF: To obtain the relative rates of the different kinetic steps in a SCF polymerization, as compared to corresponding values in a liquid solvent, it must be recognized that the partial molar volumes of dilute components in SCF normally have large negative values. From the LeChatelier principle, a bimolecular reaction which yields a single product molecule, such as the propagation or the termination by addition step, are unfavourable under these conditions. The manifestation of this effect is a reduction in the propagation (or termination by addition) rate constant. By extension, an opposite behaviour may be observed in a kinetic step like the initiation reaction, where the initiator dissociates to form two free radicals. Also, steps like the termination by disproportionation, wherein two molecules react to form two product molecules will not be affected dramatically by the presence of a SCF component in

the mixture.

An order of magnitude estimate of the reaction rate constants in SCF relative to liquid solvents may be obtained from Activated State theories, following Ehrlich (1971). Substitution of appropriate values for pressure, density and fugacity coefficients for each component show that,

$$(k_r)^{SCF} \sim [10^{-1}\text{-}10^{-2}]\ (k_r)^{liq} \qquad (6.40)$$

$$(k_i)^{SCF} \sim (k_i)^{liq} \qquad (6.42)$$

where k_r stands for the rate constants for the propagation, and termination by addition steps. The numbers deduced in Eqs (6.40) and (6.42) will be compared to rate constants obtained by fitting the transient model to experimental data presented below.

0.3.2 Experimental and Correlation Results

a. Experimental Apparatus: The setup used for the quantitative determination of SCF-phase and precipitate-phase polymer compositions consisted of a 150 ml sampling vessel equipped with two valves for charging the vessel and subsequent sampling.

Initially, the reactor was charged with freshly distilled styrene, AIBN and ethane and the quantities of each determined by weighing. The vessel was then placed in a thermostatically controlled shaker bath to ensure that the contents were isothermal and well stirred. The reaction could be conducted for any desired length of time.

In a separate set of experiments conducted in a cell that allowed for visual examination of the reaction mixture, under the same conditions, it was observed that the precipitate-phase deposited on the walls of the reactor. At the end of the reaction, therefore, in our first setup the vessel was flushed with fresh ethane at operating conditions, without losing any precipitate which was deposited on the walls (and hence not

entrained). The displaced reaction mixture is vented to atmospheric pressure through a flashing valve, when the dissolved monomer, initiator and oligomers drop out of solution and are collected in a cold U-tube. Both the SCF and precipitate phase polymers are subsequently analyzed by SEC.

b. Results: We begin our analysis of results from the polymerization experiments by considering data at a single set of operating conditions (viz. pressure, temperature, monomer concentration, initiator concentration, and reaction time); we chose experiments wherein styrene was polymerized in supercritical ethane at 333K and 17 MPa as the base case. It was found that a certain minimum monomer concentration was necessary to observe the presence of a precipitate phase. Experiments conducted with 1.65 wt% monomer (AIBN concentration was 5.83×10^{-5} g/g ethane) within the accuracy of the experimental technique, did not show the presence of a precipitated polymer, at reaction times up to 24 hours.

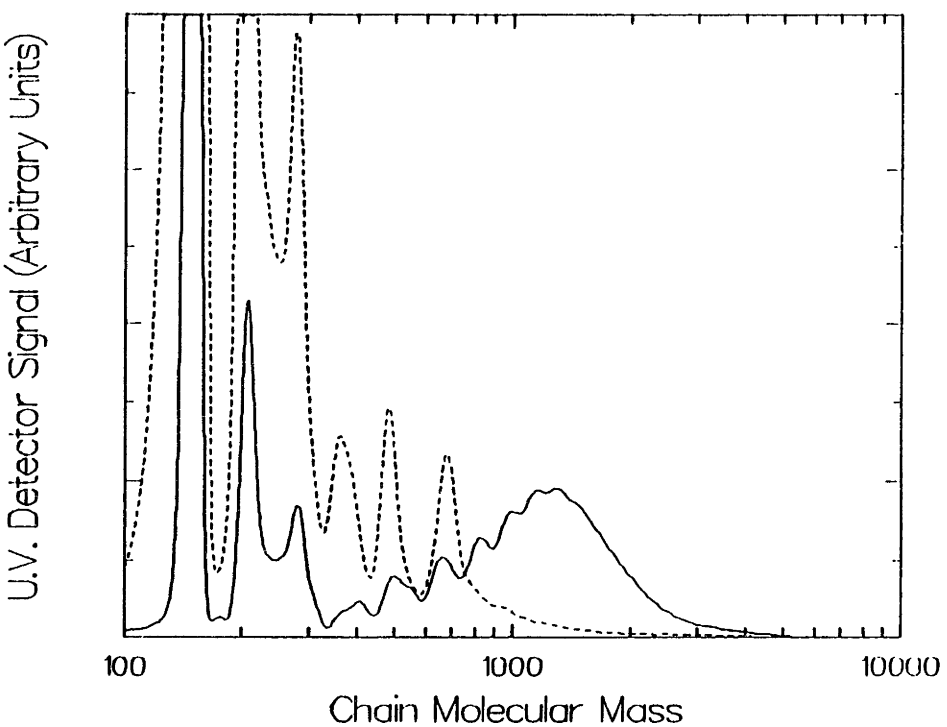

Figure 7.3: SEC traces for the product, precipitate polymer (———) and gas-phase polymers (----) at 17 MPa, 333K, for the precipitation polymerization of 3.33 wt% styrene in ethane initiated with AIBN for a reaction time of 24 hours.

Experiments were conducted at a higher monomer concentration (3.33 wt% monomer), while all other variables were held at the same values as in the earlier set of experiments. Under these conditions, at all reaction times examined (16 h $\leq t_{rxn} \leq$ 44 h), a precipitate polystyrene phase with a composition distinct from the SCF phase was observed. In Figure 7.3, SEC traces for the product, precipitate polymer and the polymer chains in the SCF are shown (t_{rxn}= 24 h). A fact to be noted is that both traces have large peaks corresponding to the monomer and dimer (or AIBN). However, the more significant fact is the presence of a peak in the precipitate phase corresponding to a molecular mass of ~1000. Also, the SCF-phase trace essentially is "cutoff" (i.e., returns to the base line) at the same molecular mass, ~1000. This verifies the presence of a strong cutoff in the solubility of polystyrene chains in the SCF-phase on the basis of chain length.

In Section 0.2, we have presented experimentally measured equilibrium partition coefficients for polystyrene chains of different degrees of

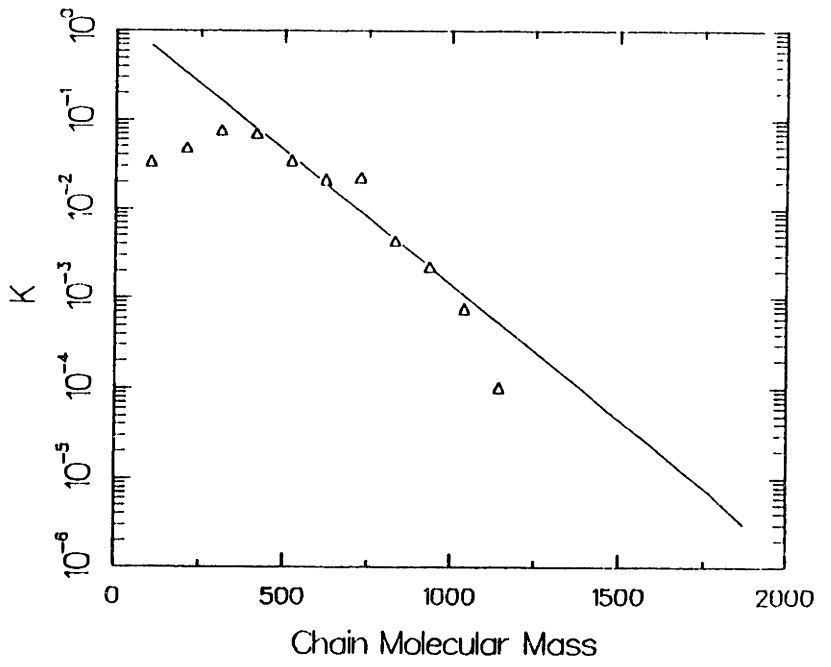

Figure 7.5: Comparison of partition coefficients of polymer chains between the polymer-rich phase and the SCF-phase as measured in solubility experiments (——), and precipitation polymerization reactions (Δ) with 3.33 wt% styrene in ethane with AIBN as radical initiator at 17 MPa and 333K.

polymerization, in SCF under different operating conditions. To examine the role of these partition coefficients in the context of precipitation polymerization reactions, in Figure 7.5 we compare K_i values as computed in solubility experiments to corresponding estimates in the reaction experiments. Some important points can be deduced by the examination of Figure 7.5:

- For molecular masses of 400-1100, there is a remarkable agreement between the partition coefficients measured in solubility experiments and in the precipitation polymerization reactions. These chains therefore, are at thermodynamic equilibrium across the two phases in a polymerization reaction, and this equilibrium is defined by the partitioning behaviour of pure polystyrene chains between a polymer-phase and an SCF-phase.
- Partition coefficients for the monomer, dimer and trimer in the polymerization experiments, however, are smaller than in the solubility experiments. Since the initiator dissociates and then propagates to form longer chains by addition to monomer, the end group for each oligomer chain necessarily possesses an initiator group. The partitioning behaviour of all chains, therefore, are influenced by the presence of the initiator group, with the smallest chains feeling the effect of this "end-group" the most.

Experiments were performed for different reaction times between 16 and 44 hours under the same operating conditions to examine the possibility of the occurrence of a Tromsdorff effect in SCF precipitation polymerizations. In all these reactions, the product polymer was observed to have different concentrations of monomer and initiator corresponding to different conversions. However, when data was examined on a first three mer-free basis, the precipitate phase compositions were found to be essentially independent of reaction time (as shown in Figure 7.6), suggesting that the precipitate-phase compositions, on this basis, are essentially in a steady-state. It is clear therefore, that no Tromsdorff effect is observed in SCF precipitation polymerizations at these conditions, although the precipitate phase contains approximately 30 wt% monomer. A potential reason for this may be that ν_{c1}

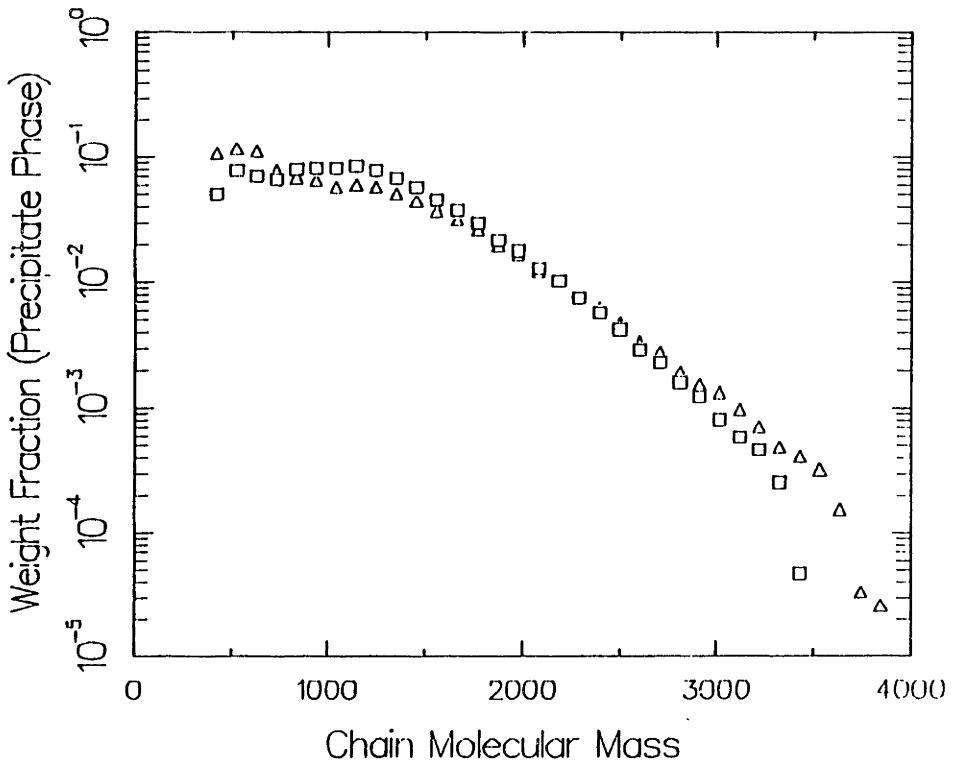

Figure 7.6: Composition of precipitate polymer, on a first three mer-free basis, for different reaction times for the precipitation polymerization of 3.33 wt% styrene in ethane, initiated with AIBN at 17 MPa and 333K. (△) is for t_{rxn}= 16 h, and (□) for t_{rxn}= 44 h.

($= k_p[M]/(k_i k_t[I])^{\frac{1}{2}}$), the kinetic chain length, is small in this case compared to liquid solvents, due to the relatively small value of (k_p/k_i). Most precipitated chains, therefore, will be terminated, providing a plausible explanation for the absence of reaction in the precipitate phase.

Solid phase compositions shown in Figure 7.6 were analyzed to determine the average molecule weight of the polymer. Numbers computed show that M_n~850, and M_w/M_n~1.25. (Monomer and dimer peaks have not been included in this calculation.) The use of the concepts of precipitation polymerization in SCF under these conditions, therefore, allow us to synthesise polystyrene with a relatively narrow molecular mass distribution, narrower than could be obtained from solution polymerization reactions in liquid solvents with radical initiators. [In the case of an "ideal" free-radical, liquid-phase solution polymerization, M_w/M_n ranges between 1.5 and 2, depending on the termination mechanism, addition or disproportionation.]

Precipitation polymerization reactions were carried out at different pressures to understand the effect of "solvent-quality" on the composition of the product polymer. It has been demonstrated in the solubility experiments, that as pressure is increased the solvent-character of an SCF moves from gas-like (low solubility, "strong" fractionation) to liquid-like (high solubility, "poor" fractionating power) continuously. As one proceeds to higher pressures, therefore, it is expected that the precipitated product obtained, will be of a broader molecular mass distribution, since the solvent now is less discriminating with respect to the fractionation of chains on the basis of molecular mass, between an SCF-phase and a polymer-rich phase.

In Figure 7.7, the molecular mass distributions of the precipitated polymer, on a first three mer-free basis, for the polymerization of 3.33 wt% styrene at three pressures of ethane (12, 17 and 25 MPa respectively) at 333K are shown; the corresponding average molecular masses are tabulated in Table 7.1. As anticipated, when one proceeds to higher operating pressures the molecular mass distributions of the precipitate phases are seen to become broader. Partition coefficients were also computed from experiments at the three pressures and were found to display the same trends as shown in Figure 7.5.

The variation of the precipitate molecular mass distribution with changes in the initial monomer concentration in the SCF-phase, constituted the next stage of our experimental work. It is known that polystyrene is soluble in styrene in all proportions. Thus, the addition of larger quantities of monomer to the ethane, will make the fractionation behaviour of SCF more liquid-like (see Section 0.2). In this sense, therefore, an increase in monomer concentration will have an effect similar to increasing the operating pressure.

In Figure 7.12 and Table 7.2, we demonstrate the molecular mass distributions of the precipitate polymer formed by polymerizing styrene at three different concentrations (3.33, 5.0 and 6.66 wt%) in supercritical ethane (at 17 MPa and 333K) with AIBN (5.83×10^{-5} gm/gm. ethane) as the radical initiator.

Table 7.1: Molecular mass data for precipitated polystyrenes at different ethane pressures at 3.33 wt% styrene concentrations and 333K with AIBN as radical initiator.

Operating Pressure (MPa)	M_n	M_w	M_w/M_n
12.0	844	1017	1.20
17.0	850	1063	1.25
25.0	938	1193	1.27

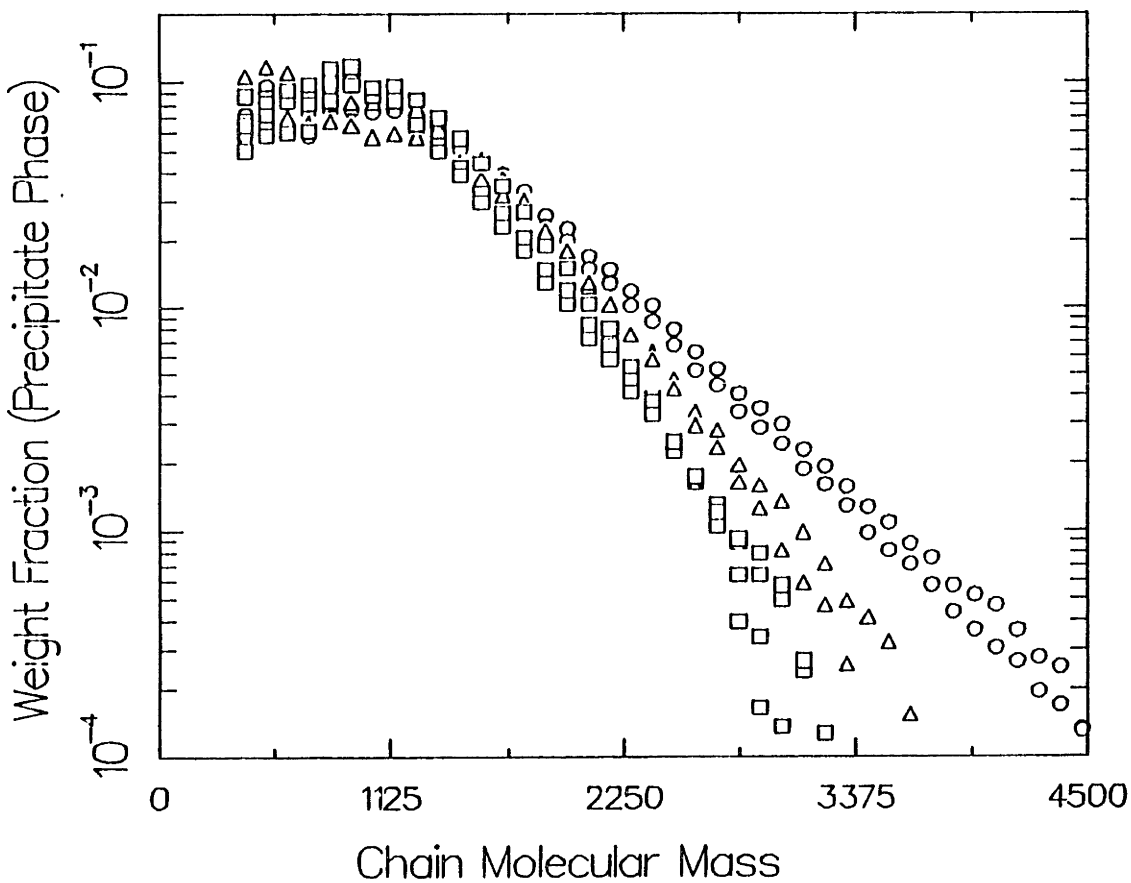

Figure 7.7: Composition of precipitate polymer, on a first three mer-free basis, at different pressures for the precipitation polymerization of 3.33 wt% styrene in ethane, initiated with AIBN at (□)12 MPa, (△)17 MPa and (o)25 MPa and 333K.

Table 7.2: Molecular mass data for precipitated polystyrenes at different monomer concentrations at 17 MPa ethane pressure and 333K with AIBN as radical initiator.

Monomer concentration wt% of SCF-phase	M_n	M_w	M_w/M_n
3.33	850	1063	1.25
5.00	1006	1249	1.24
6.66	1123	1404	1.25

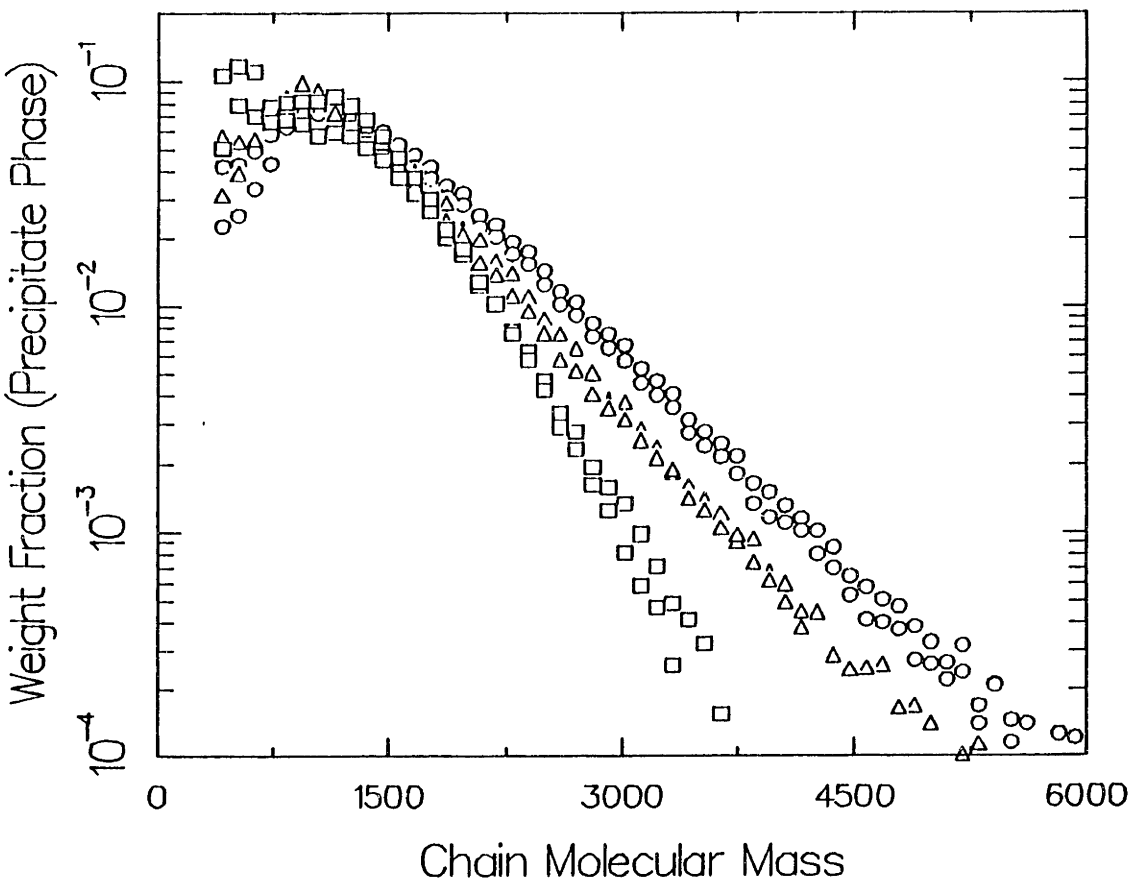

Figure 7.12: Composition of precipitate polymer, on a first three mer-free basis, for different monomer concentrations for the precipitation polymerization of styrene in ethane, initiated with AIBN at 17 MPa and 333K. (□) is at 3.33 wt% , (Δ) 5.0 wt% and (o) 6.66 wt% monomer.

Again, molecular mass distributions on a first three mer-free basis are independent of reaction time for all examined monomer concentrations, suggesting that the polymer concentrations in both phases reach a quasi-steady state at a relatively early time (i.e.,for t_{rxn}<<8 h). This also implies that almost no reaction occurs in the precipitate phase at all operating conditions considered. The molecular mass distributions of the obtained precipitate polymers are of a relatively narrow molecular mass distribution, and the absolute numbers for M_n and M_w/M_n listed in Table 7.2 demonstrate the shift of the molecular mass distribution to higher average molecular masses with increasing [M]. An interesting point to be noted in Table 7.2 is that, as one proceeds to higher monomer concentrations, M_n, the number averaged molecular mass increases, as does M_w, the weight averaged molecular mass. Their ratio (the polydispersity), which is a measure of the breadth of the molecular mass distribution, however, remains relatively unchanged.

Experiments were also conducted at different temperatures and initiator concentrations. However, the results of these experiments are not presented since the precipitate phase compositions were relatively insensitive to small changes in these variables.

c. Modelling Results: In Section 0.3.1 we have presented a model to correlate experimental results from the precipitation polymerization experiments. Also, order of magnitude estimates for the kinetic rate constants have been provided. It has been shown earlier in this section, that the partition coefficients of the first three mers in a reaction experiment are smaller than the measured partition coefficients in the solubility experiments. To account for this effect we must use the true partition coefficients as measured in the polymerization experiments for the first three mers, while using K_x from solubility data for the other mers.

In Figure 7.20, we demonstrate the quality of fits obtained to the precipitate phase compositions at one set of operating conditions (i.e., 3.33 wt% styrene polymerized in ethane at 12 MPa and 333K). As is observed

Table 7.5: A Comparison of rate constants obtained from fitting the proposed kinetic mechanism to experimental data obtained from the precipitation polymerization of 3.33 wt% styrene in ethane at 17 MPa and 333K to corresponding rate constants for the polymerization of styrene in liquid benzene at 333K and 0.1MPa.

Reaction medium	k_i (s^{-1})	k_p (ℓ $mole^{-1}s^{-1}$)	k_t (ℓ $mole^{-1}s^{-1}$)
Benzene	1×10^{-5}	100	5×10^{6}
Ethane	8×10^{-6}	1	4×10^{5}

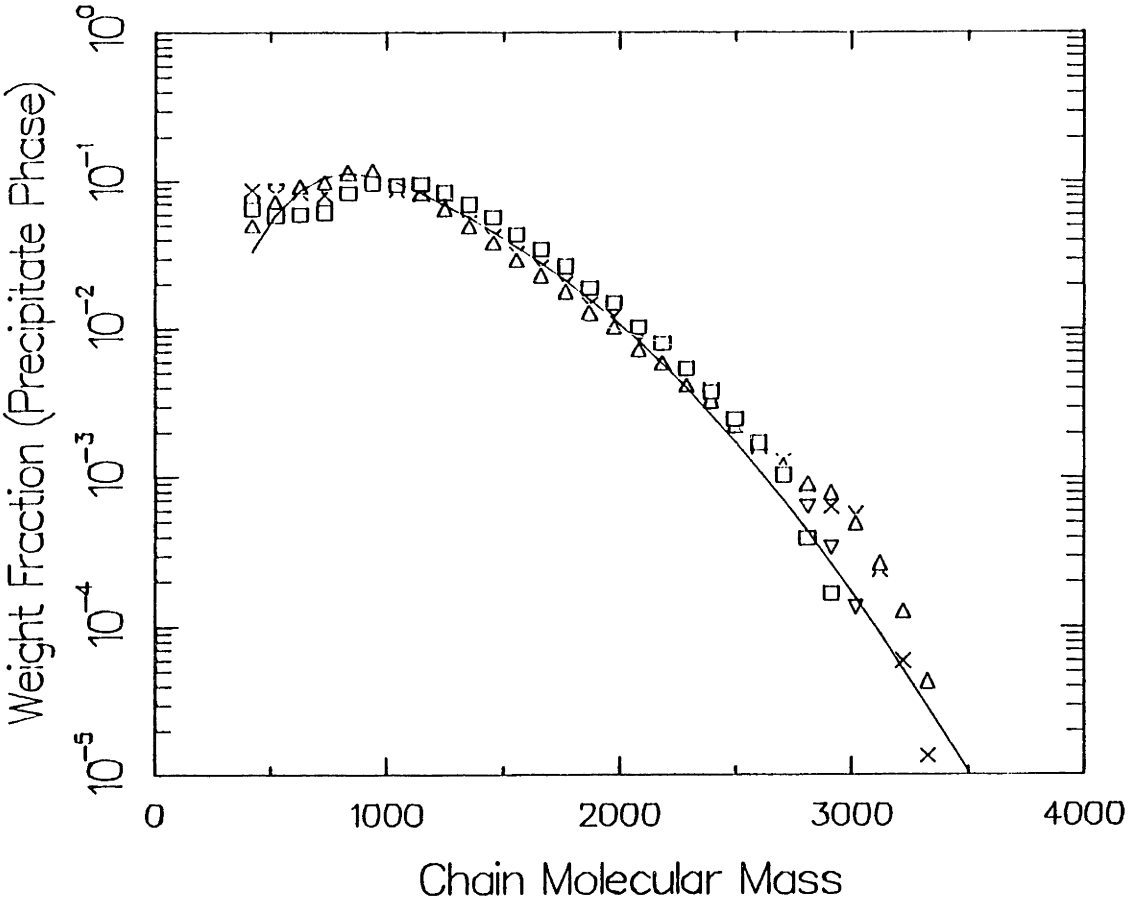

Figure 7.20: Comparison of precipitate polymer compositions, on a first three mer-free basis, for the precipitation polymerization of 3.33 wt% styrene in ethane, initiated with AIBN at 12 MPa and 333K. (□), (△), (▽) and (×) represent experimental data, while (——) is prediction of transient model.

modelling results are in good, quantitative agreement with the experimentally measured coacervate-phase compositions. The model also gives good fits to data at other pressures; however, its performance at high monomer concentrations is not as satisfactory.

In Table 7.5, we compare the kinetic constants obtained from the fitting of the model to experimental data. As deduced in Section 0.3.1, the fitted value of k_p under these conditions is approximately 2 orders of magnitude smaller in SCF, than in liquid solvents, confirming our results from the activated state theories.

d. Summary: We have shown that precipitation polymerization reactions may be conducted successfully in SCF in the presence of a minimum quantity of monomer, to produce product polymers of a small average molecular weight and of polydispersities smaller than could be obtained with the conventional, liquid-phase reactions.

Results obtained from the precipitation polymerization experiments show that polymer chains of molecular mass greater than ~400 g $mole^{-1}$ partition between the SCF-phase and the coacervate-phase following the fractionation law as determined in the solubility experiments [Eq(4.4)]. Below this molecular weight, the partitioning behaviour of chains in the polymerization experiments is affected due to the presence of the initiator, AIBN.

Also, we demonstrate that no Tromsdorff effect is observed in the precipitate phase during the course of the reactions. The use of SCF thus allows us to avoid one of the most important problems encountered in liquid-phase precipitation polymerizations.

Reactions have been conducted at different pressures and monomer concentrations, and the results of these experiments show that the precipitate compositions at higher values of pressure and monomer concentrations allow for the synthesis of higher molecular weight polymers. The reason for this phenomenon is shown to be the approach to liquid-like behaviour of the SCF

phase as P or [M] are increased.

Results obtained from the polymerization experiments have been quantitatively correlated with a transient model that has been developed for this purpose. Three parameters (k_i, k_p and k_t), are obtained from this fitting. The values of these parameters show that use of SCF solvents allows us to selectively change the rates of specific steps in the reaction mechanism (as compared to liquid solvents) to get products of a low average molecular weight.

0.4. CONCLUSIONS

SCF have been shown to be powerful fractionating media for polymers, on the basis of molecular weight. The sensitivity of the fractionating power of SCF can be varied from gas-like to liquid-like, by increasing pressure or by the addition of liquid solvents. Temperature, however, is not an important variable in the range examined. Another important deduction made from the data obtained from the solubility experiments, is that the polymer phase in contact with the SCF behaves as an ideal solution.

Partition coefficient data for the polystyrene-ethane system, at a variety of operating conditions, have been modelled with a Statistical-Mechanics based Lattice EOS, using a single adjustable parameter, δ_{12}, that is independent of pressure, temperature and polymer chain length. An analysis with the lattice EOS proves that the observed linearity of the ℓogK_i vs X_i curves in the solubility experiments represents a universally valid trend displayed by polymer-SCF systems.

Precipitation polymerization reactions in SCF have been conducted to prove the viability of this novel synthesis scheme to produce polymers of a low molecular weight and a relatively narrow molecular weight distribution. We established that polymers of chain length greater than ~400 distributed themselves across the SCF-phase and the coacervate-phase following the same partition law measured in the solubility experiments. In examining

the sensitivity of the precipitate phase compositions to changes in P and [M], it was observed that the molecular weight distributions move to higher average values with increases in each of these variables, illustrating the approach to liquid-like behaviour of the SCF solvent.

Data obtained from these experiments have been quantitatively correlated with a model developed in this work. Use of this model, along with activated state theories, illustrates the fact that the use of SCF solvents allows us to affect selectively the kinetic rates of certain steps in the mechanism, thus permitting us to produce polymers of relatively small molecular weights and polydispersity.

CHAPTER 1
INTRODUCTION

1.1 MOTIVATION

Supercritical fluid extraction (SCFE) is a unit operation in which a supercritical fluid (SCF), a substance above its critical temperature and pressure, is used as an extractant to solubilize a variety of compounds, ranging from simple molecules like benzene to complicated molecules such as cholesterol (Chrastil, 1982).

The region around the critical point is one of rapid changes in properties. The density of the substance in this regime is, in particular, very sensitive to changes in state variables and can vary from gas-like to liquid-like with relatively small changes in pressure or temperature. To illustrate this point, in Figure 1.1, a reduced pressure vs. reduced density[4] plot for a substance near its critical point is presented (Paulaitis et al., 1983). The sensitivity of the density to state variables in the vicinity of the critical point is of importance when it is considered that the solvent power of an SCF is directly related to its density (Paul and Wise, 1971).

SCF also possess other interesting properties. The specific heat, C_p, of a substance becomes infinitely large at the critical point, and thus, in the vicinity of this point, the C_p of the material can be large. Also, the kinematic viscosity, (ν), of an SCF is of the order of 10^{-7} $m^2 s^{-1}$, lower even than that of liquid metals. This fact, in conjunction with a diffusivity, (D), intermediate between liquids and gases (Table 1.1) implies that SCF have Schmitt numbers, (ν/D), of the order 10. This immediately suggests

---

[4] A reduced variable, in this context, refers to a non-dimensional number obtained by scaling the relevant variable by its value at the critical point of the material.

that, although the solvent power of an SCF is liquid-like, its Schmitt number (Sc) is gas-like. A low value for Sc is favourable in the context of SCFE since it implies that the ratio of mass transfer time to momentum transfer time is smaller than in liquids, ensuring a faster approach to a mass transport equilibrium.

SCFE has a significant advantage over conventional liquid extraction (LE) processes in that the separation of the solvent from the solute can be achieved by small variations of operating conditions, at projected

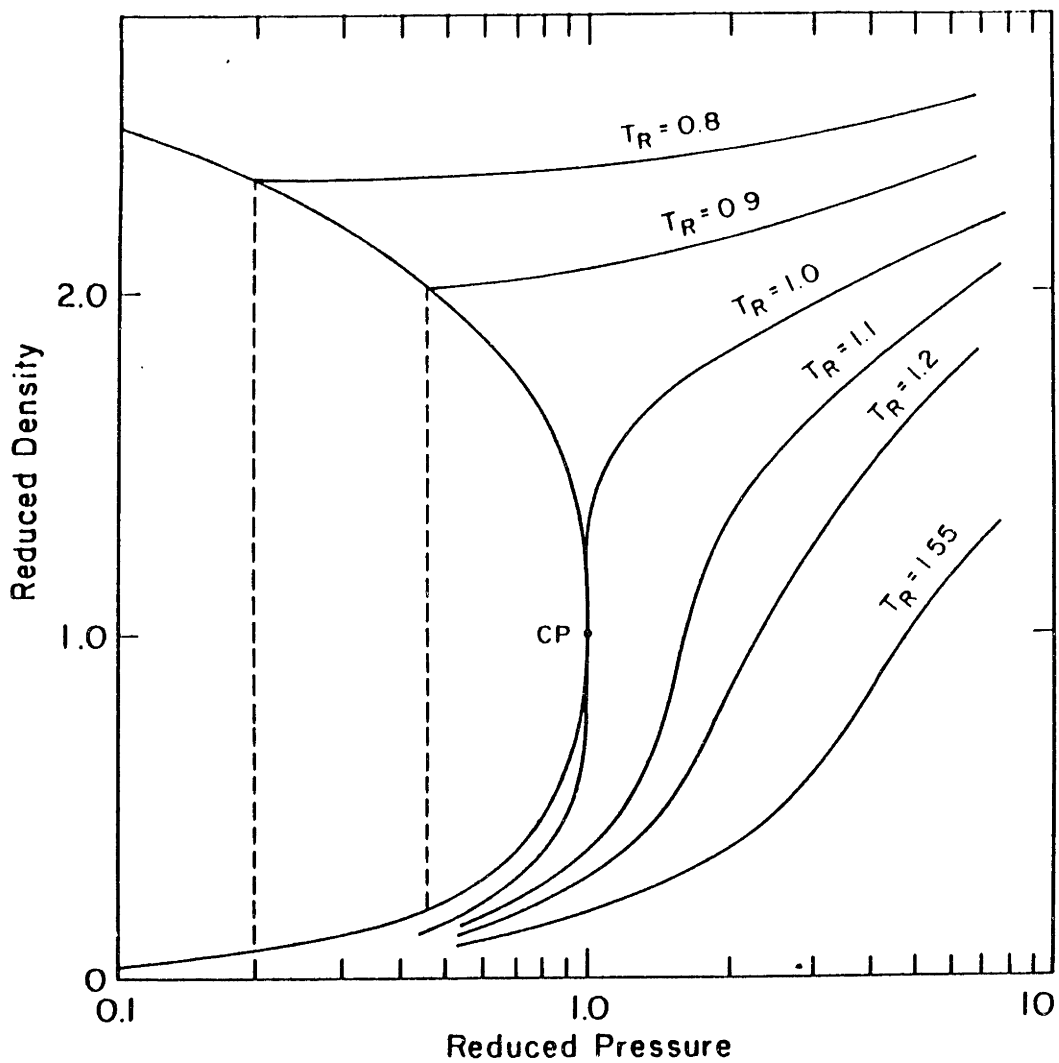

Figure 1.1: Plot of the reduced pressure vs reduced density for carbon dioxide in the vicinity of its critical point (CP). Several isotherms are shown. (Paulaitis et al., 1982)

Table 1.1: An order of magnitude comparison of the transport properties of liquids, gases and SCF.

Substance	Density kgm^{-3}	Viscosity Nsm^{-2}	Diffusivity m^2s^{-1}
Liquids	10^3	10^{-3}	10^{-9}
Gases	1	10^{-5}	10^{-5}
SCF‡	700	10^{-4}	10^{-8}

‡For CO_2 at 20 MPa, 310K

lower costs than LE. This is a direct consequence of the dependence of the solvent power of an SCF on its density: gas-like at low densities and approaching liquid-like at relatively high densities. Also, since SCF possess a high C_p, they can be used to obtain better temperature control in any unit operation in which these fluids are employed. The high operating pressures and the concomitant costs of equipment and maintainence offset this advantage. The application of SCFE is probably of most value in special extractions; viz. thermally labile products of bioreactors (Willson, 1987).

In the past, SCF have been studied mainly as alternate materials for the solubilization of low vapour pressure compounds. Examples include the dissolution of SiO_2 in supercritical water (Kennedy, 1950), simple organic solids like naphthalene, benzoic acid, anthracene, acridine and 2-aminoflourene in supercritical CO_2, ethane and several freons (Schmitt, 1984). The solubility of liquids like water, alcohols (ethanol, methanol, propanol, n-butanol) and organic acids (acetic acid, butyric acid) in supercritical CO_2 and ethane, have also been reported in a recent work (Panagiotopoulos, 1986). Another application of SCF that has been examined, is in the fractionation of mixtures of solids of low volatility. A case in point would be the fractionation of polymers on the basis of chain molecular mass with SCF solvents (Paualitis et al., 1983). It has been shown in this work that the molecular mass distribution of a polymer available commercially (polysiloxane in this case), can be narrowed by extraction with supercritical carbon dioxide. The point being emphasised here, therefore, is that most of the prior art concerns itself with the measurement of the equilibrium solubilities of compounds in supercritical fluids with little emphasis

being placed on the applications of SCF in other environments.

A few industrial applications of SCFE do exist. Prominent among these are the decaffination of coffee (Zosel, 1982; Peter and Brunner, 1982; Katz, 1981), extraction of lipids (Friedrich, 1985) and the extraction of hops (Laws et al., 1980). Again, the underlying principle in these extractions involves the utilization of the phenomenon of extractant-SCF equilibrium. It is only of late that other applications of SCF under process conditions have been examined.

An interesting example of a relatively recent application of SCF, not directly related to the areas discussed earlier, involves the production of small, essentially equal sized particles by nucleation from a solution of the material in an SCF. Krukonis (1984) has demonstrated that monodisperse particles of *ca.* 10 microns diameter can be produced by dissolving β-estradiol in carbon dioxide at 34.5 MPa and 328K and subsequently flashing the mixture to atmospheric pressure, when the dissolved solid is precipitated. This process is of significance since it is carried out at relatively mild temperature conditions and could thus be used to process thermally labile or degradable substances. An aspect of this process that has received little attention is the possibility of modifying the morphology of solids through nucleation from an SCF.

Another intriguing application of SCF involves their use in biochemical reactors, where they can be used to extract products inhibitory to the growth of the relevant microorganism, during the course of a fermentation reaction. Willson (1987) currently is investigating the use of supercritical gases in an integrated fermentation-extraction scheme in which the propionic acid produced by *Propionibacterium freudenreichii* can be abstracted from the reacting mixture, with essentially no harmful side effects.

Other processes that have received some attention in the recent past involve the use of SCF as reaction media. The high cost of SCF as extraction media makes them unattractive except in special separations. However, the possibility of altering reaction product distributions through the use of SCF as reaction

media makes them attractive candidates for further investigation, in this context. A germane example would be the use of supercritical water as a solvent for the oxidation of organic wastes, with almost no ash being produced as a byproduct (Helling, 1986).

Another potentially interesting application of SCF that combines reaction and phase equilibrium concepts is a "SCF Precipitation Polymerization". In a classical, liquid-phase precipitation polymerization reaction the monomer is dissolved in a liquid solvent that behaves as a non-solvent for the polymer. The reaction is initiated and occurs homogeneously in one phase until the polymer grows past a point when it is essentially insoluble in the liquid solution. At this instant, a second, polymer-rich phase is created by the precipitation of chains insoluble in the solvent phase. By proper adjustment of operating conditions the reaction in the precipitated "solid" polymer, which may be unterminated, can be slowed so that almost all of the reaction occurs in the solvent phase. This provides a technique to obtain a polymer with a narrow molecular mass distribution (Bamford et al.,1980). However, in liquid solvents, the product polymer is frequently a swollen gel since it is plasticized by the solvent (and sometimes the monomer). The reaction rate in the precipitate could thus be very high and often may be higher than in the solvent phase (Jenkins, 1967). The narrow molecular mass distribution that is obtained due to the precipitation might thus be destroyed, and the final product obtained would then normally be of a broad molecular mass distribution [with polydispersities, (M_w/M_n), of the order of 5-10]. Also, in liquid solvents, no control is available to vary the threshold molecular mass for polymer precipitation since the solvent power of the liquid solvents could not be varied easily.

To appreciate the utility of SCF in precipitation polymerization reactions we need to understand the position and the sensitivity of the threshold molecular mass of polymer chains for precipitation, to variations in operating conditions. In the current literature, however, little data exists to indicate the variation of solubility of the members of a homologous series of compounds in an SCF, as a function of molecular mass. It has been inferred from chromatographic techniques that the solubilities of a

series of compounds in an SCF decreases as the chain length of the solute molecule increases (Schmitz and Klesper,1983). Also, Schröder and Arndt (1976a,1976b), in their work on determining qualitatively the solubility of polymer chains (viz., PVC and polystyrene) in CO_2 observed that the equilibrium concentrations of compounds in an SCF decreases as one proceeds to solutes of longer chain lengths. This also suggests that if a mixture of compounds belonging to the same homologous series were contacted with an SCF, the lower molecular mass compounds would be preferentially dissolved into the fluid phase. This concept of preferential solubility of lower molecular mass compounds from a mixture into an SCF has been used to fractionate polydisperse polymers on the basis of molecular mass (Paulaitis et al.,1983; Krukonis, 1985; McHugh and Krukonis, 1986).

The potential use of SCF as solvents in the context of precipitation polymerization stems from the following reasons:

(i) The adjustable solvation power of SCF allows for the variation of the threshold molecular mass for polymer precipitation. The molecular mass of the product polymer may then be varied by adjusting the pressure, temperature or the composition of the SCF phase.

(ii) Since SCF are expected to be poor solvents, it is anticipated that the problem of the broadening of the product molecular mass distributions due to reactions in the precipitate will be alleviated by their use.

(iii) Subsequent to the reaction, the unreacted monomer can be recovered easily from the reaction medium, again with relatively modest changes in the operating conditions. This is in sharp contrast to classical precipitation polymerizations wherein the recovery of the unreacted monomer is a highly energy intensive process (Gutowski et al., 1983)

(iv) The high C_p of the SCF allows for the easy removal of heat of reaction thus easing a heat transfer problem that is normally encountered in precipitation polymerization reactions.

These concepts provide the motivation for the investigation of a precipitation polymerization with an SCF as a solvent medium. It must be remembered, however, that the use of SCF in this context has its disadvantages. The high pressure at which the reaction must be carried out is hazardous from

a safety consideration. The handling of solids, specially particulates, at the operating pressure is also a potential problem area if this scheme were to be extended to an industrial scale.

1.2 RESEARCH OBJECTIVES

The main focus of this work is directed toward exploring the feasibility of a precipitation polymerization of a well-studied reaction system using an SCF or an SCF mixture as the solvent medium. Styrene polymerized by a free-radical mechanism, initiated by a classic initiator such as 2,2'-azobisisobutyronitrile (AIBN) is an example polymerization system. The approach to fulfill this objective was to use experiment and theory in an integrated fashion so as to study and understand the complex phenomena involved.

1.2.1 Experimental Aspects: The experimental portion of this research relates to the operation of a polymerization system. To achieve this purpose, a well characterized reaction system is desirable. This entails that reaction rate constants as well as solubilities of oligomers in the SCF (as a function of chain length) need to be known.

- Data on the solubilities of oligomeric chains in SCF are not available. The measurement of these solubilities (as a function of chain length) was performed in the first part of this work.
- The latter part of this work then concentrated on the analysis of the chosen SCF precipitation polymerization system to prove the viability of this novel synthesis scheme to produce precipitate polymers of a narrow molecular mass distribution and a controllable average molecular mass. Also, the sensitivity of the composition of the product polymer to changes in state variables (like pressure, temperature, monomer concentration and initiator concentration) were examined to identify the controlling operating conditions.

1.2.2 Theoretical Aspects: The proper understanding of the theoretical aspects of the proposed work stems from a need to place the experimental data in a proper theoretical framework. The theoretical aspects that need to be modelled are presented below.

- The equilibrium solubilities of monodisperse polymer fractions in an SCF need to be correlated. The modelling of binary mixtures of monodisperse polymer-SCF will have to be extended to a case of a polydisperse polymer in equilibrium with an SCF.
- Data on reaction rate constants in liquid solvents are available in the current literature (Jenkins, 1967; Moore et al.,1981). However, reaction mechanisms are essentially unknown, and rate constants have not been measured for SCF polymerization reactions under the state conditions of interest. SCF precipitation polymerizations were thus performed to measure the compositions of polymer in the SCF phase and the precipitate phase to formulate an appropriate kinetic mechanism and deduce the relevant kinetic parameters. This information was used to predict the average molecular mass and molecular mass distributions of the product polymer under different operating conditions.

CHAPTER 2
EXPERIMENTAL BACKGROUND AND RESEARCH METHODOLOGY

In this chapter experimental results in the relevant areas of supercritical fluid extraction and polymer fractionation are discussed. Also, a concise introduction to precipitation polymerization is provided. This discussion will be used to rationalize the selection of the system investigated in this work.

We emphasise that the theoretical background and a detailed discussion of the theoretical methodology adopted in this work are not covered in this chapter. In the current literature, the techniques involved in the modelling of the theoretical aspects, especially the modelling of the solubility of polymers into solvents, is a highly involved field that requires an elaborate introduction. It is for this reason that this discussion has been deferred to appropriate sections in this thesis.

2.1 SUPERCRITICAL FLUID EXTRACTION

SCFE was first observed by Hannay (1880) and Hannay and Hogarth (1879) who noticed the enhancement of the solubility of a solid in a fluid near its critical point. The theoretical framework for this phenomenon was established earlier by van der Waals in his work on Equations of State in 1873. The interest in SCFE then decreased with little work being done in the field until the middle of this century. Then, the most significant study dealt with the solubility of naphthalene in SCF (Diepen and Schaeffer, 1948 and 1953). Later, this work was extended by Tsekhanskaya et al., (1964) who measured naphthalene solubilities and diffusivities in some SCF.

Much of the existing literature in this area deals with the measurement of the equilibrium solubilities of a variety of compounds in SCF (see

Chapter 1). Also, the majority of applications of SCF in the process industry involve the utilization of supercritical fluids as extraction media. The earliest use of SCF on a process scale was the deashing and supercritical extraction of coal liquids (Gearhart and Garwin, 1970). Decaffination of coffee and tea, extraction of hops and spices and fractionation of polymers are some other examples of the applications of this unit operation (Paulaitis et al.,1983; Zosel, 1978). It is only recently that the use of SCF in other aspects of process flow sheets have been considered. An example of such an application being studied currently is the utilization of supercritical fluids for the extraction of biological products from fermentation broths in a combined fermentation-extraction scheme (Willson, 1987). A book by McHugh and Krukonis (1986) provides a collection of the potential uses of SCF in industrial processes.

SCF have also been used in chromatography where the fluid is used as the carrier medium for the separation of substances with very low vapour pressures. This process has been used successfully for the separation of oligomeric and polymeric styrenes on the basis of molecular mass utilizing the fact that, in this context, SCF are strong fractionating media (Schmitz and Klesper, 1981, 1983). The principal advantage of supercritical fluid chromatography (SFC) over liquid chromatography (LC) is that the separation of a solute mixture can be obtained not only by temperature or solvent composition programming (as in the case of LC or GC) but also by pressure variations. This is a direct consequence of the sensitivity of the density, and hence solvent power of the SCF on both the temperature and pressure of operation. The height equivalent of a theoretical plate (HETP) in such separations is directly proportional to the kinematic viscosity of the carrier gas and to the diffusivity of the solute in the carrier. The very low kinematic viscosity of SCF and diffusivities intermediate between liquids and gases result in a smaller HETP in the case of SFC as compared to LC and GC (Debenedetti,1984; Klesper, 1978; see also Table 1.1), thus ensuring better fractionation of the solute on the basis of molecular mass. A review paper by Randall (1982) documents the wide range of applicability of SFC.

The separation of the product polymer from the solvent is an important problem in solution polymerization processes. This operation, which normally is achieved by the evaporation of the solvent, is energy intensive and can frequently account for *ca.* 10% of the cost of the final product. Gutowski et al., (1983) have employed SCF to facilitate the easy separation of solvents from polymers and report that this alternate method is potentially cheaper than conventionally employed techniques. McHugh and Guckes (1985) have also demonstrated that the use of SCF in this context is practically viable.

The study of the solubility of polymers in SCF was motivated mainly to understand the bulk polymerization of ethylene at operating conditions around 100 MPa and 400K, wherein the ethylene monomer is supercritical (T_c of C_2H_4 is 282.4 K and P_c is 4.9 MPa). Experimental studies in the area are almost always privy information, but there is a report by Ehrlich and Mortimer (1970) that provides some data in the form of cloud point curves for the ethylene-polyethylene system. Also, Spahl and Luft (1982) have published detailed, partition coefficient data for polyethylene chains between a polymer-phase and a supercritical ethylene phase, again in the same range of operating conditions.

Work in the area of solubility of poly(vinylchloride) in supercritical CO_2 has also been performed (Schröder and Arndt, 1976a and 1976b). In this work, light scattering was used to monitor the quantity of material dissolved in the SCF phase. Results reported cannot be quantified since they are reported as the variation of the fraction of scattered light as a function of operating variables. To infer solubility trends from light scattering data we may employ the Beer-Lambert law for light absorption,

$$B_\lambda = A_\lambda / c d_\lambda \qquad (2.1)$$

where c is the solute concentration in the SCF phase (moles m^{-3}), d_λ is the optical length of the sample cell (m) and B_λ is the molar absorbance, which has been shown to be independent of pressure (Swaid, 1982). A_λ is defined through the integral,

$$A_\lambda = \int \ell n(I_0/I)\, d\lambda \qquad (2.2)$$

where $\ell n(I_0/I)$ is the absorbance corresponding to any wavelength λ, and the integration in Eq(2.2) is performed over the wavelength spectrum of the incident beam. Schröder and Arndt (1976a,1976b) present their data as the variation of transmitted light fraction as a function of operating variables. On defining this fraction as some quantity t, we can show that,

$$c = -\ell nt/d_\lambda B_\lambda \qquad (2.3)$$

Eq.(2.3) suggests that c vs. ℓnM curves will have the same shape as Schröder and Arndt's plots of t vs M, where M represents the molecular mass of the polymer sample. Some trends for the solubility of polymers in SCF can thus be inferred from their work:

- All different molecular mass polymer samples show a sharp rise in solubility around the critical pressure of CO_2 (7.38 MPa), a characteristic displayed by low molecular mass compounds as well.
- The solubility curves tend to flatten out as one goes out to high pressures, but in a much slower fashion than the isotherms of a low molecular mass compound.
- A fact to be noted is the variation of solubility as a function of molecular mass at a given pressure and temperature, highest for low molecular masses and decreasing with increasing molecular mass (refer to Figure 2.1). Figure 2.1 demonstrates the strong dependence of the molecular mass on the solubility of a polymer into an SCF. At 100 MPa and 313K, the authors show that the transmitted light fraction depends on the molecular mass of PVC in a power-law fashion,

$$t \propto M^{-\frac{1}{4}} \qquad (2.4)$$

We can rewrite this using Eq.(2.3) as,

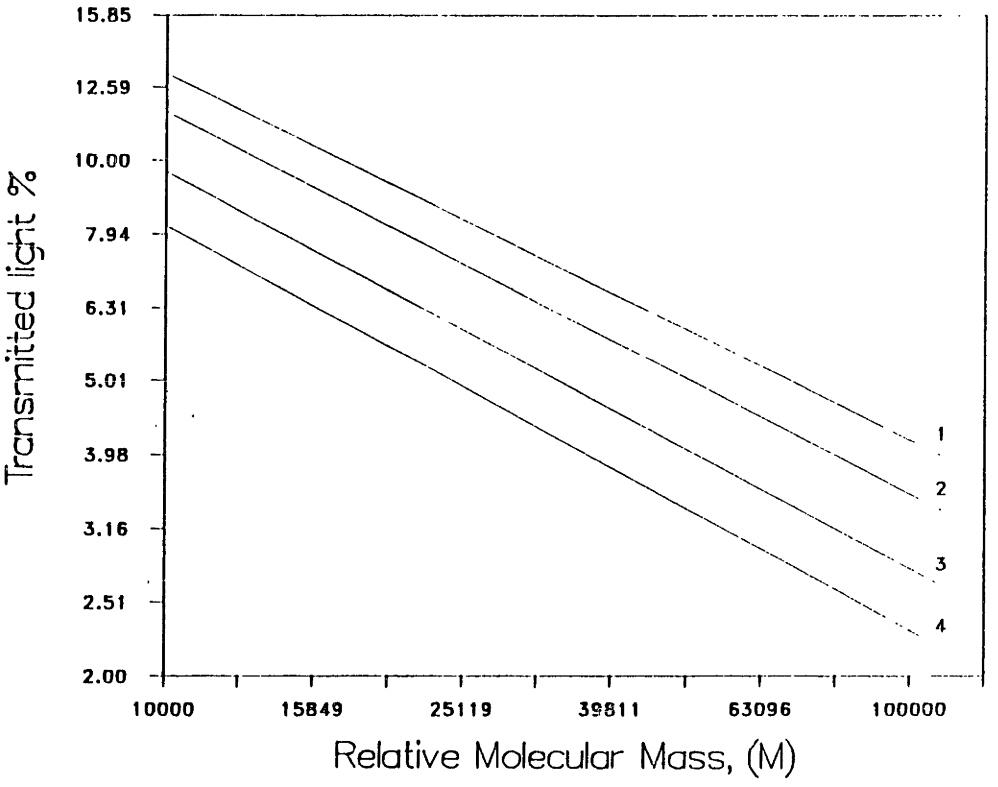

Figure 2.1 : Variation of the transmitted signal with molecular mass of the PVC sample at 313 K in CO_2. 1:100 MPa., 2: 40 MPa., 3: 20 MPa., 4:10 MPa. M is the molecular mass of the PVC fraction of interest. (Schröder and Arndt, 1976a)

$$c = \eta_1 - \eta_2 \ \ell nM \qquad (2.5)$$

where η_1 and η_2 are constants. From this work, therefore, we can surmise that the solubility of polymer samples in an SCF (in moles m^{-3}) must decrease in a linear-log fashion with increases in their molecular mass.

While it is encouraging to note that recent studies have focussed on the practical use of SCF, we must be understand that the use of high-pressure processes have not generally found much favour in the process industry; an important exception being the synthesis of polyethylene. The reason for this can be attributed to the increased costs incurred in the construction, maintainence and operation of such plants due to the extreme operating

pressures. It would thus seem reasonable to assume that large scale processes based on the use of SCF as extraction media will not be economically viable. The anticipated use of SCF probably lies in special separations (an examples of this is the extraction of thermally labile or degradable materials like products of fermentation reactions) or in unusual synthesis schemes, like the one that will be examined in this thesis. Another area that needs more careful examination is the possibility of modifying the morphology of solids, especially polymers, by nucleation from a supercritical solution.

SCF could also be used in the understanding of the fundamental behaviour of matter. It has already been shown by Panagiotopoulos (1986) that unusual phase behaviour, including substantial regions of multi-phase equilibrium are displayed by mixtures with supercritical components. High-pressure materials due to their unusual properties (see Table 1.1, for example), are excellent tools to probe the molecular interactions that determine the phase behaviour of complicated mixtures. An integration of such experimental data along with Monte Carlo or Molecular Dynamics simulations will help in delineating the factors that govern the phase behaviour of mixtures.

2.2 SOLUBILITY OF POLYMERS IN CONVENTIONAL SOLVENTS

Most of the current literature indicates that an SCF solvent may be used to fractionate polymers on the basis of molecular weight. Paulaitis et al., (1983), Krukonis (1985) and McHugh and Krukonis (1986) have demonstrated with the use of GPC traces that, by dissolving a polymer in an SCF, the product (in the SCF phase) is always concentrated in the low molecular mass chains. However, no quantitative data that illustrate the fractionating ability of SCF exist in the vicinity of their critical points.

The fractionation of polymers on the basis of molecular mass with liquids or very high pressure gases, however, is a subject that has received considerable attention in the past few decades (Schulz and Jirgensons,1940;

Flory, 1953; Koningsveld et al., 1974; Kleintjens et al., 1976; Spahl and Luft, 1982). We now examine the area of fractionation of polymers with conventional liquid or liquid-like solvents to understand qualitatively the trends to be expected when SCF solvents are used instead.

It has been demonstrated that for the fractionation of polymers with liquid-like solvents, to a first approximation, a mass-based partition coefficient for each n-mer between the two equilibrium phases depends only on the molecular mass of the chain in an exponential fashion,

$$\ell n(K_i^{old}) = \ell n(w_i'' / w_i') = -\sigma r_i + \ell n\xi \qquad (2.6)$$

where the single and double primes are used to denote the phases dilute and concentrated in polymer, respectively. w_i represents the weight fraction of the polymer chain in the relevant phase, K_i^{old} is a partition coefficient, r_i is the chain length of the polymer (or, alternately, the number of monomeric units per polymer chain) and ξ is a constant. σ, also termed as the "separation factor", determines the dependence of the partition coefficient on the molecular weight of the polymer chain, and is a function of temperature, pressure and concentration.

Schulz (1941) has derived this equation through the use of empirical arguments. The first theoretical development of Eq(2.6) was achieved by Flory (1953). Since the fractionation of a polymer occurs between a polymer-rich phase and a solvent-rich phase, it implies that polymer chains of each chain length must be in thermodynamic equilibrium across the two phases. The mathematical criterion which expresses this situation is the equality of chemical potentials of the relevant species in both the phases,

$$\mu_i' = \mu_i'' \qquad (2.7)$$

for all components i. Flory obtained expressions for the chemical potentials of each constituent of the mixture through the use of the Flory-Huggins Lattice Model (Flory, 1941,1942; Huggins, 1941,1942). On substituting these formulae in Eq(2.7), the functional form for the partition coefficient,

K_i^{old}, represented in Eq(2.6), can be recovered (Flory, 1953; Kurata, 1982).

It is to be noted here that, σ, the separation factor in Eq.(2.6) is independent of the chain length of the component i, to a zeroth order. If a narrowly distributed polymer sample were used to determine σ, therefore, the obtained value will be essentially independent of chain length. On the other hand, if a polydisperse sample were to be employed, a chain length dependent value of σ may result. An alternate way of appreciating this fact can be obtained by expanding σ in a MacLaurain series in terms of the inverse of the chain length as a parameter,

$$\sigma = \sigma_\infty + [\partial\sigma/\partial(1/r_i)]_\infty \ (1/r_i) + \cdots\cdots\cdots\cdots\cdots \qquad (2.8)$$

where the series expansion is made about the infinite chain length limit. The variation of σ with chain length is then controlled, to a first approximation, by the second term in the expansion.

To date, however, analysis techniques of sufficient accuracy do not exist to separate and analyze polymer molecular mass distributions on an individual mer by mer basis. Instead, most data reported in the literature for fractionation of polymers by liquid solvents are in the form of number or mass averaged molecular weight data. Eq(2.6), which is the governing equation for this fractionation process, however, is valid strictly only for individual mers. The calculation of σ from Eq(2.6), using average molecular mass data, will therefore not allow for an unequivocal determination of the molecular mass dependence of σ. Based on average molecular mass data for the fractionation of polymers into liquid solvents, Schulz and Jirgensons (1940) suggested that σ is a weak function of molecular mass. This observation has been subsequently verified by Breitenbach and Wolf (1967), Tsuyomoto et al.(1984) and Koningsveld and coworkers (1974). Tong et al. (1985) show that the separation factor is practically constant when dealing with a monodisperse polymer sample, and becomes dependent on the polymer molecular mass only when it is of a very broad distribution.

The solubility and fractionation of polymers (specifically polyethylene) in very high-pressure ethylene (of the order of 200 MPa.) has been reported by Spahl and Luft (1982). Again, for the polymers considered, mostly of molecular mass around 1000, they find a linear dependence of the partition coefficient on the average molecular mass of the polymer in consideration, implying that σ has a constant value in the regime investigated.

In summary, consequently, there are two points that need to be emphasised as the essential results in the literature regarding the fractionation of polymers with conventional solvents.

- The partitioning of polymer between the two equilibrium phases depends exponentially, to a zeroth order, on chain length of the relevant species following Eq(2.6) [σ is assumed to be independent of chain length]. If a broad range of chain lengths are considered, however, this simple relationship may break down and a non-linear term, still only a function of chain molecular mass, is introduced in the exponential term.
- To date there is sufficient evidence to suggest that σ may indeed be a weak function of chain molecular mass. However, no data has been published for the fractionation of polymers, on an individual mer by mer basis, to determine this dependence accurately for any system.

2.3 PRECIPITATION POLYMERIZATION

The time evolution of a precipitation polymerization is as follows: the polymerization of the monomer (either in bulk or in a homogenous solution with a diluent) is initiated either by a chemical initiator or by other means (Flory,1953), and occurs initially in a single homogenous-phase. For the case of a free radical polymerization, an initiator, such as an azonitrile compound, forms free radicals due to spontaneous thermal dissociation,

$$I \longrightarrow 2R^{\bullet} \qquad (2.9)$$

Here I is the initiator and R$^{\bullet}$ a free radical. (In all subsequent notation, the bullet, ($\bullet$), will always be used to represent a free electron that is present on a free-radical). The polymerization continues in a single phase solution through addition of monomers to free-radicals in a propagation step,

$$R^{\bullet} + M \longrightarrow RM^{\bullet} \qquad (2.10)$$

$$RM^{\bullet} + M \longrightarrow RM_2^{\bullet} \qquad (2.11)$$

$$\vdots$$

$$RM_x^{\bullet} + M \longrightarrow RM_{x+1}^{\bullet} \qquad (2.12)$$

where M stands for a monomer molecule and $RM_x^{\bullet}$ represents a chain of x monomeric units with an *unterminated* radical at the end. The propagation reaction is normally terminated either by addition or disproportionation of two active, free-radical chains to form dead polymer chains.

$$RM_x^{\bullet} + RM_y^{\bullet} \longrightarrow P_{x+y+2} \qquad \text{(Addition)} \qquad (2.13a)$$

$$\longrightarrow P_{x+1} + P_{y+1} \qquad \text{(Disproportionation)} \qquad (2.13b)$$

It is to be noted that the addition reaction involves the combination of the free electrons on the two free-radicals to form a single bond between the chains that add. In the disproportionation reaction, however, one free-radical abstracts a proton from the other to form a single bond: the other free-radical in its turn forms a double bond to satisfy the valence requirements of the carbon atoms at the end of the chain.

In precipitation polymerizations, these reactions proceed until a threshold concentration of a n-mer is reached, wherein it precipitates. The determination of the precipitation threshold is one of the least understood aspects in this mechanism since it may be affected by system-specific parameters. Barrett and Thomas (1975) present a review of the variety of theoretical techniques used to model the nucleation process. The dyna-

mically controlled threshold molecular weight for precipitation has been calculated using a theory of homogenous nucleation [(Nielsen,1964), This aspect of the literature will be addressed in Chapter 6].

The precipitated polymer still possesses some active chain ends which may react further with more monomer in a propagation step. Significant reaction in the coacervate would broaden the molecular mass distribution. Two factors dictate if further reaction occurs in the precipitate phase:

- Due to increased viscosity of glassy substances at temperatures below the T_g of the coacervate phase, the unterminated chains in this phase are more occluded than at higher temperatures. Their reactivity, therefore, is lower than that of the chains in the solution phase (Jenkins, 1967). This means that, in principle, the rate of polymerization in the precipitate is slow, and hence a product polymer with a narrow molecular mass distribution should be obtained. Bamford et al., (1980) have synthesised polystyrenes of low polydispersities ($M_w/M_n \sim 1.6$) through the free-radical precipitation polymerization of styrene in n-hexane, demonstrating the viability of this concept. At higher temperatures, however, the reactivity of the radicals in the coacervate become more important.
- The presence of large quantities of monomer or appropriate solvents however, may plasticize the polymer, thus reducing the T_g of the coacervate phase. The effect of this is similar to raising the operating temperature, i.e., the radical ends are less occluded and significant reaction with monomer may occur in this phase.

Juba (1984) and Ray and Jain (1975) have suggested that the addition of a chain-transfer agent will help in the control of the molecular mass distribution of the product polymer. The addition of a classic chain transfer agent, normally a mercaptan, helps transfer free radicals that are present on chains to monomers or other chains through the following mechanism:

$$AH + RM_x^{\bullet} \longrightarrow P_{x+1} + A^{\bullet} \qquad (2.14a)$$

$$A^{\bullet} + M \longrightarrow R^{\bullet} + AH \qquad (2.14b)$$

wherein AH is the chain transfer agent and P_x is the terminated polymer. In the first step the free radical is abstracted from the active chain by the chain transfer agent. The chain transfer agent, which now is a free radical, then reacts with either a monomer [Eq.(2.14b)], or, if the monomer concentration is low with a terminated polymer chain, in a propagation step. In this process, the active chain looses its reactivity, automatically ensuring that the broadening of the molecular mass distribution in the precipitate phase will be reduced.

Another interesting aspect of precipitation polymerization reactions is that the overall, bimolecular termination rate constant is lower in these reactions than in conventional, single phase polymerizations. This can be attributed to the fact that both terminated and unterminated chains are present in the precipitate.[5] Due to the high viscosity of this phase, the movement of the oligomeric chains in the coacervate phase is almost absent and the possibility of termination is lowered. The net effect of this phenomenon is manifested as a reduction in the value of the overall termination rate constant for the system (Jenkins, 1967).

The rate of polymerization, r_p, depends on the monomer concentration [M] and the total free radical concentration, $\sum[R_x^{\bullet}]$ through the equation:

$$r_p = k_p[M] \times \sum[R_x^{\bullet}] \qquad (2.15)$$

It must be realized, that in single phase polymerization reactions, the total radical concentration reaches a quasi steady-state relatively fast compared to the half-life of the initiator, and that this value is usually 5 to 6 orders of magnitude smaller than the monomer concentration (for more details see Flory,1953; Odian, 1985). In a solution polymerization

---

[5] The proof of the presence of active ends in the precipitate has been shown by Bamford and Jenkins (1955) with the use of electron spin resonance (ESR) measurements.

reaction, therefore, the rate of polymerization (r_p) is maximum early and slowly drops off as the conversion increases due to the depletion in monomer concentration [Eq(2.15)]. The rate of precipitation polymerization, in the absence of chain transfer agents, on the other hand, increases with time. This can be attributed to a reduced rate of termination for the precipitated radicals as compared to the termination rate in the case of solution polymerization. The concentration of unterminated radicals thus increases with time, causing an enhancement of the reaction rate in the coacervate phase. This effect termed as the Tromsdorff or autoacceleration effect is illustrated in Figure 2.2 which is reproduced from Jenkins (1967).

Solution Polymerization

Precipitation polymerization
(Without chain transfer agent)

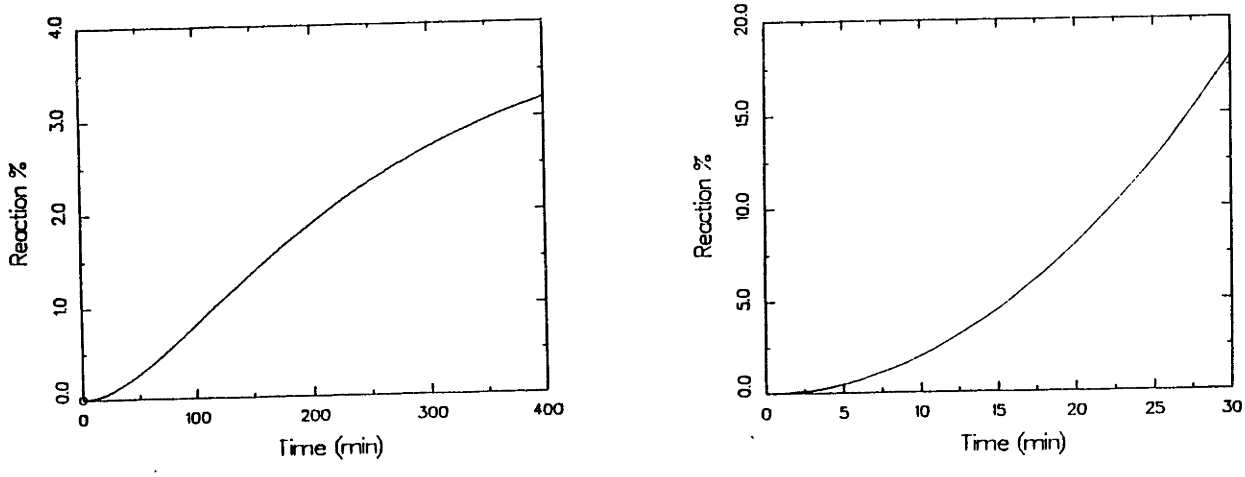

Figure 2.2: Comparison of the conversion vs. time for a solution and precipitation polymerizations (Jenkins,1967)

Historically, precipitation polymerization was discovered when methyl methacrylate was polymerized in the bulk, by a free radical mechanism in the liquid phase (Norris and Brookman,1939; Norris and Smith, 1942). Norris and Smith (1942) noted an increase in the polymerization rate with increasing conversion of the monomer and correctly attributed the source of this effect to an increase in the viscosity of the medium due to precipitation of the product poly(methylmethacrylate). An increased viscosity of the medium reduces the mobility of free-radicals, thus reducing the probability of their termination. The concentration of free-radicals thus increases with time, resulting in an increasing reaction rate following Eq(2.15). Bamford and Jenkins (1953, 1955) have subsequently verified this result for other systems, viz. the free-radical polymerization of acrylonitrile in the bulk. Other works in the area include the free radical polymerization of styrene in methanol, the bulk polymerizations of vinyl chloride and vinylidene chloride (Juba,1979).

Juba (1979) provides an overview of the field both from a theoretical and a practical standpoint. This work is also an excellent source for the current literature in the field. In the case of a homogenous-phase free radical polymerization, when termination occurs only due to addition or disproportionation, the value of M_w/M_n, termed the polydispersity, ranges between 1.5 and 2.0; the actual value depending on ratio of radicals terminated by addition to radicals terminated by disproportionation. In normal, single-phase free radical polymerizations, however, M_w/M_n normally ranges between 3 and 5, due to the presence of other termination mechanisms. Occasionally, precipitation polymerizations can yield product polymers with molecular mass distribution as low as in conventional, single-phase polymerizations. Bamford et al., (1980) report a value of M_w/M_n of approximately 1.6, for a free radical precipitation polymerization of styrene in n-hexane. Schwab (1984), also reports narrow distributions (M_w/M_n ~1.3) for the anionic dispersion polymerization of styrene in n-hexane.

Data for the reaction rate constants for some polymerization systems (viz. the free radical solution polymerization of styrene at a variety of pressures) are available in the literature (Moore et al., 1981). However,

little to no data exist for precipitation systems at high pressures, in solvents near their critical points.

2.4 RESEARCH METHODOLOGY

2.4.1 System Selection

It is the goal of this work to examine a precipitation polymerization reaction in an SCF to understand and delineate the relevant phenomena and, also, to contrast this heterogenous reaction in SCF to classical, liquid-phase precipitation polymerizations. The selection of an appropriate SCF solvent and a polymerization system will thus have to be made to successfully achieve the objectives of this work. The selected system should, preferably, meet the following criteria:

- The reaction rate in the precipitated phase can be retarded if the polymer in this phase is below its glass transition temperature. The glass-transition temperature of the chosen polymer system must be near the chosen temperature of operation. In this context, it must be remembered that the addition of a solvent, frequently, plasticizes the polymer and thus reduces the polymer's T_g.
- Also, the product polymer must be amorphous so that its equilibrium solubility can be measured unequivocally. If the product polymer were semi-crystalline, however, this would not be possible.
- The monomer and initiator must be soluble in the SCF to an appreciable degree, preferably completely soluble under the operating conditions.
- The polymer produced in the chosen system must be commercially available in samples with different molecular masses and narrow molecular mass distributions from degrees of polymerization between 1 and 50. This is essential for the measurement of the chain length dependence of the solubility of polymer chains in the chosen SCF.
- To allow for the ease of operation, it is desirable to conduct the polymerization reaction in the vicinity of room temperature, i.e., in the temperature range 303-343K. A material with a critical temperature

in this range is an ideal choice for the SCF solvent.

The selection of appropriate systems with these prerequisites can now be made. In the following discussion we present the systems chosen for this investigation.

Selection of the Polymerization System: The selection of the polymerization scheme is an important step in our system selection. As suggested earlier, a well studied polymerization system will have to be considered. The free radical polymerization of styrene is a reaction that has been carried out in a precipitation mode in a variety of solvents (Hoffman, 1976; Juba,1979), at temperatures between 298 and 353K and to yield a totally amorphous product (the glass temperature of unplasticized polystyrene is approximately 373K [Brandup and Immergut, (1975)]). Also, the various kinetic steps involved in this reaction are well understood. Polystyrene is commercially available in monodisperse polymer fractions between average molecular masses of 500 and 500,000.

Another prospective system is the anionic polymerization of PEO, a system that has also been studied in some detail in the past. However the product, PEO, is partially crystalline, which could imply a significant increase in the complexity for the understanding of the system. We thus chose the polymerization of styrene initiated by a free-radical mechanism as our model polymerization system.

SCF Selection: There are several, commonly available materials with T_c in the vicinity of room temperature. Some of these materials along with relevant thermodynamic properties are listed in Table 2.1.

Table 2.1 : Properties of some SCF

Gas	T_c (K)	P_c (MPa)
Carbon dioxide	304.2	7.38
Ethane	305.4	4.88
Ethylene	282.4	5.03
Propane	369.8	4.24

Of these SCF, CO_2 is the most frequently used SCF solvent and would be a good choice for our purposes regardless of the chosen polymerization system, since it is a well studied and fairly well understood supercritical solvent. In the past, however, almost all precipitation polymerizations have been carried out in organic media: for example, styrene in n-hexane (Bamford at al., 1980), styrene in methanol (Hoffman, 1976), methyl isopropenyl ketone in cyclohexane (Haward, 1948). (Important exceptions are the precipitation polymerizations of polymethylmethacrylate or polyacrylonitrile which are normally performed in an aqueous solution (Jenkins,1967 and all references therein), and the bulk polymerizations of vinyl chloride (Chatelain,1973), acrylonitrile (Bamford and Jenkins, 1953) or methyl methacrylate (Norris and Smith, 1942)]. The free-radical precipitation polymerization of styrene, our model polymerization system, has been conducted in the liquid phase in n-alkanes (Bamford et al, 1980). This provides us the motivation to pick ethane as the primary solvent for our exploratory work on the feasibility of precipitation polymerization in SCF solvents.

An unusual entry in Table 2.1 is propane, which with its critical temperature at 370K is outside the desired operating range. The reasoning for the inclusion of this compound is to study, if possible, the effect of tailoring the critical temperature of the SCF by the use of gas mixtures. It has been suggested in the past (Joshi and Prausnitz, 1984), that the use of SCF mixtures gives rise to synergistic effects with regard to their solvent power. This makes the use of gas mixtures of ethane and propane an attractive prospect.

Selection of free-radical initiator: Several free-radical initiators have been considered for use in polymerization reactions. Among them the most popular ones include peroxides such as cumyl peroxide, t-butyl peroxide and benzoyl peroxide, hydroperoxides such as cumyl and t-butyl hydroperoxides, and azo compounds like 2,2'-azobisisobutyronitrile (AIBN) [Odian,1985]. All these initiators form free-radicals through thermal dissociation, with AIBN being used at low temperatures ($t_{1/2}$(343K)= 4.8 h), and the peroxides being normally employed at higher temperatures ($t_{1/2}$(400K)= 6.4 h for t-butyl peroxide). Other initiators such as redox initiators, photoinitiators were not considered since it was felt that the free-radical mechanism was the best understood and hence presented the least degree of uncertainty if it were to be used. Since we chose to operate our reactions in the vicinity of room temperature, AIBN was the logical choice for the radical initiator.

2.4.2 Experimental Methodology

2.4.2.1 Solubility Experiments: Data on the solubility of polymer chains in SCF are required to understand the chain length dependence of solubility. A knowledge of the solubility allows for the prediction of the precipitation threshold in the polymerization experiments through the use of an appropriate theory of nucleation. Also, such experiments allow us to gain an understanding of the partitioning of polymer chains between the gas-phase and the precipitate-phase in the synthesis experiments.

Since the density of an SCF and hence its solvent power are sensitive to the operating variables (pressure and temperature) in the vicinity of the critical point of the solvent SCF, the variation of partition coefficient with changes in these variable will be examined. Also, as suggested, an ethane-propane mixture will be used to examine the modifying effect of an additive to the partitioning behaviour of ethane.

2.4.2.2 Reaction Experiments: The polymerization experiments are tailored to study the feasibility of the proposed "SCF Precipitation Polymerization" concept and to study the sensitivity to the following variables:

-Temperature of operation: The temperature of operation is a crucial variable due to three factors. First, that a variation in the temperature of operation would have the effect of changing the molecular mass cutoff, and thus varying the molecular mass of the resultant polymer product. Secondly, a shift in the operating temperature would cause the mobility and occlusion of the trapped radicals to vary, thus potentially affecting the molecular mass distributions of the polymer obtained. Third, reaction rates are temperature dependent and changes in temperatures are thus expected to enhance conversions from monomer to polymer, at any given time.

- Pressure of operation: The pressure of operation is an important variable since the density and hence the solvent power of an SCF are very sensitive to the value of this variable. The cutoff in molecular mass is hence expected to be a determined by this variable. We thus expect to be able to modify the molecular mass distribution of the product polymer by altering the operating pressure.

- Monomer Concentration: Since the rate of polymerization is a direct function of the monomer concentration [Eq.(2.15)] it is expected that this variable will play a pertinent role in the determination of the molecular mass distribution of the product polymer. Also, oligomers of styrene are soluble in styrene monomer, while it is expected that the SCF solvents will behave as "non-solvents" for the oligomers. The addition of appreciable quantities of styrene to the SCF can thus be expected to modify the behaviour of the solvent, thus affecting the properties of the product polymer.

CHAPTER 3

A STATISTICAL-MECHANICS BASED LATTICE MODEL EQUATION OF STATE

3.1 INTRODUCTION

The modelling of mixture VLE has normally been performed by one of the following techniques:

(a) Semi-empirical methods

(b) Monte Carlo methods

3.1.1 Monte Carlo Methods

Monte Carlo methods have been used to simulate and understand the effect of intermolecular interaction potentials between small spherical molecules, on their VLE behaviour. The review by Gubbins et al. (1983) and a recent thesis by Panagiotopoulos (1986) are excellent sources for the techniques used for the modelling of binary mixtures. However, simulations have been restricted to mixtures of small molecules of almost the same size. It is believed that Monte Carlo and Molecular Dynamics techniques will eventually find extensive use in the modelling of mixtures of molecules of disparate sizes. However, at this point in time, the excessive computational effort required in these simulation methods makes them relatively unattractive in comparison to simple, closed form equations of state (EOS).

3.1.2 Semi-Empirical methods

Helmholtz energy models of pure components and mixtures would be a natural result if a statistical mechanics approach were taken to model

mixtures of molecules. An advantage of obtaining the Helmholtz energy of a mixture, $\underline{A}$, is that it contains all the requisite thermodynamic information for the system. For example, an equation of state relating the state variables for a N component system, namely T,P,$\underline{V}$ and (N-1) mole fractions, can be obtained.

$$P = - \left. \frac{\partial \underline{A}}{\partial \underline{V}} \right|_{T,N_1,N_2 \cdots N_n} \tag{3.1}$$

Also, the chemical potentials of component i in phase j can be obtained from the $\underline{A}$ functionality.

$$\mu_i = \left. \frac{\partial \underline{A}}{\partial N_i} \right|_{T,\underline{V},N_{j \neq i}} \tag{3.2}$$

During the last decade EOS have been used increasingly to correlate and model the complex phase behaviour of molecular mixtures under a variety of conditions. Several classes of equations of state (EOS) have either been derived from, or lead to a Helmholtz energy model for a pure compound or a multicomponent mixture. Cubic EOS (van der Waals, 1873; Redlich and Kwong,1949; Soave, 1972; Peng and Robinson,1976) are examples of the more popular models that can be derived semi-empirically from an expression for the Helmholtz energy of the system of interest (Donohue and Prausnitz, 1975). These EOS can be represented in a general form as:

$$P = \frac{NRT}{\underline{V} - Nb} - \frac{N^2 a}{\underline{V}^2 + uN\underline{V}b + wN^2 b^2} \tag{3.3}$$

wherein u and w are pure numbers characteristic for each EOS and R is the universal gas constant. This genre of EOS and its modifications (Carnahan

and Starling, 1972; Dieters, 1981) have found extensive use in the field of SCFE. However, these EOS have one major limitation in that they were derived for the case of mixtures of small, essentially spherical molecules. Therefore, they should not be used for mixtures of molecules of vastly differing sizes.

To model the phase behaviour of systems of molecules of disparate sizes one needs an appropriate Equation of State (EOS) that is applicable over a large range of densities. In the past, the modelling of mixtures of molecules of dissimilar sizes has been performed by the use of either of two general techniques. The first is based on perturbation theory; an example of such an EOS is the modified perturbed hard chain EOS (PHCT) [Donohue and Prausnitz,1975; Vimalchand and Donohue,1985; Sandler,1986] which has been used successfully to model mixtures of small and large hydrocarbons. The apparent complexity and the large number of adjustable parameters in PHCT models makes them less attractive for our purposes.

The second genre of models used for polymer-solvent mixtures has been the lattice model approach. The earliest attempts to correlate polymer-solvent systems were made by Flory (1941,1942,1953), Huggins (1941, 1942) and Staverman (1950), who developed an activity coefficient model through the use of a mean-field analysis of molecules placed on a three-dimensional lattice. Most later developments in this field are attempts to alleviate the shortcomings inherent in these pioneering attempts. These improved models in their turn can be broadly classified into three categories which are discussed below.

Kleintjens (1983) and Kleintjens and Koningsveld (1982) did select the Flory-Huggins entropy term in their expression for the Helmholtz energy of the polymeric system, but departed from the older work by allowing their "enthalpic" contribution to be a function of density and composition. They also introduced empty sites in the lattice, termed "holes". The resulting EOS has been used successfully to model the phase behaviour of binary mixtures of water, carbon dioxide and decane (Nitsche et al., 1983). This model, however, is characterized by the *a-priori* assumption of a functional

form for the canonical partition function in order to derive the EOS and other thermodynamic quantities.

Flory (1970), thirty years after his initial contribution, in an attempt to obtain an EOS rather than activity coefficients, resorted to the use of a cell-theory model (Hirschfelder et al., 1954) to formulate the canonical partition function for an ensemble of pure polymer chains. This approach uses the concept of the c parameter as suggested by Prigogine (1957) to account for the external degrees of freedom of a chain molecule. The resultant EOS is a two-parameter corresponding-states model that has been extended to mixtures. Patterson and coworkers (1969,1972) have used this formulation to predict critical curves and lower critical solution temperatures (LCST) for polymer solutions. Simha and coworkers (Simha and Somcynsky, 1969; Jain and Simha, 1980) have adopted the same technique, viz. the cell-theory approach, along with different expressions for the free-volume for spherical and chain molecule fluids. These models, however, suffer from a two-fold disadvantage: first, we need to assume a functional form for the free-volume term as it cannot be assigned unequivocally from theory. Second, an extra parameter, c, which is unknown and must be obtained by fitting experimental data to the model is introduced. Also, we need to know the volume dependence of c in order that the EOS may be applicable to gas-like and liquid-like phases. If the model were extended to multicomponent mixtures, a mixing rule for the c parameter is required and this introduces an extra degree of uncertainty to mixture predictions.

Some of the difficulties encountered in the free-volume theories have been overcome in the "Lattice Fluid" theories. Sanchez and Lacombe (1976,1977) applied the more rigorous Guggenheim-Huggins-Miller approximation (Guggenheim, 1954) to enumerate the number of possible configurations when polymer chains were placed on a lattice. They also included empty sites in their lattice which they termed "holes". In their model, therefore, the number of holes plays the role of free-volume. The explicit consideration of the number of external degrees of freedom and the flexibility of a chain molecule, used to determine the functional form of the free-volume are unnecessary in this formulation. Okada and Nose (1981a, 1981b) have accounted

for the non-random distribution of free-volumes (or holes) and thus improved on the work of Sanchez and Lacombe. These models assume that a lattice cell holds exactly one small molecule or one chain segment. While this assumption will have no effect on the problem formulation for pure components, in the extension to mixtures of molecules of unequal chain segment sizes, it introduces additional complexity since we now have to account for the mixing of two quasi-lattices of unequal cell sizes. [This difficulty can be somewhat overcome if one resorts to Staverman's use of a characteristic interaction area for each type of site (Staverman,1950).] Also, in the formulation of Sanchez and Lacombe, it is (unphysically) assumed that a lattice site has an infinite coordination number.

Panayiotou and Vera (1982) improved on the "lattice fluid" model by *a-priori* setting the lattice cell size and coordination number. The lattice, therefore, is a convenient division of three-dimensional space. A unit cell does not have the function of holding exactly one small molecule or chain segment; a molecular segment can occupy a fractional number of sites. The advantage of using this method is that the extension of a pure component model to mixtures is, in principle, straightforward, since we no longer have to concern ourselves with the mixing of lattices of unequal cell size or coordination number.

It is the objective of this chapter to establish an EOS and related thermodynamic quantities for a pure component and, subsequently, closed form expressions for mixtures of molecules of any size. Panayiotou and Vera (1982) have derived an expression for pure components, and, with some approximations extended it to binary mixtures. Their formulation, however, cannot be extended to multicomponent mixtures in a closed form. We use their pure component EOS as a starting point in our modelling, and provide analytical expressions for the multicomponent EOS and chemical potentials. The utility of the lattice EOS in modelling the VLE properties of mixtures of small molecules is also examined. The necessary extensions for the modelling of polymer-SCF systems are made; however, results for these mixtures are presented in Chapter 4.

3.2 PURE COMPONENTS

3.2.1 Theoretical Development

Consider a three-dimensional cubic lattice of coordination number z and of unit cell size v_H. Each molecule is assumed to occupy r_1 lattice cells or sites (where r_1 can be fractional) and the lattice has empty sites called holes. There are N_0 holes and, correspondingly, a mole of molecules [$\equiv N_1$ molecules]. To account for the connectivity of the segments of a molecule, an "effective chain length", q_1, is defined so that zq_1 now represents the effective number of external contacts per molecule.

$$zq_1 = zr_1 - 2r_1 + 2 \tag{3.4}$$

In Eq.(3.4) it has been assumed that chains may be branched but not cyclic. The effective interaction energy between segments of molecules (species 1) is a square well potential of depth $-\epsilon_{11}$, while the interaction energy of any species with a hole (species 0) is zero. Only nearest neighbour interactions are accounted for, and pairwise additivity is assumed. The canonical partition function for this ensemble can be formally represented as:

$$\Omega = \sum_{\substack{\text{all possible} \\ \text{states } \{n\}}} \exp(-\beta E_{\{n\}}) = \Omega_{ke} \times \Omega_c \tag{3.5}$$

where β [$\equiv 1/k_B T$] is the thermodynamic temperature. Ω_{ke} is the contribution of the kinetic energy terms to the canonical partition function and is assumed to be only temperature dependent; Ω_c is the configurational part of the partition function. In the following we avoid taking temperature derivatives of thermodynamic quantities and can thus employ Ω and Ω_c interchangeably. Following the approach of Panayiotou and Vera (1982) we obtain an approximate expression for Ω_c which is valid outside the critical region of the pure component, i.e.,

$$\Omega_c \simeq \lambda(T)^{N_1} \; g(N_0, N_1, r_1, z) \; \exp[-\beta E(N_0, N_1, r_1, z)] \tag{3.6}$$

Here $g(N_0, N_1, r_1, z)$ represents a combinatorial term and the exponential term is a Boltzmann probability contribution to the maximum term in the canonical partition function. $\lambda(T)$, a temperature dependent function that accounts for the conformations of a molecule, is assumed to be independent of density, i.e., the internal configurations of a chain molecule vary only with temperature. In obtaining Eq(3.6) we have assumed that the largest term in Eq(3.3) is a good approximation to the entire summation. This concept, also termed the Mean-Field approximation, is appropriate when substances far from the critical region are considered. [The derivation of this approximation maybe obtained from standard Statistical-Mechanics texts, for example Huang (1963) or Landau and Lifschitz (1980).]

The number of configurations, $g(N_0, N_1, r_1, z)$, of placing N_0 holes and N_1 molecules on a lattice with a total interaction energy of $E(N_0, N_1, r_1, z)$ must now be enumerated. For pure components, Panayiotou and Vera (1982) have shown that assuming a random mixing of holes and molecules causes relatively small errors as compared to case where a non-random mixture of species is assumed. In our formulation, therefore, we employ the random mixture hypothesis for pure components and obtain the combinatorial term following Guggenheim (1954),

$$g(N_0, N_1, r_1, z) = \frac{(N_0 + r_1 N_1)!}{N_0!\ N_1!} \left[\frac{(N_0 + N_1 q_1)!}{(N_0 + N_1 r_1)!} \right]^{z/2} \tag{3.7}$$

where the exclamation mark (!) stands for a generalized factorial, i.e., $a! = \Gamma(a+1)$. An expression for the configurational energy, $E(N_0, N_1, r_1, z)$ may also be derived.

$$E(N_0, N_1, r_1, z) = N_{11}(-\epsilon_{11}) \tag{3.8}$$

where N_{11} represents the number of nearest neighbour 1-1 segment interactions. On substituting expressions for N_{11} we can show that,

$$E(N_0, N_1, r_1, z) = (z/2)N_1 q_1 \times \frac{N_1 q_1}{N_0 + N_1 q_1} \times (-\epsilon_{11}) \qquad (3.9)$$

Here the first term represents the number of contacts that segments of molecules (species 1) experience, and the second represents the probability that a 1 segment has another 1 segment as its nearest neighbour. Using Eqs(3.7)-(3.9) in Eq(3.6) we obtain the explicit expression for the configurational contribution to the canonical partition function for this ensemble,

$$\Omega_c \propto \lambda(T)^{N_1} \frac{(N_0 + r_1 N_1)!}{N_0!\ N_1!} \left[\frac{(N_0 + N_1 q_1)!}{(N_0 + N_1 r_1)!}\right]^{z/2} \exp\left[\frac{\beta}{2} \cdot zN_1 q_1 \epsilon_{11} \frac{N_1 q_1}{N_0 + N_1 q_1}\right] \qquad (3.10)$$

It must be emphasized here that we do not need to use the c parameter that was suggested by Prigogine (1957) to account for the external degrees of freedom for a chain molecule. Since this class of lattice models are not based on a cell model type partition function, the question of how the external and internal degrees of freedom are separated is never encountered (Sanchez and Lacombe, 1976).

The bridge from the canonical partition function to thermodynamics is through the use of standard statistical-mechanics,

$$\underline{A} = -k_B T \ \ell n\ \Omega \qquad (3.11)$$

where $\underline{A}$ is the total Helmholtz energy of the system. The EOS and related thermodynamic quantities can then be obtained through familiar techniques (Modell and Reid, 1983).

$$P = -\left.\frac{\partial \underline{A}}{\partial \underline{V}}\right|_{T,N_1} \tag{3.1}$$

$$= -\frac{k_B T}{v_H} \times \left.\frac{\partial \ell n \Omega_c}{\partial N_0}\right|_{T,N_1} \tag{3.12}$$

where $\underline{V}$, the total volume of the system is defined as,

$$\underline{V} = v_H(N_0 + r_1 N_1) \tag{3.13}$$

Using the following reducing parameters

$$-\frac{z}{2}\epsilon_{11} = P^* v_H = RT^* \tag{3.14}$$

an EOS for a pure component is obtained, i.e.,

$$\frac{\tilde{P}}{\tilde{T}} = \ell n\left[\frac{\tilde{v}}{\tilde{v} - 1}\right] + \frac{z}{2}\ell n\left[\frac{\tilde{v} + (q_1/r_1) - 1}{\tilde{v}}\right] - \frac{\vartheta^2}{\tilde{T}} \tag{3.15a}$$

Here ϑ is the effective surface area fraction of molecules in the lattice,

$$\vartheta = q_1 N_1/(N_0 + q_1 N_1) = (q_1/r_1)/[\tilde{v} + (q_1/r_1) - 1] \tag{3.15b}$$

and the tilde [~] denotes a reduced variable. All quantities except v in the EOS are reduced by the parameters in Eq.(3.14). The specific volume v is non-dimensionalized by v^*, the molecular hard-core volume, which is defined by the equation,

$$v^* = N_1 r_1 v_H, \text{ or } r_1 = v^*/(N_1 v_H) \tag{3.16}$$

Expressions for the chemical potential of a pure component can also be derived from Eq.(3.11),

$$\mu_1 = \left.\frac{\partial \underline{A}}{\partial N_1}\right|_{T,\underline{V}} \tag{3.2}$$

However, $\underline{A}$ as derived in Eq (3.11) is a function of (T,N_0,N_1), while the derivative in Eq (3.2) is taken at constant $(T,\underline{V})$. We may translate Eq(3.2) into the appropriate framework by employing the chain rule for partial differentiation,

$$d\underline{A} = \left.\frac{\partial \underline{A}}{\partial T}\right|_{N_0,N_1} dT + \left.\frac{\partial \underline{A}}{\partial N_0}\right|_{T,N_1} dN_0 + \left.\frac{\partial \underline{A}}{\partial N_1}\right|_{T,N_0} dN_1 \tag{3.17}$$

On employing Eqs(3.17) and (3.11) on Eq.(3.2) one may show that,

$$-\frac{\mu_1}{k_B T} = \tilde{r}_1(\tilde{P}/\tilde{T}) + \left.\frac{\partial \ell n \Omega_c}{\partial N_1}\right|_{T,N_0} \tag{3.18}$$

$$= \gamma(T) + \left[\frac{r_1 \tilde{P}}{\tilde{T}}\right] + \ell n q_1 - \ell n \vartheta - r_1(1-z/2)\,\ell n\,\frac{\tilde{v} + (q_1/r_1) - 1}{\tilde{v}}$$

$$- \frac{q_1 \vartheta^2}{\tilde{T}} + \frac{2q_1\vartheta}{\tilde{T}} \tag{3.19}$$

where $\gamma(T)$ represents a temperature dependent function which is constant for a species distributed between phases at equilibrium. Eqs.(3.15) and (3.19) are identical to Panayiotou and Vera's (1982) results.

3.2.2 Determination of pure component parameters

In the pure component EOS [Eq.(3.15)] there are apparently four independent, unknown parameters: we chose z, v_H, v^* and ϵ_{11}. As stated earlier a lattice cell here does not have the function usually assigned it in the lattice fluid theories, namely to hold one chain segment. In the present context the lattice merely serves to describe the number of ways neighbours in space can mutually be arranged. It is, however, mandatory, that the cells are neither excessively small nor large since Eq.(3.3) only has meaning if the cells are large enough that a small, compact molecule such as water or carbon dioxide does not occupy many adjacent sites (no "internal surfaces"). Also the cells must be small enough to allow only one small molecule or chain segment to reside in a cell. These arguments lead to a choice of a cell volume in the range 5-30 Å^3 (3×10^{-6}-18×10^{-6} m^3 mole^{-1}). A related question is the value to be chosen for z, the lattice coordination number. The lattice, having lost its literal meaning in the lattice fluid theories, nevertheless imposes its connectivity on the fluid phase. In three dimensions, the only case of interest here, a lower bound is the value for the simple cubic (or von Neumann) lattice with z=6. An upper bound is clearly the number of nearest neighbours a closest packing of identical spherical objects provides, i.e., z=12. Hence, z must fall in the range 6-12. We set z=10 and $v_H = 9.75\times10^{-6}$ m^3 mole^{-1} (corresponding to 16.2 Å^3/cell).

To model real substances we need to determine ϵ_{11} and v^*. For a pure component below its critical point the technique of Joffe et al. (1970) was employed. This involves the matching of chemical potentials of the component across the liquid and vapour phases at the vapour pressure of the substance. Also, the actual and predicted saturated liquid molar volumes were matched,

$$\mu_L = \mu_V \qquad (3.20a)$$

$$v_L(\text{actual}) = v_L(\text{predicted}) \qquad (3.20b)$$

The equation set (3.20) was solved by the use of Newton's method to yield

the pure component parameters. (The computer programs used to obtain the pure component properties are presented qualitatively in Appendix III.) In the context of the solution of Eqs (3.20) it is important to remember two facts:

- The absolute values of ϵ_{11} (J/mole) and v^* (m^3/mole) are different by approximately 8 orders of magnitude (see Table 3.1). For ease of implementation, therefore, the two parameters must be scaled so that the elements of the solution vector are of the same order of magnitude.
- v^*, the hard core volume, must always be smaller than v the molar volume. To prevent the Newton solver from straying into infeasible regions (i.e., $v^*>v$), therefore, we chose $\ell n(v/v^*-1)$ as the independent variable rather than v^*.

In Table 3.1 we list values of ϵ_{11}/k_B and v^* for some common chemicals. (The values of ϵ_{11}/k_B and v^* are temperature dependent functions.) Also, the specific choice of lattice parameters (z and v_H) was found to have little effect on the capability of the EOS to reproduce pure component vapour-liquid equilibrium (VLE) in the limits stated above ($3\times10^{-6}\leq v_H\leq18\times10^{-6}$ m^3 $mole^{-1}$; $6\leq z\leq12$).

The EOS must not be used in the vicinity of the critical point of the pure component since the mean-field approximation was evoked in its derivation. However, as for all classical EOS, the standard criteria for the critical point can be written. The critical point of a pure substance may be represented mathematically as the point where its isothermal compressibility and its partial derivative with respect to volume simultaneously diverge.

$$\partial P/\partial v]_T = \partial^2 P/\partial v^2]_T = 0 \qquad \text{at } T=T_c,\ P=P_c \tag{3.21}$$

When we use the lattice EOS in this equation set, the predicted critical point can be obtained. An analysis of the lattice EOS with the Buckingham-Pi theorem shows that there must be 5 dimensionless groups in the reduced EOS. We define four of these groups as,

Table 3.1: Pure Component Parameters for some common chemicals. z=10, v_H= 9.75×10^{-6} m^3 mole^{-1}

Chemical	T (K)	v^* (m^3 mole^{-1})	(ϵ_{11}/k_B) (K)
Water	283	17.28×10^{-6}	432.6
	293	17.82×10^{-6}	422.9
	413	19.45×10^{-6}	328.4
Methanol	293	56.97×10^{-6}	190.5
Ethanol	283	55.28×10^{-6}	163.3
	293	55.27×10^{-6}	163.0
	413	59.75×10^{-6}	136.5
n-Propanol	293	71.51×10^{-6}	147.5
n-Butanol	293	86.82×10^{-6}	140.9
n-Octanol	293	148.73×10^{-6}	129.9
t-Butanol	293	87.59×10^{-6}	123.6
n-Heptane	293	128.56×10^{-6}	98.9
n-Decane	293	184.60×10^{-6}	101.0
n-Tetradecane	293	257.40×10^{-6}	106.3
Acetone	293	68.44×10^{-6}	123.9
Benzene	293	82.68×10^{-6}	119.9
Aniline	327	88.68×10^{-6}	158.0
Naphthalene	308	106.07×10^{-6}	146.9
Anthracene	323	113.65×10^{-6}	188.7
Benzoic Acid	313	94.93×10^{-6}	202.2
Formic Acid	294	37.07×10^{-6}	219.5
Acetic Acid	293	55.83×10^{-6}	177.4
Chlorobenzene	293	98.89×10^{-6}	124.4
Cyclohexane	293	97.40×10^{-6}	108.6
o-xylene	293	111.86×10^{-6}	120.1
p-xylene	293	113.68×10^{-6}	117.0

1. All vapour pressure and liquid density data from Reid et al.(1977)
2. Additional data on ϵ_{11} and v^*, for ethanol and water as a function of temperature are presented in Table 3.3.

$$Z_H = Pv_H/RT = \tilde{P}/\tilde{T} \qquad (3.22a)$$

$$Z = Pv/RT \qquad (3.22b)$$

$$Z^* = Pv^*/RT \qquad (3.22c)$$

$$\zeta = \epsilon_{11}/RT \qquad (3.22d)$$

The coordination number, z, is then chosen as the fifth dimensionless group. The EOS can be formally rewritten as,

$$r_1(Z_H, Z^*, Z, \zeta, z) = 0 \qquad (3.23)$$

Application of the critical point criteria with the EOS will thus yield two

equations which are expressed as,

$$\tau_2(Z_H, Z^*, Z, \zeta, z) = 0 \qquad (3.24a)$$

$$\tau_3(Z_H, Z^*, Z, \zeta, z) = 0 \qquad (3.24b)$$

The equation set Eq. (3.23)-(3.24) must be solved simultaneously to yield the pure component critical point as defined by the lattice EOS. If it is assumed that the z value is a constant (equal to 10 in our case) then it can be seen that we are solving 3 equations with four unknowns. The equation set (3.23)-(3.24) has been solved with the use of a Newton's method and yields solutions in terms of a single parameter [chosen to be $(Z_H)_c$ in our case]. The formal solution to these equations can then be represented as,

$$Z_c = (Pv/RT)_c = f(Z_H)_c \qquad (3.25a)$$

$$\zeta_c = (\epsilon_{11}/RT)_c = g(Z_H)_c \qquad (3.25b)$$

$$Z_c^* = (Pv^*/RT)_c = h(Z_H)_c \qquad (3.25c)$$

It should be noted that one can obtain different values for the critical compressibilities (Z_c) by selecting different values of v_H (and therefore Z_H). Also, the critical compressibility of a material is a function of its critical pressure and temperature, thus allowing the lattice EOS to incorporate system specific thermodynamic properties (P_c and T_c) in the calculation of parameters at the critical point. This is in contrast to two-parameter cubic EOS which predict a substance independent Z_c. The point to be made here is that the predicted critical compressibility is not constant, but varies according to the critical point of the pure substance under consideration. Typically, this number ranges between 0.25 and 0.29.

Pure component parameters for supercritical components were obtained by fitting experimental P-v data on an isotherm to Eq.(3.15). (A modified Fletcher-Powell Algorithm was used in these data fitting routines.) Data for the substances tested (ethane, carbon dioxide) suggest that the computed v^* is only a weak function of temperature, and ϵ_{11} is a constant within regression error. For supercritical components modelled in this work, v^* and ϵ_{11} are assumed to be constant in the vicinity of the critical point

Table 3.2: Pure Component Parameters for ethane and carbon dioxide above their critical temperatures. z=10, v_H= 9.75x10^{-6} m^3 mole^{-1}.

Chemical	T (K)	v^* (m^3 mole^{-1})	ϵ_{11}/k_B (K)
Ethane	310-370	5.553x10^{-5}	73.732
Carbon Dioxide	310-370	3.872x10^{-5}	82.026

1. Carbon Dioxide P-v data from Angus et al.(1976)
2. Ethane data from Goodwin et al.(1976)

[typically, $T-T_c < 60K$]. In Table 3.2, we present pure component parameters for ethane and carbon dioxide above their critical temperatures.

Pure component vapour pressure data for polymeric substances are not available. Hence, we used the parameters given by Panayiotou and Vera (1982) for polymers, obtained by fitting the EOS to the thermal expansion coefficient, isothermal compressibility and thermal pressure coefficient of polymeric systems.

In summary, we have determined pure component properties in most instances (except polymers) by employing P-v data, rather than by fitting the EOS [Eq(3.15)] to properties obtained by taking temperature derivatives of thermodynamic functions (as thermal expansion coefficients). Parameters determined in the former fashion (i.e., by fitting to P-v data) are more appropriate for phase equilibrium calculations since they ensure that model predictions will always converge to the correct pressure limits when the mixture is essentially a pure component (i.e., when the mixture is infinitely dilute in the other components).

3.2.3 Discussion

The EOS given by Eq.(3.15) differs from the one suggested by Sanchez and Lacombe (1976), since the latter was developed for lattices with large coordination number. While this later approximation simplifies calculations and frees the model from the arbitrariness of a chosen value of z, a large value of z is physically unrealistic since this means that a molecule has

an infinite number of neighbours. The EOS therefore, will be inappropriate for the modelling of real VLE systems in the high z limit (see section on Mixtures: Results and Discussion). If z is set to infinity in Eq.(3.15), we recover Sanchez and Lacombe's (1977) lattice-fluid EOS,

$$\frac{\tilde{P}}{\tilde{T}} = \ell n\left[\frac{\tilde{v}}{\tilde{v} - 1}\right] + \frac{1}{\tilde{v}}\left[1 - \frac{1}{r_1}\right] - \frac{\vartheta^2}{\tilde{T}} \quad , \; z \longrightarrow \infty \tag{3.26}$$

Eq.(3.15), therefore, is simply the lattice fluid EOS for finite values of z.

In the dilute limit, Eq.(3.26) is identical to the result one obtains from the Flory approximation (1941, 1942) for the configurational part of the canonical partition function, Ω_c [see Eq.(3.6)]. This is clear if one terms the "holes" as "solvent" (with $\epsilon_{solv\text{-}solv} = \epsilon_{poly\text{-}solv} = 0$) and, also, if one makes the assumption of a dilute "solution" and employs the following definitions:

$$\tilde{v} = \phi_{pol}^{-1} \quad , \quad \tilde{T} = \chi^{-1} \quad , \; r_1 = n_{pol} \, , \; \tilde{P}/\tilde{T} = P_{osm} v_s / RT \tag{3.27}$$

Here, ϕ_{pol} is the volume fraction of the polymer, χ is the Flory-Huggins interaction parameter, n_{pol} the degree of polymerization, P_{osm} the osmotic pressure of the solution and v_s the molar volume of the solvent. One then recovers the Flory equation for the osmotic pressure (Flory, 1953) from Eq.(3.26),

$$P_{osm} = -(RT/v_s)\,[\ell n(1 - \phi_{pol}) + (1 - 1/n_{pol})\phi_{pol} + \chi\phi_{pol}^2], \quad z \longrightarrow \infty, \; \tilde{v} \longrightarrow \infty \tag{3.28}$$

To understand qualitatively the behaviour of the pure component EOS, it is examined in the limiting case of small molecules, i.e., when $q, r \longrightarrow 1$. Then, Eq.(3.15) reduces to the form,

$$\frac{\tilde{P}}{\tilde{T}} = \ell n\left[\frac{\tilde{v}}{\tilde{v}-1}\right] - \frac{1}{\tilde{T}\,\tilde{v}^2} \quad , \qquad r = q = 1 \tag{3.29a}$$

We write Eq (3.29a) in a compressibility form as,

$$Z = \frac{\tilde{P}\,\tilde{v}}{\tilde{T}} = \tilde{v}\,\ell n\left[\frac{\tilde{v}}{\tilde{v}-1}\right] - \frac{1}{\tilde{T}\,\tilde{v}} \tag{3.29b}$$

$$= Z_R - Z_a \tag{3.29c}$$

This second term in Eq (3.29b), Z_a, can be rewritten as,

$$Z_a = \frac{P_a v}{RT} = -\frac{(P^* v^{*2})}{v^2} = -\frac{a}{v^2} \tag{3.30}$$

where Z_a is termed the "attractive" contribution to the compressibility, Z (=Pv/RT), since it has the same form as the attractive term in the van der Waals EOS (van der Waals, 1873). On examining the data for P^* and v^* for ethanol and water, and computing the parameter $\underline{a}$ in Eq.(3.30) it was found that for temperature variations over a range of 150 K, this parameter always changed by less than 3% although the computed values of v^* and ϵ_{11} themselves showed a 7% variation (see Table 3.3). In the limit of small molecules, therefore, the lattice EOS has an "attractive" term that closely approximates the characteristic of the van der Waals type attractive term.

On expanding the "repulsive" term in Eq.(3.29), Z_R, in a Taylor series we obtain,

$$Z_R = (P_R v/RT) = -\tilde{v}\ell n(1-\tilde{\rho}) = 1 + \tilde{\rho}/2 + \tilde{\rho}^2/4 \cdots\cdots \tag{3.31}$$

wherein $\tilde{\rho} = 1/\tilde{v}$, and the series is valid for $\tilde{\rho} \approx 0$. Now expanding the van

Table 3.3: Pure Component parameters for ethanol and water at several temperatures (z=10, v_H=9.75 x 10^{-6} $m^3 mole^{-1}$)

	Ethanol			Water		
T(K)	ϵ_{11}	v^*	$2v_H a/z$	ϵ_{11}	v^*	$2v_H a/z$
283	1357.59	1.20	1954.93	3596.56	0.96	3314.59
293	1355.47	1.20	1951.88	3516.20	0.97	3308.39
303	1314.34	1.22	1956.26	3438.16	0.98	3302.01
313	1294.18	1.23	1957.96	3362.54	0.96	3098.92
323	1274.90	1.24	1960.29	3289.36	0.99	3223.90
333	1256.49	1.24	1931.98	3218.53	1.00	3218.53
343	1238.87	1.25	1935.73	3150.14	1.01	3213.46
353	1222.04	1.26	1940.11	3083.99	1.02	3208.58
363	1205.89	1.27	1944.98	3020.02	1.03	3203.94
373	1190.43	1.27	1920.04	2958.16	1.04	3199.55
393	1161.42	1.29	1932.72	2840.43	1.06	3191.51
413	1134.68	1.30	1917.61	2730.13	1.08	3184.42
433	1109.83	1.31	1904.58	2626.57	1.10	3178.15

ϵ_{11} is in units of J/mole, v^* in units of cm^3 g^{-1}, and *a* in units of $Jm^3(mole)^{-2}$.

der Waals repulsion term [= RT/(v-b), where b plays the same role as v^* in Eq.(3.15)] around $\tilde{\rho}$=0, after defining $\tilde{\rho}$= 2b/v, we obtain,

$$Z_R = [v/v-b] = 1 + \tilde{\rho}/2 + \tilde{\rho}^2/4 \cdot 2! + \cdots\cdots \qquad (3.32)$$

On comparing Eqs.(3.31) and (3.32) we see that the repulsion terms in the low-density range ($\tilde{\rho} \simeq 0$) are identical. Differences do appear at high densities, however; they are caused by the presence of the logarithmic functionality in this lattice-model's repulsive term. In summary, therefore, the lattice EOS behaves similar to the van der Waals EOS at low densities in the case of small molecules.

At very low densities, ($\tilde{\rho} << 1$), we can show by expanding the two logarithmic terms in Eq(3.15a), that we recover the ideal gas limit i.e.,

$$P(rv)/RT \longrightarrow 1, \quad \text{as } \rho \longrightarrow 0 \qquad (3.33)$$

where (rv) defines the molar volume of a solute with r segments.

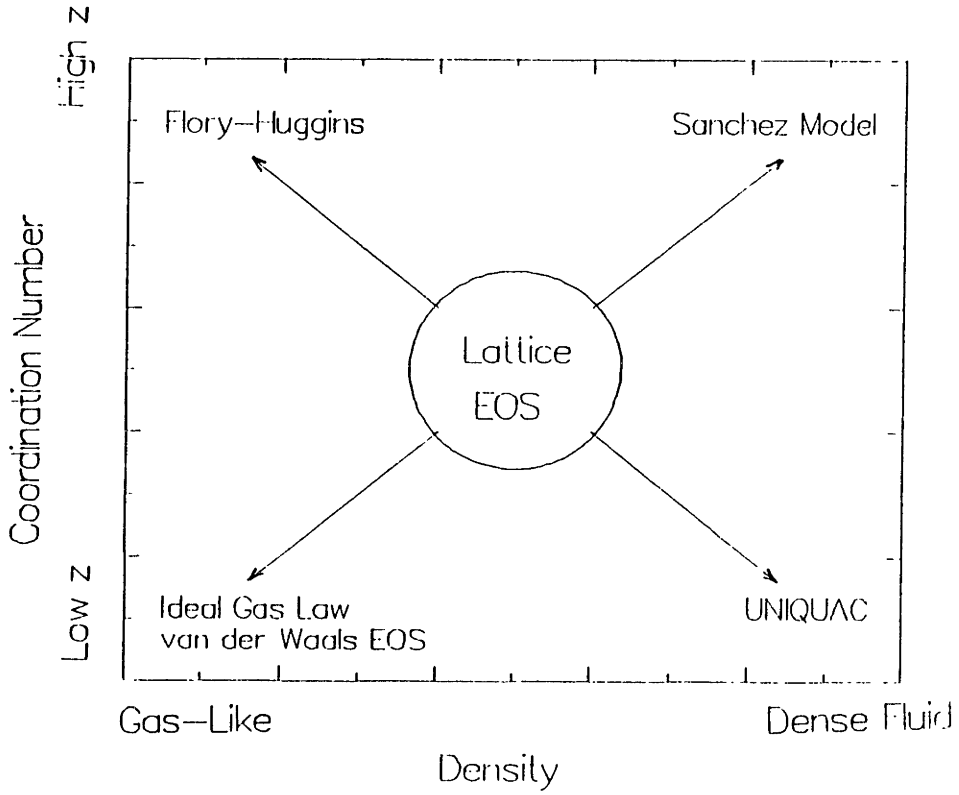

Figure 3.1: A schematic representation of the position of the lattice EOS relative to existing techniques.

From the above discussion it is clear that the EOS in Eq.(3.15) is a simple extension of well known EOS (van der Waals, 1873; Flory, 1941, 1942; Huggins, 1941, 1942; Sanchez and Lacombe, 1976, 1977; Okada and Nose, 1981a, 1981b; Panayiotou and Vera, 1982). It reduces in some limits to well known EOS both for polymer molecule and small molecule EOS (Figure 3.1) thus suggesting that it has the correct functional form for applications to systems of interest. (The lattice EOS may be used to yield a UNIQUAC type activity coefficient model for multicomponent mixtures as shown in Figure 3.1; this will be discussed in Section 3.3.2.) It also has the merit that it has only two adjustable parameters per pure component. It is expected that the physical realism built into this EOS will allow for reliable fits to experimental data using a minimum number of adjustable parameters, when it is extended to mixtures.

3.3 MIXTURES

3.3.1 Theoretical Development

Consider a mixture of N_0 holes and N_i molecules of type i (i=1,n), placed on a lattice having the same values of the coordination number (z) and the cell size (v_H) as the pure component lattices. Molecules of type i (i=1,n) have r_i segments and interact with nearest-neighbour segments of molecules j with an interaction energy $-\epsilon_{ij}$ (with $\epsilon_{0j}=0$, for all j). Pairwise additivity of interaction energies is assumed. The canonical partition function for this ensemble can be formally represented as in Eq.(3.5). We again make the mean-field approximation and write,

$$\Omega_c \propto [\Pi\lambda_i^{N_i}]\ g(N_0,\{N_i\},\{r_i\},z,\{\epsilon_{ij}\})\ \exp[-\beta E(N_0,\{N_i\},\{r_i\},z,\{\epsilon_{ij}\})] \quad (3.34)$$

where Eq.(3.34) is analogous to Eq.(3.6) and the braces, {}, denote the sets of all values of the enclosed symbol. The λ_i-factors, accounting for the internal degrees of freedom in the chains, are again assumed to be functions of temperature only. $E(N_0,\{N_i\},\{r_i\},z,\{\epsilon_{ij}\})$ represents the total potential energy of the system. To be consistent with the pure component EOS, in the following derivation, we assume that holes mix randomly.[6] Molecular segments, however, are allowed to mix non-randomly, and the partition function, therefore, has to incorporate terms that account for this effect. For convenience we can rewrite Eq.(3.34) in the form,

$$\Omega_c \propto \Pi\lambda_i^{N_i}\ g_R(N_0,\{N_i\},\{r_i\},z,\{\epsilon_{ij}\})\ g_{NR}(N_0,\{N_i\},\{r_i\},z,\{\epsilon_{ij}\})\exp[-\beta E(N_0,\{N_i\},\{r_i\},z,\{\epsilon_{ij}\})] \quad (3.35)$$

---

[6] The extension to the case where holes mix non-randomly is simple, in principle. For pure components, this has been done by Panayiotou and Vera (1982).

where g_R represents the number of configurations in a case where molecules mix randomly, and g_{NR} is a factor that corrects the combinatorial term for the effects of the non-random distribution of molecules.[7] We separate the random and the non-random contributions to g into a product, assuming that the effect of non-randomness on the number of configurations are small, i.e., we assume that g_{NR} is a small perturbation about the random value of 1. g_R can be represented, following Guggenheim (1954), as

$$g_R = \frac{(N_0 + \sum r_i N_i)!}{N_0! \ \Pi N_i!} \left[\frac{(N_0 + \sum N_i q_i)!}{(N_0 + \sum N_i r_i)!} \right]^{z/2} \tag{3.36}$$

while g_{NR} is represented following Panayiotou and Vera (1982) as,

$$g_{NR} = \frac{\Pi \bar{N}^0_{ii}! \ \ \Pi[(\bar{N}^0_{ij}/2)!]}{\Pi \bar{N}_{ii}! \ \ \Pi[(\bar{N}_{ij}/2)!]^2} \tag{3.37}$$

where

$$\bar{N}^0_{ij} = N^0_{ij}/\vartheta = (z/2)(N_i q_i)\bar{\vartheta}_i \quad (i=j) \tag{3.38a}$$

$$= 2(z/2)(N_i q_i)\bar{\vartheta}_j \quad (i \neq j) \tag{3.38b}$$

Here $\bar{N}^0_{ij}$ represents the number of i-j segment contacts on a "hole free" basis, in the case where all molecular segments mix randomly and N_{ij} are the number of i-j contacts in the non-random case.[7] $\bar{\vartheta}_i$, is area fraction of species i in the lattice on a hole-free basis,

---

[7] It must be emphasised, that, in all cases, summation indices (i,j,k,l) go from 1 to n, the number of components. If holes were assume to mix non-randomly, then the indices would go from 0 to n, where 0 would then refer to holes.

$$\bar{\vartheta}_i = \frac{N_i q_i}{\sum N_j q_j} \tag{3.38c}$$

We introduce the nonrandomness correction, Γ_{ij}, for the distribution of the segments of species i about the segments of species j. It is defined by the equation,

$$\bar{N}_{ij} = \bar{N}^0_{ij}\ \Gamma_{ij} \tag{3.39}$$

where the $\bar{N}_{ij}$'s must satisfy the mass balance constraints (Panayiotou and Vera, 1981),

$$\bar{N}_{ii} + \sum_j \bar{N}_{ij} = N_i z q_i \ , \qquad \text{for all i} \tag{3.40}$$

Since all the unlike interactions N_{ij} $(i\neq j)$ must equal N_{ji},

$$\Gamma_{ij} = \Gamma_{ji} \ , \ i\neq j \tag{3.41}$$

The potential energy of the system, $E(N_0,(N_i),(r_i),z,(\epsilon_{ij}))$, under the assumption of the pairwise additivity of interaction energies is,

$$E = \vartheta \sum\sum \bar{N}_{ij}(-\epsilon_{ij}) \tag{3.42}$$

where ϑ represents the total surface area fraction of the lattice occupied by molecular segments $[= \sum N_i q_i/(N_0+\sum N_i q_i)]$. To determine the non-randomness corrections, therefore, we must substitute Eqs.(3.36)-(3.42) in Eq.(3.35) and maximize Ω_c with respect to all the Γ_{ij}'s $(i\neq j)$. [The remaining Γ_{ij}'s $(i=j)$, can then be determined from the mass balance constraint, Eq.(3.40).] The resulting equations are also known as the quasi-chemical equations (Guggenheim, 1954) and can be represented, following the notation of Abusleme and Vera (1986), as,

$$\Gamma_{ij}^2 = \Gamma_{ii}\ \Gamma_{jj}\ \exp(\vartheta\Delta\epsilon_{ij}/k_BT), \quad i\neq j \tag{3.43a}$$

$$= \Gamma_{ii}\ \Gamma_{jj}\ \xi_{ij} \tag{3.43b}$$

where

$$\Delta\epsilon_{ij} = (\epsilon_{ii} + \epsilon_{jj} - 2\epsilon_{ij}) \tag{3.44}$$

For a multicomponent system, the resulting equations are a coupled set of quadratic equations. Clearly, these allow for an analytically closed form solution only in the case of a two-component system. However, if it is recognized that a value of ξ_{ij} different from unity represents a departure from randomness then we can expand Eq.(3.43a) as a multi-dimensional Taylor series in terms of the small parameters $(\xi_{ij}-1)$ $(i\neq j)$. The general first order solution to the equation set [Eq.(3.43a)] is,

$$\Gamma_{ij} = 1 + (1-\xi_{ij})/2 + (1/2)\sum\sum(1-\xi_{\ell m})\bar{\vartheta}_\ell\bar{\vartheta}_m - (1/2)\sum(1-\xi_{im})\bar{\vartheta}_m - (1/2)\sum(1-\xi_{mj})\bar{\vartheta}_m \tag{3.45}$$

where $\bar{\vartheta}_i$ is the surface area fraction of the segments of i molecules, on a hole free basis $(\equiv N_i q_i/\sum N_i q_i)$. This approximate solution to the quasi-chemical equations has been tested against exact numerical solutions and it was found that it is within 5% over most of the ranges tested for 3 and 4 component systems. Higher order solutions for these equations exist in the literature (Mickeleit and Lacmann, 1983) and these can be used if greater accuracy is desired.

On using Eq.(3.45) in the equation for the total energy of the system [Eq.(3.42)] one obtains,

$$E = -(z/2)[\sum N_i q_i]\vartheta\{\sum\sum\bar{\vartheta}_j\bar{\vartheta}_k\epsilon_{jk} + (1/2)\sum\sum\sum\sum\bar{\vartheta}_j\bar{\vartheta}_k\bar{\vartheta}_\ell\bar{\vartheta}_m\ \epsilon_{jk}\ (\xi_{km}+\xi_{jm}-\xi_{\ell m}-\xi_{jk})\} \tag{3.46}$$

We now define the mixing rule for the mixture parameter ϵ_M, in terms of

the pure component parameters,

$$\epsilon_M = (-E)/(\vartheta\ (z/2)[\sum N_i q_i]) \tag{3.47}$$

$$= [\sum\sum \bar{\vartheta}_j \bar{\vartheta}_k \epsilon_{jk} + (1/2)\ \sum\sum\sum\sum \bar{\vartheta}_j \bar{\vartheta}_k \bar{\vartheta}_\ell \bar{\vartheta}_m\ \epsilon_{jk}\ (\xi_{km} + \xi_{jm} - \xi_{\ell m} - \xi_{jk})] \tag{3.48}$$

Mixing rules for q_M, r_M and v_M^* are defined as,

$$q_M = \sum q_i\ x_i \tag{3.49}$$

$$r_M = \sum r_i\ x_i \tag{3.50}$$

$$v_M^* = \sum v_i^*\ x_i \tag{3.51}$$

where x_i is the mole fraction of component i in the relevant phase. The only unknown quantities in the set of equations (3.47)-(3.51) are the "unlike segment" interaction energies, ϵ_{ij}. A suitable combining rule for this parameter is suggested by Eq.(3.44),

$$\epsilon_{ij} = \epsilon_{ii} \qquad ,i=j \tag{3.52}$$

$$= 0.5(\epsilon_{ii}+\epsilon_{jj})(1-\delta_{ij}),\ i\neq j$$

δ_{ij}, is thus a measure of the departure of the mixture from randomness, i.e., when δ_{ij}'s are zero the mixture is random since the appropriate ξ_{ij} is then identically equal to unity.

The mixture EOS and related thermodynamic quantities can now be derived by the use of techniques presented earlier [Eqs(3.12) and (3.18)]. Reducing parameters for this derivation are defined in a manner analogous to Eq.(3.14) and the system volume defined as in Eq.(3.13).

$$(z/2)\epsilon_M = RT^* = P^* v_H \tag{3.53}$$

$$\underline{V} = (N_0 + \sum N_i r_i) v_H \tag{3.54}$$

We present here the final expressions for the EOS and the chemical potentials of a component i in the mixture,

$$\frac{\tilde{P}}{\tilde{T}} = \ell n\left[\frac{\tilde{v}}{\tilde{v}-1}\right] + \frac{z}{2}\ell n\left[\frac{\tilde{v}+(q_1/r_1)-1}{\tilde{v}}\right] - \frac{\vartheta^2}{\tilde{T}} + \frac{\vartheta^3}{2\tilde{T}\epsilon_M}\left[\sum\sum\sum\sum\tilde{\vartheta}_i\tilde{\vartheta}_j\tilde{\vartheta}_k\tilde{\vartheta}_l\right.$$

$$\left.\times(\xi_{ij}\Delta\epsilon_{ij}+\xi_{k\ell}\Delta\epsilon_{kl}-\xi_{kj}\Delta\epsilon_{kj}-\xi_{ik}\Delta\epsilon_{ik})/k_BT\right] - (z/8)\vartheta^2\sum\sum\sum\sum\tilde{\vartheta}_i\tilde{\vartheta}_j\tilde{\vartheta}_k\tilde{\vartheta}_l\times$$

$$[\xi_{ij}\Delta\epsilon_{ij}(2\xi_{j\ell}-\xi_{ij}-\xi_{k\ell})+(1-\xi_{ij})(2\xi_{i\ell}\Delta\epsilon_{il}-\xi_{ij}\Delta\epsilon_{ij}-\xi_{k\ell}\Delta\epsilon_{k\ell})]/k_BT \tag{3.55}$$

$$-\frac{\mu_i}{k_BT} = \gamma_i(T) + \left[\frac{r_i\tilde{P}}{\tilde{T}}\right] + \ell nq_i - \ell n\vartheta\vartheta_i - r_i(1-z/2)\,\ell n\,\frac{\tilde{v}+(q_M/r_M)-1}{\tilde{v}}$$

$$-\frac{q_i\vartheta^2}{\tilde{T}} + \frac{q_i\vartheta}{\tilde{T}\epsilon_M}\left[\sum 2\tilde{\vartheta}_j\epsilon_{ij} - \sum 2\tilde{\vartheta}_j\tilde{\vartheta}_k\tilde{\vartheta}_\ell\tilde{\vartheta}_m\epsilon_{jk}(\xi_{km}+\xi_{jm}-\xi_{\ell m}-\xi_{jk}) + \sum\sum\sum\tilde{\vartheta}_j\tilde{\vartheta}_k\tilde{\vartheta}_l\times\right.$$

$$\{\epsilon_{jk}\times(\xi_{ki}+\xi_{ji}+\xi_{k\ell}+\xi_{jl}-2\xi_{i\ell}-2\xi_{jk}) + \epsilon_{ji}\times(\xi_{ik}+\xi_{jk}-\xi_{\ell k}-\xi_{ji}) + \epsilon_{ki}\times(\xi_{kj}+\xi_{ij}-\xi_{\ell j}-$$

$$\left.\xi_{ki}) + \vartheta(1-\vartheta)\sum\sum\sum\sum\tilde{\vartheta}_j\tilde{\vartheta}_k\tilde{\vartheta}_\ell\tilde{\vartheta}_m\epsilon_{jk}(\xi_{km}\Delta\epsilon_{km}+\xi_{jm}\Delta\epsilon_{jm}-\xi_{\ell m}\Delta\epsilon_{\ell m}-\xi_{jk}\Delta\epsilon_{jk})/k_BT\right]$$

$$+(z/8)q_i\times\sum\sum\sum\sum\sum\tilde{\vartheta}_j\tilde{\vartheta}_k\tilde{\vartheta}_\ell\tilde{\vartheta}_m\{(1-\xi_{jk})(4\xi_{jm}-2\xi_{jk}-3\xi_{\ell m}+\xi_{im}-2\xi_{ji}-\xi_{\ell i}) - (1-\xi_{ik})\times$$

$$(2\xi_{im}-\xi_{ik}-\xi_{\ell m}) - (1-\xi_{ji})(2\xi_{jm}-\xi_{jk}-\xi_{\ell m})\} + (z/8)q_i\vartheta(1-\vartheta)\sum\sum\sum\sum\tilde{\vartheta}_j\tilde{\vartheta}_k\tilde{\vartheta}_\ell\tilde{\vartheta}_m/k_BT\times$$

$$(\xi_{jk}\Delta\epsilon_{jk}(2\xi_{jm}-\xi_{jk}-\xi_{\ell m})-(1-\xi_{jk})(2\xi_{jm}\Delta\epsilon_{jm}-\xi_{jk}\Delta\epsilon_{jk}-\xi_{\ell m}\Delta\epsilon_{\ell m})\} \tag{3.56}$$

The first three terms in the mixture EOS are identical to the terms in the pure component EOS [Eq.(3.15)]. The additional terms in Eq.(3.55) account for the non-random distribution of molecule segments. In Eq.(3.56), $\gamma_i(T)$ is a temperature dependent function [same as the $\gamma(T)$ for the appropriate pure component i in Eq.(3.19)], and the last two terms account for the non-random distribution of molecular segments.

For all binary mixtures examined, simpler forms of Eqs.(3.55) and (3.56) may be used with little loss of accuracy. For example, in Eq(3.55), for all binary mixtures tested, it was found that the 4^{th} and 5^{th} terms which represent the contributions of the non-randomness terms, are always 4 orders of magnitude smaller than the first three terms. These last two terms in Eq(3.55) may thus be neglected. This approximation, shown below, has been tested for binary mixtures only, however, and may not be sufficiently accurate for mixtures with more than two components.

$$\frac{\tilde{P}}{\tilde{T}} = \ell n\left[\frac{\tilde{v}}{\tilde{v}-1}\right] + \frac{z}{2}\ell n\left[\frac{\tilde{v}+(q_1/r_1)-1}{\tilde{v}}\right] - \frac{\vartheta^2}{\tilde{T}} \qquad (3.57)$$

$$-\frac{\mu_i}{k_B T} = \gamma_i(T) + \left[\frac{r_i\tilde{P}}{\tilde{T}}\right] + \ell n q_i - \ell n(\vartheta\tilde{\vartheta}_i) - r_i(1-z/2)\,\ell n\,\frac{\tilde{v}+(q_M/r_M)-1}{\tilde{v}}$$

$$-\frac{q_i\vartheta^2}{\tilde{T}} + \frac{q_i\vartheta}{\tilde{T}\epsilon_M}\left[\sum 2\tilde{\vartheta}_j\epsilon_{ij} - \sum\sum\sum\sum 2\tilde{\vartheta}_j\tilde{\vartheta}_k\tilde{\vartheta}_\ell\tilde{\vartheta}_m\epsilon_{jk}(\xi_{km}+\xi_{jm}-\xi_{\ell m}-\xi_{jk})\right] \qquad (3.58)$$

It is to be noted that the simplified mixture EOS [Eq(3.57)] has exactly the same functional form as the pure component EOS [Eq(3.15)], but that Eq (3.58) is slightly different from Eq (3.16). Panayiotou and Vera's EOS for

binary mixtures is identical to Eq (3.57) although they state that they had explicitly accounted for the non-random distribution of molecular segments. An approximation must thus have been made by Panayiotou and Vera for them to have obtained the same formal expression for both the pure component and binary mixture EOS.

3.3.2 Discussion

The chemical potential expression for individual species in a multicomponent mixture has been presented in Eq.(3.56). If we were to consider the high-density limit (i.e., essentially no holes in the lattice) and derive activity coefficients from this chemical potential functionality we would obtain a functional form similar to UNIQUAC (Abrams and Prausnitz, 1975). The main differences in our formulation and the one of Abrams and Prausnitz are:

1. The UNIQUAC equation has been derived by employing the Staverman (1950) expression for the combinatorial term, developed for mixtures of molecules of arbitrary sizes and shape. This factor is similar to the one employed in our derivation, but does not explicitly account for the coordination number z.
2. Pure component EOS have not been derived in the development of UNIQUAC; instead, only activity coefficient expressions for components in a binary or higher mixture have been presented. The UNIQUAC equation, therefore, does not lend itself to be readily applied to mixtures with supercritical components.

However, the more relevant observation is the fundamental similarity of the lattice EOS and the UNIQUAC formulation, which is highlighted by the increasing use of UNIQUAC-type activity coefficient expressions in group-contribution schemes like UNIFAC (See Reid et al., 1977 and appropriate references therein.) A problem frequently encountered in the application of UNIFAC schemes is the non-availability of an EOS that is thermodynamically

consistent with the activity coefficients of mixture components. One potentially promising route to improve on existing techniques, therefore, will be to employ these same group contribution methods to the lattice EOS, which may then be employed as a *predictive* tool for the correlation of the multi-phase behaviour of complex mixtures at supercritical temperatures (where UNIQUAC is not appropriate) and elevated pressures.

3.3.3 Implementation Aspects

The expressions derived for the mixture EOS and the chemical potential of component i in a multi-component mixture were used to model the phase equilibria of binary mixtures. A set of non-linear equations were obtained;

$$\mu_i^s = \mu_i^t \quad \text{at constant T,P} \tag{3.59}$$

Eq (3.59) is valid for all components i across all phases s and t. These equations were solved by the use of Newton's method to yield the equilibrium phase compositions. In the solution of the equation set (3.59) we must also solve the EOS to obtain the phase molar volumes.

The algorithm used, therefore, was an imbedded Newton's method, with the internal loop utilized to solve the EOS for volume and the external loop for the convergence of the mole (or mass) fractions of the different species. Some relevant aspects of the solution procedure are:

- To ensure that the solution vector of mixture compositions ($0 \leq x_i \leq 1$, for all i) did not stray into infeasible regions, each element in the open set (0,1) was mapped into a $(-\infty,\infty)$ set. The one-to-one mapping employed was,

$$\psi_i = \tan[(x_i - 0.5) \times \pi) \tag{3.60}$$

- For subcritical temperatures, it was found that the solution of

EOS for volume had a familiar van der Waals type shape, with only three real roots. This fact, which is not apparent from the complex functional form of the EOS, allows for a relatively easy search for phase volumes.

The computer programs used in the solution of the phase equilibrium problem were written in standard FORTRAN 77 and are described in Appendix III.

3.3.4 Results and Discussion

The capability of the lattice EOS to fit experimental VLE data for mixture of molecules was examined next. Mixtures of small molecules (acetone-benzene, ethanol-water) were considered first. In Figures 3.2 and 3.3 a comparison is made between the fitted and experimental low-pressure VLE data for these systems (Weisphart,1975; Pemberton and Mash, 1978). An excellent fit to the data is obtained in both cases, with the use of one binary parameter (δ_{ij}).

The interesting aspect of this modelling is the temperature independence of δ_{ij}. It has been shown above that, for pure components consisting of small molecules, the lattice EOS has an attractive term with an essentially temperature independent "van der Waals" parameter, a. Extending this argument to mixtures results in the prediction of the temperature independence of δ_{ij} for binary mixtures of small molecules.

In examining the sensitivity of the model to the assumed value of z, it was found that, for the ethanol-water system, the model results were insensitive to z values in the vicinity of z=10 (i.e., for $4 < z < 15$). For unrealistic values of z ($z > 15$), however, the model was incapable of even qualitatively fitting mixture VLE behaviour. It is speculated that the reason for the failure of the model in the limit of large z lies in the fact that a molecular segment is presumed to have more nearest neighbours than possible even in a cubic closed packed lattice.

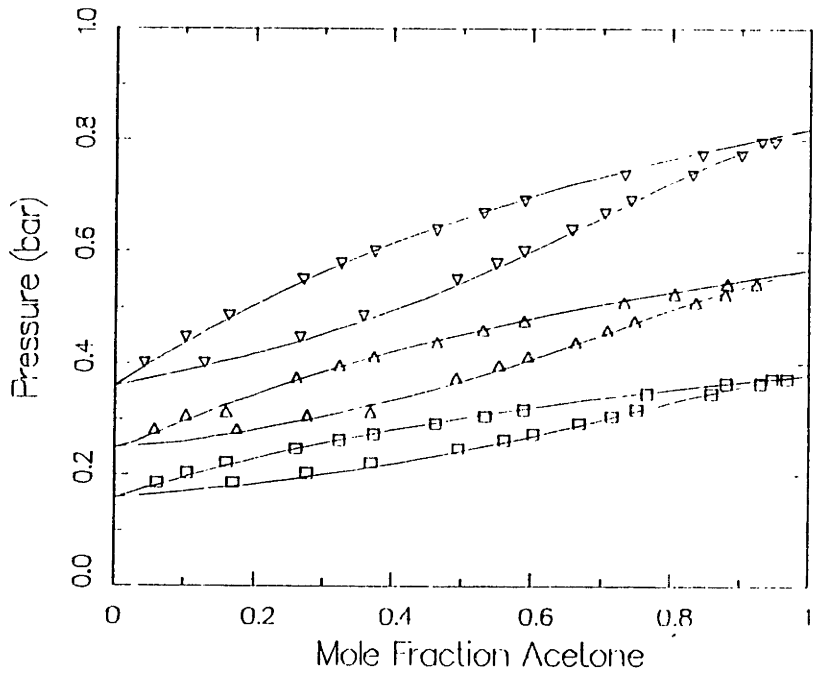

Figure 3.2: Comparison of (——) lattice model predictions and experimental data of Weisphart (1975) for the acetone-benzene binary mixture at (□) 303K, (△) 313 K, (▽) 323K with δ_{ij}=0.022.

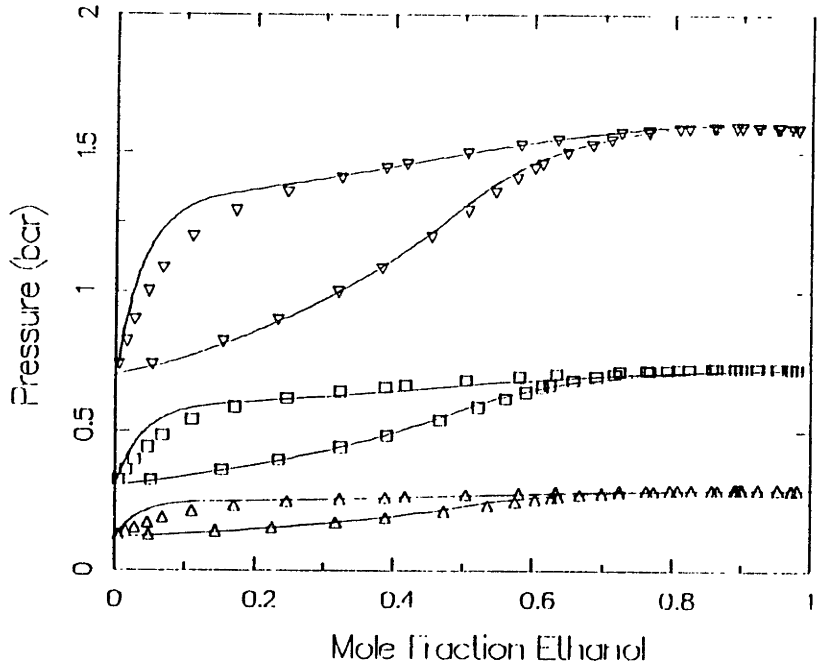

Figure 3.3: Comparison of the experimental data of Pemberton and Mash (1978) for the ethanol-water binary at (△) 323K, (□) 343K and (▽) 363K with (———) lattice model predictions with δ_{ij}=0.085.

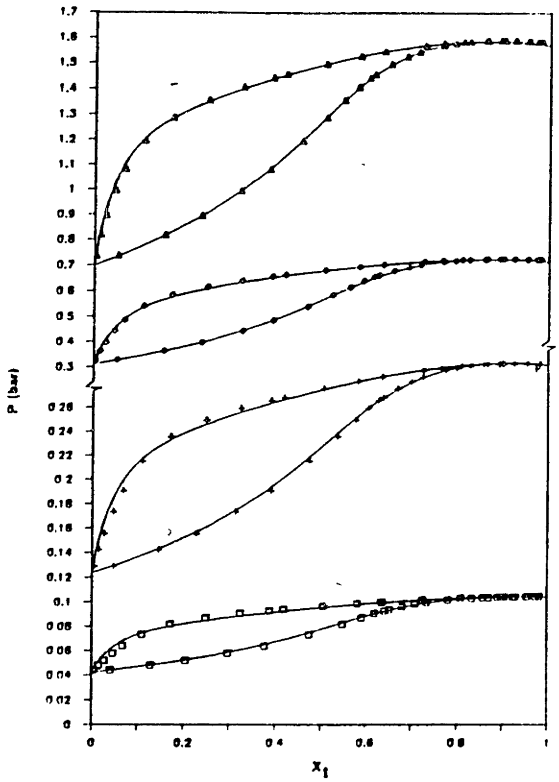

Figure 3.4: Comparison of the experimental data of Pemberton and Mash (1978) for the ethanol-water binary at (□) 303K, (+) 323K, (◊) 343K and (Δ) 363K with (———) predictions of a modified Peng-Robinson EOS (Panagiotopoulos, 1986).

In Figures 3.3 and 3.4 we compare the relative quality of fits to the experimental data for the ethanol-water system from the lattice EOS and a modified Peng-Robinson EOS (Panagiotopoulos, 1986). From visual inspection, it can be deduced that, for this system, the lattice EOS performs almost as well as the more conventional technique. The advantage of the lattice EOS is the constant value of the interaction parameter, δ_{ij}, that has been employed; in the Peng-Robinson EOS the adjustable parameter (δ_{ij}) is a temperature-dependent function.

The capability of the lattice EOS in the modelling of the VLE of mixtures of molecules of different sizes at a moderate pressure was examined next. The results for the H_2S-n-heptane system at 310 K and 352 K are shown in Figure 3.5 (Ng et al., 1980). For the temperatures considered, it is seen that there is good agreement between the correlation and the experimental data. The lattice model thus provides the capability to obtain good, quantitative fits to experimental VLE data for binary mixtures of molecules below their

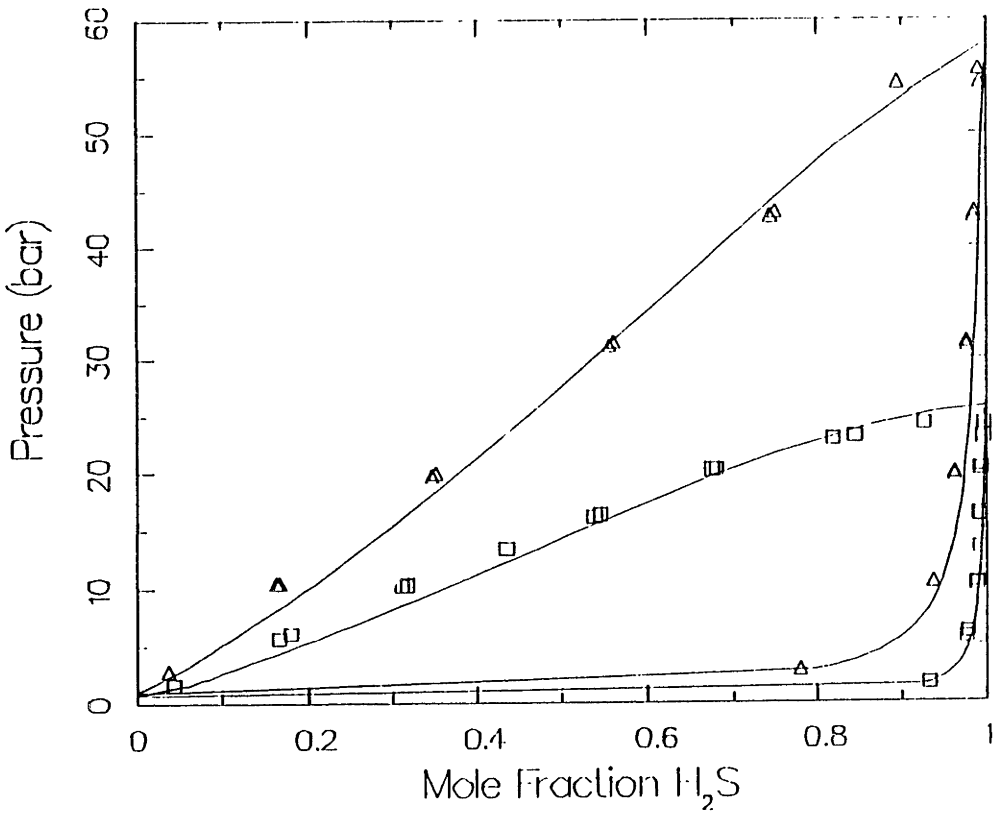

Figure 3.5: Comparison of (———) lattice model predictions and experimental data of Ng. et al. (1980), at (□) 310K and (△) 352K with δ_{ij}=0.09 for the H_2S-n-heptane system.

critical point.

The model was then applied to two-phase compositionally symmetric binaries with a supercritical component and a liquid solute. In Figure 3.6, the model calculations are compared to experimental data for the carbon dioxide-acetone system at two temperatures [313K and 333K; Katayama et al,1975; Panagiotopoulos, 1986]. A single, temperature independent binary interaction parameter was employed in the fitting of the model to data. Fits to the data are in good agreement with the measured data and correlations using the modified PR EOS (Figure 3.7 from Panagiotopoulos, 1986), outside the critical region. Since the model formulation makes use of the mean-field approximation, it is not expected to perform well in the critical region.

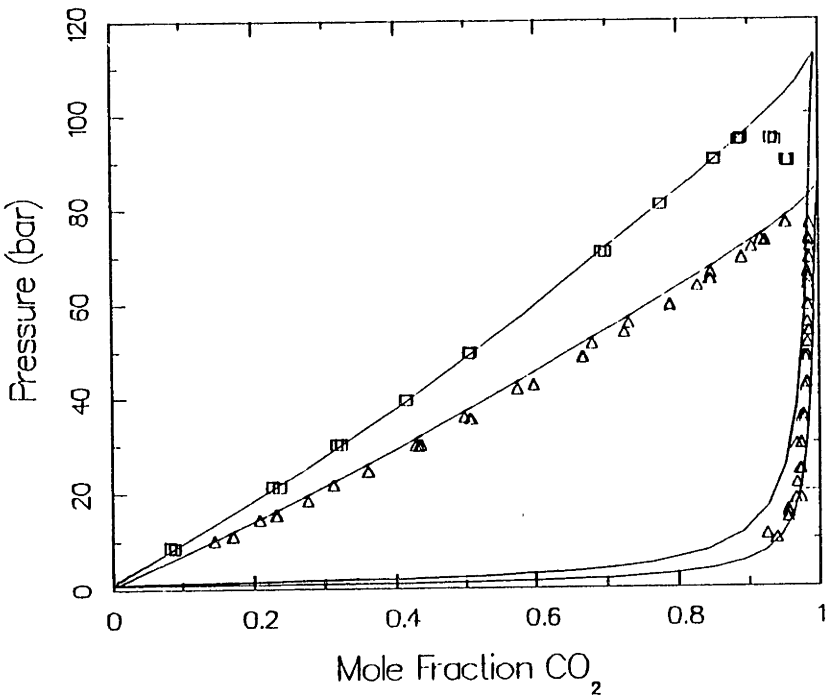

Figure 3.6: Comparison of the experimental data for the acetone-CO_2 binary at (△) 313K and (□) 333K with (——) lattice model predictions with δ_{ij}=0.0.

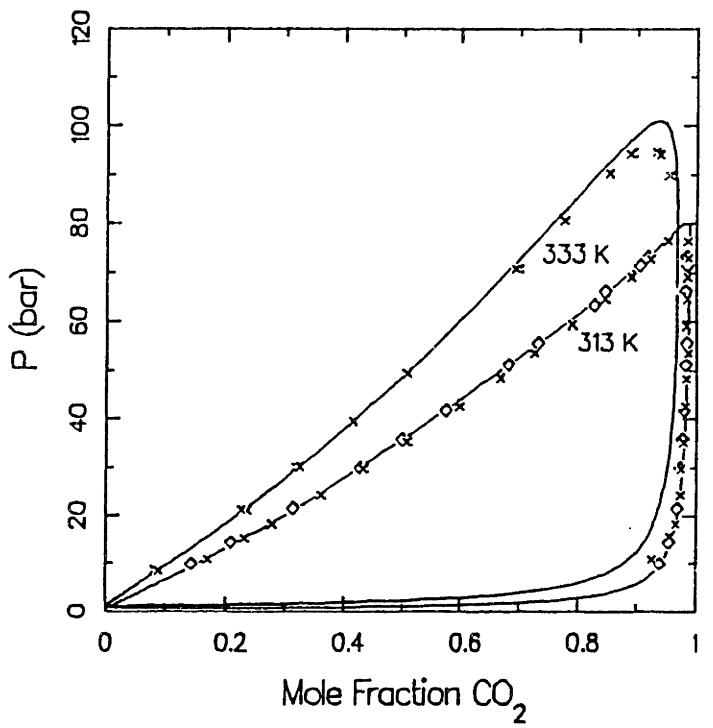

Figure 3.7: Comparison of the experimental data for the acetone-CO_2 binary to PR EOS fits. (□) are data of Katayama et al (1975) and (×) of Panagiotopoulos, 1986 (from Panagiotopoulos, 1986).

It has been suggested that a lattice model can be made to fit the behaviour of substances in the vicinity of the critical point, with the use of a "decorated lattice model" (Gilbert and Eckert, 1986). This genre of models builds the critical exponents into the problem, and thus can model the critical region with greater accuracy. For our purpose, however, the near-critical region (i.e., $|T-T_c|/T_c<0.1$, $|P-P_c|/P_c<0.1$) has not been considered.

In Figure 3.8, the model behaviour is compared to experimental data for the benzoic acid-carbon dioxide binary at three temperatures [318K, 328K and 343K, Schmitt,1984]. Since the solid benzoic acid phase is crystalline, in our modelling of this system it was therefore assumed that the solid phase was pure. (The two phases in equilibrium are therefore compositionally asymmetric). Outside the critical region, the lattice EOS provides a good fit to the

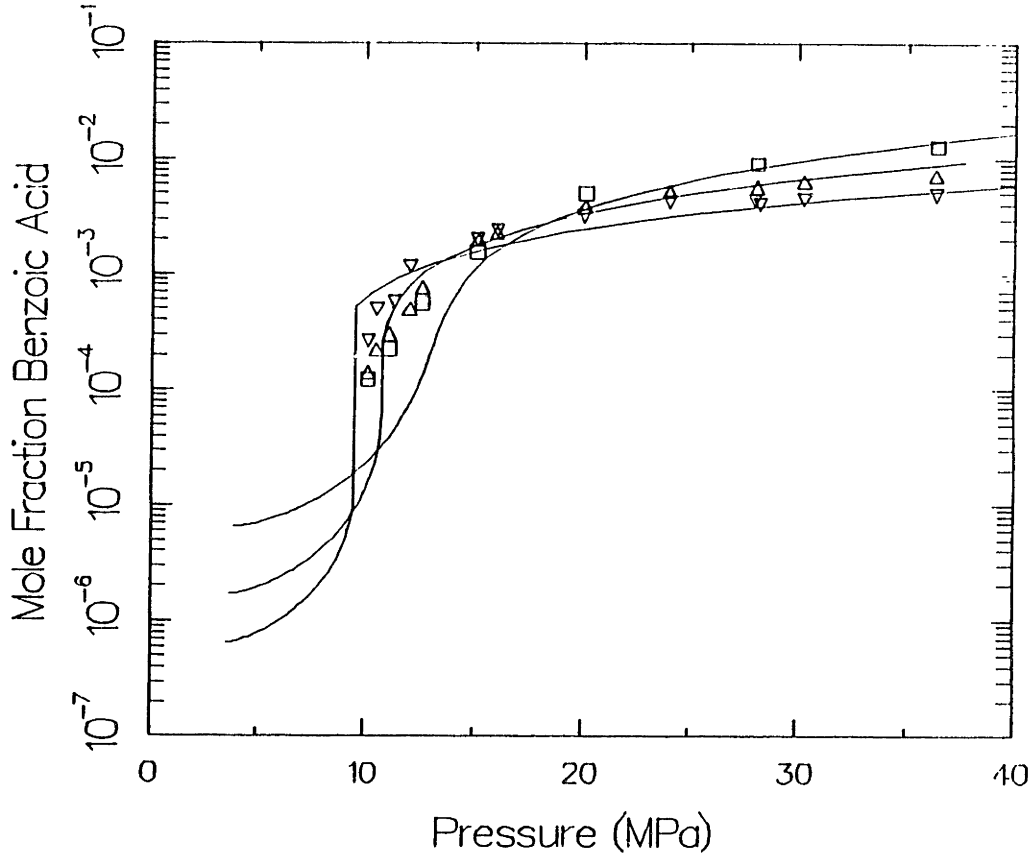

Figure 3.8: Lattice model predictions (——) compared to experimental data on the benzoic acid-CO_2 at (▽) 318K, (△) 328K and (□) 343K with δ_{ij} = 0.12 (318K), 0.10(328K) and 0.092(343K).

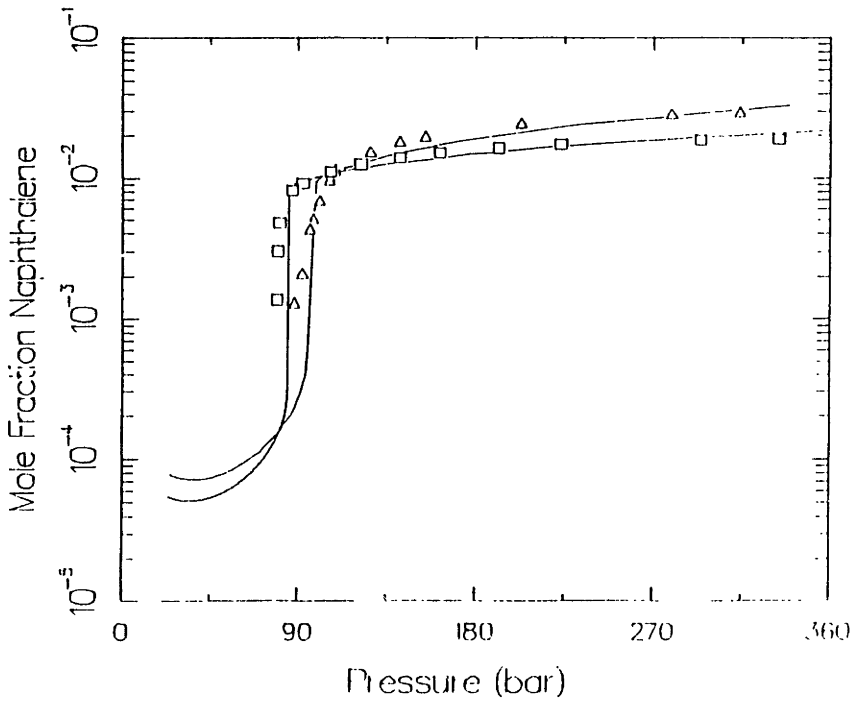

Figure 3.9: Lattice model predictions (——) at with experimental data on the naphthalene-CO_2 at (□) 318K and (△) 328K with δ_{ij} = 0.14 (318K) and 0.135(328K).

measured data. In the critical region, however, at one pressure, the equation of state predicts the presence of a three phase region. This is the cause for the discontinuity of the curves in the region of sharp rise in solubility. Similar behaviour is also observed for the naphthalene-CO_2 system (Tsekhanskaya et al., 1964; Figure 3.9) at two different temperatures.

The model also provided a good fit to the volumetric properties of other solid-supercritical systems. In Figure 3.10 and 3.11, we show plots of the solubility of acridine and anthracene respectively, in carbon dioxide as function of density at two different temperatures. The goodness of fit displayed by these plots along with Figure 3.12 and 3.13 suggests that the lattice model EOS has the correct functicnal form to reproduce the P-v properties of dilute binaries in the supercritical region.

In summary, for solid-supercritical fluid systems, the lattice model can reproduce experimental data to within experimental accuracy outside the

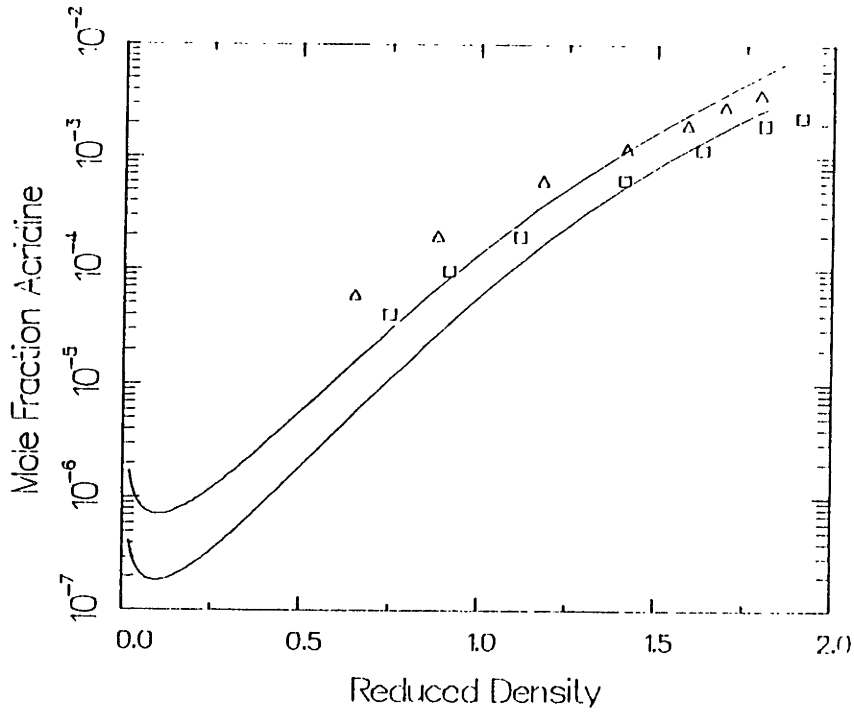

Figure 3.10: Solubility of acridine in CO_2, plotted against the reduced density of the CO_2 phase at (□) 328K and (△) 343K compared to lattice model predictions (——) with δ_{ij}=0.135. Experimental data are of Schmitt (1984).

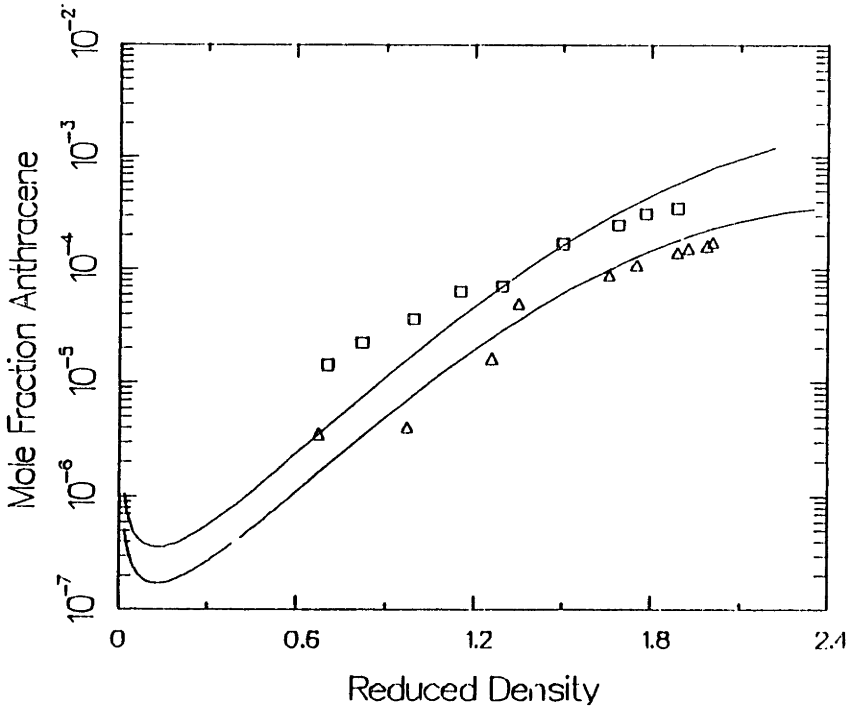

Figure 3.11: Solubility of anthracene in CO_2, plotted against the reduced density of the CO_2 phase at (△) 323K and (□) 343K compared to lattice model predictions (——) with δ_{ij}(323K)=0.22 and δ_{12}(343K)=0.19. Experimental data are of Röβling and Franck(1983).

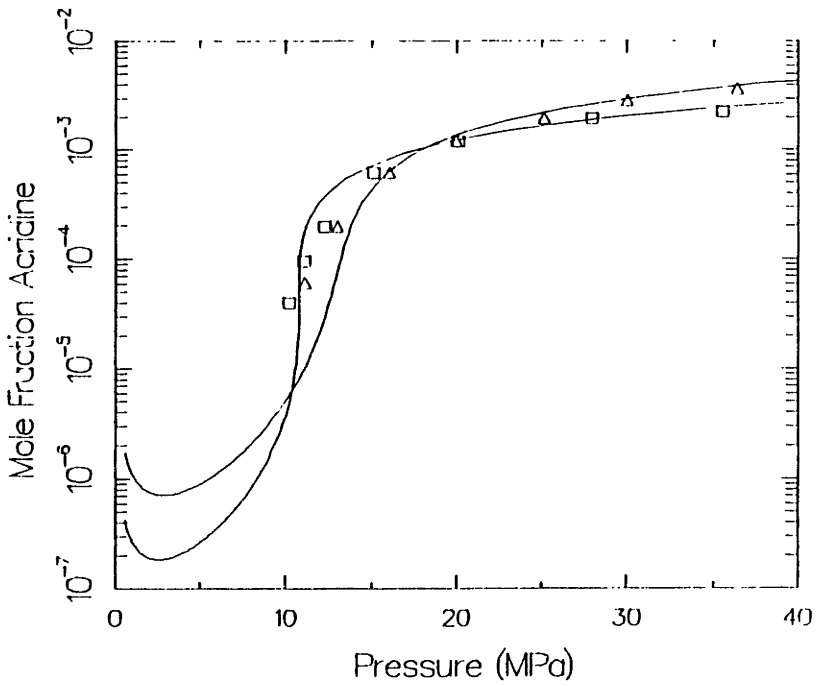

Figure 3.12: Comparison of the experimental data for the solubility of acridine in CO_2, at (□) 328K and (△) 343K with lattice model predictions (——) with δ_{ij}=0.135.

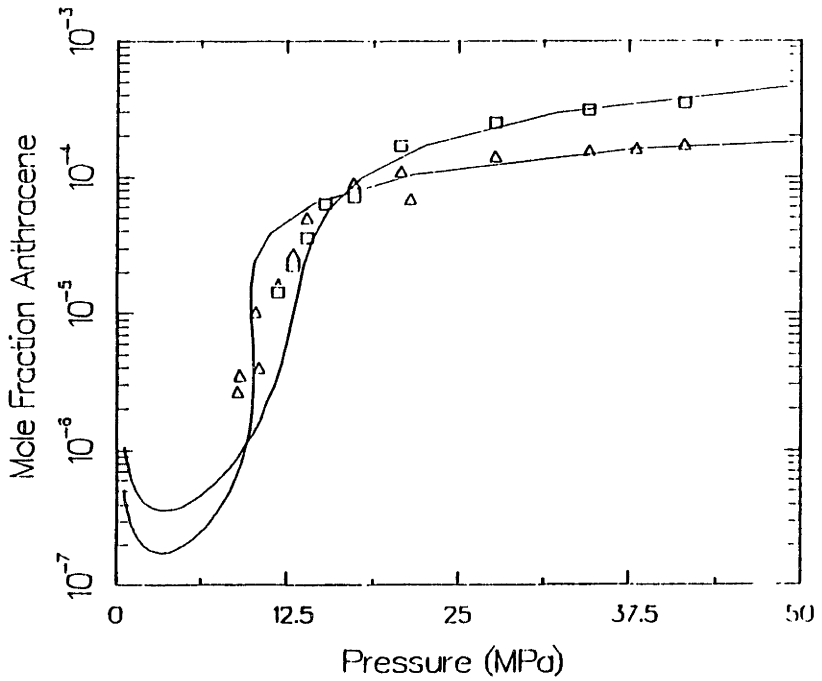

Figure 3.13: Comparison of the experimental data for the solubility of anthracene in CO_2, at (△) 323K and (□) 343K with lattice model predictions (——) with δ_{ij}(323K)=0.22 and δ_{12}(343K)=0.19.

critical region. Volumetric properties of these systems are also well predicted.

For the eight different systems examined, covering a range of pressures and phase behaviour, the capability of the lattice EOS to correlate phase equilibria for mixtures of "small" molecules is comparable to traditionally employed techniques (for example the single parameter Peng-Robinson EOS). While we do not present quantitative comparisons (as average absolute deviations or standard deviations), the point to be emphasised is the utility of the lattice EOS, developed mainly for the correlation of mixtures of molecules of disparate sizes, to model mixtures of small molecules of essentially the same size.

3.4 EXTENSION TO POLYMER-SCF SYSTEMS

Since we will be dealing with the equilibrium of polymers of a known molecular mass distribution and an SCF, we need the pure components parameters associated with each of the mixture components. Parameters for the SCF were obtained by fitting P-v data on the respective isotherms, as stated before.

Parameters for polystyrene above its glass transition temperature (~380K) are available in the existing literature (Panayiotou and Vera, 1982). These parameters were employed in our modelling in the temperature range 313-333K, with the following two assumptions:

(i) ϵ_{11} and v^* (in units of $m^3\ kg^{-1}$) were assumed independent of chain length. This assumption has been made due to lack of thermodynamic data for polymers of different chain lengths.

(ii) As the presence of compressed gases reduces the glass transition temperature of a polymer (Wang et al., 1982) we assume that polystyrene in the temperature range 313-333K, in the presence of supercritical ethane, is above its glass-transition temperature.

The validity of these assumptions will be examined in Chapter 4, when the model is employed for the correlation of experimental data for the polystyrene-

ethane system.

We now examine the predictions of the lattice EOS with respect to polymeric systems at some well known limits:

Ideal "Macromolecular" Gas Mixture: Under the assumption of an energetically non-interacting gas mixture with one small and one large component, at approximately zero pressure, one may show from Eq (3.59) that,

$$-\frac{\mu_i}{k_B T} = \gamma_i(T) + \ell n q_i - \ell n \tilde{\vartheta}_i \; (q_M/r_M)/\tilde{v} \tag{3.61}$$

wherein the definition of ϑ_i [Eq (3.38c)] has been employed. Since we have a small component in the gas-phase, we approximate q_M/r_M to unity. On using the definition of an ideal gas,

$$\tilde{P}\tilde{v}/T = 1 \tag{3.62}$$

we may reduce Eq(3.61) to the form,

$$\mu_i = \gamma'(T) + k_B T \ell n(\tilde{\vartheta}_i P/q_i) \tag{3.63}$$

which now represents the "Ideal Macromolecular Gas Limit". This should contrasted to the chemical potential definition for an ideal-gas mixture (IGM),

$$\mu_i = \gamma''(T) + k_B T \ell n(P x_i) \tag{3.64}$$

It is to be noted in this context that Eq(3.63) explicitly accounts for the difference in sizes between the component molecules with the presence of q_i (a size parameter) and ϑ_i, the surface area fraction of the component macromolecule. Also, Eq(3.63) will reduce to the ideal-gas limit [Eq(3.64)] when the two mixture components are small and of approximately the same size since ϑ_i may be replaced by x_i and q_i is approximately equal to 1.

Eq(3.63) thus redefines, in a more general fashion, the ideal gas mixture from which the conventional IGM may be deduced as a limit.

Ideal "Macromolecular" Liquid Solution: If we examine a dense phase, energetically non-interacting mixture of a small molecule and a macromolecular compound, from Eq.(3.58) we can show that,

$$\mu_i = \eta'(T,P) + k_B T \ell n \tilde{\vartheta}_i / q_i \qquad (3.65)$$

This should be contrasted to the normally employed definition of the ideal solution for mixtures of small molecules,

$$\mu_i = \eta'(T,P) + k_B T \ell n x_i \qquad (3.66)$$

Again, Eq(3.65) may be reduced to Eq(3.66) under the special assumption that the mixture components are of the same size and small. Eq(3.65) therefore represents a more general definition of an ideal solution, and is valid for mixtures of molecules of differing sizes, while Eq(3.66), the familiar expression, is valid only in special cases.

The implication of these two definitions will be the need for the reformulation of mixture thermodynamics to include mixtures of molecules of disparate sizes. In essence, we need to redefine quantities as fugacity ($\hat{f}$) and activity (a) so that polymer mixtures may be managed with the same set of operational definitions used for mixtures of small, equally-sized molecules.

CHAPTER 4

SOLUBILITY OF POLYMERS IN SUPERCRITICAL FLUIDS: MEASUREMENT, RESULTS AND DISCUSSION

4.1 EXPERIMENTAL APPARATUS

The experimental apparatus employed for the measurement of solubilities of polymer chains in SCF was a flow-through apparatus shown schematically in Figure 4.1. The main features of the setup are discussed below:

- SCF Feed: The SCF from the tank is pumped to pressure by a diaphragm compressor (Aminco, J46-13411 rated to 70 MPa) and fed into a 2 litre tank that served as a surge vessel. Pressure in the tank was maintained to ±0.5 bar with a pressure controller (Ashcroft, 0-37 MPa).

- Extraction Column: The polymer to be extracted was loaded into a 2.54 cm diameter column (Autoclave Engineers, 316 Stainless Steel) which is maintained isothermally in a water bath with a mixer-stirrer (Thermomix 1460) and at constant pressure with a pressure regulator (Matheson, Model #3064, to within ± 0.5 bar). All lines downstream of the column were maintained at the temperature of water bath to prevent precipitation of any polymer dissolved in the SCF. [This was achieved by recirculating water from the bath through jackets that surrounded the lines using a centrifugal pump (March Manufacturing, Model TE-MDX-MT-3).]

- Measurement of Temperature and Pressure: The pressure in the reactor was monitored continuously with a Heise pressure gauge with an accuracy of ±0.01 MPa (Heise gauge, 0-40MPa) and the temperature measurements were performed with iron-constantan thermocouples accurate to ±0.2K.

- Safety Considerations: The column was equipped with a rupture disk

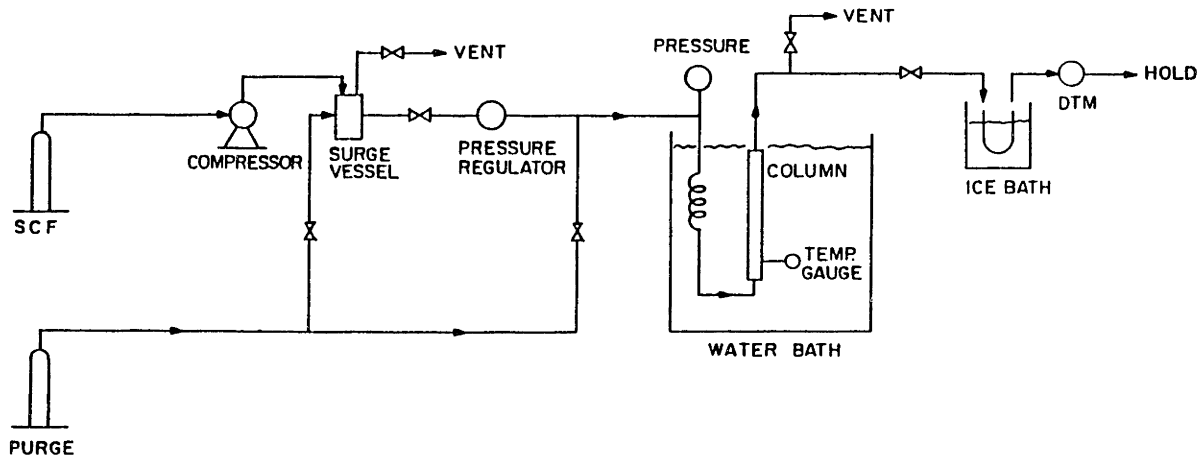

Figure 4.1: A Schematic representation of the solubility apparatus.

(Autoclave Engineers) rated at 40 MPa; this limit was less than the rating of the extraction column (50 MPa). The tubing volume was small, less than *ca.* 10% of the volume of the column. Therefore, the tubes were not specifically protected against pressure surges. Also, the holding vessel for the SCF was equipped with a rupture disk (Autoclave Engineers). All vessels were equipped with vent valves so as to ensure that the entire system could be manually vented to the hood in less than 2 min. A combustible gas detector (Sears Gas Alarm) was installed in the laboratory to warn the operator of possible leaks in the system.

- Operating Procedure: Gas from the surge tank was introduced into the bottom of the extraction column in a continuous fashion. The flow rate

of the SCF through the extraction vessel was maintained at a value (~ 1 standard liter/minute) such that the gas removed from the top of the column was in "equilibrium" with the polymer. This "loaded" SCF phase was then flashed to atmospheric pressure with a metering valve (Autoclave Engineers) which was maintained at a temperature at least 20K above the glass-transition temperature of the pure polymer to prevent "plugging". The precipitated polymer was collected in U-tubes, subsequently dissolved in a measured amount of tetrahydrofuran (E.M. Sciences, TX0282-1, Omnisolv Grade) and analyzed by Size Exclusion Chromatography (Hewlett Packard liquid chromatograph model 1090A with Waters' Ultrastyragel columns #10570, 10571 and 10572 in series) for total mass and degree of polymerization distribution (see Appendix I for the procedure employed in the chromatographic analysis). The integrated gas flow was measured with a dry-test meter (Singer, DTM 115).

- Materials Used: High purity ethane (99.9%, Matheson Gas Products), carbon dioxide (99.9%, Matheson Gas Products) and a gas mixture (87% ethane, 13% propane by mole, Matheson Gas Products) were the SCF used in the experiments. Heptane (Mallinckrodt) was also employed as a solvent in our tests. Two narrowly distributed polystyrene standards (Pressure Chemicals, M_n = 2060 g mole^{-1}, M_w/M_n~1.2 and M_n= 800 g mole^{-1}, M_w/M_n~1.25) were the polymers used in the experiments. For the chromatographic analysis, tetrahydrofuran stabilized with 20 ppm hydroquinone (E.M. Sciences, TX0282-1, Omnisolv Grade) was used.

4.2 RESULTS AND DISCUSSION

4.2.1 Results at a Single Pressure

It is the goal of this section to understand the solubility of polymers, on the basis of chain length, into an SCF phase. We begin by examining qualitative trends for the solubility of polystyrene chains in supercritical ethane. In Figure 4.2, chromatograms for an unextracted polystyrene (M_n ~2060 g mole^{-1}) and 4 extracts (each obtained successively

by contacting the initially unextracted polymer with approximately 10 standard litres of ethane at 25 MPa and 333K), are presented. There are two important trends that may be noted from this figure:

- Although the unextracted polystyrene has a narrow molecular weight distribution (with M_n~2060 g $mole^{-1}$), and hence has little of the low molecular weight oligomers, the extracts are concentrated in the low molecular weight species. This suggests that ethane under these conditions is a very selective fractionating medium for polystyrene on the basis of chain length, with the smallest oligomers being the most soluble. The concept of preferential solubility of lower molecular weight compounds from a mixture into an SCF has been used in the past to fractionate a polydisperse polymer on the basis of molecular weight (McHugh and Krukonis, 1986).

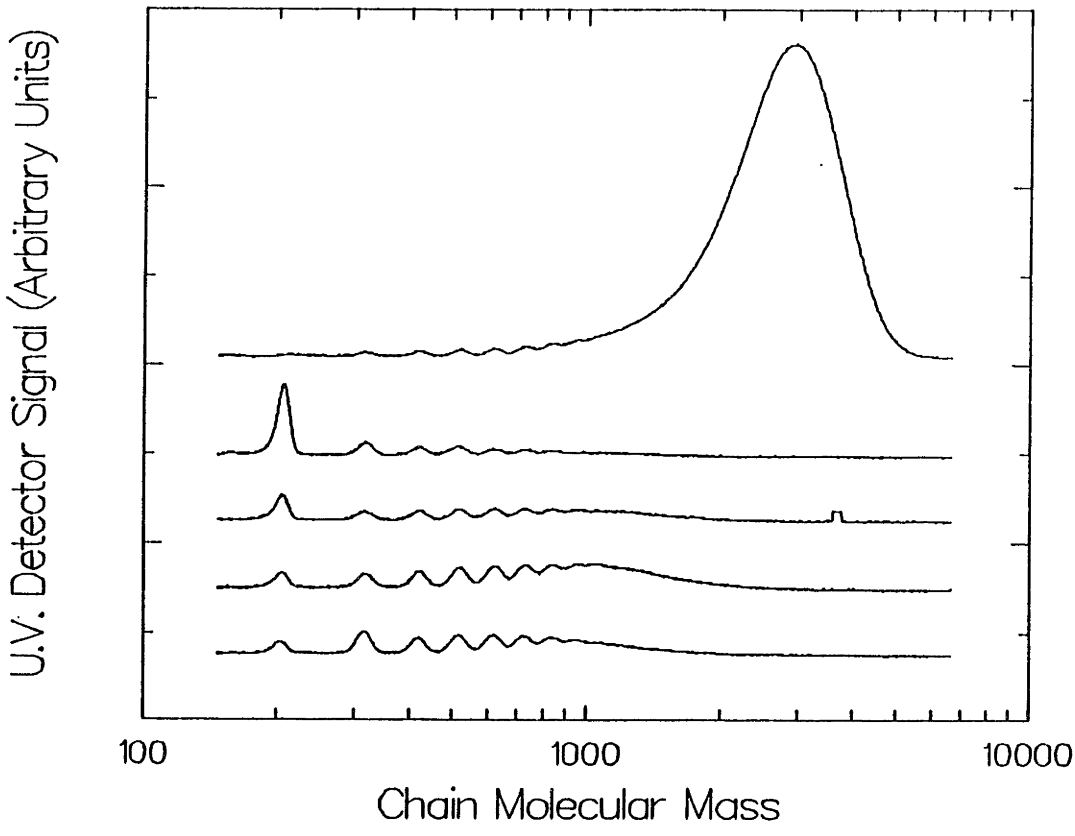

Figure 4.2: Chromatograms, (from top to bottom), for an unextracted polystyrene, and 4 successive extracts obtained by contacting the polymer with 4 × ~10 standard liters of ethane at 25 MPa and 333K.

- As one proceeds from samples 1 to 4 (the first to the last), the relative quantities of dimer are lower in each successive extract. This reduction in the relative concentration of dimer may be due to diffusional limitations in the polymer which prevent the SCF from contacting and extracting the dimer to its equilibrium value in the gas-phase (See Section 4.3.1).

In summary, therefore, qualitative trends obtained from these experiments suggest that ethane is a powerful fractionating medium for polystyrene chains on the basis of molecular mass, with the smallest oligomers being the most soluble in the SCF phase. To quantify this result we define a partition coefficient, K_i, for the distribution of a polymer of chain length i between an SCF-phase and a polymer-phase,

$$K_i = w_i^v / w_i^s \tag{4.1}$$

where w_i^v is the mass fraction of the i-mer in the solvent phase (in units of kg i-mer/kg solvent) while w_i^s is the mass fraction of the same i-mer in the SCF-free polymer phase (in units of kg mer/kg SCF-free solid). This is in contrast to K_i^{old} as defined in the current literature for the solubility of polymers in liquid solvents,

$$K_i^{old} = w_i'' / w_i' \tag{4.2}$$

where the mass fractions of the appropriate chain in both phases (with the solvent) are used to calculate the separation factor, K_i^{old}.[8]

---

[8] We employed the solid-phase compositions on a SCF-free basis in Eq(4.1) due to the difficulty encountered in the measurement of the amount of SCF dissolved in the polymer phase in our experimental setup. Since the amount of SCF dissolved in the polymer does not vary much with average molecular mass of the polymer employed (for masses >~600 g $mole^{-1}$, see Section 4.3.2) our definition of K_i, Eq (4.1), will incorporate all the essential physics regarding the solubility of polymer chains in SCF.

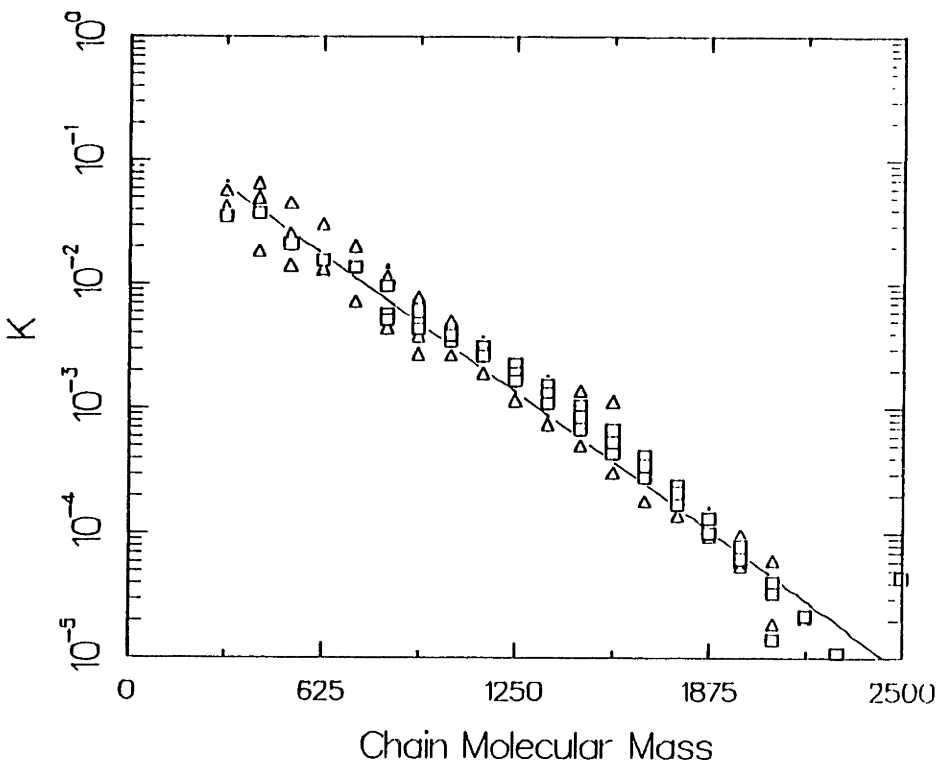

Figure 4.3: Experimental data for the partition coefficients of different styrene oligomers between a polymer-rich phase and an ethane-rich phase at 25 MPa and 333K. (□) is data obtained with a polymer of average molecular mass of 2060, and (△) from a polymer of molecular mass 800.

In Figure 4.3, then, we examine the variation of K_i with polymer chain length when a polystyrene sample is extracted with ethane at 25 MPa and 333K. The data presented were obtained from polystyrenes of M_n~ 2060 g $mole^{-1}$ (from Figure 4.2) and 800 g $mole^{-1}$. There are three important results that may be deduced from the analysis of this figure :

- The sharp, monotonic decrease of K_i with chain length observed on this graph verifies the strong fractionating ability of SCF under these operating conditions, as deduced from Figure 4.2.
- There is a log-linear dependence of the partition coefficients on molecular weight. This result along with experimental information on the behaviour of partition coefficients in liquid and liquid-like solvents [Eq(2.6) and Figure 2.1] suggest the validity of the relationship,

$$\log_{10}(K_i) = A(T) + B(T)\, X_i \qquad (4.3)$$

between K_i and the chain length of the relevant polymer, X_i, for fractionation of polymers using *liquids or SCF as extraction media*. Here A(T) and B(T) are temperature dependent constants. An important difference between our results and the information in the existing literature is that the data presented here are for individual chain lengths, while, in the past, reported results have been based on average molecular weight data only. Since Eq(4.3) and correspondingly Eq(2.6) for conventional solvents are strictly valid only on a *mer by mer* basis. Figure 4.3, to our knowledge, thus represents the first complete data for the solubility of individual polymer chains into extracting solvents.

- The measured values of K_i for the various oligomers from both the polystyrene samples fall on the same straight line. This has important connotations. First, it demonstrates that the partition coefficient of any chain from the polymer-rich phase to the supercritical phase is *independent* of the composition of the parent polymer. Figure 4.3 therefore, confirms that the observed linearity represents a general, universal behaviour for the solubility of polystyrene chains into supercritical ethane at these operating conditions. In addition, the composition-independence of K_i in Figure 4.3 implies that the equilibrium solubility of a polystyrene chain into a supercritical ethane phase occurs as if the condensed phase were an ideal solution. In essence, therefore, we are dealing with a linear combination of independent quasi-binaries of SCF with the individual chain length polymers. We shall use this important deduction as a starting point in our modelling.

In modelling the experimental data a Statistical-Mechanics based Lattice Model EOS (Chapter 3) was employed. In Figure 4.4, the experimental data presented in Figure 4.3 are compared to the results obtained from the lattice EOS for these two-phase quasi-binary systems. A single interaction parameter, δ_{ij} (=0.018), independent of chain length was employed. The model results are in good agreement with the experimental data at all

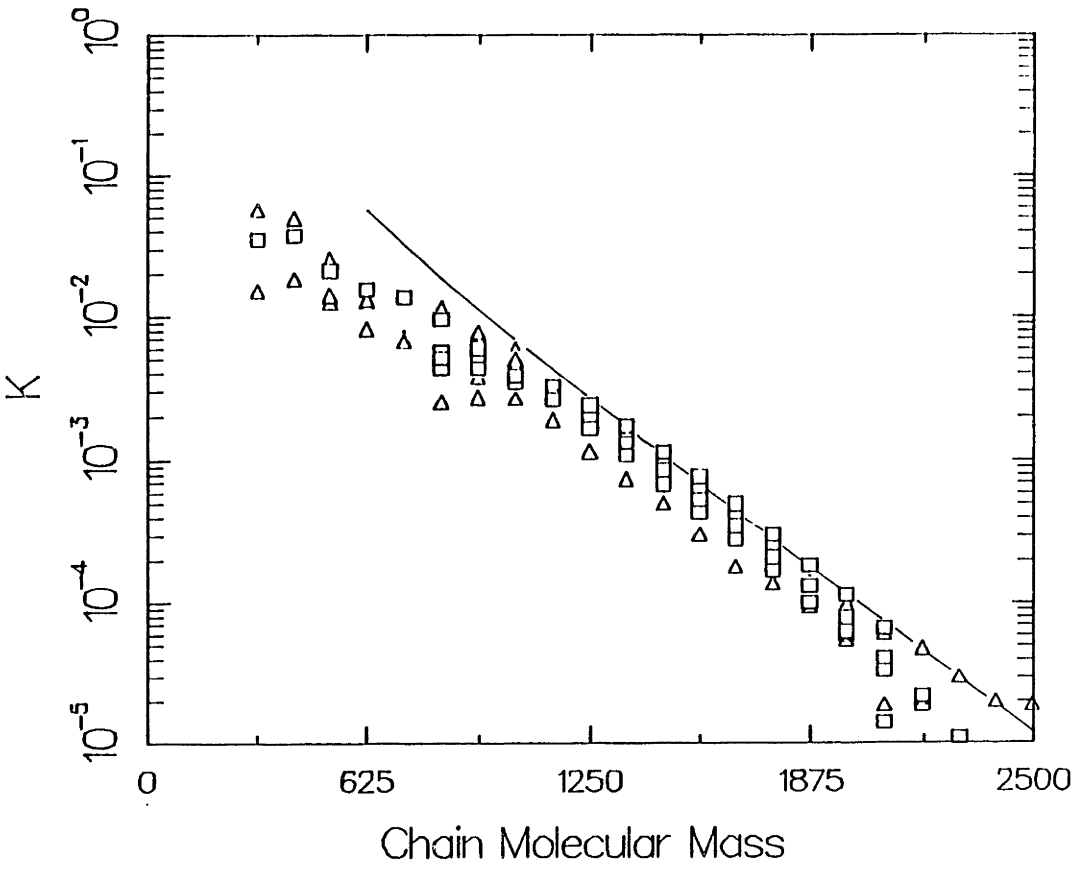

Figure 4.4: Comparison of the lattice model predictions (———), with experimental partition coefficient data for the polystyrene-ethane system at 333K and 25 MPa [(□) and (Δ)].

chain lengths beyond a relative molecular mass of 1200 g $mole^{-1}$. The reason for the disagreement between the model and experiment below this molecular weight is speculated to be due to two factors.

- First, we assume that segments of all polystyrene chains interact with the same energy per contact area, ϵ_{11} (Section 3.4). Clearly, this assumption breaks down for shorter chains when end effects become important.
- Also, the results shown in Figure 4.4 are valid only as long as there are two phases in equilibrium; however, pure styrene monomer is completely soluble in ethane at pressures greater than 9.0 MPa at 333K (see Chapter 7). Results predicted with a two-phase, quasi-

binary model are therefore unreliable for the smallest oligomers.

In summary, results obtained for the solubility of polystyrene chains in ethane at 25 MPa and 333K verify that supercritical ethane is a strong fractionating medium for polystyrene on the basis of chain length. An important conclusion from this study is that the polystyrene phase in contact with SCF ethane behaves as an ideal solution. This result allows for the easy correlation of experimentally measured partition coefficients with the lattice EOS, since we may now deal with a linear combination of several n-mer-SCF quasi-binary mixtures rather than a multicomponent polymer-SCF equilibrium. Modelling results using this assumption show that we can reproduce experimental trends, above a certain chain molecular mass, with a single adjustable parameter, δ_{12}, that is independent of chain length.

4.2.2 Results from Conventional Solvents

We now compare the fractionating power of supercritical ethane to conventionally employed solvents (liquids and ideal gases). In Figure 4.5 we present a plot of the equilibrium solubilities of polystyrene chains in n-heptane at 298 K. These data were obtained from the polystyrene sample with M_n ~2060 g mole^{-1}. On the same plot we also show the fractionation expected if an ideal gas (ethane, in this case) at a pressure of 1 MPa and 333K were used as a solvent. With the use of a gaseous solvent, pronounced fractionation on the basis of polymer chain length is obtained, as indicated by the large slope of the line of ℓn K vs molecular weight. However, the loading of polystyrene chains in the gas phase is low. On the other hand, liquid solvents offer poor fractionation as suggested by the small absolute value of the slope of the ℓogK vs. molecular mass. However, these solvents afford higher loadings of polymer. The two lines shown in this figure thus represent the two extreme cases of fractionation that can be achieved through the use of conventional solvents. Since the solvent-power of gas and liquid solvents cannot be altered easily, these also represent the fractionation that is normally achievable with such solvents. In contrast, ethane at 25 MPa and 333K has a behaviour intermediate between a gas-like

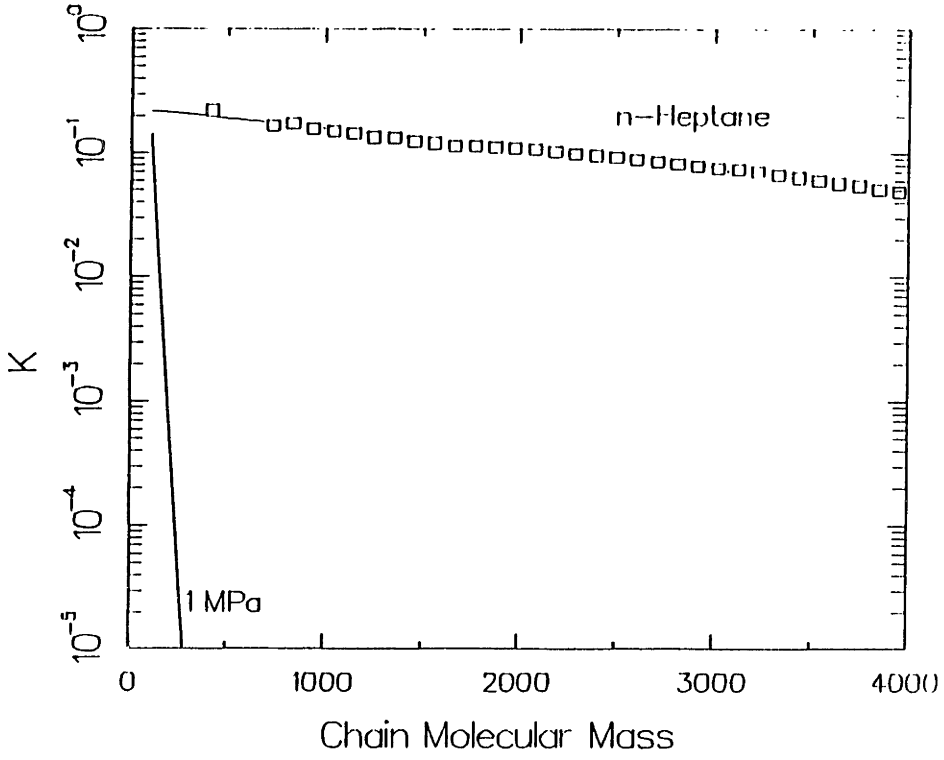

Figure 4.5: Comparison of the partitioning behaviour of n-heptane (298K) and ethane (at 1 MPa and 333K) for polystyrene oligomers between a polymer-rich phase and a solvent-rich phase. (□) are experimental data and the line through the points is a best-fit straight line. Ethane results are simulated from the ideal gas law.

and a liquid-like solvent. Thus, the use of SCF solvents permits one to access regions in the partition coefficient diagram that are not approachable with conventional solvents.

We will now examine the sensitivity of the fractionating ability of SCF to the following changes in operating conditions.

(i) Pressure (8.5-34 MPa)

(ii) Temperature (313-333K)

(iii) Solvent (CO_2, ethane, and a mixture of ethane and propane)

Predictions from the lattice EOS will also be presented to explore the relevance of this theoretical tool for the correlation of experimental data.

4.2.3 Results at Different Pressures

4.2.3.1 Experimental and Modelling Results

The partitioning ability of an SCF is expected to be a strong function of operating pressure since the density (and hence the solvent power) of the SCF has been shown to vary from gas-like to liquid-like in a continuous fashion with increasing pressure (see Figure 1.1, Paulaitis et al, 1983). The partitioning behaviour of an SCF solvent with respect to polymers, is therefore expected to vary from gas-like ("strong" fractionation, "poor" loading) to liquid-like ("poor" fractionation, "good" loading) in a *continuous* fashion as one increases pressure.

In Figure 4.6 we present averaged experimental data for partition coefficients of polystyrene chains as a function of chain molecular mass at several ethane pressures between 8.5 and 34 MPa, at 333K. (The lines through the points are best fit straight lines.) Again, these include data from both the 800 and 2060 g $mole^{-1}$ polystyrene samples (detailed results are presented in Appendix II). The partition coefficient data from Figure 4.5 (with n-heptane at 298K, and ethane at 1MPa and 333K as solvents) are also shown for comparison.

At all examined pressures we have a log-linear dependence for K_i on the chain molecular mass. At the lowest pressure (8.5 MPa), the partition coefficient line is steep, indicating a pronounced fractionation. As one proceeds to higher pressures the density and solvent power of ethane approach a liquid-like value. The loading of the SCF phase with polystyrene chains of higher masses thus increase; however, the fractionation obtained becomes less selective.

The data in Figure 4.6 were fitted to a line of the form,

$$\ell og_{10}(K_i) = C_0 - (\text{Degree of Polymerization})_i \times C_1 \qquad (4.4)$$

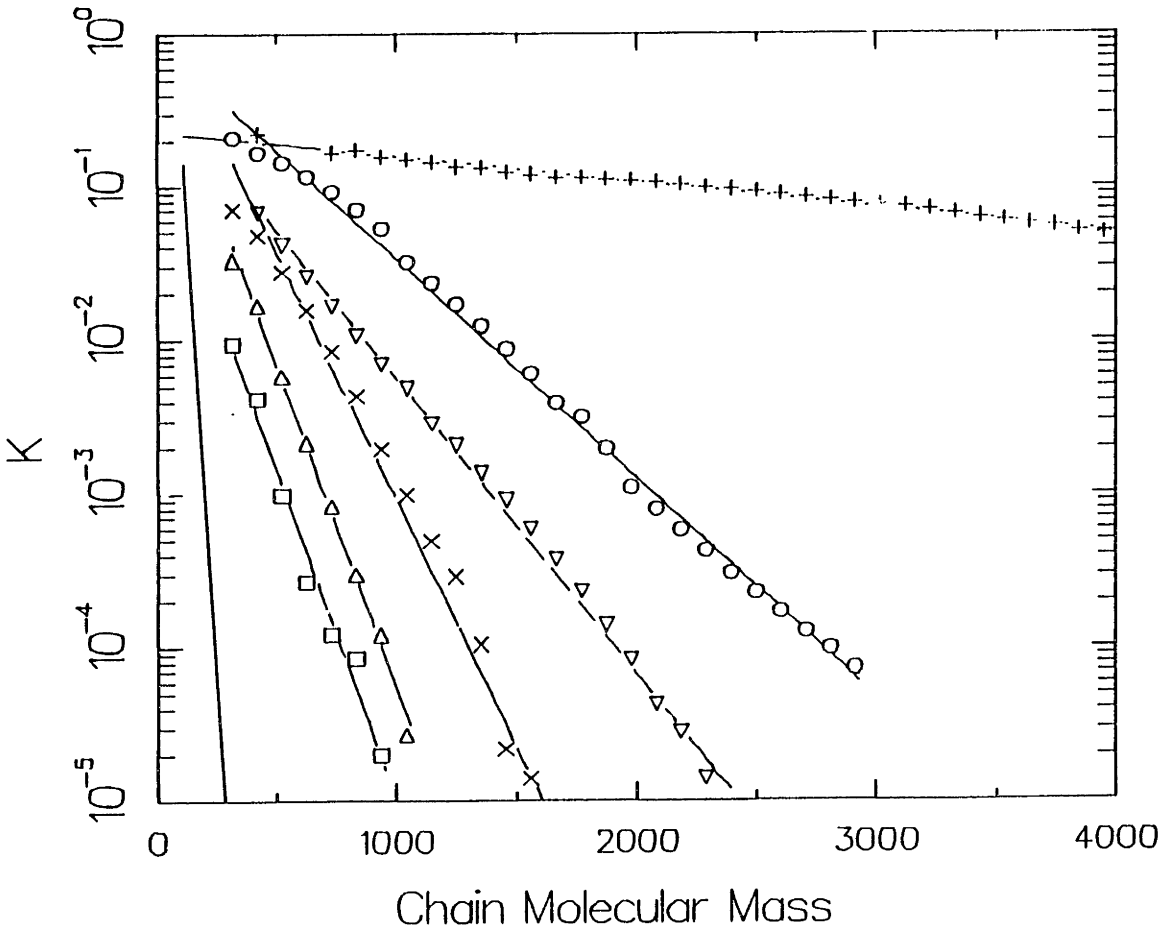

Figure 4.6: Experimental data for the solubility of polystyrene in various solvents. [The lines are best-fits.] (+) are data for partition coefficients in n-heptane at 298K. All other data are at 333K with ethane as solvent. (□) at 8.5 MPa, (△) 10 MPa, (×) 15 MPa, (▽) 25 MPa and (○) 34 MPa. The line with no points is ethane at 1 MPa.

and the "best fit" values of C_0 and C_1 are shown in Table 4.1. The dependence of C_1 [the slope in Eq(4.4)] on pressure reflects the strong dependence of the selectivity of the supercritical ethane on operating conditions. C_0, however, does not follow a trend explainable in a similarly simple fashion, and the observed variations may only be the result of experimental error.

Table 4.1
Variation of C_0 and C_1 with pressure at 333K

Pressure (MPa)	C_0	$10^3 C_1$
8.5	-0.74	4.23
10.0	-0.08	4.17
15.0	0.16	3.19
25.0	-0.34	1.92
34.0	-0.16	1.37

Experimental data for the partitioning of polystyrene chains in ethane at the 3 different pressures (10, 15, and 34 MPa) were correlated with the lattice model EOS. The single interaction parameter (δ_{12}) employed at these different pressures, at all chain lengths, was the same as the δ_{12} value obtained by fitting experimental data at 25 MPa (i.e., δ_{12}=0.018). In

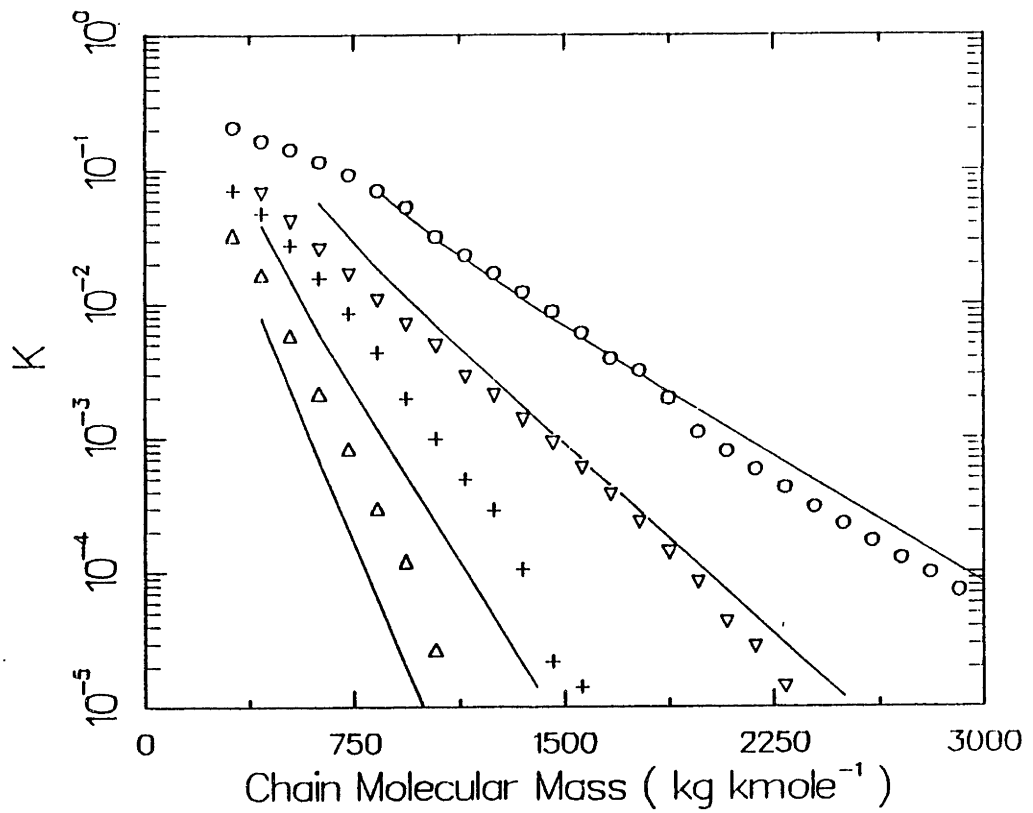

Figure 4.7: Comparison of the lattice model predictions [δ_{12}=0.018 (———)], with experimental partition coefficient data for the polystyrene-ethane system at 333K and (Δ) 10 MPa, (+) 15 MPa, (∇) 25 MPa and (O) 34 MPa.

essence, the model results at these three pressures are *predictions*. The results of the lattice model at 10, 15, 25 and 34 MPa are compared to experimentally measured partition coefficients in Figure 4.7. The important point in this context is the utility of the mean-field lattice EOS in the quantitative correlation of experimental data for the polystyrene-ethane system across variations in pressure and polymer chain length with a single adjustable parameter, δ_{12}, that is independent of these variables.

Although the lattice model EOS quantitatively reproduces most of the relevant features of the partition coefficient diagrams, it must be used only outside the immediate vicinity of the critical point of the SCF (*ca.* $|T-T_c|/T_c < 0.05$ and $|\rho-\rho_c|/\rho_c < 0.05$) since the EOS is a mean-field equation. For this reason, modelling results at a pressure of 8.5 MPa are not presented.

The data in Figure 4.6 were cross-plotted so that the variation of the partition coefficient with pressure could be observed for different chain length polymers (Figure 4.8). The lattice model reproduces the experimental trends accurately for the examined polystyrene chain lengths. At the lowest molecular mass presented, (624 g $mole^{-1}$ in this case), the partition coefficients increase rapidly at a pressure around 8 MPa (corresponding to ρ_c) and begin to level off at higher pressures (ca. 10 MPa). This is consistent with observed trends for the solubility of small molecule compounds in SCF (e.g., naphthalene or acridine in supercritical CO_2, see Section 3.3.4), where a sharp increase in solubility is observed in the region where the density of the SCF increases rapidly. As one proceeds to the higher molecular mass chains this increase in solubility is not as steep and also extends to higher pressures. For example, model predictions for the partition coefficient of the polystyrene chain of molecular mass 2040 g $mole^{-1}$ show that its solubility is still increasing at a relatively high pressure of 40 MPa. The behaviour of macromolecular compounds in SCF is thus qualitatively very different in character from the behaviour of small molecule compounds.

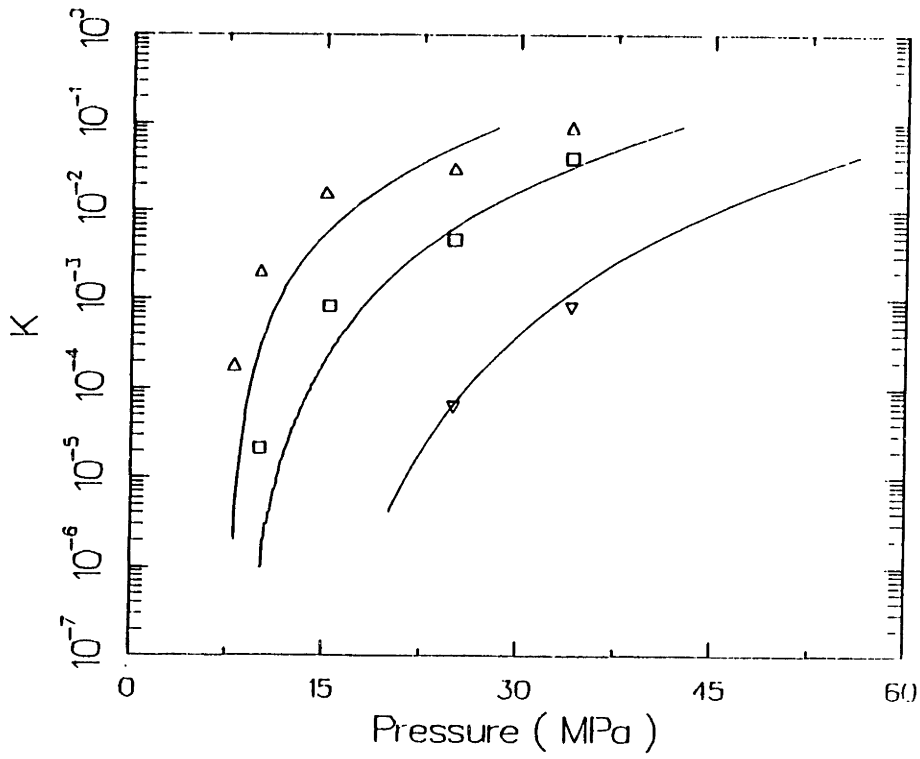

Figure 4.8: Experimental data and lattice model predictions (———) for the partition coefficients of individual polystyrene chain lengths in ethane at 333K plotted as a function of pressure. Polymers of molecular masses (△) 624 , (□) 1040 and (▽) 2040 g mole^{-1} are examined.

To reiterate the usefulness of the EOS in the modelling of the partition coefficients of polystyrene into ethane, we present in Figure 4.9 a plot of cutoff molecular mass at different pressures, both from experiment and model predictions. A cutoff molecular mass represents the polymer chain of the largest molecular mass that could be detected in the SCF phase after it was contacted with the polymer sample. (The criterion used for determining this molecular mass was to find the polymer chain that had a K_i value of 10^{-6}). Again, model predictions (obtained with δ_{12}=0.018), outside the critical region of the solvent, are seen to be in good agreement with experimental results. An interesting implication of this diagram is that as pressure is increased, the cutoff molecular mass rises, and, at a pressure of 50 MPa it is at a molecular mass of ca. 10,000 g mole^{-1}. At these elevated pressures, as expected, ethane begins to behave akin to a conventional liquid solvent.

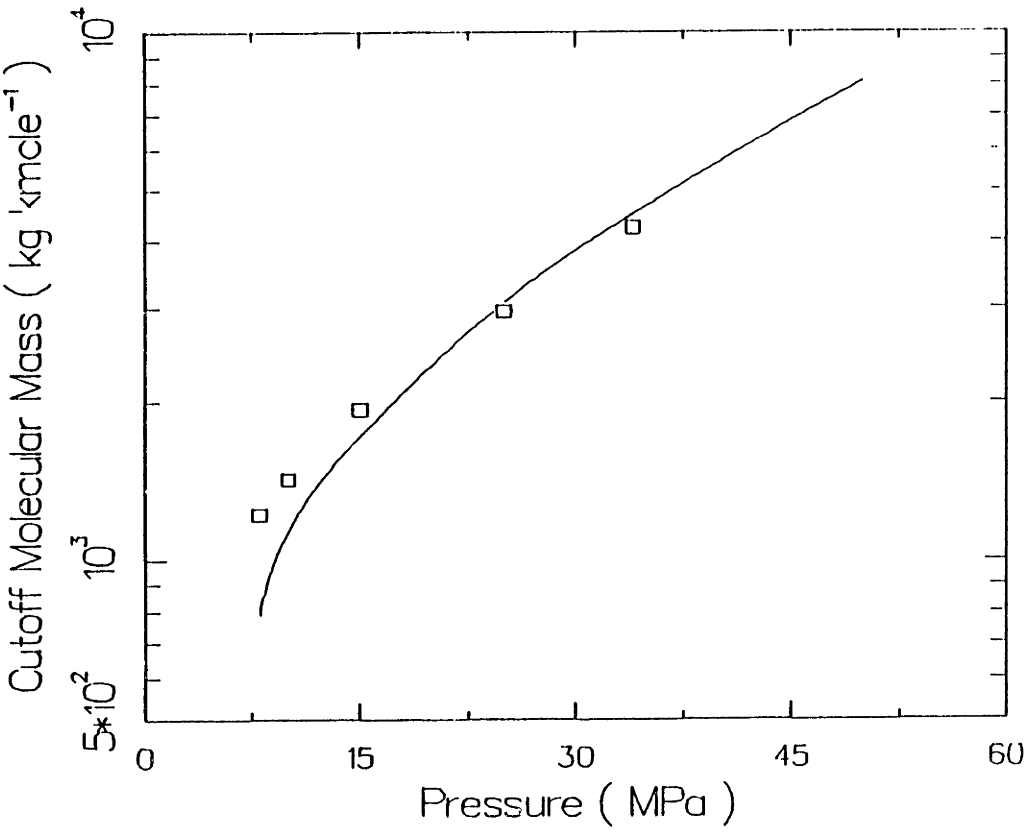

Figure 4.9: Experimental data (□) and lattice model predictions (———) for the molecular weight cutoff of polystyrene chains in ethane at 333K, plotted as a function of pressure.

4.2.3.2 Theoretical Aspects

There are two results presented in section 4.2.3.1 that need to be understood theoretically to generalize the results obtained from the polystyrene-ethane system to any polymer-SCF equilibrium. They are,

(i) The linearity of $\ell n\ K_i$ vs polymer chain length, X_i

(ii) The dependence of K_i on pressure, for all X_i.

(i) *The linearity of $\ell n\ K_i$ vs polymer chain length*: To explain the observed linearity for the partition coefficients with polystyrene chain lengths, at all ethane pressures, it must be realized that we are dealing

with a situation where polymers of all chain lengths and the SCF are at a thermodynamic equilibrium between the two phases. The mathematical condition that represents this phase equilibrium is an equality of chemical potentials of each component in both phases,

$$\mu^{v}_{SCF} = \mu^{s}_{SCF} \tag{4.5a}$$

$$\mu^{v}_{i} = \mu^{s}_{i} \tag{4.5b}$$

The expression for the chemical potential of a component in a binary mixture, as obtained from the lattice EOS, has been presented in Eq. (3.58).

$$-\frac{\mu_i}{k_B T} = \gamma_i(T) + \left[\frac{r_i \tilde{P}}{\tilde{T}}\right] + \ell n q_i - \ell n \vartheta \tilde{\vartheta}_i - r_i(1-z/2)\,\ell n \frac{\tilde{v} + (q_M/r_M) - 1}{\tilde{v}}$$

$$-\frac{q_i \vartheta^2}{\tilde{T}} + \frac{q_i \vartheta}{\tilde{T}\epsilon_M}\left[\sum 2\tilde{\vartheta}_j \epsilon_{ij} - \sum\sum\sum 2\tilde{\vartheta}_j \tilde{\vartheta}_k \tilde{\vartheta}_\ell \tilde{\vartheta}_m \epsilon_{jk}(\xi_{km}+\xi_{jm}-\xi_{\ell m}-\xi_{jk})\right] \tag{3.58}$$

We now make some reasonable approximations and examine Eq(4.5) under the assumption of independent n-mer-SCF quasi-binaries,

(i) We hypothesise that non-randomness corrections do not make significant contributions to μ_i under these conditions., i.e, we assume that all $\xi_{ij} = 1$.

(ii) For simplicity, it is also assumed that phase volumes (v, in units of $cm^3 g^{-1}$) and the ratio q_M/r_M are essentially independent of the specific polymer chain length considered in the n-mer-SCF equilibrium.

On applying Eq (3.58) in Eq (4.5b) under these approximations, we may show that,

$$\ell n(\bar{\vartheta}_i^v/\bar{\vartheta}_i^s) = \alpha_0 + \alpha_1 q_i \qquad (4.6)$$

where α_0 and α_1 are SCF specific constants that are indcpendent of polymer chain length, X_i, but are functions of pressure (P) and temperature (T). Eq(4.6), thus represents a general result obtained from the lattice EOS for a polymer-SCF quasi-binary, contingent on the assumptions stated earlier. To deduce the experimental relationship between K_i and X_i, [Eq (4.4)], from Eq (4.6) it must be realized that q_i is the effective chain length of the polymer. Also, the ratio of area fractions of the polymer in the two phases may be related to the ratio of the respective weight fractions, i.e.,

$$\bar{\vartheta}_i^v = (x_i q_i)^v/\sum(x_j q_j)^v \sim w_i^v/X_i(MW)_1 \qquad (4.7a)$$

$$\bar{\vartheta}_i^s = (x_i q_i)^s/\sum(x_j q_j)^s \sim \Phi \; [\neq f(P)] \qquad (4.7b)$$

where it has been assumed that the polymer chains are present in dilute concentrations in the SCF phase, and that the weight of the SCF dissolved in the solid phase is independent of the polymer chain length. On substituting Eq(4.7) in Eq(4.6) we obtain a result identical to Eq (4.4).

$$\ell n(K_i) = \ell n(w_i^v/w_i^s) \sim \xi_0 + \xi_1 X_i \qquad (4.8)$$

The functionality of the partition coefficient of a polystyrene oligomer on its chain length as deduced from Figures 4.3 and 4.6 [Eq(4.4)] therefore *represents a general result* that may be expected from all polymer-SCF systems that do not violate the general assumptions made in the derivation of Eq(4.8). Although several assumptions have been made in deriving Eq(4.8), none are unreasonable within the framework of the systems examined. Clearly, exceptions will arise when the assumptions made break down; a specific case being a situation where the loading of polymers in the SCF become large.

(ii) *The dependence of K_i on Pressure*: In Figures 4.4 and 4.8 it has been shown that K_i for polystyrene chains increase with increasing ethane pressure. Also, we have shown that as one proceeds to longer chain length polystyrenes the region of rise in solubility (when plotted against pressure) becomes less pronounced and extends to higher pressures. At this point, therefore, we would like to investigate the theoretical reasons for the manifestation of these phenomena.

Partition coefficients, as defined in Eq(4.1), are the ratio of the weight fraction of the specific polymer chain length in the SCF phase to the corresponding weight fraction in the SCF-free solid phase. The pressure derivative of ℓnK may therefore be shown to be related to the corresponding rate of change of the mole fraction of the polymer in the SCF phase,

$$\left.\frac{\partial \ell nK_i}{\partial P}\right)_{T,\sigma} = \left.\frac{\partial \ell n(w_i^v/w_i^s)}{\partial P}\right)_{T,\sigma} \sim \left.\frac{\partial \ell n[x_i^v (MW)_i/(MW)_{SCF}\Phi]}{\partial P}\right)_{T,\sigma} \qquad (4.9)$$

Here, σ implies that the derivatives are taken along the saturation curve, and the translation from weight fractions to mole fractions has been achieved through the use of Eq(4.7). $(MW)_i$ and $(MW)_{SCF}$ represent the molecular weights of the polymer chain and the SCF respectively. The derivative $\partial \ell nx_i^v/\partial P]_{T,\sigma}$, under the assumption of a pure solid phase has been shown to take the form (Kurnik, 1981),

$$\left.\frac{\partial \ell nx_i^v}{\partial P}\right)_{T,\sigma} \sim \frac{V_i^s - \bar{V}_i}{RT} \qquad (4.10)$$

outside the critical region of the solvent. V_i^s represents the molar volume of the solute, and $\bar{V}_i$ represents the partial molar volume of the polymer in the SCF-phase. We employed Eq (4.10) in Eq (4.9) as an approximation, with the clear understanding that this assumption of a pure solid was not appropriate in the case of the polystyrene-ethane system. However, the approximation would be more reasonable if the quantity of SCF dissolved in

the solid phase did not change substantially with pressure. From this mathematical procedure, one may then show that,

$$\left.\frac{\partial \ell n K_i}{\partial P}\right)_{T,\sigma} \sim -\frac{V_i^s - \bar{V}_i}{RT} \qquad (4.11)$$

In the past it has been shown for polymeric systems that $\bar{V}_i$ scales approximately linearly with the chain length of the polymer in consideration (Abraham and Ehrlich, 1975). On employing this fact along with the assumption that V_i^s, the molar volume of the solute, also scales with X_i, one can finally show that,

$$\left.\frac{\partial \ell n K_i}{\partial P}\right)_{T,\sigma} \sim X_i \times \frac{(V_i^s - \bar{V}_i)}{RT} \qquad (4.12)$$

The pressure derivative of the partition coefficient of a polystyrene chain (into supercritical ethane), therefore, scales linearly with its chain length. So, although the isotherms for low molecular weight compounds (as the monomer and dimer) essentially level out at pressures greater than ~15 MPa, the isotherms for higher molecular weight polymers will continue to rise since their rate of increase with pressure is magnified by their chain lengths, as suggested by Eq(4.12).

To examine the validity of Eq(4.12) and the assumptions made in its derivation, in Figure 4.10 we present plots of the quantity $(1/X_i)\partial \ell n K_i/\partial P]_{T,\sigma}$ against pressure for three different polystyrene chain lengths (of molecular weight 624, 1040 and 2080 g mole^{-1}), as predicted from the lattice model. If Eq.(4.12) were valid we would obtain a single curve that is independent of polymer chain length. Results shown in Figure 4.10 illustrate that this result is strictly valid near the critical density of ethane. At higher pressures, however, discrepancies arise, but the point to be emphasised here is the remarkable agreement of the slopes for the different chain lengths in the vicinity of the sharp rise in the density of the solvent SCF. The

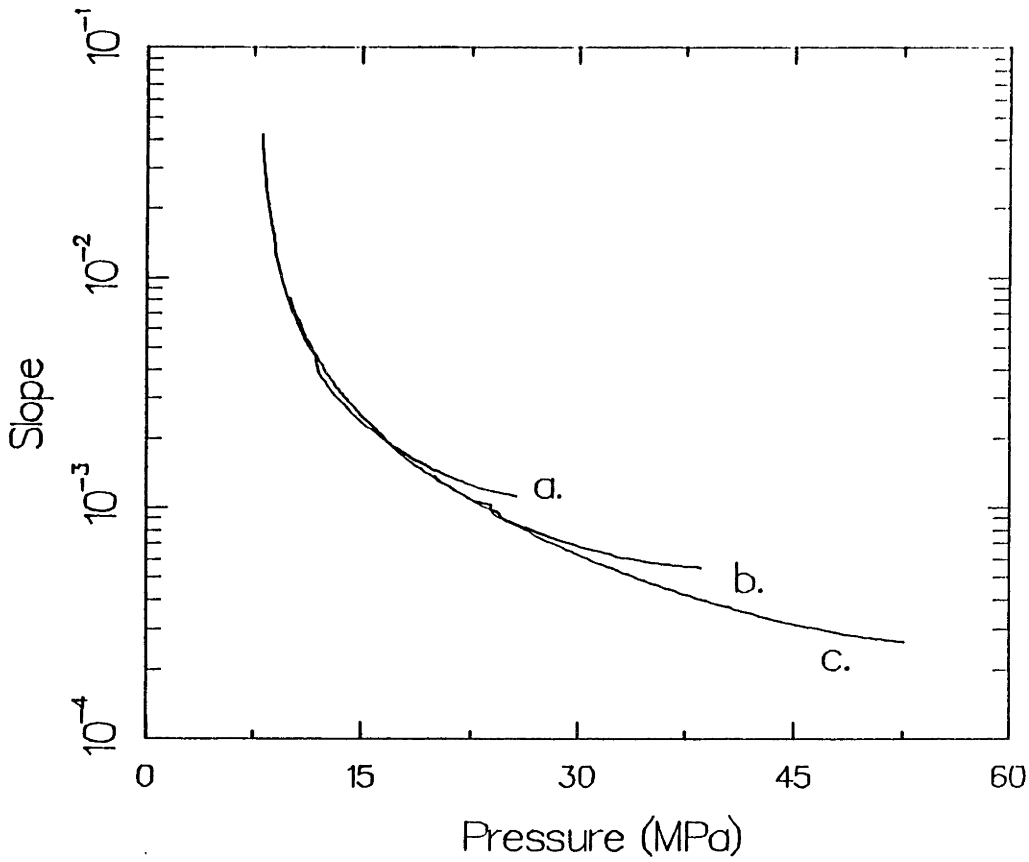

Figure 4.10: Lattice Model Predictions with δ_{12}=0.018 for the quantity $(1/X_i)\partial\ell nK_i/\partial P]_{T,\sigma}$ (in units of bar^{-1}) for the solubility of polystyrene chains (of molecular weights a. 624, b. 1040 and c. 2080 g $mole^{-1}$) in ethane at 333K.

important deduction that may be made on the basis of Figure 4.10 is that the qualitative differences noted in the behaviour of small and large molecular weight compounds when dissolved in SCF is a manifestation of the difference in chain lengths of the solutes. While Eq (4.12) stresses the differences in behaviour between a small and a macromolecular compound, the identical value of slopes noted in the pressure regime < 20 MPa verifies the presence of a governing universality determining the solubility of different sized molecules in SCF.

In summary, the following conclusions may be drawn from the experimental and theoretical results that have been presented to demonstrate the sensitivity of the partitioning behaviour of SCF to changes in operating pressure:

- Results at all ethane pressures show that the partition coefficient of any chain length polystyrene, K_i, is independent of the composition of the polymer phase. The polystyrene phase in contact with ethane therefore, behaves as an ideal solution at all operating pressures.
- As the pressure of operation is increased, the solvent quality of an SCF varies continuously from gas-like to liquid-like. The use of an SCF solvent thus allows one to access regions of the partition coefficient diagram that could not be obtained by the use of conventional gas or liquid solvents.
- The partition coefficient vs chain molecular mass curves are log-linear at all pressures examined, with the absolute value of the slope of the line decreasing as pressure was increased. This is another manifestation of the approach of the SCF to liquid-like behaviour as P is increased.
- All experimental data for the polystyrene-ethane system, outside the critical region of the SCF, have been correlated with a lattice model EOS with a single adjustable parameter, δ_{12}, that is independent of chain length and pressure.
- Through the use of simple thermodynamic arguments we have shown that the lattice EOS predicts the log-linear behaviour of the partition coefficient vs chain molecular weight line observed for the polystyrene-ethane system. This relationship is expected to be valid generally across most commonly encountered polymer-SCF systems.
- We have shown that the behaviour of the solubility isotherms (K_i plotted against P), of polystyrene chains of high molecular weight are qualitatively different from the character displayed by the corresponding curves for small molecules. However, if we account for the size of the polymer molecule, then the presence of a certain universality can be demonstrated in the solubility characteristics of different chain length polymers.

4.2.4 Results at Different Temperatures

Temperature of operation affects the partition coefficients of polystyrene chains dissolving into ethane in two opposing directions:

(i) Since the vapour pressure of substances increase with increasing temperature, a larger amount of each chain length polymer may be expected to be in the SCF phase at equilibrium, if the pressure and density of the SCF remained unchanged.

(ii) As the temperature of a SCF-polymer mixture is increased, at constant pressure, the density of the SCF will decrease (see Figure 1.1). It has been shown, in Section 4.2.2 that the fractionating behaviour of SCF becomes more "gas-like" as its density is decreased. This effect will, therefore, reduce the loading of polymer chains in SCF as temperature is increased.

To quantify these results we begin by writing the derivative $\partial \ell nK_i / \partial(1/T)]_{P,\sigma}$ in the form,

$$\left.\frac{\partial \ell nK_i}{\partial(1/T)}\right]_{P,\sigma} = \left.\frac{\partial \ell nK_i}{\partial(1/T)}\right]_{P,\rho} + \left.\frac{\partial \ell nK_i}{\partial \rho}\right]_{P,T} \times \left.\frac{\partial \rho}{\partial(1/T)}\right]_{P,\sigma} \qquad (4.13)$$

The first term in Eq(4.13) will only contain the effects of temperature on the vapour pressure of the pure polymer chain. In other words, this term represents the negative of the enthalpy of sublimation of the polymer chain under these conditions, and would always be negative in sign,

$$\left.\frac{\partial \ell nK_i}{\partial(1/T)}\right]_{P,\rho} = - \frac{\Delta H^{sub}}{R} \qquad (4.14)$$

Then, the second term in Eq (4.13) represents the effects of changing solvent density on K_i. Clearly, this term should be positive for all

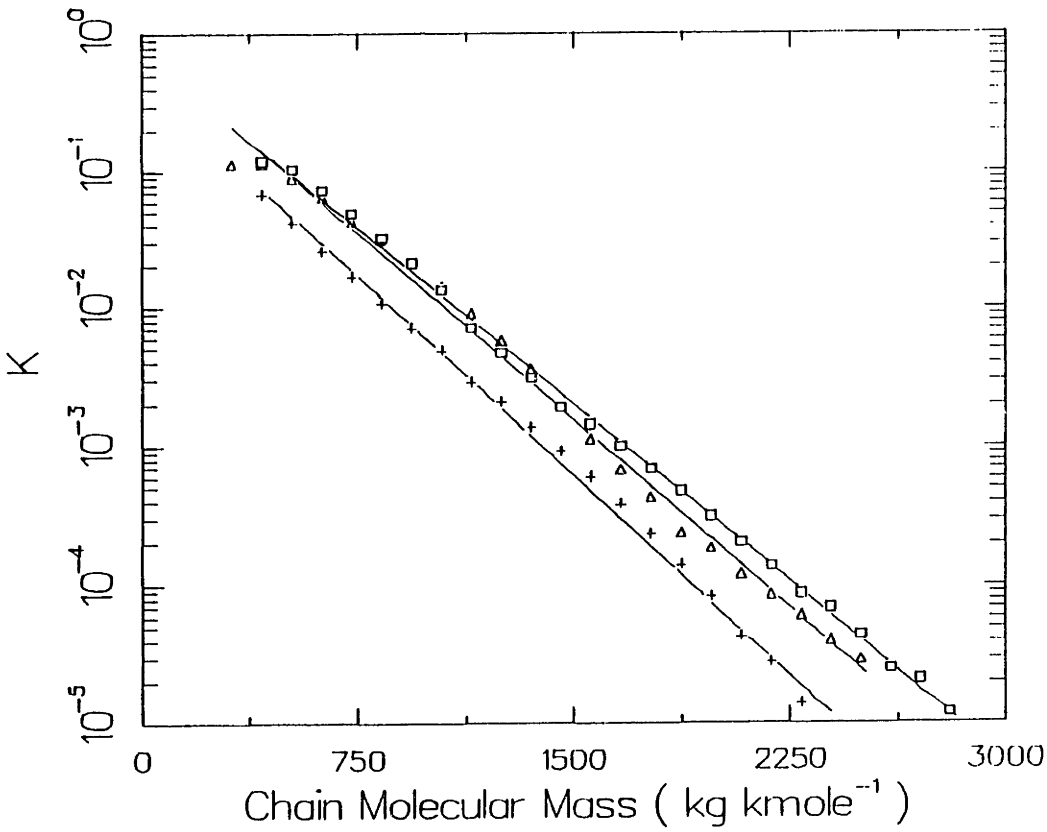

Figure 4.11: Experimental partition coefficient data for the polystyrene-ethane system at 25 MPa and (□) 313K, (Δ) 323K and (+) 333K. The lines represent best fit straight lines.

conditions considered since it is a product of two positive factors. The exact dependence of partition coefficients on temperature will therefore be governed by the dominant term in Eq (4.13).

In Figure 4.11, the averaged K_i values for polystyrene chains into ethane at a pressure of 25 MPa and three different temperatures (313, 323 and 333K respectively) are presented. Data for this graph were obtained from polystyrenes of M_n~ 2060 and 800 g mole^{-1}, exactly as in the previous experiments.

The partition coefficient curves for the polystyrene-ethane system are not as sensitive to temperature changes as they are to variations in pressure. This could be due to the fact that, at these conditions, ethane has an

essentially liquid-like density (~300 kg m^{-3}) which is not very sensitive to relatively small changes in temperature.

Data at these three temperatures were fitted to an equation of the form presented in Eq.(4.4) and the results are reported in Table 4.2.

Table 4.2: Variation of C_0 and C_1 with temperature at 25MPa

Temperature (K)	C_0	$10^3 C_1$
313	-0.11	1.73
323	-0.08	1.82
333	-0.34	1.92

The lattice model EOS was again used to fit the experimental data. It was found that the same value of δ_{ij} (= 0.018) that was used at 333K could be used over the temperature range of interest. Data fits obtained with this value of the binary interaction parameter are demonstrated in Figure 4.12. The lattice model thus allows for the quantitative reproduction of experimental data for the polystyrene-ethane system across variations in chain length, pressure and temperature with one apparently constant value of the interaction parameter, δ_{ij}. The utility of the lattice model in the correlation of such systems, in principle, is emphasised by its capability of predicting quantitative trends by fitting it to a single datum point for the system of interest.

An interesting feature of Figures 4.11 and 4.12 is that the curves corresponding to lower temperatures fall above the ones at higher temperatures. Also C_1, the slope of the K_i line (in Table 4.2), shows that the fractionating power of an SCF becomes more "gas-like" as one proceeds to higher temperatures. From the discussion presented earlier in this section it is inferred that the small effect of changes in SCF density due to temperature variations dominate the variation of K_i observed in these experiments.

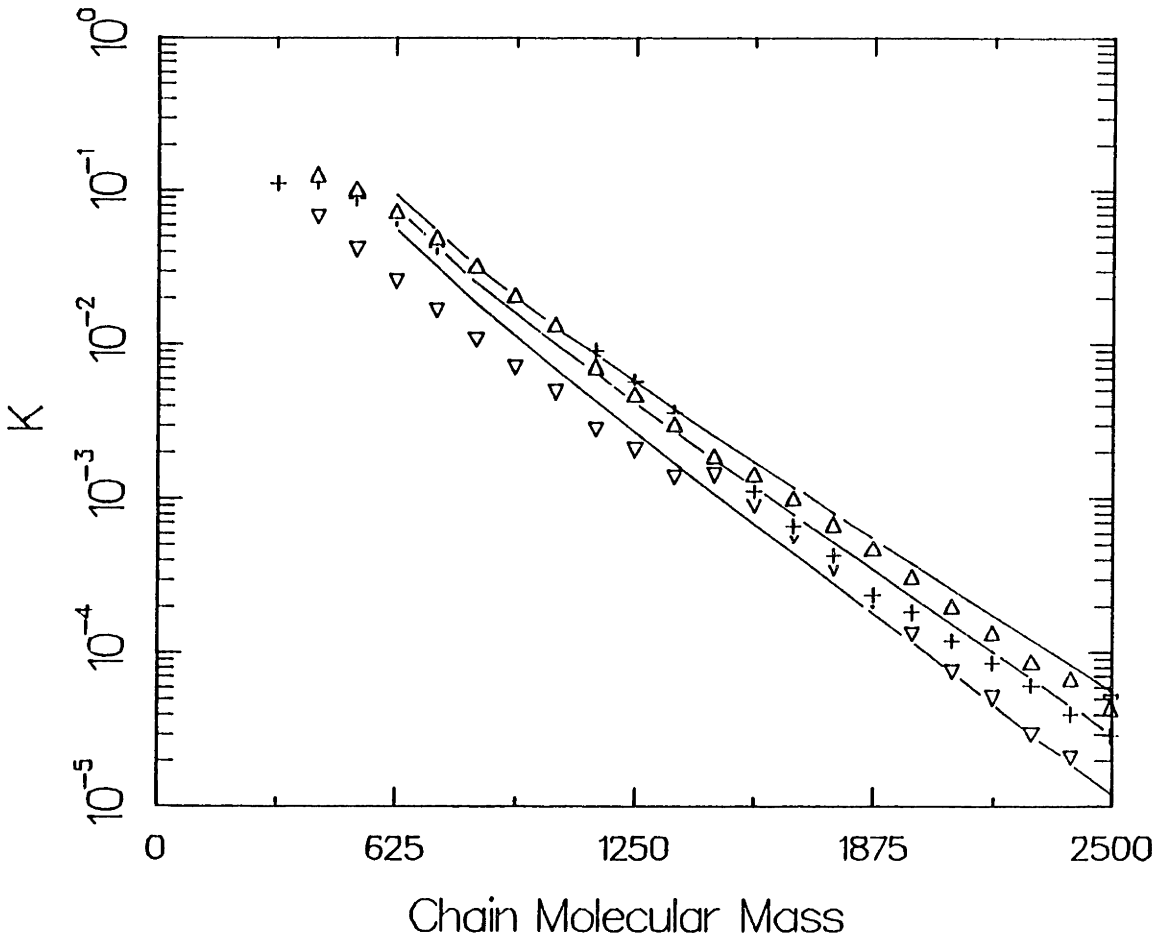

Figure 4.12: Comparison of the lattice model predictions [δ_{12}=0.018, (———)] with experimental partition coefficient data for the polystyrene-ethane system at 25 MPa and (△) 313K, (+) 323K and (▽) 333K.

This would imply that a lower temperature would afford a higher loading of the longer polystyrene chains (than a higher temperature). This apparently anomalous result can be understood if the lattice model predictions for the solubility of a single molecular mass polystyrene chain (1040 g mole^{-1} in this case) in ethane are examined as a function of pressure and temperature (Figure 4.13). It is seen that the predictions at lower temperatures always lie above the corresponding curves at higher temperatures, verifying

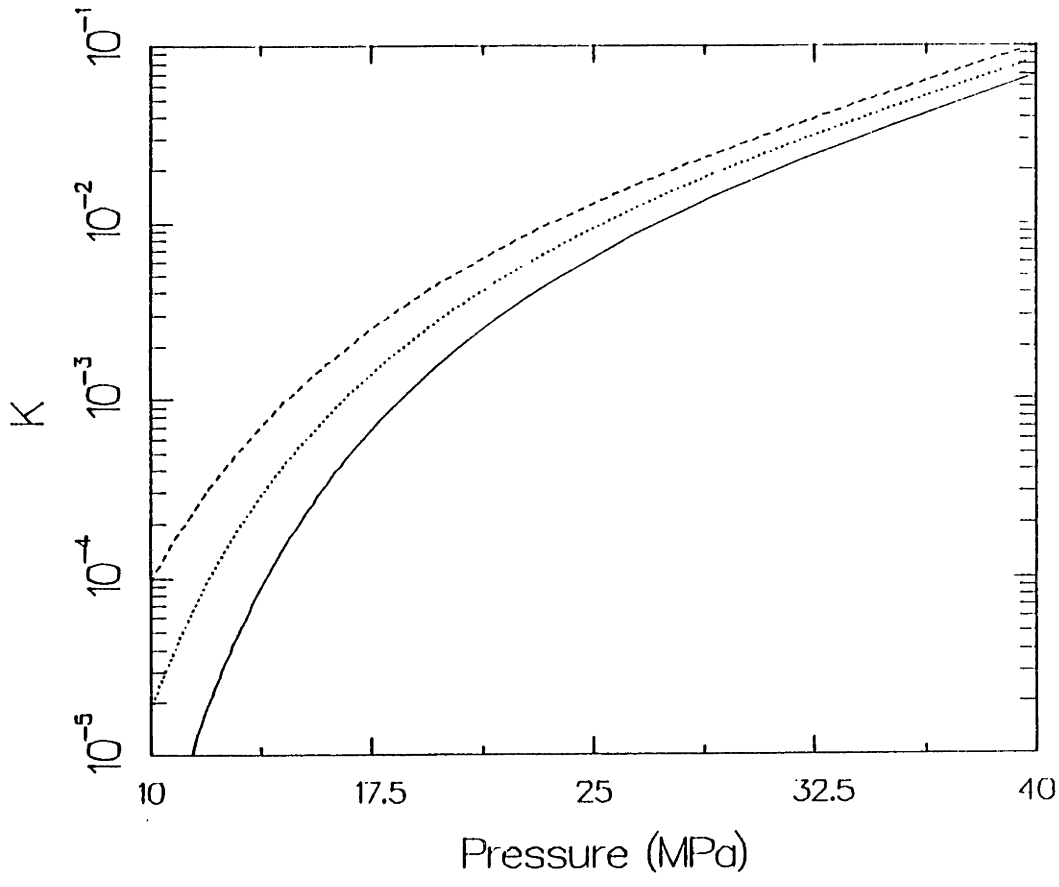

Figure 4.13: Lattice model predictions for the variation of partition coefficients of a 1040 g mole^{-1} polystyrene in ethane, across changes in pressure. The curves represent different isotherms. (——) 333K, (· · · ·) 323 K and (----) 313 K.

that changes in SCF density determine the behaviour of partition coefficients with variations in temperature.

This result should be contrasted to corresponding results obtained for the solubility of a low molecular weight compound in an SCF (e.g., acridine or anthracene in CO_2, see Figures 3.10-3.13. In these diagrams, the mole fraction of the solute in the gas-phase plays a role analogous to K_i in Figure 4.13.) In the case of small solutes there is a region in the diagram, called the retrograde region, where the lower temperature solubilities are higher than at higher temperatures. At higher pressures, however, an opposite trend has been observed. In the case of a macromolecular species this opposite effect at high pressures is not seen, suggesting again that

the behaviour of macromolecular compounds in SCF is very different from that of small molecule solutes.

In conclusion, variations of temperature in the range examined do not have a pronounced effect on the partition coefficients of the different polystyrene chain lengths in ethane at 25 MPa. As temperature is increased, the density (and hence the solvent power) of the SCF becomes more "gas-like", and the loading of polymer chains in the fluid-phase decrease. Data obtained at the three different temperatures (313, 323 and 333K) have been correlated across changes in chain lengths and temperatures employing the lattice EOS with one adjustable parameter that is independent of operating conditions. The potential of the lattice EOS as a predictive tool for this system across variations in temperature, pressure and chain length is thus verified, since the EOS can correlate data across all states with a single value of the interaction parameter, δ_{12}.

4.2.5 Results with different solvents

The effect of the variation of solvent quality on the partition coefficient curves was also examined. Ethane and two other solvents were used: CO_2, one of the popular supercritical solvents, and a mixture of ethane and propane (*ca.* 87:13 by mole). Since propane is a liquid under the experimental conditions its partitioning behaviour with respect to polystyrene chains is expected to be similar to n-heptane. A mixture of ethane and propane was used to examine if the fractionation obtained with this system corresponded to a behaviour between ethane and a conventional liquid solvent. The averaged experimental data for the partition coefficients of polystyrene chains of various molecular masses in the different gases at 333K and 25 MPa along with lattice model fits are shown in Figure 4.14.

Carbon dioxide is seen to be the worst solvent at these conditions. One reason for this could be attributed to the fact that at 25 MPa CO_2 is at a lower reduced pressure (and hence lower reduced density), than the other two solvents. However, a comparison of ethane and CO_2 at the same reduced

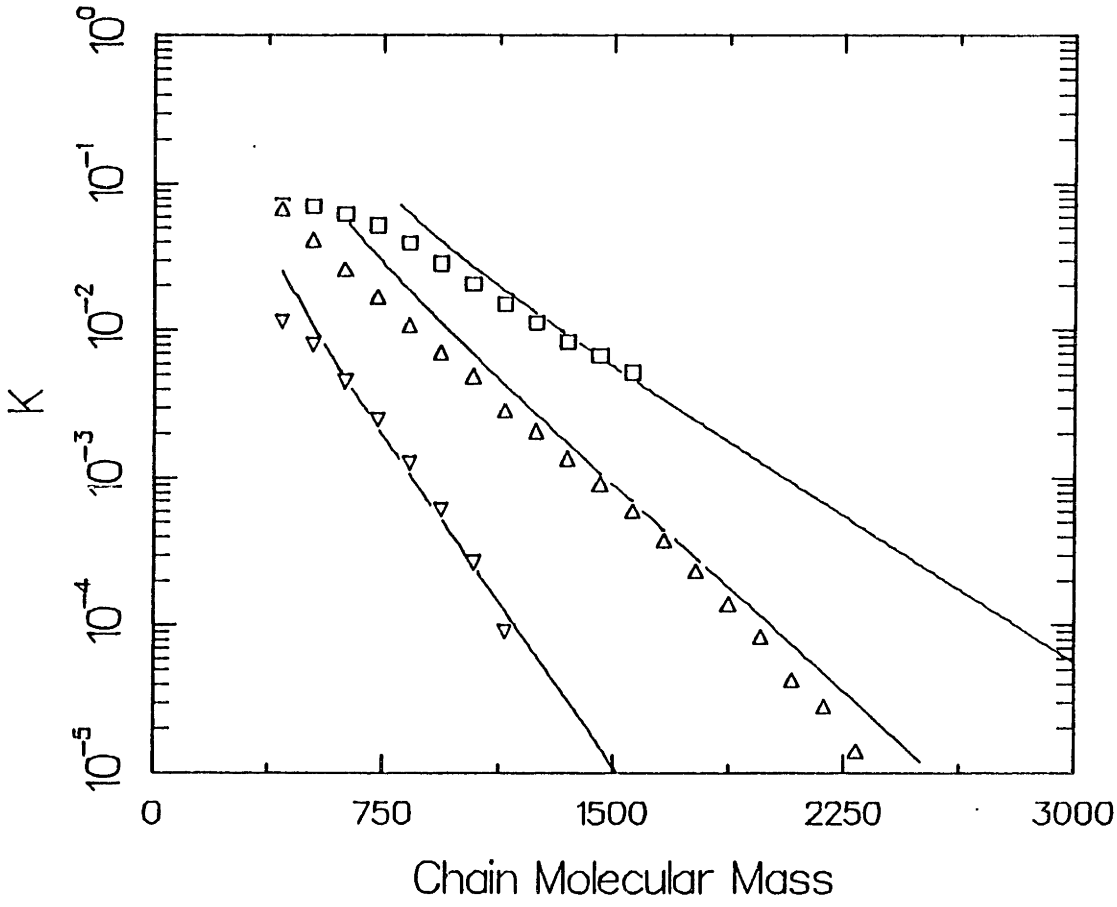

Figure 4.14: Comparison of lattice model fits (———) to experimental data for the fractionation of polystyrene chains with: (Δ) ethane (δ_{12}=0.018), (∇) CO_2(δ_{12} = 0.08) and (□) ethane+ 13% propane (δ_{12}= 0.03).

pressure (i.e., ethane at 17 MPa and CO_2 at 25 MPa) showed that CO_2 is still a poorer solvent than ethane (see Appendix II). The mixture of ethane and propane, however, is a better solvent (and consequently a poorer fractionating medium) than pure ethane. This leads us to the important conclusion that a "better" solvent may be obtained simply by adding a small quantity of a higher member of the same homologous series to a relatively poor solvent.

The experimental data in Figure 4.14 have been modelled by the lattice EOS.

Again quantitative fits were obtained with the use of a single adjustable parameter per binary, across variations in polymer chain length. However, the different systems are not modelled with the same value of the interaction parameter, δ_{12}.

4.3 EXPERIMENTAL AND THEORETICAL CONSIDERATIONS

4.3.1 The Role of Diffusion

An equilibrium solubility of an oligomer in the SCF phase can be measured when the gas phase is in equilibrium with the bulk of the condensed phase. A high average molecular mass polymer with a narrow molecular mass distribution has relatively small quantities of both low and very high molecular weight chains. The small concentrations of the lowest molecular mass chains in the 2060 g mole^{-1} polystyrene used (M_w/M_n~1.2), coupled with their inherently high solubilities ensures that the surface of the polymer will be depleted in these oligomers when it is contacted with an SCF. With respect to these oligomers, equilibrium between the bulk and surface of the condensed phase will then have to be reestablished by diffusional processes. In Figure 4.1 we have demonstrated that for four runs performed successively, the dimer concentrations in the extracts decrease monotonically. It is clear that, in these runs, the measured concentration of dimer in the extract phase represents a diffusionally controlled value.

For chains with molecular weights close to the peak molecular mass in the distribution, diffusion is no longer controlling because sufficient material is present on the particle surface to saturate the gas phase.

Solubility data of the polystyrene chains in ethane at 25 MPa and 333K, measured under transport limitations, are presented in Figure 4.15. (These data were measured with the polystyrene sample with M_n~ 2060 g mole^{-1}). Ethane was placed in contact with the polystyrene for 25 hours before sampling.

The measured solubility of the trimer is 7×10^{-5} kg/kg ethane. As expected, the measured solubility of the tetramer is dramatically lower. As one progresses to higher molecular masses, the observed solubility is seen to rise due to the larger quantity of the oligomer being present in the parent polymer. The solubility reaches an equilibrium value, as deduced from the linearity of solubility plot, around a molecular mass of 1200 g $mole^{-1}$. Most reported equilibrium solubilities from the polystyrene of molecular mass 2060 g $mole^{-1}$ are therefore, only for oligomers of mass higher than 1200 g $mole^{-1}$.

To obtain a mathematical understanding of the relative time scales involved in the diffusional process we examine, as a simple model, the diffusion of a low concentration oligomer out of an inert polymer sphere of radius R, which is placed in contact with an infinite quantity of SCF. The governing transport equation for this process, in spherical coordinates is,

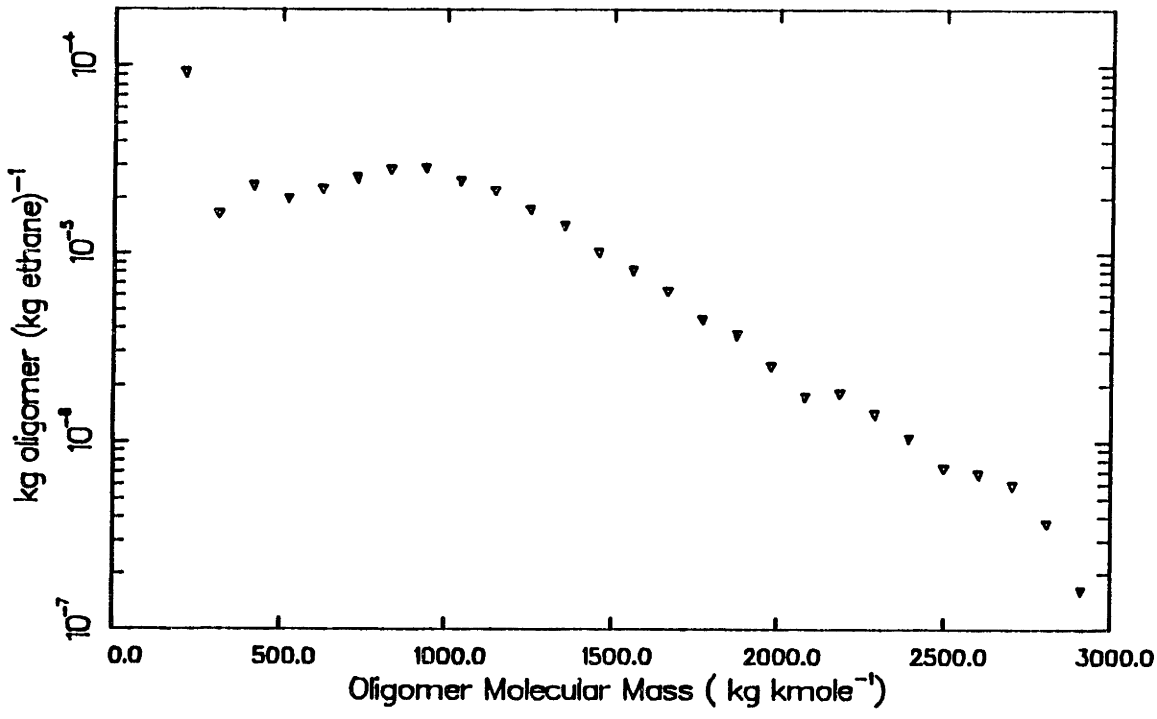

Figure 4.15: Measured solubilities of various oligomers of a polystyrene of average molecular mass 2060 g $mole^{-1}$ in ethane at 25 MPa and 333K.

$$\frac{\partial c_A}{\partial t} = \frac{D}{r^2}\frac{\partial}{\partial r}\left(r^2\frac{\partial c_A}{\partial r}\right) \tag{4.15}$$

where c_A is the concentration of species A at any radial distance r from the centre of the sphere, at any time t. D is the diffusion coefficient of the species A, assumed to be independent of c_A and r. The boundary conditions for this problem are,

$$\text{at } t=0, \quad \text{for all } r, \quad c_A = c_{A0} \tag{4.16a}$$

$$\text{for all } t, \quad r=0, \quad \partial c_A/\partial r = 0 \tag{4.16b}$$

$$\text{for all } t\ (\neq 0), \quad r=R, \quad c_A = 0 \tag{4.16c}$$

While the solution to this problem has been performed by the use of a standard separation of variables technique, no final results are reported here. We however, examine the characteristic diffusion time associated with this formulation,

$$t_D = R^2/D \tag{4.17}$$

If we use reasonable estimates for polymer particle diameter (~200 μm) and the diffusion coefficient for the dimer (~ 10^{-12} cm^2s^{-1}) we obtain diffusion times of 10^4 s. Under these assumptions, therefore, the equilibration of dimer between the SCF phase and the bulk of the polymer phase requires a time of the order of a few hours.

This observation has important practical connotations when it is desired to strip low molecular mass oligomers from high molecular weight polymers. Under these conditions, it is not an equilibrium solubility but one controlled by transport restrictions that is of primary significance.

4.3.2 Quantity of SCF dissolved in Polymer

In the definition of K_i, [Eq(4.1)], the solid phase weight fractions of polystyrene chains have been used on an SCF-free basis. The implicit assumption in using SCF-free solid phase compositions is that this definition of K_i incorporates all the physics necessary in describing the fractionation process. This supposition will be justified, if we can show that the quantity of SCF dissolved in the polymer phase does not change with variations in the molecular weight of the polymer.

The equilibrium solubility of SCF in the polystyrene phase cannot be measured in our apparatus since it is not possible for us to sample the solid phase when it is contacted with the extracting fluid. We therefore

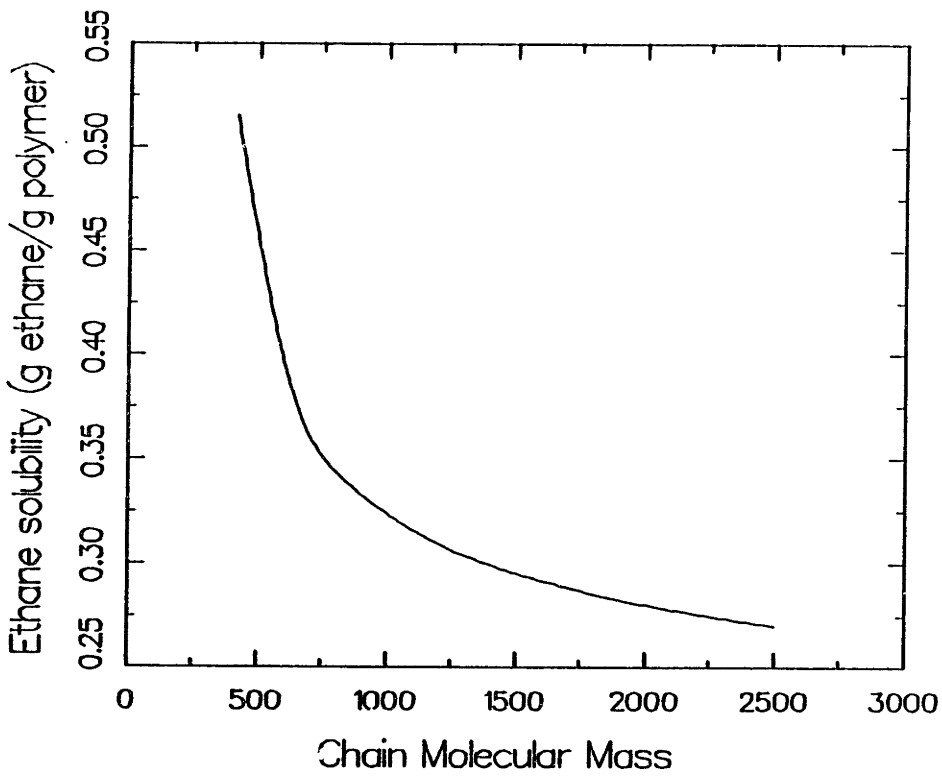

Figure 4.16: Lattice model predictions for the solubility of ethane in polystyrene at 8.5 MPa and 333K, with δ_{12}= 0.018.

employed the lattice EOS to estimate the variation of the amount of SCF dissolved in the solid phase, as the molecular weight of the polymer changed. In Figure 4.16 we show lattice model predictions for ethane solubilities in different molecular mass polystyrenes at 8.5 MPa and 333K (δ_{12} =0.018). The quantity of ethane dissolved in the polystyrene phase (in units of g ethane/g polymer) levels out asymptotically to a value of 0.25 g ethane/g polymer. At a molecular weight of 800 g mole^{-1} the solubility has a value of 0.32 g ethane/g polymer, while at 2000 g mole^{-1} the corresponding number is 0.26 g ethane/g polymer. Since we employ polystyrenes of M_n 800 and 2060 g mole^{-1}, therefore, the assumption of using solid phase compositions on a SCF-free basis will not cause large errors.

4.3.3 Sensitivity of Lattice Model Predictions

The lattice model fits to experimentally measured partition coefficients were obtained with the use of a single adjustable parameter, δ_{12}. In this section we examine the sensitivity of the lattice model predictions to changes in δ_{12}.

We examine a single case: the solubility of polystyrene chains in a ethane-propane mixture (*ca.* 87:13 by mole), which was correlated with the lattice model with a δ_{12} =0.03. On performing a sensitivity analysis we show that,

$$\left.\frac{\partial \ell og_{10} K_i}{\partial \delta_{ij}}\right]_{T,P} = 2.39 - 3.32\, X_i \qquad (4.18)$$

Eq(4.18), which represents a generally observed qualitative trend for the polystyrene-SCF mixtures examined in this work, shows that both C_0 and C_1 [the slope and intercept defined in Eq(4.4)] as predicted by the model are

sensitive to the actual value of δ_{12}. This proves further that the lattice model is appropriate for the modelling of polymer-SCF equilibria since we can reproduce accurately both the intercept and slope of the K_i vs X_i line with the use of a single adjustable parameter, δ_{12}.

CHAPTER 5

SOLUBILITY OF POLYMERS IN SUPERCRITICAL FLUIDS: SUMMARY OF EXPERIMENTAL AND MODELLING RESULTS

In Chapter 4 we have presented experimental measurements for the solubility of polystyrene chains in SCF at several operating conditions. Also, these data have been correlated with a statistical-mechanics based lattice equation of state that was developed to model mixtures of molecules of disparate sizes (Chapter 3). In this chapter we summarize the important results related to the fractionation of polymers using SCF.

5.1 SOLUBILITY OF POLYMERS IN CONVENTIONAL SOLVENTS

First, we examined the solubility of polystyrene in conventional solvents: liquids and ideal-gases. A partition coefficient, K_i, was defined for the distribution of a polymer of chain length i between the solvent phase and the polymer phase,

$$K_i = w_i^v / w_i^s \tag{4.1}$$

Here w_i represents the mass (or weight) fraction of the relevant chain length polymer in the appropriate phase: v represents the solvent phase composition and s represents the polymer phase compositions on a solvent free basis.

When the partition coefficients obtained from the solubility of polystyrene chains in n-heptane were plotted against the chain molecular weight the resultant relationship was a log-linear one. Alternately, the partition coefficients of any mer may be correlated to its chain length X_i, by the equation,

$$\ell og_{10} K_i = A(T) + B(T)\ X_i \qquad (4.3)$$

This relationship between K_i and X_i has already been reported in the literature. However, the data presented here are for individual chain lengths, while in the past results based only on average molecular weights have been reported for liquid solvents.

Analysis of the results obtained from the solubility of polystyrene in n-heptane at 298K [Figure 4.5] show that liquid solvents are poor fractionating media for polymers on the basis of molecular weight, and hence allow for a relatively large loading of the longer chains in the solvent phase. With the use of a gaseous solvent, however, good fractionation can be obtained, but the loading of polymers in the gas phase is low. Liquid and gaseous solvents thus represent the two extreme cases of fractionating behaviour obtainable by the use of conventional solvents.

5.2 SOLUBILITY OF POLYMERS IN SCF

We then examined SCF to explore the possibility of obtaining a fractionating behaviour intermediate between a gaseous and a liquid-like solvent. To this end we employed ethane at 25 MPa and 333K to solubilize two different polystyrene samples (M_n~ 2060 g mole^{-1}, M_w/M_n~ 1.2; M_n~ 800 g mole^{-1}, M_w/M_n~ 1.1). The important results from this investigation are summarized below:

- Data, when plotted as ℓnK_i vs. polymer chain length [Figure 4.3], show that SCF are intermediate in their fractionating behaviour under these conditions; i.e., the partition coefficients for different chain length polymers lie between the values obtained from n-heptane and an ideal gas. Data in this figure also demonstrate that Eq(4.3), which is valid for conventional solvents is also applicable to the ethane-polystyrene system at 25 MPa and 333K.
- In Figure 4.3 it is also seen that K_i values obtained from the two different polystyrene samples fall on the same straight line. K_i,

therefore, is essentially independent of the composition of the parent polymer, suggesting that the polymer phase in contact with the ethane behaves as an ideal solution. We employ this important deduction as the starting point in our modelling since we may now deal with a linear combination of several n-mer-SCF quasi-binaries rather than a multicomponent polymer-SCF equilibrium.

- Solid phase compositions have been employed on a solvent-free basis in the definition of K_i [Eq (4.1)]. From a theoretical analysis we show that the quantity of SCF dissolved in the polymer does not change appreciably with polymer molecular weight for the samples employed in our experiments. This definition of K_i will, therefore, incorporate all the essential physics regarding the solubility of polymers into SCF.
- Modelling of the experimental data has been performed with a statistical-mechanics based lattice model equation of state with the use of a single adjustable parameter, δ_{12}. We show that all data at this operating condition, above a molecular of ~1200 g $mole^{-1}$, can be correlated with a constant value of δ_{12} ($\simeq$ 0.018). Also, in this modelling it has been assumed that polystyrene under all experimental conditions is at a thermodynamic equilibrium state; i.e., we assume that the polymer is above its glass transition temperature.

The sensitivity of the partitioning behaviour of SCF to changes in following operating conditions was then studied:

(1) Pressure (8.5-34 MPa)
(2) Temperature (313-333 K)
(3) Solvent (CO_2, ethane and a mixture of ethane and propane).

Results from these experiments are summarized below.

a. Changes in Pressure: The density (and hence the solvent power) of an SCF changes continuously from gas-like to liquid-like as its pressure is raised. Increases in pressures were thus effected to verify the approach to liquid-like behaviour of supercritical ethane.

Results reported in Section 4.2.3.1 demonstrate that as the ethane pressure is increased from 8.5 MPa to 34 MPa (at 333K) the partition coefficients of the various styrene oligomers increase and continuously approach the value obtained in the experiments conducted with n-heptane. As expected, the behaviour of the SCF approaches a liquid-like character as its pressure is increased. As at 25 MPa, the data at all pressures show a log-linear dependence of K_i on chain length. A theoretical analysis with the lattice EOS also showed that the log-linear dependence of K_i on polymer chain length is a universal result that is expected to be valid across most commonly encountered polymer-SCF systems.

Data obtained at these pressures were correlated with the statistical mechanics based lattice EOS, at all chain lengths and pressures, employing the same value of δ_{12} (= 0.018) that was employed at 25 MPa. The lattice EOS thus provides us with a predictive tool for the polystyrene-ethane system since it can correlate experimental data across variations in pressure and chain length (above 1200 g $mole^{-1}$) using a constant value of δ_{12}.

On plotting the data for different chain length polymers on a K_i vs pressure basis we showed that the behaviour of the isotherms for macromolecular compounds is qualitatively different from the character of the corresponding curves for small molecule solutes. For example, for the lowest molecular mass considered (624 g $mole^{-1}$ in this case), the partition coefficients increases rapidly at a pressure around 8 MPa (corresponding to ρ_c of the SCF solvent) and begin to level off at pressures near 10 MPa. However, model predictions for the partition coefficient of the polymer chain of molecular mass 2040 g $mole^{-1}$ show that its solubility does not rise very sharply at 8 MPa, but that it is still increasing at a relatively high pressure of 40 MPa.

From a theoretical analysis we showed that although the K_i vs P curves for different chain length polymers have different qualitative natures, if we examined the quantity $(1/X_i)\partial \ell nK_i/\partial P]_{T,\sigma}$ as a function of

pressure then the data for all molecular weights collapse to a single curve. We thus have demonstrated the existence of a governing universality in the behaviour of different polystyrene chain lengths when they were dissolved into supercritical ethane.

b. Variations in Operating Temperature: Changes in the temperature of operation affect the partitioning of polymer chains into an SCF due to two conflicting effects. First, as temperature increases at a constant pressure, the vapour pressures of compounds increase. This effect should enhance the solubility of materials into SCF. However, the density of the SCF decreases with increasing temperature making the partitioning behaviour of the fluid more "gas-like".

Data presented in section 4.2.4 show that the partition coefficients for all chain length polystyrenes (with ethane as the SCF) decrease slightly as temperature is raised from 313K to 333K. This illustrates that the dominant effect of changing temperature is a reduction in the solubilities of the different chain length polymers due to a decrease in the density of the fluid phase.

The lattice EOS was employed for the correlation of experimental data at the three different temperatures (313, 323 and 333K respectively). It was found that the value of δ_{12} employed at 333K could also be used for quantitatively fitting experimental trends at the other two temperatures. The lattice EOS thus allows us to model the polystyrene-ethane system across variations in chain length, pressure and temperature with a single interaction parameter (δ_{12}) that is independent of these variables.

c. Data obtained using different solvents: The effect of the variation of solvent quality was also examined. Three different solvents were employed in the analysis (CO_2, ethane and a 87:13 by mole mixture of ethane and propane at 25 MPa and 333K). Data for these systems were also correlated by the lattice EOS, again by using a single value of δ_{12} across variations of chain length for each system.

Of the three solvents studied, CO_2 was shown to be the most gas-like under these conditions. A reason for the poor solvent nature of CO_2 can be understood when the interaction parameter employed in the lattice EOS for the polystyrene-CO_2 is examined (=0.08). The corresponding δ_{12} value for the polystyrene-ethane system is 0.018. Since a large value of δ_{12} implies that the interaction between unlike molecule segments is energetically less favourable than the energy of interaction between like segments, this offers an explanation for the relatively poor solvent quality of supercritical carbon dioxide.

Since propane is a liquid solvent at these operating conditions, a mixture of ethane and propane is expected to display a fractionation behaviour intermediate between ethane and a conventional liquid solvent. Experimental results for the ethane-propane mixture show that it indeed is a more liquid-like solvent than ethane at 25 MPa and 333K. This deduction also suggests that, the effect of pressure on the partitioning behaviour of a SCF can be duplicated by adding varying quantities of liquid additives to an SCF solvent.

CHAPTER 6

MODELLING OF PRECIPITATION POLYMERIZATION IN SUPERCRITICAL FLUIDS

6.1 INTRODUCTION

Reactions in supercritical fluids (SCF) represent a nascent discipline and to date little work has been done in this area. A review paper by Bala Subramaniam and McHugh (1986) documents the existing literature in this field. To our knowledge, precipitation polymerization reactions in SCF have not been reported. In the ensuing discussion, therefore, we will attempt to focus our attention on the two areas of interest to us, viz.

- The existing literature in the field of precipitation polymerizations in liquid solvents.
- A review of modelling homogenous, single-phase polymerization reactions conducted at high-pressure.

The goal of this chapter is to combine the existing knowledge in these areas along with the theory developed for the partitioning of polymers into SCF (Chapters 3 and 4) to predict average molecular masses, molecular mass distributions and other relevant information for precipitation polymerization reactions in SCF.

6.1.1 Modelling of Precipitation Polymerization Reactions

There exists almost no references in the literature on the modelling of precipitation polymerization reactions. This is attributable to the fact that in the case of precipitation polymerizations in liquid solvents, the product polymer is seldom glassy and hence reaction continues in the

coacervate phase. The final polymer compositions are thus system dependent: the number of particles, the surface area to volume ratios of the particles, stirring rate etc., may become the dominating effects. The understanding of these two aspects hinge on the appreciation of the relevant nucleation phenomena that govern the formation of precipitate particles. Fitch and Tsai (1970) present a theoretical approach to the modelling of the nucleation process. Ray and Jain (1975) and Barrett and Thomas (1975) attempt to explain the phenomenon of precipitation in a qualitative manner. According to both these groups the nucleation process can occur either due to "self nucleation" (when a chain becomes so long that it can nucleate by itself) or "aggregate nucleation" (when several chains aggregate and form a nucleus). Ray and Jain (1975) state that the controlling nucleation process is dictated by temperature, with self nucleation controlling at high temperatures. They also claim that, at low temperatures perhaps 10-25 chains aggregate and form a stable nucleus that then precipitates.

Barrett and Thomas (1975) present a detailed review of the variety of theoretical techniques used to model dispersion polymerization systems, including the nucleation process. The dynamically controlled threshold molecular weight for precipitation has been calculated in this work using a theory of homogenous nucleation (Nielsen,1964). The knowledge of the solubility of chains in the specific solvent is required in order that this theory may be applied. This solubility was obtained using the Flory-Huggins model for the excess Gibbs energy of the mixture (Flory, 1953,1941,1942; Huggins, 1941,1942). The threshold chain length also depends on the kinetics of the propagation step and on the surface tension of the polymer-solvent interface. Subsequent to the first particle being formed, the concept of homogenous nucleation is no longer relevant since the particles formed now act as nuclei for the growing oligomers in solution. This fact has been substantiated by the evidence that, after the initial nucleation burst, the number of particles remains essentially constant (Hoffman, 1976). The oligomers in solution thus, can be captured by the existing particles either "irreversibly", or can participate in an "equilibrium" with the particle surface. Theories exist for both these

processes but they have not been substantiated with experimental data (Fitch and Tsai, 1970).

The precipitated polymer has chains that are both terminated and unterminated. If the threshold of precipitation is higher than the average degree of polymerization achieved in the solution phase, then, most of the chains that precipitate will be terminated. If,on the other hand, the degree of polymerization is higher than the threshold, most of the precipitated oligomers will have active chain ends. The reactivity of the unterminated radicals in the precipitate is determined by the quantity of monomer present in the precipitate, the nature of the solvent and the temperature of operation. The temperature of operation is an important variable since, in the case of polymers below their glass transition temperature, as the temperature is reduced, the chains tend to coil and occlude the radicals thus reducing their reactivity.

6.1.2 Reactions in High-Pressure Gases

The understanding of reactions under high-pressure entails the appreciation of the structure and properties of the reaction transition state. Eckert (1972) provides an overview of the field and teaches the relationship between the structure and properties of the transition state and the measured activation volumes. Ehrlich (1971) and Abraham and Ehrlich (1975) also demonstrate that the proper understanding of the activation volumes of the reactants and transition state is essential for the interpretation of reaction rate parameters for the bulk polymerization of ethylene at elevated pressures (~100 MPa).

In transition state theories (Moore and Pearson, 1981) a bimolecular reaction can be represented as,

$$A + B \rightleftharpoons (AB)^{\ddagger} \longrightarrow AB \qquad (6.1)$$

where a true thermodynamic equilibrium has been assumed between the

transition state, $(AB)^{\ddagger}$, and the reactants A and B. The reaction rate for this bimolecular reaction, k_r, can be expressed in terms of the transition state and reactants as

$$k_r = (k_B T/h)\ K_c^{\ddagger} \tag{6.2}$$

where k_B is the Boltzmann's constant, T the temperature in Kelvin, h the Planck's constant and $K_c^{\ddagger}$ is the equilibrium constant between the activated complex and the reactants based on concentrations (Ehrlich, 1971).

$$K_c^{\ddagger} = \frac{[AB^{\ddagger}]}{[A][B]} \tag{6.3}$$

where the square brackets represent concentrations. This constant can be rewritten following Ehrlich (1971) as,

$$K_c^{\ddagger} = \frac{\rho f(AB^{\ddagger})/P\phi(AB^{\ddagger})}{[\rho f(A)/P\phi(A)]\times[\rho f(B)/P\phi(B)]} \tag{6.4a}$$

where the fundamental relationship between the fugacity of a component (f), and its corresponding fugacity coefficient (ϕ) has been invoked. ρ is the molar density of the SCF mixture and P the operating pressure. Now, we may rewrite Eq.(6.4a) as,

$$K_c^{\ddagger} = \frac{K_f^{\ddagger}}{(\rho/P)\ K_{\phi}^{\ddagger}} \tag{6.4b}$$

where $K_f^{\ddagger}$ is the equilibrium constant based on fugacities, defined in fashion analogous to Eq.(6.3). $K_\phi^{\ddagger}$ is then the equilibrium constant based on fugacity coefficients. The pressure dependence of k_r, the reaction rate constant, can now be derived from standard thermodynamics, through the use of the equation set (6.2)-(6.4) (Ehrlich,1971).

$$\left.\frac{\partial \ell n k_r}{\partial P}\right]_{T,y_A} = -\sum \nu_i (\bar{v}_i/RT - \kappa_T) \qquad (6.5)$$

Here, y_A is the mole fraction of component A in the mixture, κ_T the isothermal compressibility of the reacting mixture and overbars denote the partial molar volumes of the appropriate mixture component. In precipitation polymerizations conducted in vicinity of the critical point of the solvent, two facts are of significance: the isothermal compressibility, κ_T, is very large. Also, in this regime, the partial molar volumes of dilute, non-volatile components can take on large values, negative or positive (Eckert, 1972; Abraham and Ehrlich, 1975). The value of the reaction rate constant, k_r, therefore, can take on values in this regime, very different from values in liquid solvents.

For the bulk polymerization of ethylene at elevated pressures (~100 MPa at T~400 K), however, Ehrlich and Mortimer (1970) report propagation rate constant values, k_p, of the same order of magnitude as those found in the polymerization of vinyl polymers in liquid solvents. Abraham and Ehrlich (1975) emphasise, therefore, that the anomalous values of reaction rate constants due to pressure effects are valid only in the immediate region around the critical point of the solvent.

Apart from the effect of the solvent on the absolute value of reaction rate constants, Ehrlich and Mortimer (1970) suggest that the mechanism of a free-radical initiated polymerization in high-pressure gases is similar to the corresponding reaction mechanism in liquid solvents. That is, the steps occurring normally in a free-radical polymerization system: free-

radical initiation, propagation and termination due to addition and disproportionation all happen in this system. This is a rational conclusion, since the steps involved are chemical in nature and it is reasonable to assume that we cannot affect the chemical steps in a kinetic process purely by physical means, as in this case. However, SCF have been used to alter the selectivity of a reaction towards the formation of a desired product over an undesired one (Subramaniam and McHugh, 1986).

6.2 MODELLING OF SCF PRECIPITATION POLYMERIZATION

The time evolution of a precipitation polymerization reaction in an SCF can be thought of as occurring in three, distinct phases:

- Initially, the reaction mixture, composed of a known quantity of SCF, monomer and initiator is in a *single-phase, homogenous* solution. Reaction begins through the decomposition of initiator to form free-radicals. These free-radicals then add monomer to form longer chain-radicals in a propagation step. The reaction is terminated by a bimolecular addition or disproportionation [Eqs.(2.9)-(2.13)].
- As the reaction proceeds in time, the concentrations of polymer chains (in principle, both terminated and unterminated) increase, and at some point they nucleate to form a second, solid phase.
- Subsequent to this precipitation step, at all times, polymers of all chain-lengths equilibrate across the two phases, following a partition law. A relevant example would be the partition law presented in Chapter 4 for the distribution of polymer chains between a coacervate-phase and an SCF-phase; however, partition coefficients for the various chain length polymers, as determined from reaction experiments (presented in Chapter 7) will be employed. Reaction continues to occur in the SCF phase; it is assumed that no reaction occurs in the precipitate-phase.

We shall now formulate each of these steps into a mathematical model and discuss the solution procedure adopted to solve the set of equations so obtained.

A point to be emphasised in this case, is that we assume that no reaction occurs in the precipitate phase. Extrapolation of the results of Wang et al., (1982) suggest that the glass transition temperature for polystyrene in the presence of CO_2 at our temperature of operation (333K, P > 10 MPa) is in the vicinity of 325K (see Figure 6.1). So, while the coacervate may not necessarily be a glass at these conditions, its viscosity is still very high, suggesting that the reaction rate in this phase may be very small. These same trends may be expected from ethane, and we assume this to be valid since no data exists to show the effect of ethane on the glass-transition temperature of polystyrene. [This assumption will be verified in Section 7.2.3.1.] Also, it must be highlighted that if reaction were to occur in the precipitate phase, then, a model for the reaction may need to be system specific.

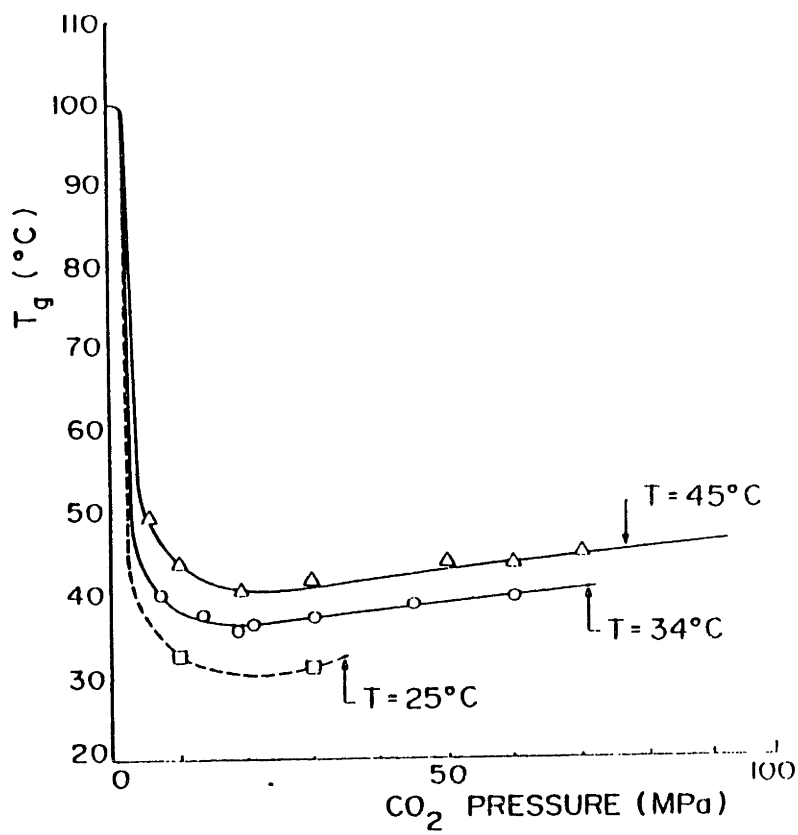

Figure 6.1: Glass transition temperatures of polystyrene at different temperatures and CO_2 pressures (Wang et al., 1972)

6.2.1 Modelling of a Polymerization prior to precipitation

The modelling of a single-phase polymerization involving initiation, propagation and termination is available in the existing literature [Flory, 1953; Odian, 1985]. The following reactions are assumed to occur in this step,

$$I \xrightarrow{k_i} 2R^{\bullet} \tag{6.6}$$

$$R^{\bullet} + M \xrightarrow{k_p} RM^{\bullet} \tag{6.7}$$

$$RM_x^{\bullet} + M \xrightarrow{k_p} RM_{x+1}^{\bullet} \qquad \text{(for any } x > 0\text{)} \tag{6.8}$$

where k_i refers to rate constant of the initiation step and k_p for the chain-propagation reaction. Also, note that steps (6.7) and (6.8) have the same reaction rate constant, k_p, although Flory (1953) has suggested that these two rate constants may be different. These reactions are followed by the termination of the propagating radicals.

$$RM_x^{\bullet} + RM_y^{\bullet} \xrightarrow{k_t} P_{x+1} + P_{y+1} \tag{6.9}$$

where P_{x+1} and P_{y+1} are terminated chains, one of which contains a double bond. In this context, it must be stressed that the termination mechanism in Eq(6.9) represents the extinction of free-radicals by a disproportionation mechanism. It is the underlying assumption therefore, that the termination of radicals by addition is not a significant step in our model. The rationale for this assumption will be investigated in Section 6.4. The general rate equations governing this reaction sequence can be written following Flory (1953) as,

$$\frac{d[I]}{dt} = -k_i[I] \tag{6.10}$$

$$\frac{d[R^\bullet]}{dt} = k_i[I] - k_p[M][R^\bullet] - k_t[R^\bullet]\times\sum[RM_x^\bullet] \qquad (6.11)$$

$$\frac{d[RM_x^\bullet]}{dt} = k_p[M][RM_{x-1}^\bullet] - k_p[M][RM_x^\bullet] - k_t[RM_x^\bullet]\times\sum[RM_x^\bullet] \qquad (6.12)$$

$$\frac{d[P_{x+1}]}{dt} = k_t[RM_x^\bullet]\times\sum[RM_x^\bullet] \qquad (6.13)$$

There are a few points that need clarification in the formulation of the equation set (6.10)-(6.13).

-In Eq.(6.6) it is seen that an initiator molecule dissociates to form two free-radicals. However, in Eq.(6.11), it is formulated that only one free-radical reacts with the monomer. In the formulation of free-radical mechanisms, a factor *f* is normally introduced to account for the fraction of the free-radicals created, that add a monomer in a propagation step. Flory (1953) states that the initiator efficiency, *f*, is around 60%. For convenience, therefore, *f*, is taken to be 0.5, and together with the factor 2 incorporated in the numerical value of k_i.

- The reaction rates, in Eq.(6.10)-(6.13), are written in terms of *concentrations*. Erickson (1987) has suggested that for mixtures in the vicinity of their critical points it is more appropriate to rewrite these equations in terms of *fugacities*. However, Ehrlich and Mortimer (1970) suggest that the use of fugacities are more appropriate for reactions in systems at gas-like densities. Since the issue is still unclarified, we will proceed to work with concentrations, but choose to obtain order of magnitude estimates for the change in reaction rate constants (due to pressure effects) from fugacities. This, and other ramifications of using fugacities rather than concentrations will be discussed in section 6.4.

- In Eq.(6.13), it has been assumed that chain termination occurs only by disproportionation. It will be shown in Section 6.4 from the use of transition state theories that the free radicals in the system are terminated mainly by disproportionation since the rate constant for the termination by addition step is slowed due to the presence of the SCF

solvent.

In this context, it must be recognized that to maintain a mass balance we need to formulate an equation that will ensure the conservation of mass for the monomer.

$$[M] = [M]_0 - \sum x[RM_x^{\cdot}] - \sum x[P_x] \qquad (6.14)$$

Here $[M]_0$ is the initial monomer concentration, and [M] represents the monomer concentration at any instant of time. The formulation of the rate expressions in a single-phase reaction medium is now complete. We must highlight here that several, simplifying assumptions have been made in the preceding formulation. This must be placed in perspective when it is recognized that the thrust of this work is aimed at obtaining an understanding of the important underlying phenomena in this new area of research. All assumptions are therefore made towards retaining the important points in the mathematical model, while avoiding complexities, which at this point would only lead to relatively small corrections in the ultimate solution.

6.2.2 Modelling of Nucleation Phenomena

As stated earlier, there exist theories based on classical thermodynamics (Modell and Reid, 1983) which predict particle sizes and threshold concentrations of different chains in a supersaturated phase. To predict the rate of nucleation, these theories require a knowledge of the degree of supersaturation, and surface tension between the mers in the solid, precipitate phase and the gas-phase (Nielsen,1964). Due to these prerequisites, therefore, the implementation of such a model is not easy.

An alternate formulation would be to allow the single phase polymerization, described in the preceding section, to proceed until a mer of a certain length reaches its spinoidal, or its limit of stability. The limit of stability of a polymer of any given chain-length, in a mixture

with n components, can be obtained by the solution of an algebraic equation of the type,

$$y^{(n)}_{n+1,n+1} = 0 \qquad (6.15)$$

where $y^{(n)}_{n+1,n+1}$, represents the second partial derivative of the n^{th} Legendre transform of the basis function, $\underline{U}$ (the internal energy). More details of this calculation are presented in Modell and Reid (1983) and Kumar and Reid (1986). To be able to obtain numerical values for the limits of stability we need to have an appropriate EOS. The lattice EOS presented in Chapter 3 would be an appropriate tool in this context.

In the application of the model to real precipitation polymerization systems this calculation would be of importance in the determination of the number of particles, the particle sizes and other relevant information. However, these aspects lie beyond the scope of this work since we are at this point, interested primarily in predicting the molecular mass distributions of the polymers in the precipitate and the SCF phase. It was found in our analysis with the model that the final, product molecular mass distributions were independent of the theory of nucleation selected, and depended primarily on kinetic rate constants and partition coefficient data (See Chapter 7 for details).

In the course of this work, therefore, a simple theory of nucleation was employed. This involved the location of the first chain length that reached its binodal concentration in the gas-phase. The binodal concentration of a chain can be determined from the partition law,

$$\ell og_{10}(K_x) = \ell og_{10}(w^v_x/w^s_x) = C_0 - C_1 X_x \qquad (4.4)$$

by setting w^s_x equal to unity. We would like to emphasised here, that this "theory of nucleation" is appropriate only in this context. If more detailed information such as particle sizes, or volume to surface area ratios of the particles formed are desired then a more exact theory of nucleation, as outlined earlier in this section must be employed.

6.2.3 Modelling subsequent to precipitation

Following precipitation, it is assumed that the solid phase is inert and no further reaction occurs in this phase; the reaction set, Eq.(6.6)-(6.9) continues to be valid in the SCF phase. It is assumed that the polymer chains in the SCF and the precipitate phase are always at thermodynamic equilibrium. (Experimental data will be examined in Chapter 7 to verify this assumption.) The differential equation set Eq.(6.10)-(6.13) will now have to be reformulated to allow for the presence of the solid phase that is in equilibrium with the reaction-phase.

In this case, the initiator mass balance equations can be written in a difference form as,

$$([I]_{t+\Delta t}-[I]_t)(MW)_I/\rho_{SCF} = -k_i[I]_t\,\Delta t(MW)_I/\rho_{SCF} - (MW)_I((m_s[I])_{t+\Delta t} - (m_s[I])_t)/K_2\rho_{SCF} \quad (6.16)$$

where ρ_{SCF} is the density of the SCF (in kg m^{-3}) and $(MW)_I$ is the relative molecular mass of the initiator. K_2, is the partition coefficient of the initiator between the gas-phase and the precipitate-phase and m_s is the *mass of precipitate per unit mass of the SCF phase*. The left hand side of Eq(6.16) represents the net accumulation of the initiator in the SCF phase (in units of kg initiator/kg SCF), between times t and t+Δt. The first term on the right hand side is the destruction of initiator to form free-radicals in the same time period, and is analogous to the appropriate term in Eq(6.10). The second term then represents the rate of precipitation of initiator into the precipitate phase in the appropriate time interval, t to t+Δt.

Dividing Eq.(6.16) by Δt and taking the limit as $\Delta t \longrightarrow 0$, the final differential equation for the concentration of the initiator in the SCF-phase can be obtained.

$$\left(1+\frac{m_s}{K_2}\right)\frac{d[I]}{dt} = -k_i[I] - \frac{[I]}{K_2}\frac{dm_s}{dt} \tag{6.17}$$

dm_s/dt represents the rate of change of the mass of the solid phase (per unit mass of SCF phase) as a function of time. In a fashion similar to Eqs.(6.16) and (6.17) we can now develop the governing differential equations for the radicals and polymers of all chain lengths in the gas-phase.

$$\left(1+\frac{m_s}{K_1}\right)\frac{d[R^\bullet]}{dt} = k_i[I] - k_p[M][R^\bullet] - k_t[R^\bullet]\sum[RM_x^\bullet] - \frac{[R^\bullet]}{K_1}\frac{dm_s}{dt} \tag{6.18}$$

$$\left(1+\frac{m_s}{K_x}\right)\frac{d[RM_x^\bullet]}{dt} = k_p[M][RM_{x-1}^\bullet] - k_p[M][R^\bullet] - k_t[RM_x^\bullet]\times\sum[RM_x^\bullet] - \frac{[RM_x^\bullet]}{K_x}\frac{dm_s}{dt} \tag{6.19}$$

$$\left(1+\frac{m_s}{K_{x+1}}\right)\frac{d[P_{x+1}]}{dt} = k_t[RM_x^\bullet]\times\sum[RM_x^\bullet] - \frac{[P_{x+1}]}{K_x}\frac{dm_s}{dt} \tag{6.20}$$

In these equations, K_x represents the partition coefficient of the polymer chain of length x monomeric units. In this formulation, we have assumed that unterminated radicals and terminated polymer chains of the same chain length partition between the SCF phase and the polymer phase in exactly the same fashion. To complete this representation, the mass balance equation for the monomer is,

$$[M] = [M]_0 - \sum x[RM_x^\bullet] - \sum x[P_x] - m_s[M]/K_1 - \sum x[\lambda_x]m_s/K_x \tag{6.21a}$$

$$= ([M]_0 - \sum x[\lambda_x](1+m_s/K_x))/(1+m_s/K_1) \tag{6.21b}$$

where $[\lambda_i]$ is the concentration in the gas-phase of *all* species of chain-length i (i.e., both terminated and unterminated chains) and $(MW)_i$ is the

molecular mass of the species.

$$[\lambda_i] = [RM^{\bullet}_{x-1}] + [P_x] \tag{6.22}$$

The time derivative of the monomer concentration, [M], can now be easily obtained from Eq.(6.21). The only unknowns in Eq.(6.21) are m_s and dm_s/dt. m_s can be tracked simply by closing the mass balances for each mer at every instant of time. The calculation of dm_s/dt, however, is not straightforward. It must be remembered that polymer chains in the SCF and the precipitate phase are in equilibrium at all times. Since,

$$K_i = w_i^v/w_i^s \tag{4.1}$$

is always valid, we can write that,

$$w_i^s = [\lambda_i](MW)_i/\rho_{SCF}K_i \tag{6.23}$$

where w_i^s is the mass fraction of the i^{th} mer in the precipitate phase. Since the w_i^s must always add up to unity, we get,

$$\sum[\lambda_i](MW)_i/\rho_{SCF}K_i = 1 \tag{6.24}$$

or that,

$$\sum d[\lambda_i]/dt\ (MW)_i/\rho_{SCF}K_i + d[M]/dt\ (MW)_1/\rho_{SCF}K_1 = 0 \tag{6.25}$$

The respective derivatives required in Eq.(6.25) can now be obtained from Eq.(6.17)-(6.21), and it is seen that the only unknown is dm_s/dt. Analytical expressions can thus be obtained for this derivative,

$$\frac{dm_s}{dt} = \frac{k_p[M]\sum(MW)_i([RM^{\bullet}_{i-2}] - [RM^{\bullet}_{i-1}])(K_1-K_i-m_s)/(m_s+K_i)}{\sum[\lambda_i](MW)_iK_i/(m_s+K_i)K_i + [M]/K_1} \tag{6.26}$$

where the summation in the numerator goes from 2 to infinity. The mathematical formulation for the polymerization subsequent to precipitation is now complete.

6.2.4 Digression: A Steady-State Model

In the past it has been common practice to model free-radical polymerization processes as reactions in which radicals are at a steady state (Flory, 1953; Odian, 1985; Froment and Bischoff,1979). This simplifying assumption has been found to work relatively successfully for the understanding of conventional single-phase, free-radical polymerizations. This genre of models has an advantage in that it allows for a closed form, analytically tractable solution to the set of algebraic equations that govern a steady state polymerization. Controlling variables can thus be identified, and experiments designed with these criteria. It was therefore our aim to explore the feasibility of using a steady-state model for the better understanding of our system.

Prior to precipitation, the steady-state model may be derived by assuming that all radical concentrations as dictated by Eqs.(6.11) and (6.12) must be at a steady state. The left hand sides of these two equations must therefore be set to zero to obtain the "steady-state" radical concentration profiles preceding precipitation. In this time period, however, it must be realized that terminated polymer chains will not be at a steady-state since polymers will be formed continuously by the termination of radicals. In this model, therefore, the rate equation for polymer chains, Eq.(6.13), will continue to be valid. Radical concentrations may be obtained from solving Eqs.(6.11) and (6.12) after setting the respective derivatives to zero,

$$[RM^{\bullet}_{x-1}] = \frac{k_p[M][RM^{\bullet}_{x-2}]}{k_p[M] + k_t \times \sum[RM^{\bullet}_{x}]} \qquad (6.27)$$

On summing Eq.(6.11) and (6.12) for all values of x, one may show that,

$$\sum[RM_x^\bullet] = (k_i k_t [I])^{1/2} \tag{6.28}$$

Thus,

$$[RM_{x-1}^\bullet] = \frac{k_p [M][RM_{x-2}^\bullet]}{k_p [M] + (k_i k_t [I])^{1/2}} \tag{6.29}$$

$$\sim (k_i [I]/k_p [M])\ e^{-(x\ (k_i k_t [I])^{1/2}/k_p [M])} \tag{6.30}$$

$$\sim (k_i [I]/k_p [M])\ e^{-x/\nu_{c1}} \tag{6.31}$$

where ν_{c1} [$= k_p[M]/(k_i k_t [I])^{\frac{1}{2}}$] is the kinetic chain length obtained during the reaction. We now examine the appropriateness of the application of this "steady-state" model to SCF precipitation polymerizations before precipitation. Two cases may be envisaged:

- If ν_{c1} is larger than $(1/C_1)$ [in Eq.(4.4)], then this model suggests that precipitation must occur at zero time. In this case, the "steady-state" model is, therefore, be invalid until the instant of precipitation.
- However, in the special case where ν_{c1} is smaller than $(1/C_1)$, this model will predict non zero precipitation times and may thus be used to predict gas-phase concentrations prior to precipitation.

Subsequent to precipitation, let us assume that all concentrations (on a monomer and initiator free basis), in both phases are constant. The steady state model thus assumes that all mers, not including the monomer and the initiator, are at quasi-steady states. The only change then, will correspond to a increase in mass of the solid due to precipitation. On

solving the algebraic equation set [Eq.(6.17)-(6.21)], obtained by setting the left hand sides to zero, we obtain the steady-state gas phase concentrations,

$$[RM_x^\bullet] = \frac{(k_i/k_p)\,([I]/[M])}{\prod_j (1 + (k_t/k_p)(\sum[RM_x^\bullet])/[M]) + (dm_s/dt)/K_j k_p [M])} \tag{6.32}$$

$$[P_{x+1}] = K_{x+1} \frac{k_t \sum[RM_x^\bullet]}{(dm_s/dt)} [RM_x^\bullet] \tag{6.33}$$

This also allows for the definition of dm_s/dt as,

$$\frac{dm_s}{dt} = \frac{k_i [I]}{\rho_{SCF}} M_n \tag{6.34}$$

where M_n is defined through the expression,

$$M_n = \frac{1}{\sum w_x/(MW)_x} = \frac{\sum n_x (MW)_x}{\sum n_x} \tag{6.35}$$

w_x and n_x are the weight fraction and the number fraction of the x^{th} mer in the <u>precipitate</u> phase, respectively, and $(MW)_x$ its molecular mass. It is seen that the rate of precipitation is proportional to the average molecular mass of the <u>solid</u> in equilibrium with the SCF-phase, and that the appropriate average is the number averaged molecular mass of the precipitated polymer.

The accuracy and validity of the assumptions made in the derivation of this model will be discussed in Chapter 7, where it is employed for the correlation of experimental data obtained from SCF precipitation polymerizations.

6.3 IMPLEMENTATION ASPECTS

The implementation of the transient model was performed in three stages. At time 0, it was assumed that only monomer and initiator were present in the SCF phase. Initially, the reacting mixture was a homogenous single phase, and the relevant rate equations [Eqs (6.10) to (6.13)] were solved by a marching technique, where time was incrementally increased and the set of equations iterated upon to yield the radical and terminated polymer concentrations at that time.

The instant of precipitation, then, was determined when an appropriate chain length polymer reached its binodal concentration. At this instant, this chain was assumed to form a second phase. Also, all other chains were assumed to precipitate, such that the gas and the precipitate phases were in equilibrium. The mass of the precipitate, m_s, at this instant was obtained by performing a mass balance on the whole system, i.e.,

$$\sum [\lambda_i]^{eq}(MW)_i/\rho_{SCF} + \sum w_i^s m_s = \sum[\lambda_i](MW)_i/\rho_{SCF} \qquad (6.36)$$

where $[\lambda_i]^{eq}$ represents the concentration of i^{th} chain-length subsequent to the precipitation, in the SCF-phase. $[\lambda_i]$ is the concentration of the same mer *prior* to precipitation, and $[\lambda_i]^{eq}$ and w_i^s are related through Eq.(6.23). The mass of the solid, m_s, was obtained at the instant of precipitation by the iterative solution of Eq.(6.31); a simple, bisection method was found to be robust enough to deal with this solution.

Subsequent to this step, the transient model was solved by the numerical integration of Eq.(6.18)-(6.21), again through the use of the same marching technique used earlier. The mass of the precipitate was updated through the

use of Eq.(6.26). A variable integration step had to be used, with the step size determined through the equation,

$$\Delta t << m_s/(dm_s/dt) \qquad (6.37)$$

A variable time step was necessary since, at the instant of precipitation, the time derivatives of concentrations were large and picking a large time step causes numerical instabilities to appear in the solutions for the concentrations of the chains in the precipitate phase.

6.4 REACTION RATE CONSTANTS FROM ACTIVATED STATE THEORIES

To obtain the relative rates of the different kinetic steps in an SCF polymerization it must be realized that the partial molar volumes of dilute components in SCF, normally, have large negative values. From the LeChatelier principle, a bimolecular reaction which yields a single product molecule, such as the propagation or the termination by addition step, are unfavourable under these conditions. The overall manifestation of this effect is a reduction in the propagation (or termination by addition) rate constant. By extension, an opposite behaviour may be observed in a kinetic step, like the initiation reaction, where the initiator dissociates to form two free radicals. Also, steps like the termination by disproportionation, wherein two molecules react to form two product molecules, will not be affected dramatically by the presence of a SCF component in the mixture.

We now attempt to obtain an order of magnitude estimate for the value of the propagation rate constant under these conditions, using an activated state theory developed by Ehrlich (1971). Eqs. (6.2) and (6.4) provide mathematical expressions relating the reaction rate constant, k_r, in terms of the fugacities and fugacity coefficients of the reactants and the activated state. Now, $K_f^{\ddagger}$ is independent of pressure since it is based on a unity reference state (Ehrlich,1971). Eqs (6.2)-(6.4) thus imply that,

$$(k_r P K_\phi^\ddagger / \rho) \neq f(P) \tag{6.38}$$

We may now expand $K_\phi^\ddagger$ in terms of the fugacity coefficients of the respective mixture components,

$$K_\phi^\ddagger = \frac{\phi(AB)^\ddagger}{\phi(A)\ \phi(B)} \tag{6.39}$$

Let us now assume that all the three fugacity coefficients to be of the same order of magnitude: approximately 10^{-4} or smaller [T_r~1.5, P_r~1.5, under infinitely dilute conditions (Debenedetti and Kumar, 1986a,1986b)]. $K_\phi^\ddagger$, thus, under supercritical conditions, is of the order of 10^4 or larger. Under the conditions where precipitation polymerizations are conducted, i.e., for ethane at ~ 15MPa and 333K, ρ is of the order of 10^4 mole m^{-3}. For conventional liquid solvents, $K_\phi^\ddagger$ lies between 0.1 and 1 at pressures of 0.1 MPa and densities of ~10^4 mole m^{-3}. Using Eq.(6.33) suggests therefore, that

$$(k_r)^{SCF} \sim [10^{-1}\text{-}10^{-2}]\ (k_r)^{liq} \tag{6.40}$$

The reaction rate constants for the propagation and the termination by addition steps for a polymerization in a SCF solvent, in the vicinity of its critical point, are approximately 2 orders of magnitude smaller than the corresponding values in a liquid solvent.

By the same rationale let us now examine the effect of the use of SCF on the rate of the initiation step. The initiation step may be thought of as occurring in the following manner,

$$I \rightleftarrows (R^\bullet R^\bullet)^\ddagger \longrightarrow 2R^\bullet \tag{6.41}$$

Application of Eq.(6.38) will immediately suggest that the initiation step will not be affected substantially due to the presence of the SCF solvent,

i.e.,

$$(k_i)^{SCF} \sim (k_i)^{liq} \qquad (6.42)$$

It has been suggested by Subramaniam and McHugh (1985) that the initiator step will be accelerated due to the lower viscosity of the SCF, which reduces the so called "cage-effect". While this may be true, the point to be emphasised here is that the relative rates of initiation and propagation in the reaction mechanism in SCF solvent are substantially altered from the corresponding values in conventional, liquid solvents.

In summary, the use of activated state theories suggest that for the polymerization reactions in SCF solvents near their critical points, the ratio of reaction rate constants based on concentrations for the propagation step to the initiation step is approximately 2 orders of magnitude smaller than corresponding values in liquid solvents. Also, the rate of termination by addition under these conditions is substantially smaller than in liquid like conditions. The other rate constants remain relatively unaltered, suggesting that termination by disproportionation is probably the dominant termination mechanism in this regime. Since the ratio of the propagation to the initiation rate constant is reduced in SCF solvents as compared to liquid solvents, it is to be expected that smaller kinetic chain lengths would result in SCF polymerizations. The use of SCF fluids as solvents for polymerization reactions, therefore, offers us a probe of the mechanism of free-radical polymerizations, since the presence of the SCF selectively affects the rates of some steps, while leaving the others essentially unaltered.

CHAPTER 7

PRECIPITATION POLYMERIZATIONS IN SUPERCRITICAL FLUIDS: MEASUREMENT, RESULTS AND DISCUSSION

7.1 EXPERIMENTAL APPARATUS

Experiments to demonstrate the feasibility of precipitation polymerization reactions in SCF were carried out in two different setups, both of which are discussed below. The first incorporated a reactor that allowed for the visual observation of the reaction medium, but could not be used for obtaining quantitative data. The second apparatus then corrected this problem; however, no visual observation was possible.

7.1.1 Reactor Setup Allowing Visual Observation

A schematic representation of this setup is shown in Figure 7.1. The main elements of this apparatus are:

- Reactor: A high pressure optical cell (Jerguson gage model 19-TCH-40) was used as the reactor. The cell is a rectangular channel of approximate dimensions 32cm × 1.3cm × 1.3cm (internal volume ~ 50 ml), between two high-strength borosilicate glass plates and a 316 stainless steel enclosure. The cell afforded a full view of the contents of the reactor and was used to monitor the onset of precipitation, which manifested itself as a increased turbidity in the contents.

- Recirculation System: The reaction mixture was removed from the bottom of the gage and recirculated externally to the top of the reactor with a double head minipump (Milton Roy, double head, explosion proof, 46/920 ml/hour minipump) to ensure complete mixing of the contents.

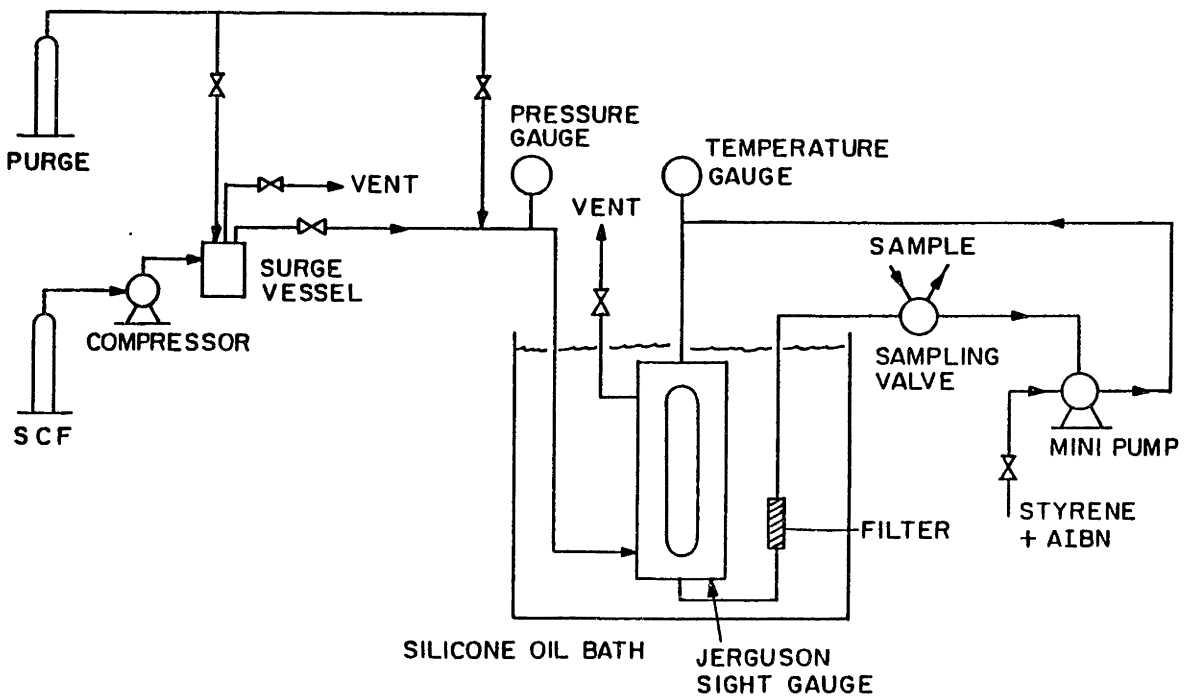

Figure 7.1: Schematic of apparatus with visual observation

- SCF feed: The solvent gas from the cylinder was pumped to the necessary pressure by a diaphragm compressor (Aminco, J46-13411) and fed into a 2 litre tank that served as a surge vessel. This vessel ensured

that required quantities of the SCF at pressure were available when necessary. The SCF, from this tank, was introduced into the bottom of the Jerguson gage through $1/8^{th}$ inch, 316 stainless steel tubes.

- Temperature Control: The reactor was placed in a silicone oil bath (Dow Corning DC200) and thermostatically controlled to ±0.01K with a Thermomix 1460 temperature controller. All recirculation tubes were jacketed with heating tape to ensure that they were isothermal.

- Measurement of Temperature and Pressure: The pressure in the reactor was monitored continuously with a Heise pressure gauge with an accuracy of ±0.01 MPa (Heise gauge, 0-40MPa) and the temperature measurements were performed with iron-constantan thermocouples accurate to ±0.2K.

- Safety Considerations: The reactor was equipped with a rupture disk (Autoclave Engineers) with a burst pressure of 30 MPa which was smaller than the pressure rating of the Jerguson gage (35 MPa). The tubing volume was small, <*ca.* 10% of the reactor volume, and therefore, the tubes were not specifically protected against pressure surges. Also, the holding vessel for the SCF was equipped with a rupture disk (Autoclave Engineers). All vessels were equipped with vent valves so as to ensure that the entire system could be manually vented to the hood in less that 2 min. A combustible gas detector (Sears Gas Alarm) was installed in the laboratory to warn the operator of possible leaks in the system. Other safety devices such as rubber gloves and eye goggles were also constantly employed.

Operating Procedure: A known quantity of freshly distilled styrene (Polysciences, stabilized with 20 ppm hydroquinone) mixed with AIBN (Polysciences, 99% pure) was metered into the sight gage by the minipump. The SCF was now introduced into the reactor at the desired pressure. The contents were recirculated until the solution was homogenous and in a single-phase. Recirculation continued and after approximately 15 min, the solution turned turbid due to the precipitation of polymer chains from solution. Later, *ca.* after 15 more minutes, the solution turned clear again and small particles of precipitate were deposited on the walls of the reactor.

The experiment was continued for an additional 4-6 hours. Small quantities of filtered reacting mixture (*ca.* 25 μl) were obtained using a sampling valve (Valco Instruments, 6 port HPLC valve) at different times during the course of the reaction. This sample was subsequently flashed to atmospheric pressure, where the dissolved styrene and other oligomers in the SCF phase dropped out of solution. This precipitate was collected in a U-tube and analyzed by SEC. (See Appendix I for details of the SEC analysis.) No reliable analysis of the gas phase polymers could be obtained since the quantities of the monomer and the oligomers in the 25 μl SCF sample were extremely small. This situation could have been alleviated by obtaining a larger SCF-phase sample; however, if macroscopic samples (~ 1 ml) were taken, the conditions in the reactor would not remain unchanged.

At the end of the reaction, the Jerguson gage was flushed with fresh ethane, and finally vented. Since the precipitated polymer was deposited on the walls of the reactor, it was not blown out by this venting process. The precipitated polymer was dissolved in THF (Omnisolv Grade, EM Sciences, TX0282-1) and analysed by SEC. Since a large quantity of THF was required to wash the reactor thoroughly the sample was too dilute to be analyzed successfully by SEC. The product polymer in this THF was not concentrated further i.e., by heating or vacuum distillation, since it was believed that the polystyrene would react further in this step. The time and effort required to prepare the reactor after a reaction also made the use of this setup inefficient for data collection. (Results obtained from these experiments are summarized in Section 7.2.1). An alternate experimental apparatus was therefore employed for determining quantitatively the gas and solid phase compositions.

7.1.2 An Alternate Experimental Setup

The new technique was planned to improve on the deficiencies of the older method and was chosen to satisfy the following criteria:

- The reactor should hold enough material to determine both the SCF-phase and polymer-phase compositions accurately and reproducibly.

- Reactor contents must be stirred to maintain spatially uniform concentrations of all species in the reactor.
- The setup should be so designed so that experiments could be run without constant observation.
- Pressure and temperature in the reactor should be monitorable, preferably continuously.

The new setup consisted of a 150 ml, 316 stainless steel sampling vessel rated to 34.5 MPa, that served as a reactor (Whitey, 50D4-150). This reactor was equipped with two valves (Nupro, SS-4PDM4-F4) for charging the vessel and subsequent sampling. Reactor pressure was monitored by pressure gauges (Matheson, 0-35 MPa) and each vessel was equipped with a release valve, that could be set for any desired operating pressure (Nupro,SS-4R3A1-G).

Initially, the reactor was charged with styrene, AIBN and ethane and the quantities of each determined by weighing. The vessel was then placed in a thermostatically controlled, variable speed shaker bath (Blue M) to ensure that the contents were isothermal and well stirred. The water bath temperature was determined by a mercury thermometer of accuracy ±0.1K, and subsequently monitored by an iron-constantan thermocouple. The reaction could be conducted for any desired length of time since the reaction is conducted in the hood and the release valve can be set so that the contents can be maintained at the desired pressure.

At the end of the reaction, the vessel was flushed with fresh ethane at operating conditions. The displaced reaction mixture is vented to atmospheric pressure through a flashing valve, when the dissolved monomer, initiator and oligomers drop out of solution and are collected in a cold U-tube. The reactor is vented and subsequently washed with a small, carefully measured quantity of THF which is then analyzed by SEC. The SCF-phase sample, in the U-tube, is also dissolved in THF and analyzed by SEC.

7.2 EXPERIMENTAL RESULTS

7.2.1 Preliminary Polymerization Experiments

Initial experiments in the Jerguson sight gage were conducted at relatively high concentrations of monomer (~ 20 wt% monomer and ~0.1 wt% of initiator) at 12 MPa and 333K with ethane as the SCF solvent. Under these conditions, it was demonstrated that the concept of precipitation polymerization in SCF is a sound one. The time evolution of such a reaction, as observed from these experiments, can be summarized into three distinct time regimes:

- At the outset, the mixture of SCF, monomer and initiator are present in a single, homogenous phase.
- After a small duration of time, *ca.* 15 min after commencement, the solution turns turbid. This turbidity is believed to be due to the precipitation of a product polymer that is insoluble in the SCF-phase.
- Subsequently, after approximately another half an hour, the solution became clear. We believe this change was due to deposition of the product polymer onto the walls of the Jerguson sight gage.

No further, visible changes occurred in the reactor contents (with continuous recirculation), even after 10 hours. As stated earlier, no quantitative data were obtained from this experimental setup, and the alternate technique was used in all subsequent reactions.

Precipitation polymerization of styrene in liquid n-heptane under comparable operating conditions, (i.e., all variables except pressure were maintained at similar values in both reactions), were also performed to contrast the mechanism of precipitation polymerizations in SCF to similar reactions in liquid solvents. It was observed that, qualitatively, the reaction mechanism in both systems seemed to follow similar time evolutions, i.e., the three time regimes discussed earlier also occur for reactions in n-heptane although the time for initial turbidity was longer (~ 2h). This

suggests that the use of SCF solvents, at least in principle, do not alter the physical processes that occurred in such reactions. However, the time scales in the reaction are smaller for SCF solvents, and this fact can be attributed to the relatively "poorer" solvent quality of SCF as compared to liquid solvents (In this context, a poorer solvent is one that affords better fractionation than liquid solvents, at the expense of solute loading).

7.2.2 Solubility of Monomer and Radical Initiator in SCF

Since the monomer, in relatively high concentrations, was found to be soluble in ethane at 12 MPa at 333K, no experiments were conducted to measure the VLE behaviour of styrene in ethane. Preliminary experiments for the solubility of styrene in CO_2 have been conducted (McHugh and Krukonis, 1986) and show that styrene and CO_2 are completely miscible under similar operating conditions (i.e., 12 MPa and 333K).

The styrene-ethane system (or the CO_2-styrene system), when viewed on a P-T projection has a continuous mixture critical line between the critical points of the two mixture components. This mixture, which is classified as Type I in the notation of Rowlinson and Swinton (1982), must therefore display complete miscibility above a certain pressure, at each supercritical temperature. A rough estimate of this pressure, at temperatures close to the critical point of ethane (305K), is the pressure that corresponds to the maximum change in density on the relevant isotherm (for example ~8.5 MPa at 333K). This argument is meant to be qualitative and if one desires to use operating pressures near the pressure of complete miscibility, careful experiments must then be performed to understand the phase behaviour of this binary mixture in this regime.

The solubility of the free-radical initiator (AIBN) in ethane at 333K and at several pressures has, however, been measured in this work. In Figure 7.2, experimental solubility data for AIBN in ethane along with predictions from the lattice model EOS are presented. The data shown are in the form of partition coefficients, defined as in Eq(4.1). (The partition coefficient

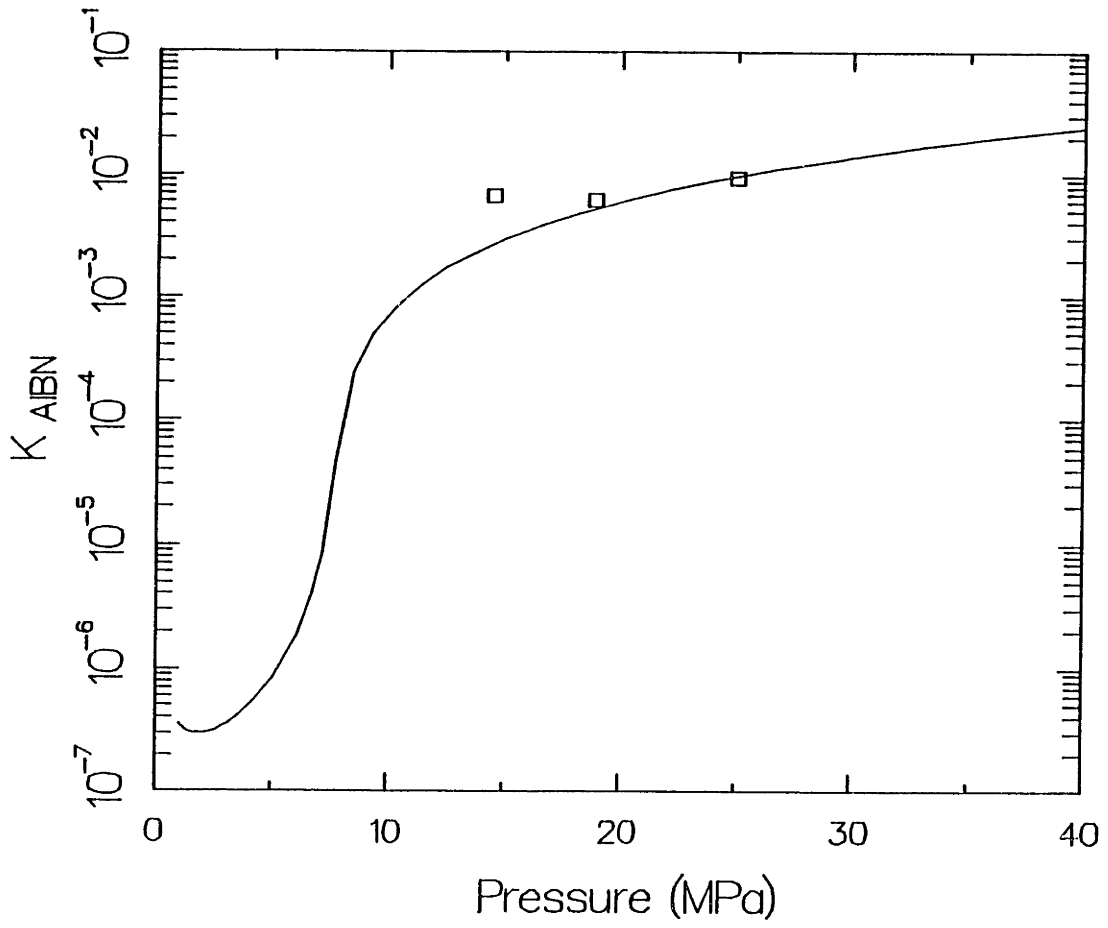

Figure 7.2: Solubility of AIBN in ethane at 333K. (□) are experimental data and (———) is the lattice model prediction with ϵ_{AIBN} *= 1590 J mole*$^{-1}$*,* v^**= 0.7 cc/g and* k_{ij}*=0.07.*

in this case, therefore, represents the mass fraction of AIBN in the SCF phase.) Figure 7.2 shows that AIBN is soluble to approximately 0.6 wt% in ethane under operating pressures of greater than 12 MPa at 333K.

In this context, the solubility of AIBN in ethane shows the trends with pressure expected for the solubility of small molecule solutes in SCF: i.e., that it increases sharply in the vicinity of the critical density of ethane, and subsequently levels out at a near constant value. This is in sharp contrast to the behaviour of polymeric chains of relatively high molecular mass (~2080 g mole^{-1} for polystyrene) in SCF under at the same

temperature, wherein the solubility is seen to rise even at pressures near 50 MPa (see Figure 4.8).

Another point to be emphasised is that, although the molecular mass of AIBN (162) is approximately that of a styrene dimer (208), the partition coefficients for the two are dramatically different. For example, at 333K and 12 MPa,

$$K\ (\text{AIBN}) \sim 0.006 \qquad (7.1a)$$

$$K\ (\text{Dimer}) \sim 0.35 \qquad (7.1b)$$

It is therefore, reasonable to expect that a ternary mixture of AIBN, ethane and styrene (monomer or dimer) *will not* behave as an ideal solution, and the effects of solution non-idealities have to be accounted when the modelling of the polymerization reaction is considered. Also, since the polymerization process is initiated by a free-radical formed by the thermal dissociation of an initiator molecule, there must be a initiator group at the end of each oligomeric chain. Short chain length polymers, therefore, should feel the effect of this end-group when they partition between the SCF-phase and the polymer-phase in a polymerization reaction. (These aspects will be considered in sections 7.2.3.1 and 7.3.2.)

7.2.3 Results from Alternate Polymerization Apparatus

7.2.3.1 Analysis of a Base Case

We begin our analysis of results from the "quantitative" polymerization experiments by considering results at a single set of operating conditions (viz. pressure, temperature, monomer concentration, initiator concentration, and reaction time); we chose experiments wherein styrene was polymerized in supercritical ethane at 333K and 17 MPa as the base case. It was found that a certain minimum monomer concentration was necessary to observe the presence of a precipitate phase. Experiments conducted with 1.65 wt% monomer (AIBN concentration was 5.83×10^{-5} gm/gm ethane), within the accuracy of the experimental technique, did not show the presence of a precipitated polymer at reaction times upto 24 hours. At this operating condition, apparently, no polymer precipitation occurs, and, this is attributable to the fact that the concentrations of oligomers produced will be smaller at lower [M]. It is reasonable to visualize therefore, that at this operating condition, the oligomer concentrations in the SCF phase are so small that they do not reach their saturation concentrations during the course of the reaction and thus do not nucleate out of the SCF-phase to form a precipitate.

Experiments were conducted at a higher monomer concentration (3.33 wt% monomer), while all other variables were held at the same values as in the earlier set of experiments (i.e., 5.83×10^{-5} gm initiator/gm ethane, 17 MPa and 333K). Under these conditions, at all reaction times examined (16h $\leq t_{rxn} \leq$ 44 h), a precipitate polystyrene phase with a composition distinct from the SCF phase was observed. In Figure 7.3, SEC traces for the product polymer and the polymer chains in the SCF are shown (t_{rxn} =24h). Both traces have large peaks corresponding to the monomer and dimer (or AIBN), thus indicating that both phases are constituted essentially of the monomer and the initiator. However, the more significant fact is the presence of a peak in the precipitate phase corresponding to a molecular mass of ~1000. Also, the SCF-phase trace essentially is "cutoff" (i.e., returns to the base line) at a molecular mass corresponding to the peak molecular mass in

the precipitate-phase. This verifies the presence of a strong cutoff in solubility of polystyrene chains in the SCF-phase on the basis of chain length. Although, for all examined reaction times, the same qualitative trends were obtained from the SEC traces, for smaller reaction times, the peak at a molecular mass of 1000 in the precipitate phase is attenuated, indicating a lower conversion of monomer to precipitated polymer. Intuitively, since we would expect the conversion to scale directly with some simple function of reaction time, this is not an unexpected result. (The effect of reaction time on polymer compositions is discussed later in this section.)

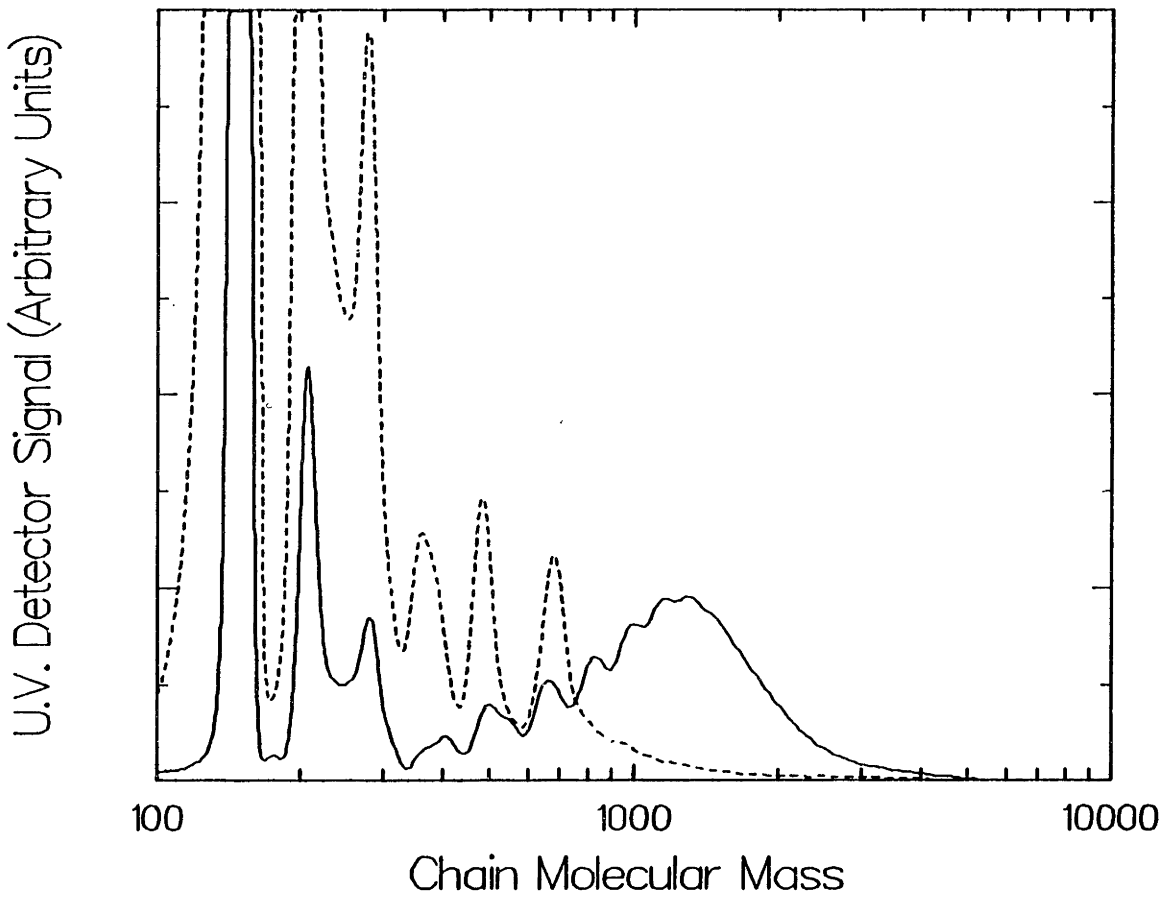

Figure 7.3: SEC traces for the product, precipitate polymer (———) and gas-phase polymers (----) at 17 MPa, 333K, for the precipitation polymerization of 3.33 wt% styrene in ethane initiated with AIBN for a reaction time of 24 hours. The two chromatograms are plotted on arbitrary scales and have different spans on the y-axis.

To understand further the mechanism of precipitation polymerization reactions, the SEC curves in Figure 7.3 were analyzed to obtain mass fractions of individual mers in each of the two phases. In Figure 7.4, we show the solid-phase (in units of gm. mer/gm. ethane-free solid) and gas-phase polymer compositions (in units of gm.mer/gm.ethane) as obtained from this analysis. Some conclusions can be made by examining these results:

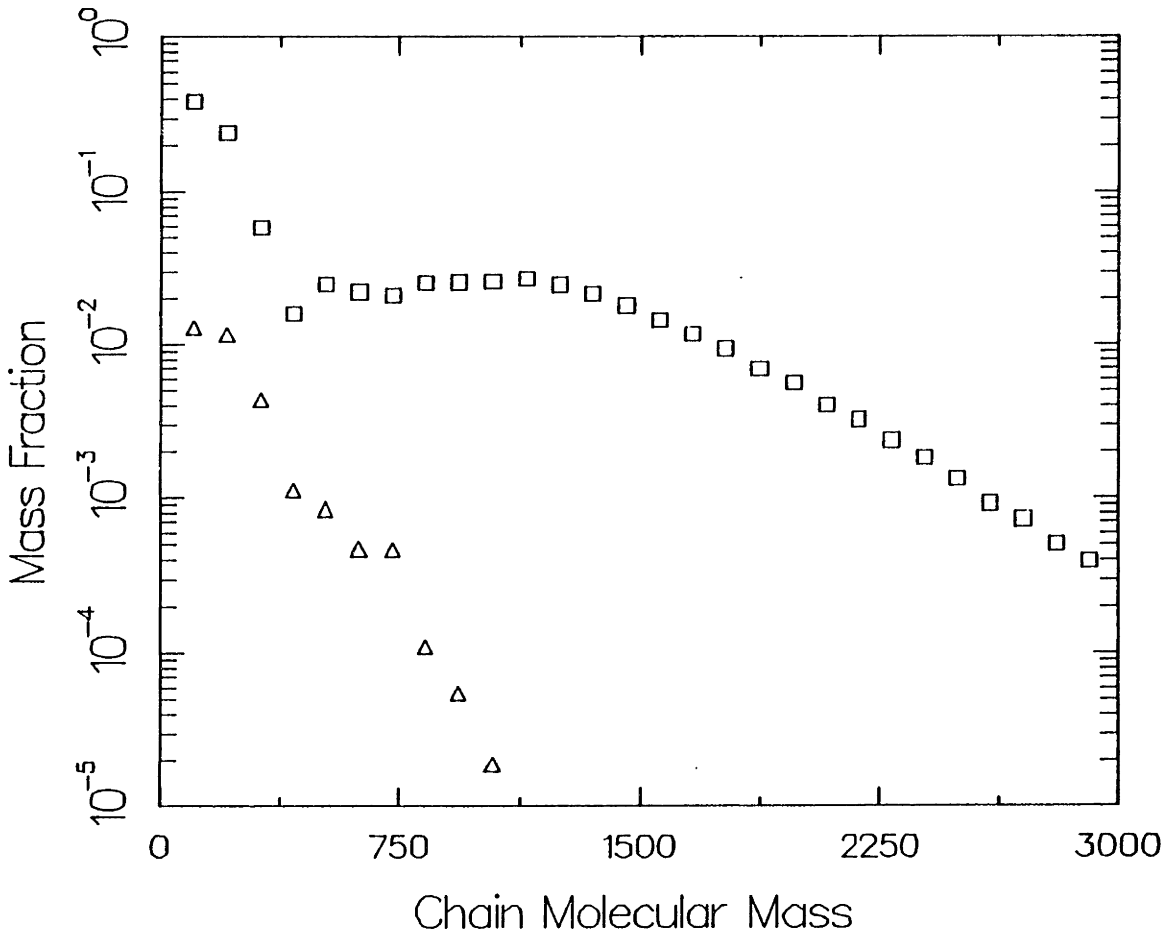

Figure 7.4: Compositions of the product, precipitate polymer (□; in units of gm. mer/gm. ethane-free solid) and gas-phase polymers (△, in units of gm mer/gm. ethane) at 17 MPa, 333K, for the precipitation polymerization of 3.33 wt% styrene in ethane initiated with AIBN for a reaction time of 24 hours.

- As stated earlier both phases are predominantly composed of monomer and dimer.
- Solid phase compositions show a peak in the vicinity of molecular mass ~ 1000. Beyond this molecular mass, the mass fraction of chains in this phase drop off *in a log-linear* fashion. Calculation of average molecule masses show that M_n~850, and M_w/M_n~1.25. (Monomer and dimer peaks have not been included in this calculation.) Precipitation polymerization reactions in SCF under these conditions, thus allows one to synthesise polystyrene with a relatively narrow molecular mass distribution, narrower than could have been obtained from solution polymerization reactions in liquid solvents with radical initiators. [In the case of an "ideal" free-radical, liquid-phase solution polymerization, M_w/M_n ranges between 1.5 and 2, depending on the termination mechanism, disproportionation or addition (also see Chapter 2).]
- The gas-phase compositions decrease in an essentially log-linear fashion with increasing chain molecular mass. Also, as stated earlier the quantity of chains above molecular mass ~ 1000, is too small to be detected by the analysis technique employed. To appreciate the shape of the molecular mass distribution in this phase, one must realize that in the gas-phase there are two competing steps: chain propagation [Eqs (6.7) and (6.8)] vs. precipitation of the relevant chain into the solid-phase. Qualitatively, it would be reasonable to expect that longer chains would preferably partition into the solid-phase. The rate of propagation of chains thus decreases with increasing chain length due to the reduced concentrations of longer chains in the gas-phase. The controlling aspect, therefore, is the governing law for the partitioning of chains between the solid-phase and the SCF-phase.

To infer the underlying partitioning law therefore, in Figure 7.5, we show the partition coefficients [defined as in Eq.(4.1)] calculated from data presented in Figure 7.4. These values are then compared to the partition coefficients for polystyrene chains between a polymer-phase and an ethane-phase under the same pressure and temperature conditions, as measured in

the solubility experiments [discussed in Section 4.2]. Some important points can be deduced by the examination of Figure 7.5:

- For molecular masses of 400-1100, there is a remarkable agreement between the partition coefficients measured in solubility experiments and in the precipitation polymerization reactions. These chains, thus, are at thermodynamic equilibrium across the two phases in a polymerization reaction, and that this equilibrium is defined by the partitioning behaviour of pure polystyrene chains between a polymer-phase and an SCF-phase.
- Partition coefficients for the monomer, dimer and trimer in the

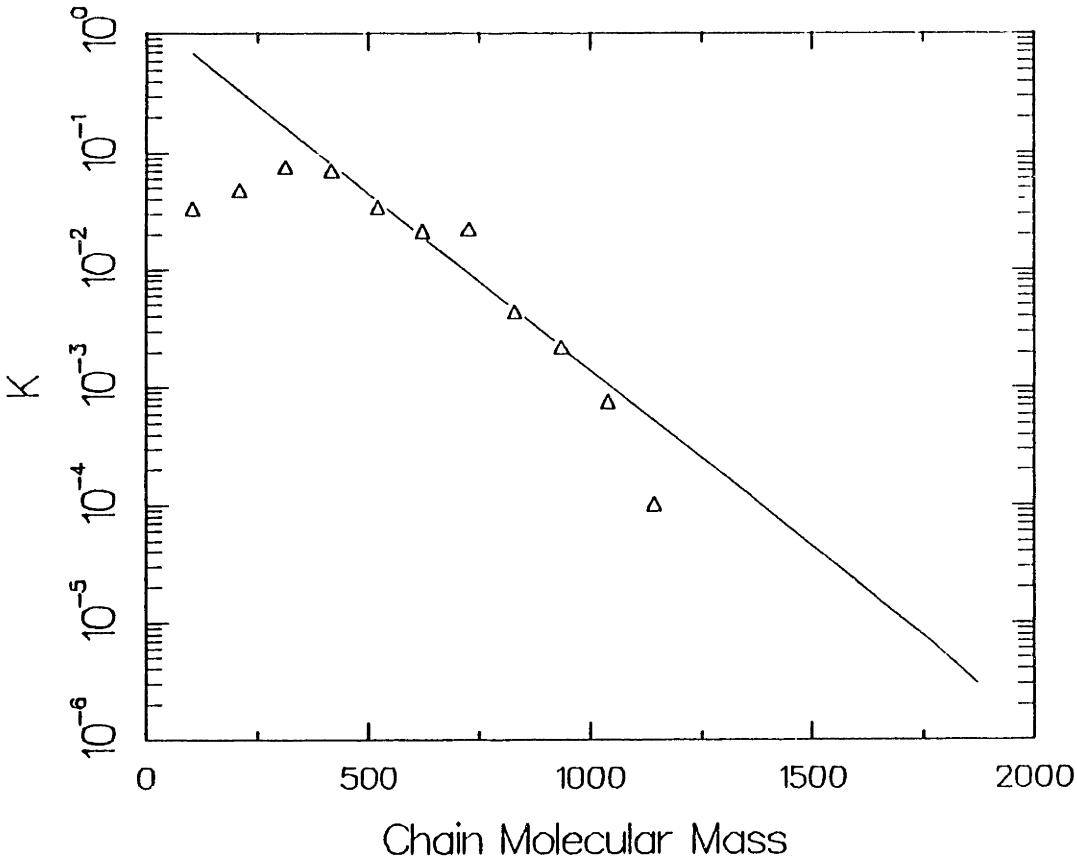

Figure 7.5: Comparison of partition coefficients of polymer chains between the polymer-rich phase and the SCF-phase as measured in solubility experiments (——), and precipitation polymerization reactions (Δ) with 3.33 wt% styrene in ethane with AIBN as radical initiator at 17 MPa and 333K.

polymerization experiments, however, are smaller than in the solubility experiments. It is believed that the presence of the initiator, which has a partition coefficient much smaller than the dimer molecule, modifies the behaviour of the smallest chains. This modification may be manifested in two different ways:

(a) Since the initiator dissociates and then propagates to form longer chains by addition to monomer, the end group for each oligomer chain necessarily possesses an initiator group. The partitioning behaviour of all chains, therefore, are influenced by the presence of the initiator group, with the smallest chains feeling the effect of this "end-group" the most. Since the partition coefficient of the AIBN is smaller than the corresponding styrene oligomer, the addition of this end-group will reduce the partition coefficient of a chain as compared to a "pure" polystyrene chain of the same degree of polymerization.

(b) Since the monomer and initiator molecules are dissimilar in properties (for example styrene, a liquid, is completely soluble in ethane under these conditions, while AIBN is soluble to only 0.6 wt% in ethane), it is expected that a ternary mixture of styrene-AIBN-ethane must necessarily possess some solution non-idealities, which might manifest themselves as a lower partition coefficient for the monomer and possibly the smallest chains. At higher molecular masses, the polymer chains and AIBN are now qualitatively similar in partitioning behaviour and hence do not feel the influence of solution non-idealities.

- Beyond a molecular mass of ~1000, the agreement between the partition coefficients measured in reaction and solubility experiments is not very good. This may be a manifestation of the lack of accuracy in our analysis technique in measuring mass fractions less than *ca.* 10^{-6}.

In summary, the phenomenon of precipitation polymerization in SCF is believed to be governed by a *dynamic equilibrium* of polystyrene chains of different molecular masses between the solid, precipitate-phase and the SCF-phase. For molecular masses greater than ~400 the equilibrium partition coefficients as measured in the solubility experiments control this fractionation, while below this molecular mass the equilibrium is affected due to the presence of dissolved initiator.

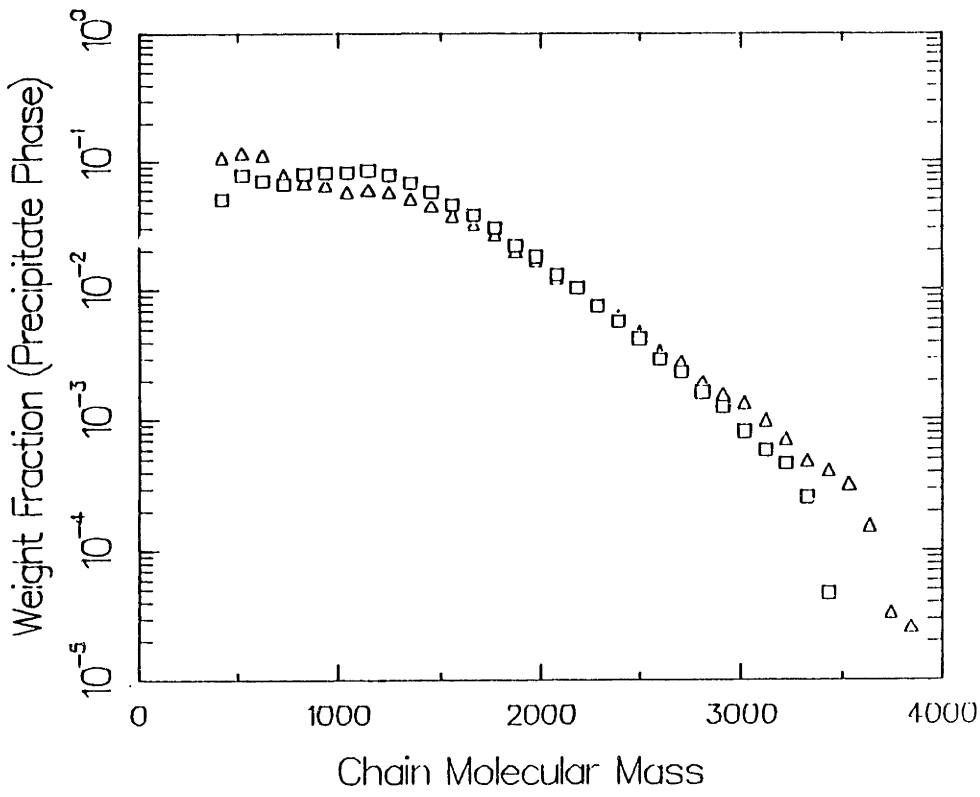

Figure 7.6: Composition of precipitate polymer, on a first three mer-free basis, for different reaction times for the precipitation polymerization of 3.33 wt% styrene in ethane, initiated with AIBN at 17 MPa and 333K. (Δ) is for t_{rxn}= 16 h, and (□) for t_{rxn}= 44 h.

It has already been mentioned that results obtained at different reaction times have the same qualitative trends. Experiments were performed for reaction times between 16 and 44 hours under the same operating conditions (i.e., 5.83×10^{-5} gm initiator/gm ethane, 3.33 wt% monomer at 17 MPa and 333K) to quantify these similarities. It was found that in all these reactions the product polymer had different concentrations of monomer and initiator, corresponding to different conversions. However, when data were examined on a first three mer-free basis,[9] the precipitate phase compositions were found to be essentially independent of reaction time. Compositions of

[9] We employ compositions on a first three mer-free basis since the AIBN elution time in the chromatographic analysis overlaps the peak times for the dimer and trimer.

the precipitate phase at two different times, on a first three-mer free basis are shown in Figure 7.6, to demonstrate this fact. Although the precipitate phase contains approximately 30 wt% monomer, no broadening of the molecular mass distribution seems to occur as one proceeds to longer reaction times, i.e., no Tromsdorff effect is observed. The reason for this is speculated to be due two factors:

- The precipitate phase has a high viscosity due to the presence of the higher molecular mass chains and initiator (the precipitate has ~20 wt% initiator, which is essentially crystalline in the pure state). The presence of these materials ensures that little diffusion of monomer occurs to the unterminated chains. Therefore, no reaction can occur in this phase.
- Also, ν_{c1}, the kinetic chain length, is small in this case due to the relatively small value of (k_p/k_t), as shown in Section 6.4. Most precipitated chains, therefore, will be terminated, providing a plausible explanation for the absence of reaction in the precipitate phase.

Convincing arguments for the absence of reaction in the precipitate phase may be provided only if macroscopic quantities of polymer are synthesised and analyzed for unterminated radicals, say by ESR.

The main results from the polymerization experiments at 17MPa, 333K, 3.33wt% monomer and 5.83×10^{-5} gm AIBN/gm.ethane are:

- The concept of precipitation polymerization in SCF solvents is feasible and product polymers of a *narrow* molecular mass distribution may be synthesized by this technique.
- The governing mechanism in these reactions is a thermodynamic phase equilibrium of polymer chains (of molecular masses > 300 g $mole^{-1}$) between the SCF-phase and precipitate-phase. This equilibrium is dictated by the pressure and temperature of operation for a chosen polymer-SCF system, as discussed in Chapter 4.
- The presence of initiator, which has a partition coefficient that is approximately two orders of magnitude smaller than the styrene

oligomer of a corresponding chain molecular mass, apparently governs the partitioning of low-molecular mass chains (molecular mass ≤300), between the precipitate-phase and the SCF-phase.

- Since the precipitate molecular mass distributions do not broaden as one proceeds to larger reaction times we assume that little or no reaction occurs in this phase at these operating conditions.

The effect of other operating conditions on the product polymer compositions must now be studied to complete this analysis. For this purpose, the influence of the changes in the following variables on the precipitate compositions were examined:

a. Pressure (12MPa, 17MPa and 25MPa)
b. Monomer Concentration (3.33 wt%, 5.0 wt% and 6.66 wt%)
c. Initiator Concentration (5.83×10^{-5}, 2.90×10^{-5} and 0 gm/gm. SCF)
d. Temperature (333K and 343K)

The results from these investigations are presented in the following sections of this chapter.

7.2.3.2 Experiments at Different Pressures

Precipitation polymerization reactions were carried out at different pressures to understand the effect of "solvent-quality" on the composition of the product polymer. It has been demonstrated in Chapter 4 that as pressure is increased, the solvent-character of an SCF moves from gas-like (low solubility, "strong" fractionation) to liquid-like (high solubility, "poor" fractionating power). At higher pressures, the solvent is less discriminating with respect to the fractionation of chains on the basis of molecular mass between an SCF-rich phase and a polymer-rich phase. At higher pressure, therefore, it is expected that the product obtained will be of a broader molecular mass distribution.

In Figure 7.7, the molecular mass distributions on a first three

Table 7.1: Molecular mass data for precipitated-polystyrene at different ethane pressures at 3.33 wt% styrene concentrations and 333K with AIBN as radical initiator.

Operating Pressure (MPa)	M_n	M_w	M_w/M_n
12.0	844	1017	1.20
17.0	850	1063	1.25
25.0	938	1193	1.27

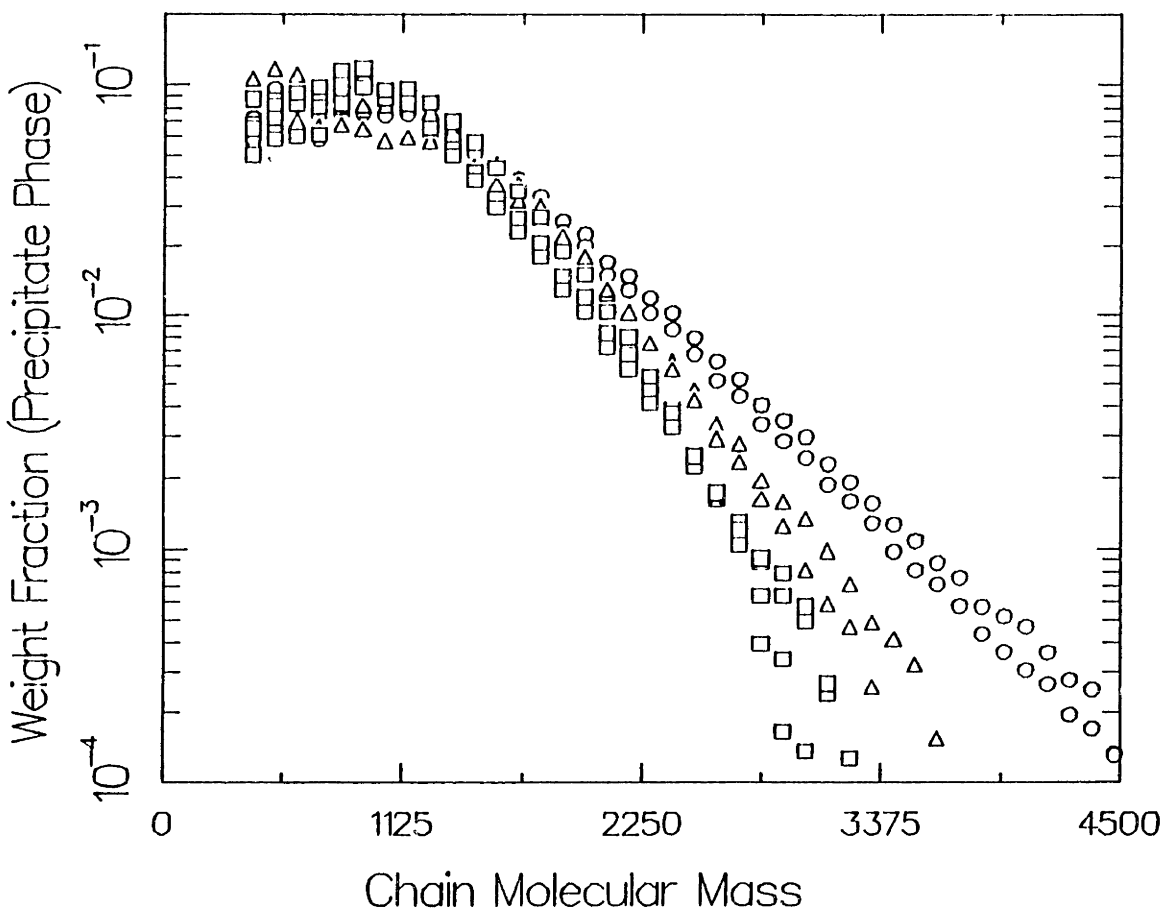

Figure 7.7: Composition of precipitate polymer, on a first three mer-free basis, at different pressures for the precipitation polymerization of 3.33 wt% styrene in ethane, initiated with AIBN at (□)12 MPa, (△)17 MPa and (o)25 MPa and 333K.

mer-free basis, for the precipitation polymerization of 3.33 wt% styrene at three pressures of ethane (12, 17 and 25 MPa at 333K) are shown. The corresponding average molecular masses are tabulated in Table 7.1. As was anticipated, when one proceeds to higher operating pressures, the molecular mass distribution of the precipitate phase are seen to become broader. (This is indicated by the smaller slope of the molecular mass distributions at high chain lengths.) An interesting point about the three pressure results shown in Figure 7.7 is that the peak molecular mass, apparently, is independent of the operating pressure and occurs in the vicinity of molecular mass ~1000 (i.e., degree of polymerization ~ 10). The peak molecular mass is, in the ranges of operation considered, probably determined by the kinetics of the reaction, along with the gross operating conditions, while being relatively unaffected by the density changes due to pressure variations. The breadth of the molecular mass distribution, in contrast, is sensitive to the operating conditions, and is governed essentially by the pressure of operation. This is a direct implication of the responsiveness of the solvent power of an SCF solvent to relatively small changes in operating pressure, as discussed in Chapter 4.

The partitioning behaviour of polystyrene chains between a polymer-rich and an SCF-rich phase in a precipitation polymerization reaction with an ethane solvent at 17 MPa and 333K has been presented in Figure 7.5. To study the effect of pressure on this partitioning behaviour, in Figures 7.8 and 7.9 we present experimental data for the compositions of the two phases; comparison of measured partition coefficients in the polymerization reaction and solubility experiments at 12 MPa and 25 MPa (monomer concentration is 3.33 wt% and AIBN concentration is ~ 5.8×10^{-5} gm/gm. ethane, and T is 333K) are also shown in Figures 7.10 and 7.11. Data at these two pressures corroborate the information regarding the partitioning behaviour obtained from experiments at 17 MPa, i.e., that the first three-mers have partition coefficients significantly smaller than the K values measured in solubility experiments. At 12 MPa it is seen that beyond the first three mers, agreement between the partition coefficients is excellent. At 25 MPa, the agreement is not as good, and the reason for this disagreement is speculated to be due to experimental error.

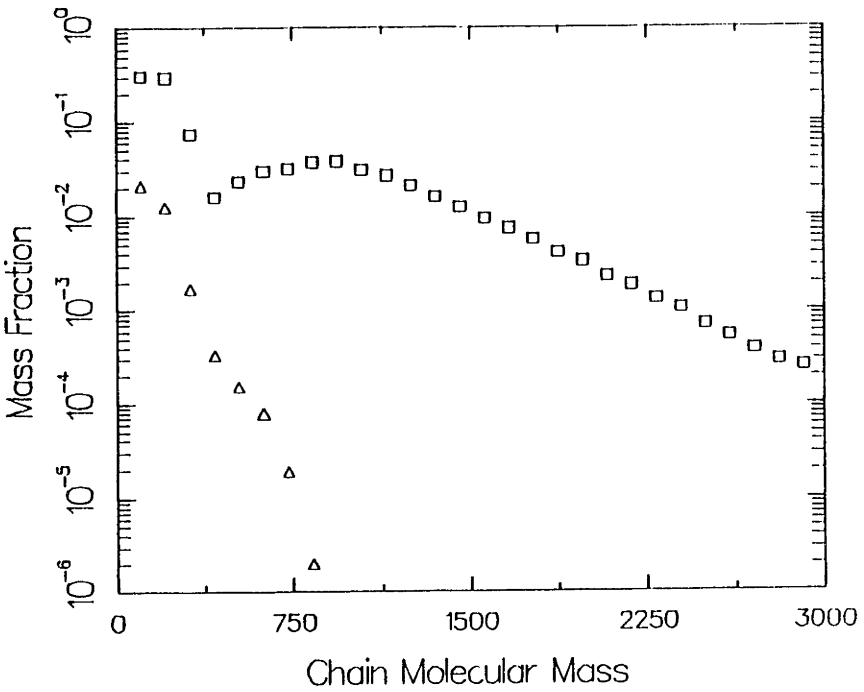

Figure 7.8: Compositions of the product, precipitate polymer (□; in units of gm. mer/gm.SCF-free solid) and gas-phase polymers (Δ, in units of gm mer/gm. ethane) at 12 MPa, 333K, for the precipitation polymerization of 3.33 wt% styrene in ethane initiated with AIBN for a reaction time of 24 hours.

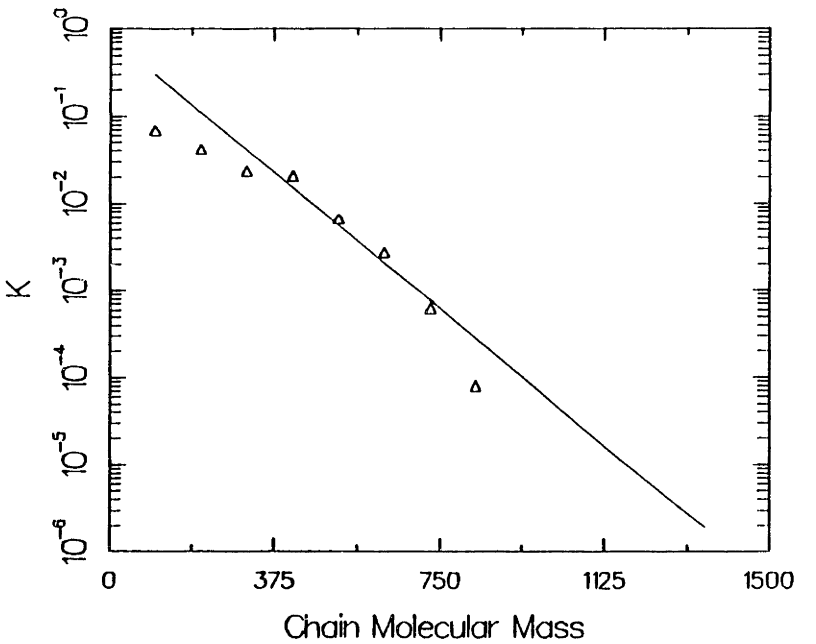

Figure 7.9: Comparison of partition coefficients of polymer chains between the polymer-rich phase and the SCF-phase as measured in solubility experiments (——), and precipitation polymerization reactions (Δ) with 3.33 wt% styrene in ethane with AIBN as radical initiator at 12 MPa and 333K.

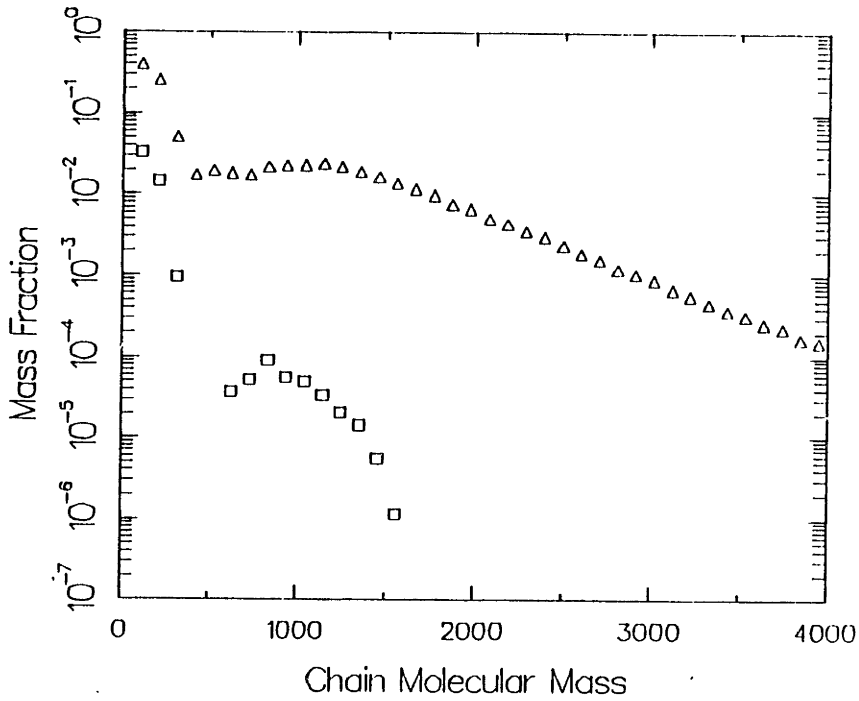

Figure 7.10: Compositions of the product, precipitate polymer (△; in units of gm. mer/gm.SCF-free solid) and gas-phase polymers (□, in units of gm mer/gm. ethane) at 25 MPa, 333K, for the precipitation polymerization of 3.33 wt% styrene in ethane initiated with AIBN for a reaction time of 24 hours.

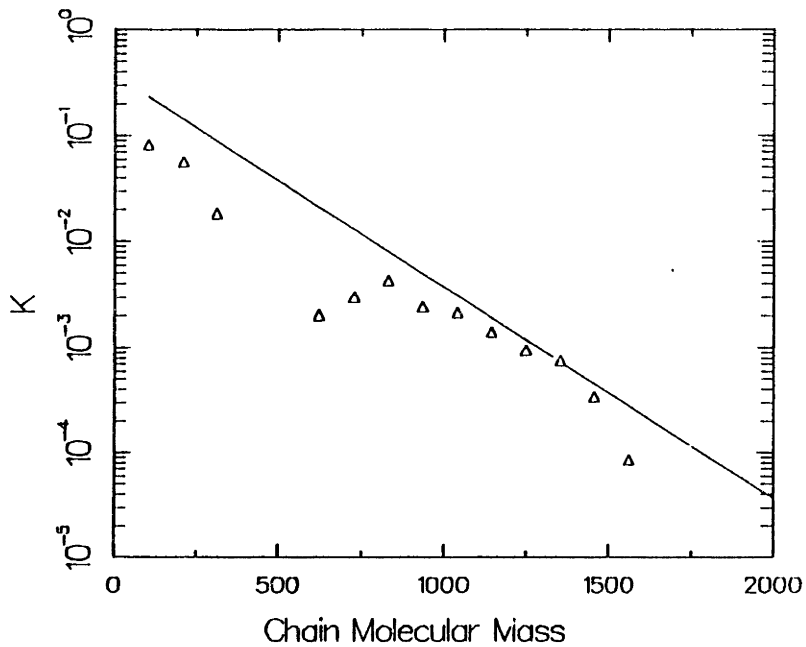

Figure 7.11: Comparison of partition coefficients of polymer chains between the polymer-rich phase and the SCF-phase as measured in solubility experiments (——), and precipitation polymerization reactions (△) with 3.33 wt% styrene in ethane with AIBN as radical initiator at 25 MPa and 333K.

To recapitulate, therefore, the variation of pressure causes essentially no change in the peak of the molecular mass distribution of the precipitated polymer. However, the breadth of the molecular mass distribution is increased as one proceeds to higher pressure, illustrating the approach to liquid-like behaviour of the SCF-solvent. The partitioning of chains between the SCF-phase and the precipitate-phase, beyond a chain length of 3, apparently follows the same behaviour as noted in the solubility experiments. The unusual behaviour of the first three mers is attributed to the presence of the initiator that is of a chemical character different from that of the monomer.

7.2.3.3 Experiments at Different Monomer Concentrations

The variation of the precipitate molecular mass distribution with changes in the initial monomer concentration in the SCF-phase constituted the next stage of our experimental work. Monomer concentration is an important variable, for two different reasons.

- The rate of formation of radicals and terminated chains, both before and subsequent to precipitation, have been shown to depend directly on the concentration of monomer (see Section 6.2 for mathematical arguments). It is expected, therefore, that the final product molecular mass distributions will be affected by changes in monomer concentrations. However, the exact nature of these changes cannot be deduced since the equations presented in Section 6.2 are complicated, and a functional dependence of molecular mass distributions on [M] cannot be immediately derived.
- It is known that polystyrene chains of all molecular weights are soluble in styrene in all proportions. The addition of finite quantities of monomer is thus expected to modify the solvent power of supercritical ethane, and to have an effect similar to the modification of the fractionation ability of ethane, by the addition of propane, as demonstrated in Chapter 4. As one proceeds to higher monomer concentrations, therefore, it is expected that the precipitate

polymer will possess larger quantities of longer chain molecules. In this sense, therefore, an increase in monomer concentration will have an effect similar to increasing the operating pressure.

In Figure 7.12, we demonstrate the molecular mass distributions of the precipitate polymer formed by polymerizing styrene at three different concentrations (3.33, 5.0 and 6.66 wt%) in supercritical ethane (at 17 MPa and 333K) with AIBN (5.83×10^{-5} gm/gm. ethane) as the radical initiator. Again, molecular mass distributions on a first three mer-free basis are independent of reaction time for all examined monomer concentrations. Polymer concentrations in both phases must therefore reach constant values at a relatively early time (i.e.,for t_{rxn}<<8 h). This also implies that

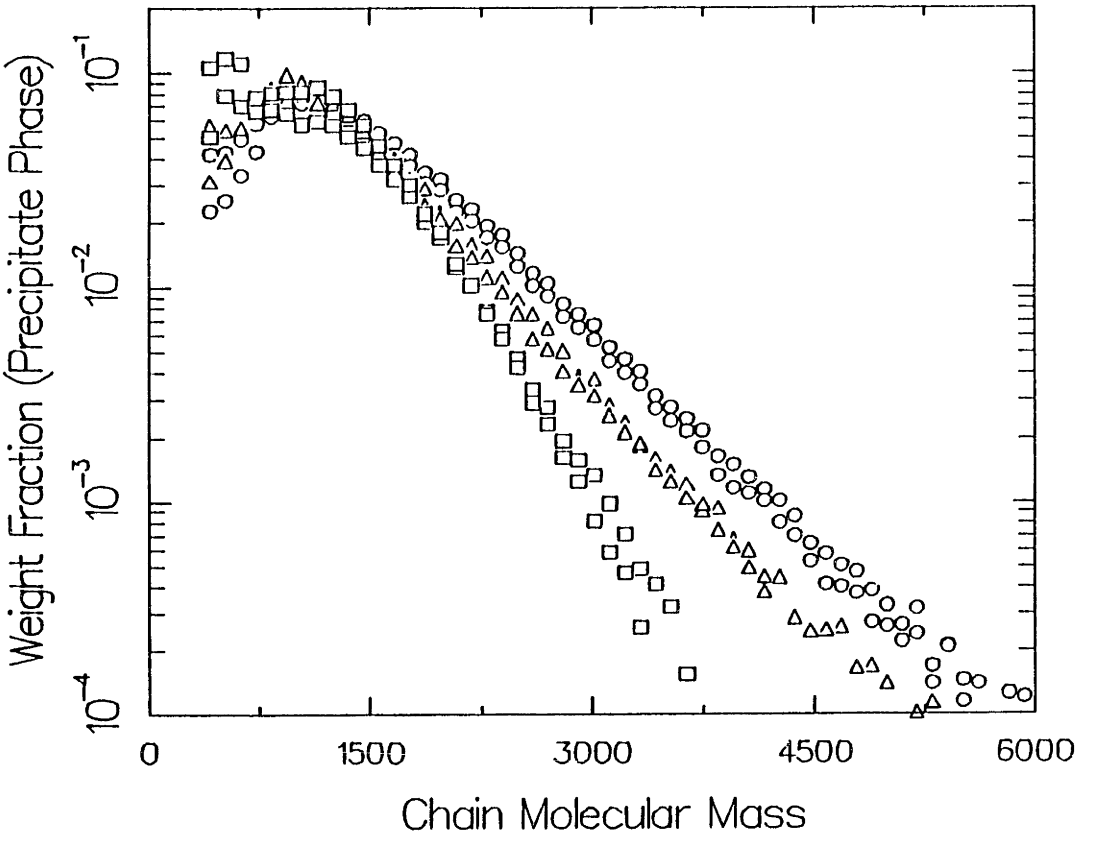

Figure 7.12: Composition of precipitate polymer, on a first three mer-free basis for different monomer concentrations for the precipitation polymerization of styrene in ethane, initiated with AIBN at 17 MPa and 333K. (□) is at 3.33 wt% , (△) 5.0 wt% and (o) 6.66 wt% monomer.

Table 7.2: Molecular mass data for precipitated-polystyrene at different monomer concentrations at 17 MPa ethane pressure and 333K with AIBN as radical initiator.

Monomer concentration wt% of SCF-phase	M_n	M_w	M_w/M_n
3.33	850	1063	1.25
5.00	1006	1249	1.24
6.66	1123	1404	1.25

almost no reaction occurs in the precipitate phase. The point to be emphasised in Figure 7.12, is that the peak molecular mass, again, is not a function of the variable which has been altered in these experiments, i.e., monomer concentration. This confirms the surmise that the peak molecular mass is controlled, to a large extent, by the chosen precipitation polymerization system, and is basically not affected by relatively small variations in operating conditions. The average molecular weight, in contrast, shifts to higher molecular masses at higher [M]. The molecular mass distributions of the precipitate polymers are relatively narrow, and the absolute numbers for M_n and M_w/M_n listed in Table 7.2 demonstrate the shift of the molecular mass distribution to higher average molecular masses with increasing [M]. An interesting point to be noted in Table 7.2 is that, as one proceeds to higher monomer concentrations, M_n, the number averaged molecular mass increases, as does M_w, the weight averaged molecular mass. However, their ratio, the polydispersity, which is a measure of the breadth of the molecular mass distribution, remains relatively unchanged. This is in sharp contrast to the results presented in Table 7.1 where both M_n and M_w/M_n increase as one goes to higher operating pressures.

To understand these phenomena we examine the variation of the number fractions of the different chain-length polymers in the precipitate phase at the different monomer concentrations in Figure 7.13.

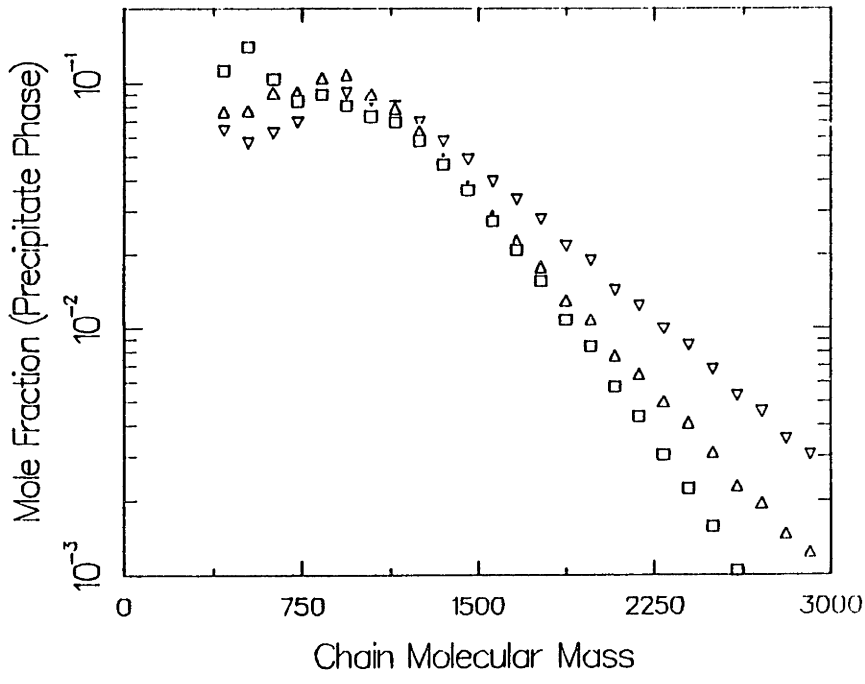

Figure 7.13: Composition on a mole fraction basis precipitate polymer, on a first three mer-free basis for different monomer concentrations for the precipitation polymerization of styrene in ethane, initiated with AIBN at 17 MPa and 333K. (□) is at 3.33 wt% , (△) 5.0 wt% and (▽) 6.66 wt% monomer.

Again data are presented on a first three mer-free basis. This Figure reiterates two facts that were illustrated in Figure 7.12.

- The peaks in the precipitate phase for all three monomer concentrations are approximately at a molecular mass ~ 1000.
- The molecular weight distributions, at high molecular masses, drop off less sharply at higher monomer concentrations (as compared to data at lower monomer concentrations.) To be able to close the mass balances ($\sum w_x^s$ =1), therefore, the curves at higher monomer concentrations must be less concentrated in the low molecular mass chains. This trend is clearly illustrated in Figure 7.13. The other interesting aspect of this diagram is that the three molecular mass distributions cross over at approximately the peak molecular mass in the distribution. The suggests that the phenomena controlling this peak molecular mass are important in the understanding of precipitation polymerization reactions.

Here, we make some observations regarding the mechanism of precipitation

polymerizations on the basis of Figure 7.13:

- The concentrations of the various mers (in units of mole ℓ^{-1}) in the precipitate and the SCF phases *cannot have a simple, linear dependence on the monomer concentration*. This is clear because a linear dependence for the concentrations of the various mers would dictate that precipitate compositions (on a mole or mass fraction basis) and hence, M_n, would be independent of the monomer concentration. For example,

$$M_n = \frac{\sum n_i (MW)_i}{\sum n_i} \tag{7.1}$$

would be independent of [M] if the various n_i's (the moles of species i in the relevant phase) depended linearly on the monomer concentration. Also, if this were true, then, M_w and consequently M_w/M_n would also be independent of monomer concentrations.

- It is not possible to explain the shape of the molecular mass distribution as shown in Figure 7.13 as an effect of <u>only</u> the variation of the solvent power of the SCF due to the addition of the monomer. If the change in solvent power alone were the controlling variable, then, while the higher molecular mass chains would be present in larger quantities, the concentrations of the lower molecular mass chains, including the molecular weight corresponding to the peak, must be relatively reduced to account for the mass balance constraints. The fact that the concentration of the peak in the molecular mass distributions is essentially insensitive to changes in [M] suggest that some other phenomenon must occur at this point in the distribution to balance the effect of the change in solvent quality.

We now attempt to achieve a mathematical understanding of the changes occurring in the precipitate molecular mass distribution as monomer concentrations are increased. At low molecular masses, in the gas phase, from Eq.(6.32),

$$[RM_x^\bullet] = \frac{(k_i/k_p)\,([I]/[M])}{\prod_j (1 + (k_t/k_p)(\sum[RM_x^\bullet]/[M]) + (dm_s/dt)/K_j k_p [M])} \qquad (6.32)$$

By assuming that $k_t \times \sum[RM_x^\bullet]/K_p[M] \ll 1$,[10] and that at the low molecular mass end the third term in the denominator is $\ll 1$ [since $dm_s/dt \ll 1$], we can show that,

$$[RM_x^\bullet] \sim k_i[I]/k_p[M] \qquad (7.2)$$

independent of x. This result can be understood qualitatively by realizing that the rate of propagation of radicals is dependent directly on monomer concentration [Eq.(6.12)]. Therefore, although "larger" quantities of a specific chain are produced at higher monomer concentrations, a corresponding "larger" fraction is lost in the formation of longer chains. The kinetic chain lengths, as defined in Eqs(6.30) and (6.31) are larger, suggesting that longer chains will be produced in larger quantities as [M] is increased. So, if no precipitation were to occur, the obtained molecular mass distribution would be flatter and tend to higher molecular masses.

From Eq.(7.2) we can make two conclusions regarding the behaviour of the molecular mass distributions of the precipitate polymer compositions at the lowest molecular masses:

(a) From Eq.(7.2) it is clear that as monomer concentrations increase, the concentrations of the smallest oligomers in the gas phase decrease. Also, the terminated polymer concentrations in SCF phase, which are proportional to $[RM_x^\bullet]$, must decrease with increasing [M]. The mass fraction of each oligomer in the solid phase will also drop when [M] increases,

---

[10] The rationale for this is that $k_p[M][RM_x^\bullet]$, which is the propagation rate of any radical x is larger than the termination rate of the radicals, $k_t[RM_x^\bullet] \times \sum[RM_x^\bullet]$ (see Table 7.4, for absolute numbers).

$$w_x^s = \{[RM_{x-1}^{\cdot}]+[P_x]\}\times(MW)_x/\rho_{SCF}K_x \propto 1/[M]K_x \qquad (7.3)$$

(b) We now attempt to rationalize the initial increase of polymer concentrations with chain length in the precipitate, as demonstrated in Figures (7.12) and (7.13). It has been shown in Chapter 4 that K_x decreases as one proceeds to higher x, [Eq.(4.4)],

$$\ell og_{10}K_x = \ell og_{10}(w_x^v/w_x^s) = C_0 - C_1X_x \qquad (4.4)$$

From Eqs(7.2) and (7.3), at the low molecular mass end the mass fraction of chains in the solid phase increases with increasing chain length, i.e.,

$$w_x^s \propto 10^{[-C_0+C_1X_x]}/[M] \qquad (7.4)$$

The derivation of Eq(7.4) is contingent on the assumption that the last term in the denominator of Eq.(6.32) is much smaller than 1, which will be valid for the smallest chain lengths. As one proceeds to higher chain lengths, however, the last term in the denominator in Eq.(6.32) (corresponding to precipitation), increases and is of order 1 or higher. Beyond this molecular mass, gas phase compositions drop off exponentially with increasing chain length as do the solid phase compositions. The behaviour of long-chain molecules are therefore governed by the precipitation phenomenon and, also, the need to complete the mass balance in each of the two phases. *The peak in the solid phase molecular mass distribution therefore, represents the point where the reaction in the gas-phase goes from kinetic control [Eq.(7.4)] to precipitation control [Eq.(6.32)].*

Qualitatively, the change of the shape of the precipitate polymer molecular mass distributions with monomer concentration can thus be explained. However, the effect of the addition of relatively large quantities of monomer to supercritical ethane on the partitioning behaviour of the SCF-phase has not been addressed. To appreciate this, we present in Figure 7.14 and 7.15, partition coefficients for polystyrene chains between the precipitate-

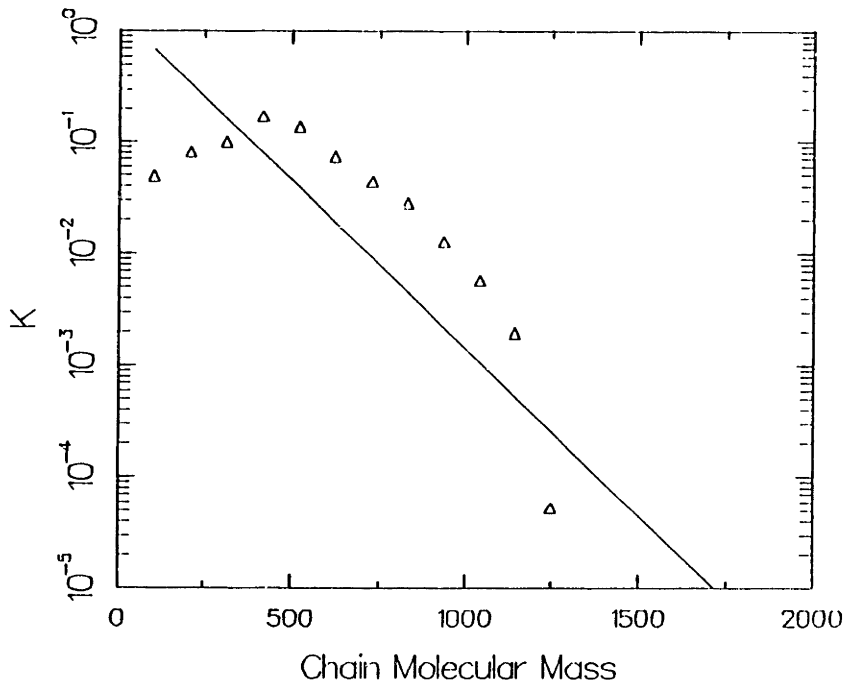

Figure 7.14: Comparison of partition coefficients of polymer chains between the polymer-rich phase and the SCF-phase as measured in solubility experiments (——), and precipitation polymerization reactions (Δ) with 5.0 wt% styrene in ethane with AIBN as radical initiator at 17 MPa and 333K.

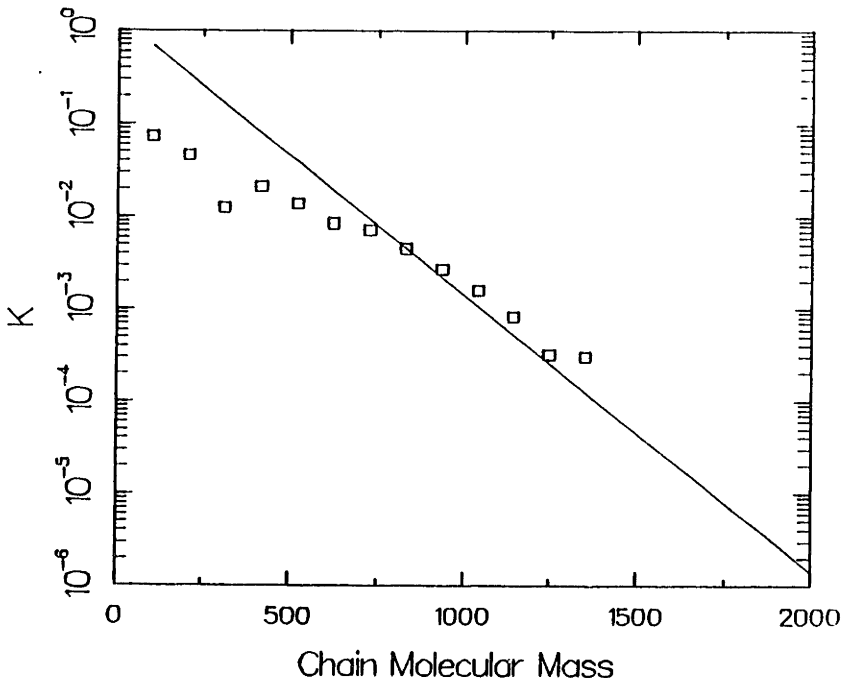

Figure 7.15: Comparison of partition coefficients of polymer chains between the polymer-rich phase and the SCF-phase as measured in solubility experiments (——), and precipitation polymerization reactions (□) with 6.66 wt% styrene in ethane with AIBN as radical initiator at 17 MPa and 333K.

phase and the SCF-phase as calculated from polymerization experiments at 5.0 and 6.66 wt% styrene in ethane at 17 MPa and 333K, respectively. These results are then compared to partition coefficients of polystyrene chains in pure ethane at the same temperature and pressure of operation as measured in solubility experiments.

Results in Figure 7.14 and 7.15, in essence, are in accordance with trends obtained in the experiments at 17MPa and 333K at lower monomer concentration. These plots suggest that partition coefficients for polystyrene chains are not affected due to the increased concentration of monomer in the experiments. Results in Figure 7.14 for the 5.0 wt% monomer, do show some variation, but results for the 6.66 wt% monomer revert to the same trends demonstrated by the reaction with 3.33 wt% monomer (Figure 7.5). We conclude, therefore, that these experiments do not provide enough evidence to study the effect of increased monomer concentration on the partitioning behaviour of the SCF phase, at least for the oligomers in the molecular mass range 400-1100. For our modelling, therefore, we assume that the presence of up to 7.0 wt% monomer has little effect on the fractionating behaviour of the SCF.

In summary, the effect of changes in monomer concentration on the precipitation polymerization of styrene in ethane are:

- Average molecular masses (M_n and M_w) of the precipitated polymer increase as one increases monomer concentration. However, the polydispersity, M_w/M_n, remains unchanged. The variation of monomer concentration, therefore, allows one to synthesise polymers of different average molecular masses while not changing the polydispersity of the product.
- Neither the position nor the concentration of the peak molecular mass in the precipitate phase are sensitive to variations in monomer concentration. This can be qualitatively explained when it is recognized that the peak molecular mass corresponds to the point where the reaction in the gas phase goes from kinetic control to precipitation control, and therefore must remain unchanged as long as the fractionation power of the solvent remains relatively unchanged.

- The partitioning behaviour of the SCF for polymers of molecular mass 400-1000 remains essentially unchanged due to the addition of up to 6.66 wt% monomer. This is in contrast to experimental results presented in Chapter 4, where the addition of 10 mole% propane to ethane is shown to cause a significant change in the partitioning behaviour of the SCF. However, more careful solubility experiments must be performed with styrene-ethane solvent mixtures before this point may be clarified. Also, measurements of the partition coefficients from polymers synthesised in SCF polymerization reactions would help in resolving this issue.

7.2.3.4 Reactions at Different Initiator Concentrations

The rate of creation of free radicals, at any instant of time depends linearly on the concentration of the initiator in the reaction medium [Eq.(6.10)]. In normal, single-phase solution polymerization reactions, therefore, the change in initiator concentrations serves to change the time scale of the reaction [Eq.(6.11)-(6.13), or see Flory, 1953 for mathematical details]. Also, the average molecular masses of the product may be affected when initiator concentrations are varied (Bovey and Winslow, 1979),

$$M_w = (1+\xi)/(1-\xi) \tag{7.5a}$$

$$M_n = 1/(1-\xi) \tag{7.5b}$$

$$M_w/M_n = 1+\xi \tag{7.5c}$$

where, ξ, is the time-independent probability that a given radical will propagate rather than terminate and, in this case, is defined through the equation,

$$\xi = \frac{1}{1 + (k_i k_t [I])^{\frac{1}{2}}/k_p [M]} \tag{7.6}$$

It has been assumed in the formulation of Eq.(7.6) that disproportionation is the only termination mechanism. Frequently, in a liquid phase reaction, ξ is close to 1 since propagation is favoured over termination. Changes in [I], therefore, have very small effects on the average molecular masses or polydispersity of the product polymer.

SCF precipitation polymerizations were conducted at different [I], to study the effect of initiator concentrations on the molecular mass distributions of the precipitated polymer. It was observed that, as long as some initiator was present ($\sim 5\times10^{-6}$ to 6×10^{-5} gm AIBN/gm ethane at 3.33 wt% monomer at 17 MPa and 333K), the molecular mass distribution of the product polymer, on a first three mer-free basis, remain unchanged. This is consistent with results obtained from solution polymerization. Also, qualitatively, the conversion of monomer to precipitate polymer was reduced as initiator concentration decreased. Results for these experiments have not been presented due to their inaccuracy, especially when [I] was very small.

In the case when there was no initiator present, however, no polymer was found in the SCF-phase, and hence no precipitate phase was observed even after reaction times of ~ 180 h. This experimental outcome suggests that the dominant initiation mechanism is the formation of free-radicals by the dissociation of initiator (i.e., thermal initiation by the addition of two monomers to form a free-radical is, for all practical purposes, absent).

In summary, the presence of finite quantities of initiator (at [M] > 3.33 wt% at 17 MPa and 333K), therefore, does produce a precipitate polymer whose composition on a first three mer-free basis is independent of the initiator concentration. Qualitative results show that the conversion of the monomer to precipitated polymer scales linearly with the initiator concentration at any given reaction time.

7.2.3.5 Experiments at Different Temperatures

The variation of operating temperature is anticipated to affect an SCF precipitation polymerization in two ways:

- As temperature increases, at a given pressure, the density of the SCF phase decreases. The effect of this phenomenon is to make the fluid phase a stronger fractionation medium, i.e., its behaviour

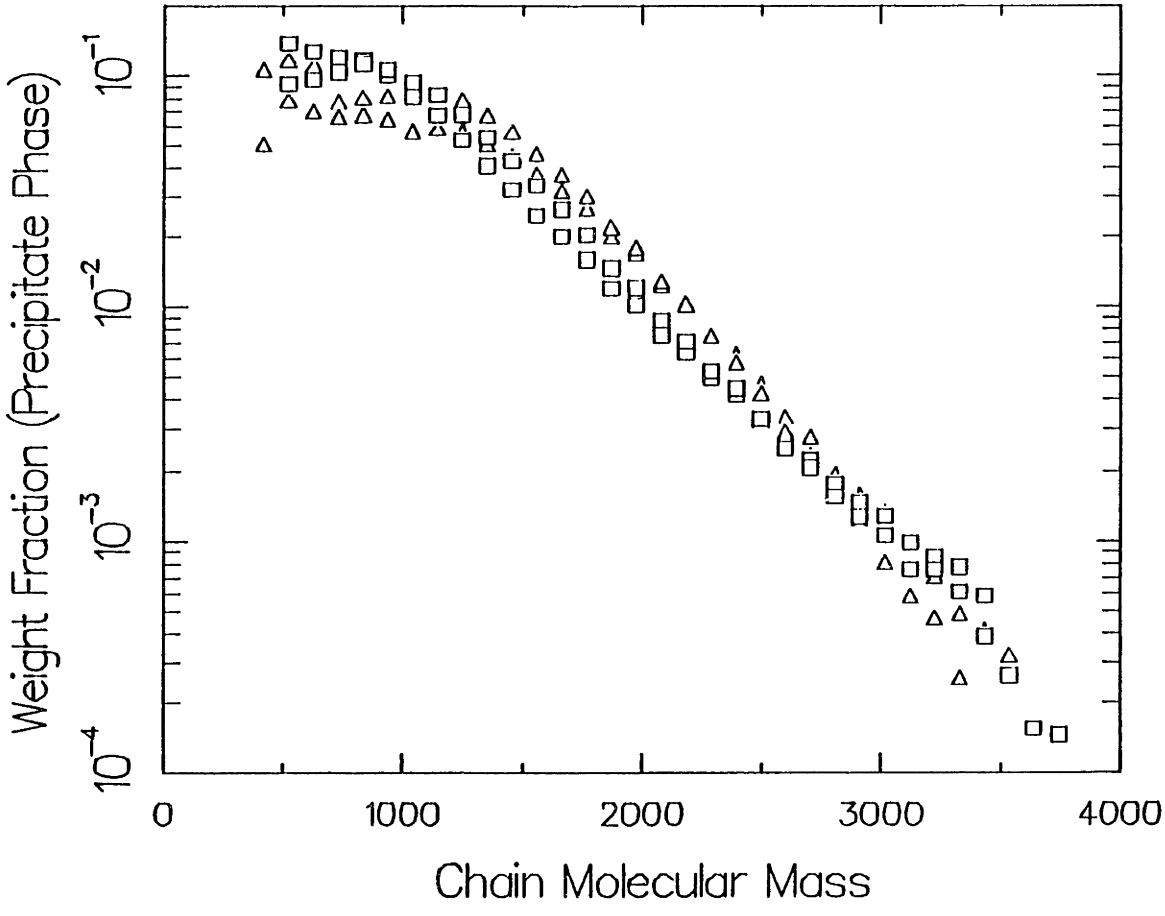

Figure 7.16: Composition on a mole fraction basis precipitate polymer, on a first three mer-free basis for different monomer concentrations for the precipitation polymerization of styrene in ethane, initiated with AIBN at 17 MPa and 3.33 wt% monomer at (Δ) 333K and (□) 343K.

Table 7.3: Molecular mass data for precipitated-polystyrene at two temperatures at 3.33 wt% styrene concentrations with AIBN as radical initiator at 17MPa.

Operating Temperature (K)	M_n	M_w	M_w/M_n
333	850	1063	1.25
343	884	1039	1.18

becomes more gas-like (see Chapter 4). This will result in narrower molecular mass distributions for the product polymer.

- As temperature increases, the reaction rate constants, and hence the reaction rates are expected to increase. The manifestation of this phenomenon will be in the broadening of the precipitate molecular mass distribution, and also result in higher conversions of monomer to precipitate polymer at any given reaction time.

With respect to the molecular mass distribution of the precipitate, therefore, the increase of operating temperature has two conflicting phenomena, and the overall effect of a temperature change will depend on which of these two steps dominate.

Data in Figure 7.16 and Table 7.3, show that the compositions of the precipitate polymer phase at the two temperatures, 333K and 343K respectively, are essentially unchanged within experimental error. It can be inferred therefore, that the two competing mechanisms discussed earlier balance each other for this temperature change (10K). Data not shown, however, demonstrate that the conversion of monomer to polymer at a reaction time of 24 h is higher at 343K than at 333K (~0.7% at 343K to ~0.3% at 333K).

The increase of operating temperature potentially may have an undesired effect i.e., as temperature is increased, the product polystyrene which could have been below T_g at lower temperatures, now is an "equilibrium liquid". The diffusion of monomer through the polymer which has some unterminated chains is thus easier, and the reaction rate in the precipitate phase could be increased. The manifestation of this effect would be the broadening

of the molecular mass distribution at higher temperatures. However, at the two temperatures examined, no broadening of the molecular mass distribution seems to occur suggesting that the diffusion of the monomer to unterminated polymer chains still does not occur. At even higher temperatures (~ 373K), it is expected that appreciable reaction may occur in the precipitate phase.

7.3 MODELLING OF EXPERIMENTAL DATA

7.3.1 Single Phase Reactions

In Section 7.2.3.1 we stated that a minimum monomer concentration is necessary to observe experimentally the presence of a precipitate phase polymer. Reactions conducted at approximately 1.5 wt% styrene monomer fall below this threshold monomer concentration and yield no precipitate. These data have not been used up to this point since they were not directly relevant to the understanding of SCF precipitation polymerizations. We may, however, as we discuss below, use data obtained for these single phase reaction conditions to determine, independently, the ratio of kinetic rate constants.

It has been shown by Flory (1953) and others (Bovey and Winslow, 1979, Odian, 1985) that the composition of polymer produced by single-phase polymerization may be modelled by a most probable distribution with a propagation probability, ξ, as stated in Section 7.2.3.4,

$$\xi = \frac{1}{1 + (k_i k_t [I])^{\frac{1}{2}}/k_p [M]} = \frac{1}{1 + (1/\nu_{c1})} \qquad (7.6)$$

The composition of the product polymer, in the single-phase polymerization may thus be computed by the expression,

$$w_x^v = x\xi^{x-1}(1-\xi)^2 \qquad (7.7)$$

and the probability of propagation, ξ, be obtained by fitting Eq(7.7) to

Table 7.4: Data obtained from the single phase polymerization of styrene in ethane at 333K and various pressures.

P (MPa)	ξ	ν_{cl}	$(k_i k_t)^{-\frac{1}{2}} k_p$ $(l/mole)^{\frac{1}{2}}$	$(\nu_{cl})_{liq}/(\nu_{cl})_{SCF}$
13	0.39	0.639	0.0488	64.72
17.5	0.46	0.852	0.0658	48.58
20	0.50	1.000	0.0764	41.38

experimental data obtained in these experiments. Values of ξ and other related quantities are reported in Table 7.4.

Several conclusions about the mechanism of polymerizations in SCF may be drawn by examining Table 7.4:

- The probabilities of propagation, ξ, increase as one proceeds to higher pressures. This is consistent with the fact that the behaviour of SCF becomes more liquid-like at higher pressures. In this context it must be remembered that the probability of propagation in normal liquid-phase polymerizations are frequently higher than 0.99.
- At low monomer concentrations, the kinetic chain lengths in SCF systems are small, and frequently of order 1. This is a direct manifestation of the reduced value of k_p, which ensures that termination of reacting chains is a more dominant phenomenon in SCF polymerizations than in liquid phase polymerizations. Kinetic chain lengths in the case of SCF systems are compared to liquid systems at similar values of [I] and [M] in the last column of Table 7.4, where it is seen that kinetic chain lengths in SCF are approximately 2 orders of magnitude smaller than in liquid systems.
- Use of this data also allows us to specify the ratio $(k_i k_t)^{\frac{1}{2}}/k_p$ in SCF systems. In the correlation of experimental data for the precipitation polymerization using the transient model, therefore, we have an independent check of the values of the fitted parameters: k_i, k_p and k_t (see Section 7.3.2 and 6.2).
- In Eq(7.5), it has been shown that the polydispersity of the

resultant polymer sample is $(1+\xi)$. Therefore, polymers produced in a single phase reaction, under SCF conditions, have smaller polydispersities than corresponding values than in an "ideal" liquid-phase reaction, where $M_w/M_n \sim 2$.

7.3.2 The Transient Model

In Chapter 6, we have presented two models for the correlation of experimental data obtained in the SCF precipitation polymerization reactions. We begin our modelling by considering data obtained by the polymerization of 3.33 wt% styrene in ethane at 17 MPa and 333K.

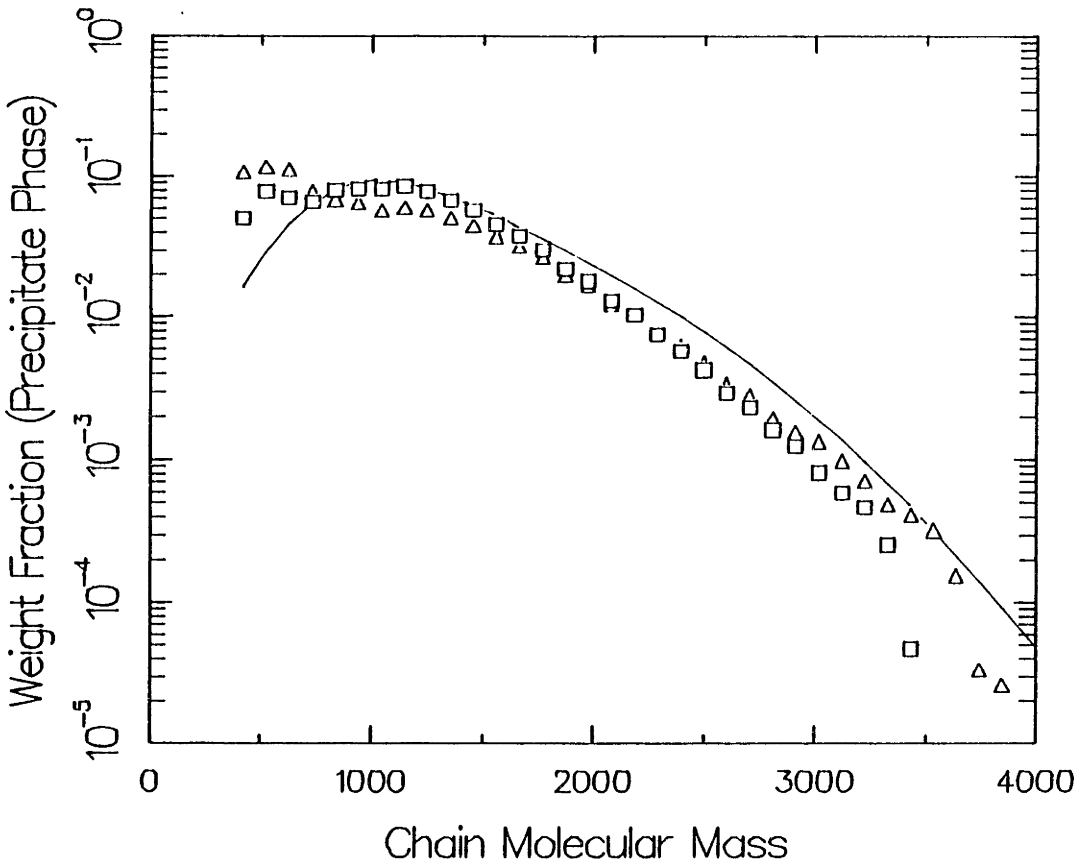

Figure 7.17: Comparison of precipitate polymer compositions, on a first three mer-free basis for the precipitation polymerization of 3.33 wt% styrene in ethane, initiated with AIBN at 17 MPa and 333K. (△) and (□) represent experimental data, while (——) is prediction of transient model.

It has been shown in section 7.2.3.1, that the partition coefficients of the first three mers are smaller than the measured partition coefficients in the solubility experiments (see Chapter 4). To account for this effect we must use the true partition coefficients, as measured in the polymerization experiments for the first three mers, while using K_x from solubility data for the other mers. Also, arguments presented in Section 6.4, suggest that while k_t (the termination rate constant) has a value that is in the same order of magnitude as corresponding values in liquid solvents, k_p (the propagation rate constant) is 1-2 orders of magnitude smaller in SCF than in liquid systems.

With a knowledge of these facts we proceed to model the base case (17 MPa, 333K, 3.33 wt% styrene in ethane with 5.83×10^{-5} gm AIBN/gm. ethane), with the use of the transient model developed in Section 6.2. In Figure 7.17, the experimental data for the precipitate phase composition (on a first three mer-free basis) are compared to the fit obtained from the transient model (with $k_i=8\times10^{-6}$ s^{-1}, $k_p=$ 1.0 ℓ $mole^{-1}s^{-1}$, $k_t=$ 4×10^5 ℓ $mole^{-1}$ s^{-1}, $(k_i k_t)^{-\frac{1}{2}}k_p=0.559$). Under these conditions, the agreement between experiment and theory is excellent and is within the experimental error. All facets of the behaviour of the experimental data are reproduced by the model, implying that the correct physics have been included in its formulation.

Of the three parameters used, it was observed that k_p controls the position of the maximum in the molecular mass distribution and k_t the shape of the molecular mass distribution at high molecular masses. As in the case of liquid phase polymerization reactions, k_i essentially affects only the rate of conversion of monomer to precipitate polymer. The sensitivity of the model results to variations in the fitted parameters will be discussed later in this section.

The mechanism of precipitation polymerization as predicted by this model, at this operating condition, can be depicted in the following steps:

- Initially, only monomer and initiator are dissolved in the SCF-phase and are present in a homogenous solution. Radicals and terminated polymer chains are then formed, and the absolute quantities of each

at any instant of time can be obtained by numerically integrating the equation set Eq.(6.10)-(6.14).

- At zero time there are no oligomers in solution (except the monomer); with increasing time the SCF phase compositions rise and, at the instant of precipitation the plot of gas phase oligomer concentrations vs molecular mass is tangential to the binodal curve. This occurs at t_{rxn}=180 s where the concentration of the polymer chains of degree of polymerization 50 reaches its binodal value and thus precipitates out of solution. The SCF phase polymer compositions at the instant of precipitation and the binodal concentration of each mer are shown in Figure 7.18 to illustrate this point.

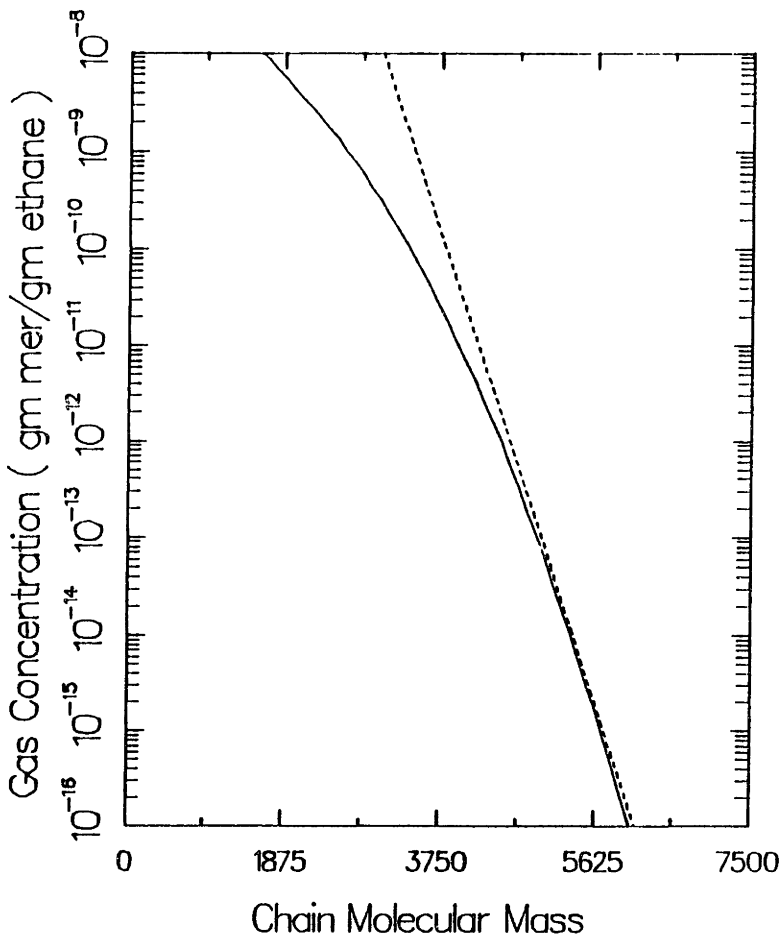

Figure 7.18: Comparison of the model predictions for the gas phase (——), and the binodal polymer compositions (----) at the instant of precipitation (180 s) for the polymerization of 3.33 wt% styrene in 17 MPa ethane at 333K with AIBN as radical initiator.

- Beyond this instant in time, two phases (an SCF phase and a polymer phase) are in equilibrium, and reaction continues only in the gas phase. Solid-phase compositions, on a first three mer-free basis, are found to be essentially independent of time.

We may also determine the composition of the SCF phase polymer in equilibrium with this "time independent" precipitate phase. In Figure 7.19, a comparison is presented between the experimentally measured SCF phase compositions and the model predictions. The agreement between the model and experiment is good at low molecular masses; at higher molecular masses the model has the right qualitative trend, although the quantitative agreement is poor. The point to be emphasised is that model is fitted to precipitate phase

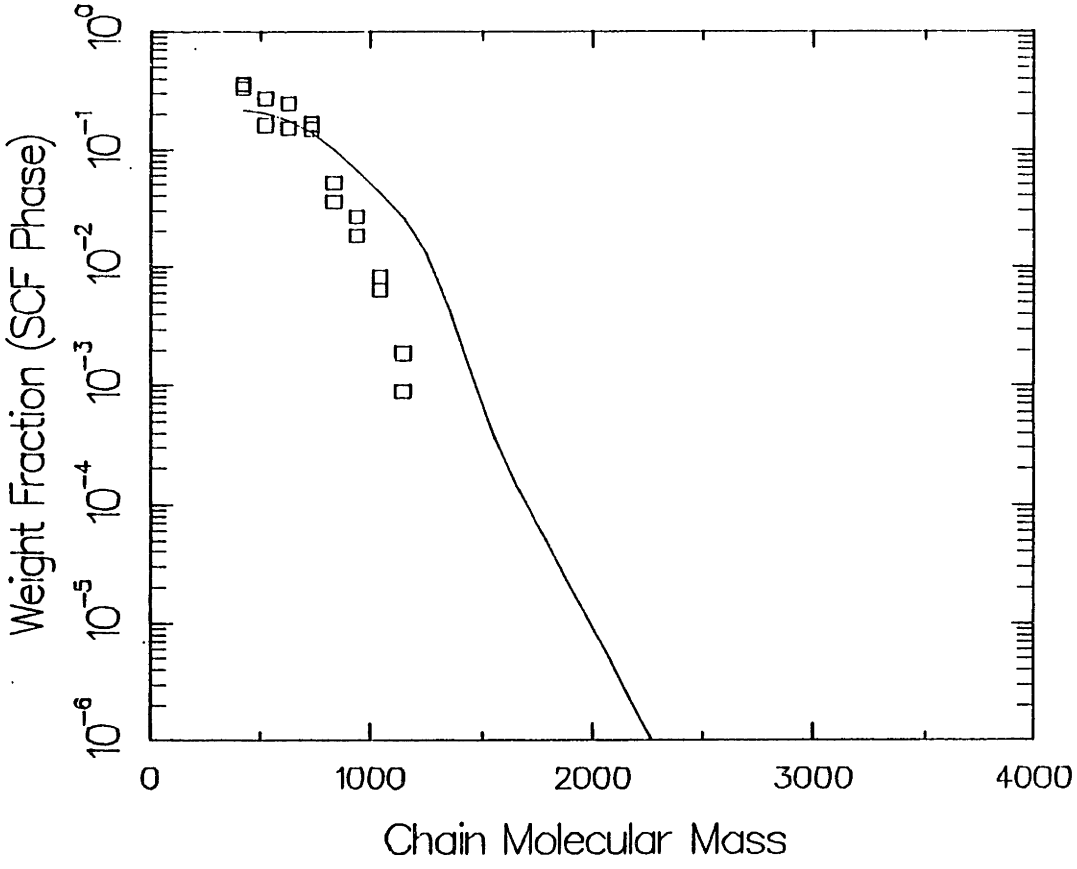

Figure 7.19: Comparison of SCF-phase polymer compositions, on a first three mer-free basis for the precipitation polymerization of 3.33 wt% styrene in ethane, initiated with AIBN at 17 MPa and 333K. (□) represent experimental data, while (——) is prediction of transient model.

Table 7.5: A Comparison of rate constants obtained from fitting the proposed kinetic mechanism to experimental data obtained from the precipitation polymerization of 3.33 wt% styrene in ethane at 17 MPa and 333K to corresponding rate constants for the polymerization of styrene in liquid benzene at 333K and 0.1MPa.

Reaction medium	k_i (s^{-1})	k_p (ℓ $mole^{-1}s^{-1}$)	k_t (ℓ $mole^{-1}s^{-1}$)
Benzene	1×10^{-5}	100	5×10^{6}
Ethane	8×10^{-6}	1	4×10^{5}

data, and so the SCF phase compositions are predictions. Also, the disagreement between the experimental data and model predictions are at a molecular mass where the concentrations of the relevant mer is small (*ca.* $< 10^{-4}$ gm/gm. ethane) and is thus at the limit of resolution of the analytical technique employed.

The kinetic parameters employed in fitting the model to the experimental data at 17 MPa (i.e., k_i, k_t and k_p) are listed in Table 7.5, and are compared to corresponding numbers for the polymerization of styrene in a conventional liquid solvent. As suggested in Section 6.4, the k_i and k_t values in the two systems are essentially the same, while k_p is approximately 2 orders of magnitude smaller in SCF. It has been suggested in the existing literature (for example, Subramaniam and McHugh, 1986; Eckert, 1972) that the rate of the initiation and termination steps may indeed be higher in SCF than in liquid phase systems due to the increased diffusivity of species in SCF. Since we have fit three variables to one set of compositions, the kinetic constants listed in Table 7.5 do not necessarily reflect absolute values, but rather represent order of magnitude estimates for these parameters. The point being stressed here, however, concerns itself with the anomalously small value of k_p in SCF systems, a phenomenon that has not been suggested in the literature to date. This unusually small value of the propagation rate constant is the dominant effect in SCF polymerization reactions, since it this constant that dictates the "growth rate" of the polymer chain as compared to the termination rate. The effect of enhanced initiation and possibly, termination rates, are therefore even furthered by this unusually small value of propagation rate constant,

resulting in smaller reaction rates for the monomer and relatively low average molecular mass polymers.

If the operating pressure is to be increased to the order of approximately 50 MPa, the SCF must now begin to behave increasing like a liquid solvent as indicated in the solubility experiments. The liquid like behaviour of the SCF solvent under such conditions is thus expected to lead to higher propagation rates and hence higher average molecular mass polymers. This same effect, may, in principle, may be achieved by the addition of liquid additives (viz. propane), as suggested by the fractionation experiments. In summary, the effect of SCF solvents on the reaction rate will be a maximum at the critical point of the solvent (where partial molar volumes will be the most negative) and will be progressively smaller as one proceeds to higher pressures wherein the SCF is anticipated to behave akin to a liquid solvent.

A related issue is the width of the molecular mass distribution (as expressed by M_w/M_n) of the precipitate polymer, which is smallest at low pressures (near P_c) and increases as the operating pressure is increased. The explanation for this may be understood by the examination of Eqs.(7.5) and (7.6), which are valid in the SCF phase. However, in the case of a precipitation polymerization, the probability of propagation, ξ, must account for the "termination" of chains due to precipitation from the reacting phase. The probability of propagation, ξ, is, therefore, now chain length dependent due to the inherent chain length dependence of the precipitation rate, i.e. at a quasi-steady state,

$$\xi_i = \frac{k_p[M][RM_i^\bullet]}{k_p[M][RM_x^\bullet] + k_t[RM_i^\bullet]\times\sum[RM_x^\bullet] + [RM_i^\bullet]/K_i\, dm_s/dt} \qquad (7.7)$$

The probability of a propagation, beyond a certain chain length, will be controlled by the K_i term, making the dependence of ξ_i on chain length i,

an exponential one.

For fluids near the critical point therefore, the probability of propagation to longer chain lengths becomes smaller as one proceeds to longer chain lengths, due to the inherently strong fractionation ability of fluids in this regime. Polymers in the SCF phase (and hence the precipitate-phase) must have a narrowly distributed molecular weight distribution. As one proceeds to higher operating pressures, the partitioning behaviour of the SCF is less pronounced, and hence higher concentrations of longer chains are produced. The net effect of this phenomenon is that polymers of a broader molecular mass distribution are produced. In the limit of very high pressure, the SCF behaves akin to a liquid solvent. The precipitation rate is therefore essentially a constant across chain lengths, leading to a constant value of ξ. The polydispersity of polymers produced in a SCF precipitation polymerizations at very high pressures will therefore be close to the ideal value of 2. Also, as pressure increases, the k_p value is expected to increase and approach liquid-like values (as the partial molar volume anomaly begins to disappear.) The rate of polymerization is thus anticipated to rise with an increase in the operating pressure. However, this is compensated by a broadening of the molecular mass distributions. Also, at higher pressures higher average molecular mass polymers will result.

The model predictions for the precipitate polymer at the two other operating pressures, viz. 12 and 25 MPa are shown in Figures 7.20 and 7.21. An excellent fit to the experimental data is obtained at the two other pressures with essentially the same parameters employed in the modelling at 17 MPa. This again confirms the surmise that the behaviour of precipitation polymerization systems under these conditions is dominated by the small value of k_p, and any variations caused by the changes of the kinetic constants with pressure is overshadowed by this unusually small value of k_p.

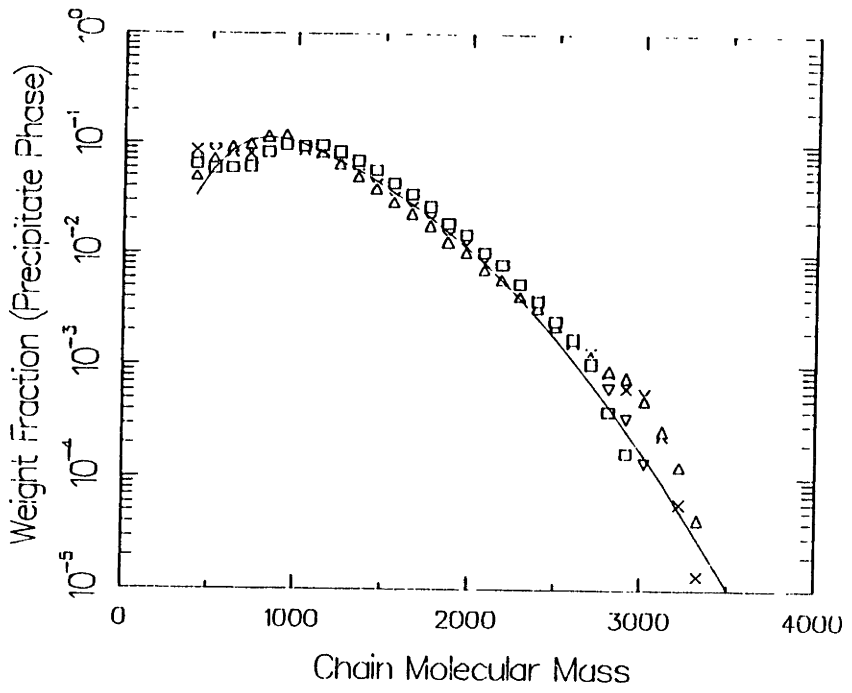

Figure 7.20: Comparison of precipitate polymer compositions, on a first three mer-free basis for the precipitation polymerization of 3.33 wt% styrene in ethane, initiated with AIBN at 12 MPa and 333K. (□), (△), (▽) and (x) represent experimental data, while (——) is prediction of transient model.

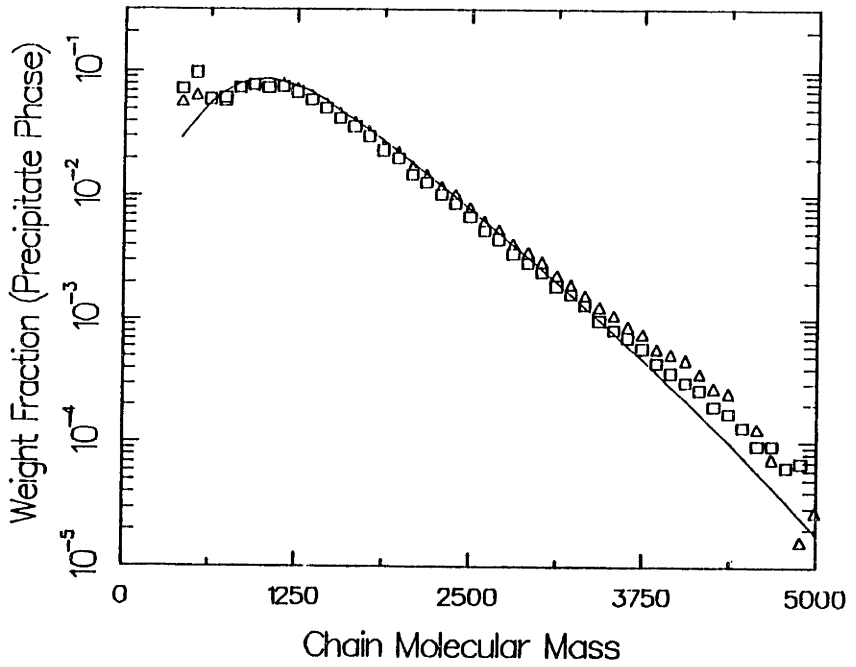

Figure 7.21: Comparison of precipitate polymer compositions, on a first three mer-free basis for the precipitation polymerization of 3.33 wt% styrene in ethane, initiated with AIBN at 25 MPa and 333K. (△) and (□) represent experimental data, while (——) is prediction of transient model.

Model results for the reactions at 17MPa at the different monomer concentrations (5.0 and 6.66 wt%) are presented in Figures 7.22 and 7.23. The partitioning law used in these cases was the same as was employed in the correlation of the polymerization data of 3.33 wt% styrene. As can be seen the agreement between the model and experiment is good at the low molecular masses but there is some disagreement as one proceeds to larger molecular masses. The region of disagreement is one where no experimental data on the partition coefficients can be measured in the polymerization experiments, due to the low concentrations of the corresponding mers in the SCF phase.

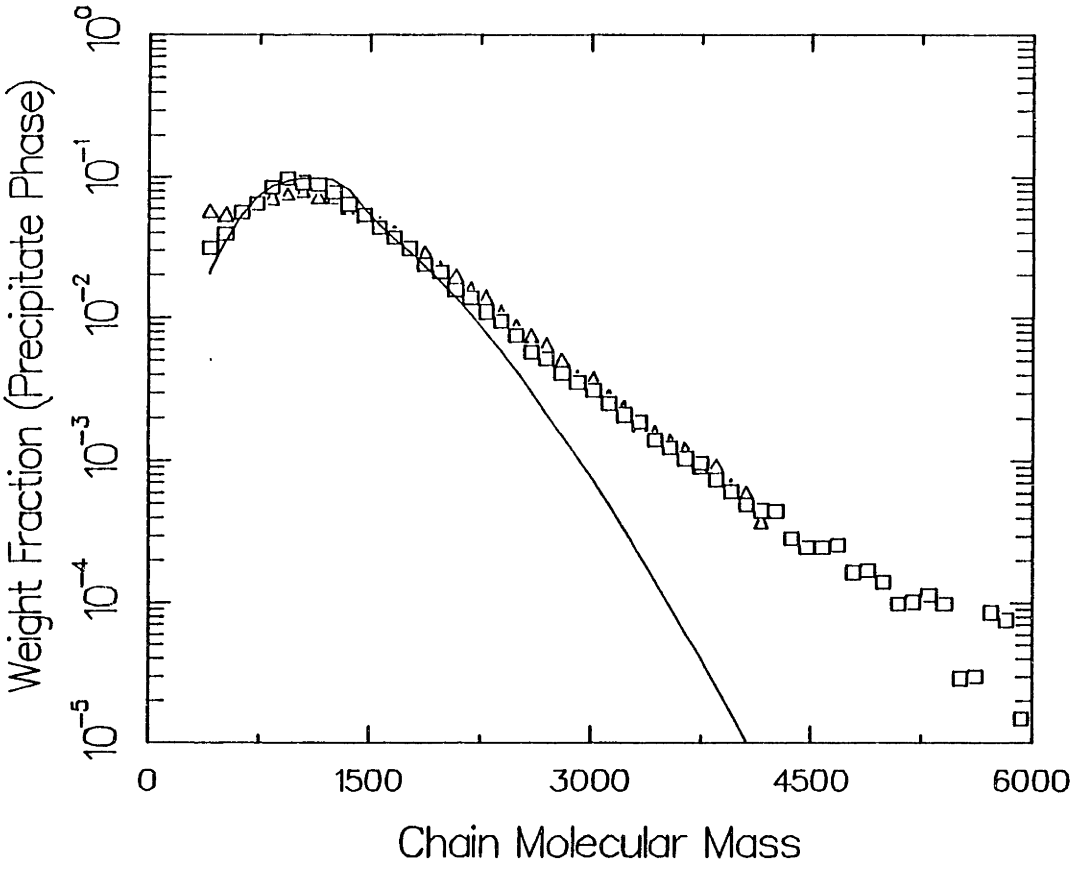

Figure 7.22: Comparison of precipitate polymer compositions, on a first three mer-free basis for the precipitation polymerization of 5.00 wt% styrene in ethane, initiated with AIBN at 17 MPa and 333K. (□) and (Δ) represent experimental data, while (——) is prediction of transient model.

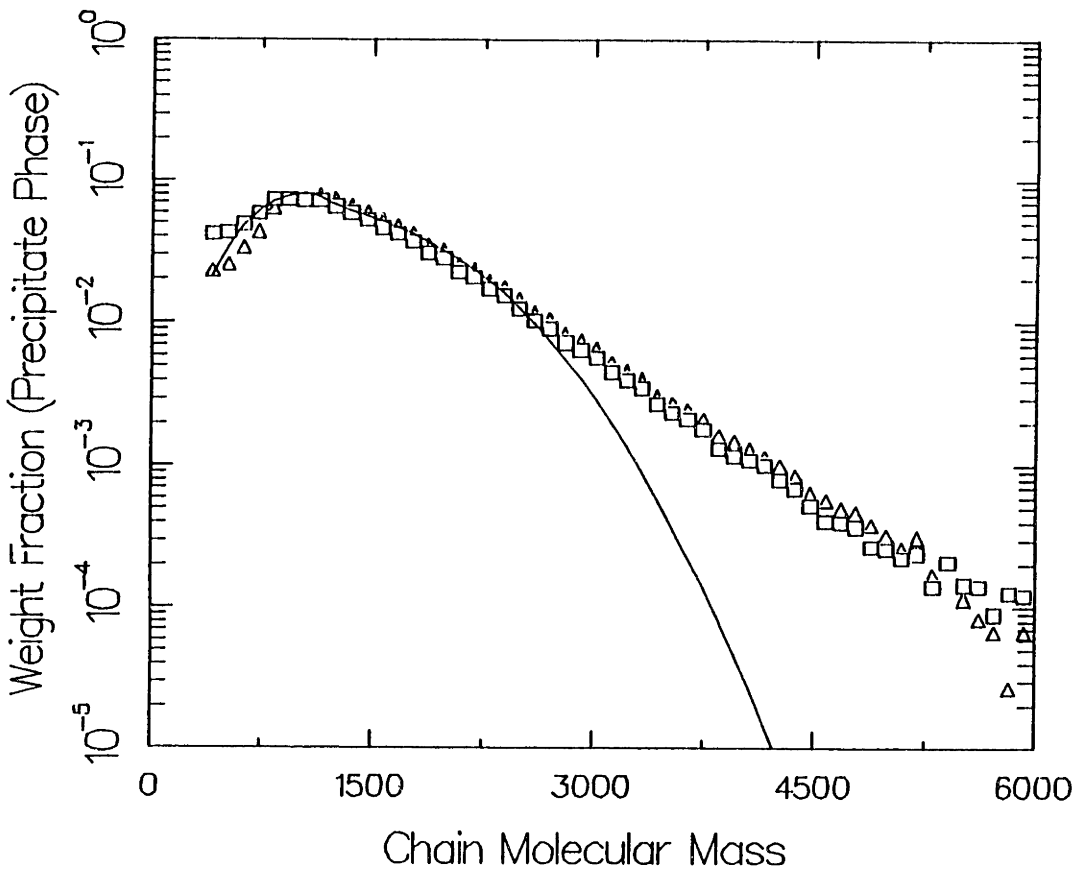

Figure 7.23: Comparison of precipitate polymer compositions, on a first three mer-free basis for the precipitation polymerization of 6.66 wt% styrene in ethane, initiated with AIBN at 25 MPa and 333K. (□) and (△) represent experimental data, while (——) is prediction of transient model.

It is speculated that at this high molecular mass end the partitioning behaviour of individual chains is modified due to the presence of a larger quantity of the monomer, with the larger chains feeling the effect more substantially than the small chains. This situation may be clarified further if solubility experiments were to be conducted with polymer obtained under polymerization conditions.

To understand the sensitivity of model results to changes in the three parameters: k_i, k_p and k_t, the variations of the precipitate polymer compositions at 17 MPa and 333K (3.33 wt% styrene in ethane) were examined with changes in the kinetic constants. In Figures 7.24, 7.25 and 7.26 the model predictions for different values of k_i, k_p and k_t, respectively, are examined. It is to be noted that the predictions of the precipitate phase

compositions on a first three mer-free basis are relatively insensitive to variations in the values of k_i and k_t. However, the model predictions are sensitive to variations in the propagation rate constant, k_p, and when the k_p value is raised from 1.0 ℓ $mole^{-1}s^{-1}$ to 5 ℓ $mole^{-1}s^{-1}$, the predicted compositions are different, even qualitatively. The variations of model predictions to changes in the kinetic constants may be summarized in the following points:

- The variation of k_i (4.0×10^{-6} $s^{-1} \leq k_i \leq 1.6\times10^{-5}$ s^{-1}) slightly changes the position of the maximum in the precipitate polymer composition. However, the general shape of the curves at the different k_i values are the same suggesting that k_i values do not change the qualitative shape of the curves.

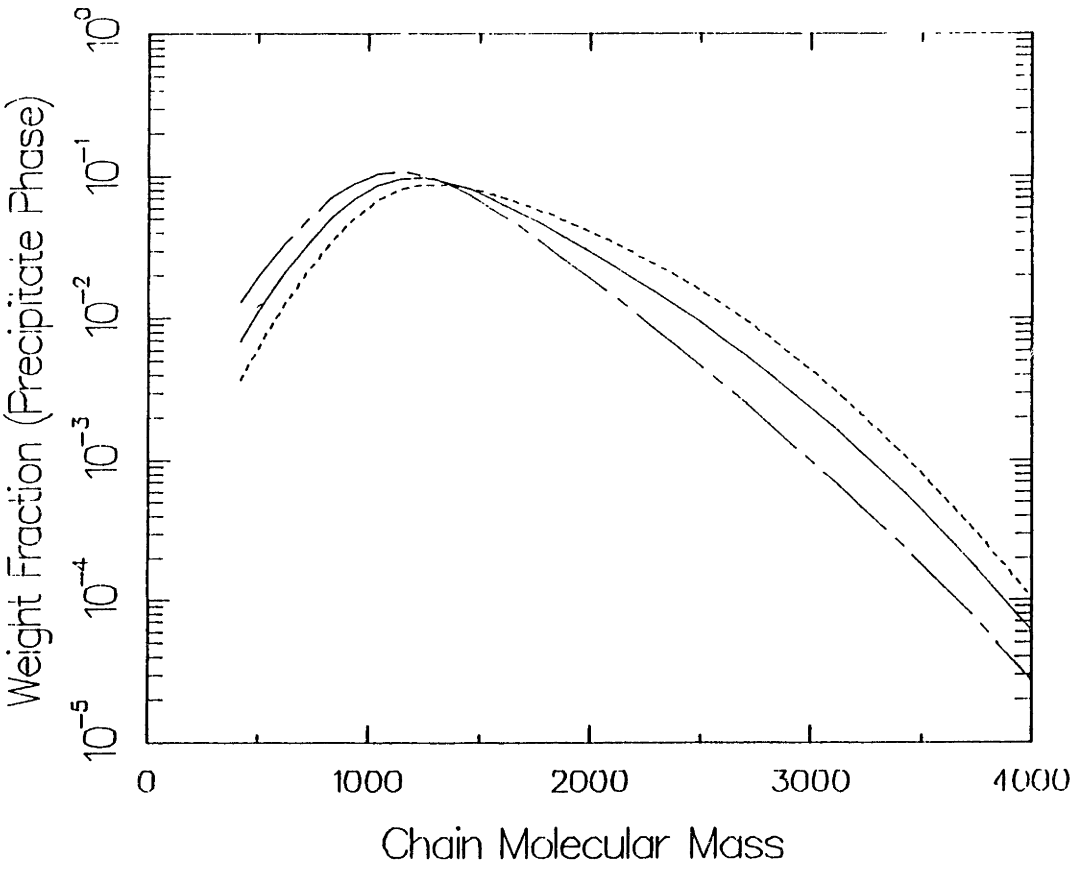

Figure 7.24: Comparison of predicted precipitate polymer compositions, on a first three mer-free basis for the precipitation polymerization of 3.33 wt% styrene in ethane, initiated with AIBN at 25 MPa and 333K for different value of k_i. (---) 4.0×10^{-6} s^{-1}, (——) 8×10^{-6} s^{-1}, (— - —) 1.6×10^{-5} s^{-1}.

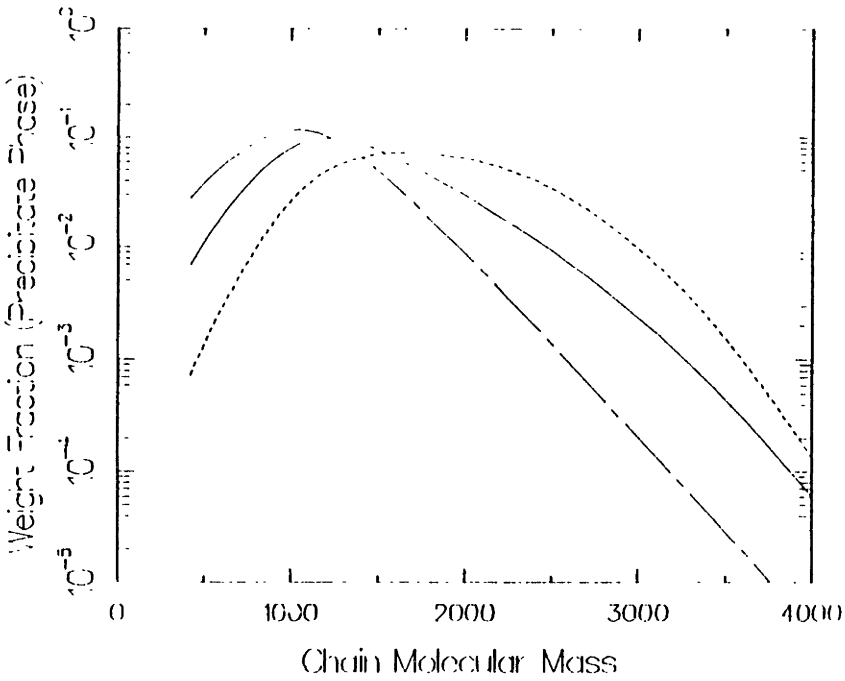

Figure 7.25: Comparison of predicted precipitate polymer compositions, on a first three mer-free basis for the precipitation polymerization of 3.33 wt% styrene in ethane, initiated with AIBN at 25 MPa and 333K for different values of k_p. *(---)5ℓ mole^{-1}s^{-1}, (——) 1ℓ mole^{-1}s^{-1}, (— - —)0.5ℓ mole^{-1} s^{-1}.*

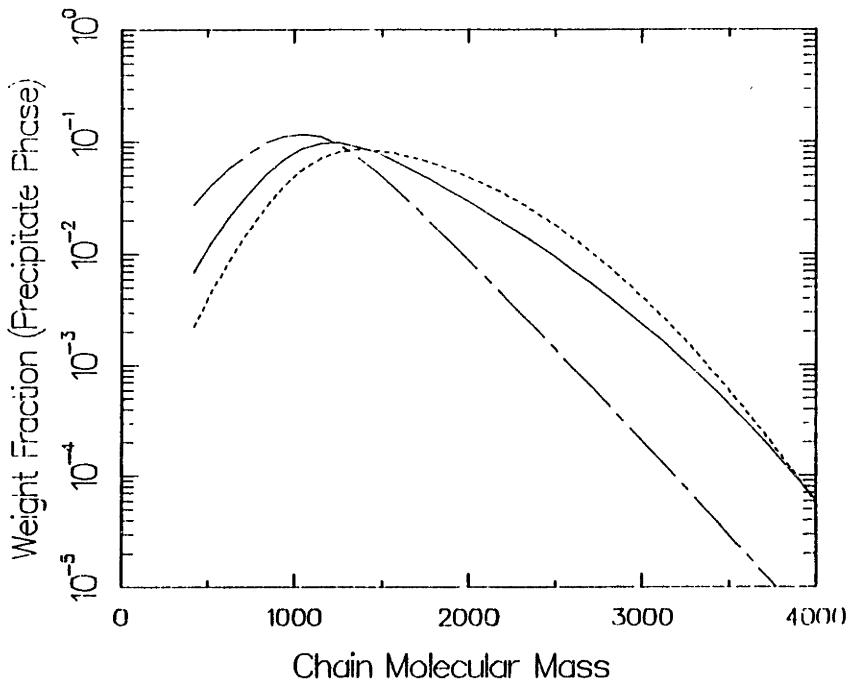

Figure 7.26: Comparison of predicted precipitate polymer compositions, on a first three mer-free basis for the precipitation polymerization of 3.33 wt% styrene in ethane, initiated with AIBN at 25 MPa and 333K for different value of k_t. *(---) 1.0×10^{5}ℓ mole^{-1}s^{-1}, (——) 4×10^{5}ℓ mole^{-1}s^{-1}, (—— - —) 1.6×10^6 ℓ mole^{-1}s^{-1}.*

- The precipitate composition, however, is very sensitive to changes in k_p, and when k_p is changed from 0.5 ℓ $mole^{-1}s^{-1}$ to 5.0 ℓ $mole^{-1}$ s^{-1} the maximum is seen to change from about a degree of polymerization of 10 to approximately 20. Also, the peak becomes flatter as one proceeds to higher k_p. The predicted molecular mass distributions in the precipitate phase (and hence the SCF-phase) are thus dependent strongly on the k_p value employed in the modelling.
- Changes in the termination rate constant, k_t, also, do not have an appreciable effect on the predicted molecular mass distribution. Variations of k_t do not effect the peak in the molecular mass distribution, although the shape of the distributions are altered somewhat by changes in k_t.

In summary, therefore, the transient model may be employed to estimate quantitatively all observed trends in the precipitate polymer composition with variations in pressure at low monomer concentrations. At higher monomer concentrations, however, the model predictions, especially at high molecular masses, is not very good and may be attributed to the fact that the addition of large quantities of the monomer may change the partitioning behaviour of the SCF solvent. Gas phase polymer concentrations are also well reproduced at the low molecular mass end; at higher molecular masses the trends are qualitatively reproduced although there is no quantitative agreement between the model predictions and the experimental data. The model predictions are sensitive to variations in k_p, and changes in this variable alter the peak molecular mass and the shape of the molecular mass distribution of the precipitate polymer. Variations in k_i and k_t, however, do not have as pronounced an effect as variations in k_p, although changes in these variables do cause some changes in the absolute numbers predicted.

7.3.3 The Steady-State Model

In Section 6.2.4 we have developed a steady-state model for the modelling of SCF precipitation polymerization reactions in a fashion analogous to steady-state models for single-phase liquid polymerizations. In this section we examine the fits to experimental data obtained by employing this steady-state model and examine its utility in this context.

We do not utilize the steady-state model to predict precipitation times, and molecular mass distributions until after the instant of precipitation. This is because our interest is in mainly obtaining the compositions of the precipitate and SCF-phase polymers at large times, which we have shown in Section 7.2.3.1 to be time independent when examined on a first three mer-free basis.

In the correlation using the steady-state model, we employed essentially the same values of k_i, k_t and k_p that were utilized in the transient model for the correlation of the precipitation polymerization results for 3.33 wt% styrene in ethane at 17 MPa and 333K. (We present results at only one operating condition, as an example. The predictions at the other pressures have essentially the same trends.) In Figure 7.27 and 7.28, we demonstrate the fits obtained by employing the steady-state model. It can be observed, that in contrast to the transient model, the steady-state model gives an excellent fit to the gas-phase data, while the precipitate-phase compositions are not well correlated. There are two possible reasons for this behaviour of the steady state model:

- Both, the transient and the steady-state models, fit the experimental data quantitatively only in a single phase. The disagreement of the models is seen to be accentuated at molecular masses >1000, where we have no measured partition coefficient data from the precipitation experiments. It is our surmise that polymers of molecular mass > 1000 are present in such small quantities (*ca.* $< 10^{-4}$ mass fraction) in the precipitate phase that equilibrium between the two phases may not be achieved due to diffusional limitations (as discussed in

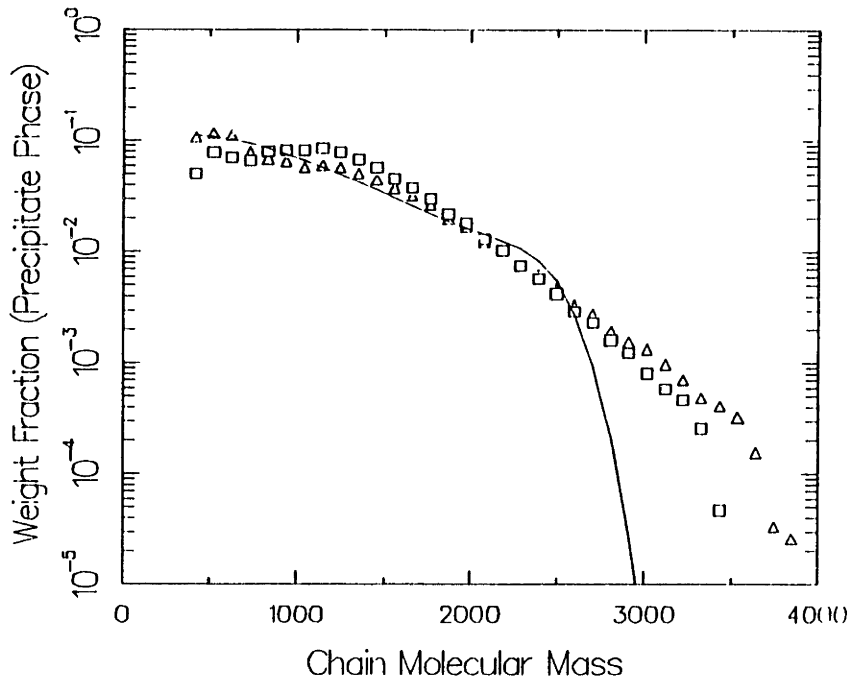

Figure 7.27: Comparison of precipitate polymer compositions, on a first three mer-free basis for the precipitation polymerization of 3.33 wt% styrene in ethane, initiated with AIBN at 17 MPa and 333K. (□) and (△) represent experiment, while (——) is prediction of the steady-state model.

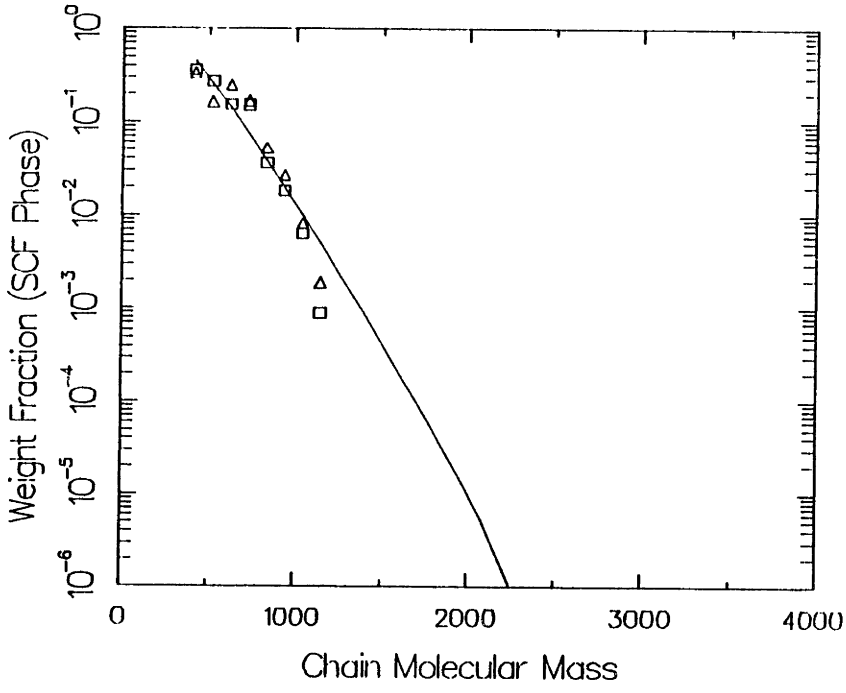

Figure 7.28: Comparison of SCF polymer compositions, on a first three mer-free basis for the precipitation polymerization of 3.33 wt% styrene in ethane, initiated with AIBN at 17 MPa and 333K. (□) and (△) represent experimental data, while (——) is prediction of the steady-state model.

Chapter 4). This provides us with the rationale of expecting quantitative fits by our models to data from only a single phase. This disagreement may be resolved by the inclusion of diffusion control in any future models that may be developed. A related problem then would be the accurate measurement of diffusion coefficients of the polymer chains as a function of pressure, temperature and chain length.

- An important question to be answered relates to the difference in behaviour of the transient and the steady-state models for the prediction of the compositions of the two equilibrium phases. It is seen (in Figure 7.17) that the transient model fits the precipitate phase well, a fact that may be rationalized when it is realized that this model is fit to precipitate polymer compositions. However, the steady-state model is seen to correlate the SCF phase data with parameters employed in the transient model. One likely solution may be that the transient equations for the SCF phase [Eq.(6.27)-(6.35)], for the low molecular mass polymers, do not feel the effect of the solid phase, since m_s and $dm_s/dt \ll 1$. In essence therefore, we solve two uncoupled problems, the gas-phase and precipitate-phase compositions. For the steady-state model, however, from Eq.(6.32), it is clear that the gas-phase compositions depend directly on the solid-phase compositions through dm_s/dt. In this case therefore, the solution of the equations yielding the compositions of the two phases are not decoupled. This may partially explain the discrepancy in the results obtained from the two models.

In summary, therefore, there exist differences between the predictions of the two models. It is the conclusion of this work, therefore, that this inconsistency between the models may be caused due to our lack of knowledge of the partitioning behaviour of polystyrene chains above a molecular mass of 1100 g $mole^{-1}$ in the polymerization experiments. Experimental results obtained in the measurement of partition coefficients in Chapter 4 suggest that diffusion of polymer chains in the coacervate phase may be an important effect for chains present in small quantities. These chains may thus not be at a true, thermodynamic equilibrium across the SCF and the precipitate phases, under reaction condition. It is our anticipation that model predictions

would be more consistent if diffusion limitations were incorporated in the formulation.

CHAPTER 8

PRECIPITATION POLYMERIZATIONS IN SUPERCRITICAL FLUIDS: SUMMARY

Results have been presented in Chapter 7 to demonstrate the viability of SCF precipitation polymerizations to produce polymers of a narrow molecular mass distribution. Also, models developed in Chapter 6 have been employed to correlate quantitatively experimental data on the compositions of the SCF and precipitate polymers. The main results of Chapter 6 and 7 are summarized below.

8.1 SINGLE PHASE POLYMERIZATION RESULTS

It has been demonstrated that an initiator is necessary to observe, experimentally, the presence of *any* polymer in the SCF phase. Also a minimum concentration of monomer (~3.3 wt% monomer in ethane at 17 MPa and 333K) is required to observe the presence of a *precipitate polymer* phase.

Reactions conducted below the minimum monomer concentration yield no precipitate phase polymer, at least within the accuracy of our experiments. Data from these *single phase reactions* may be employed to evaluate the probability of propagation of a radical of chain length i to form a chain of length i+1, ξ_i, under these conditions. ξ_i, in its most general form is defined as,

$$\xi_i = \frac{\text{Rate of propagation of radicals of length i}}{\text{Rate of propagation + Rate of termination of radicals}} \qquad (8.1)$$

For the case of a single phase polymerization we have observed, (following Flory (1953) and others [Odian (1985); Bovey and Winslow (1979)]) that ξ_i

is independent of chain length. Also, we have shown that under supercritical conditions the dominant termination mechanism is disproportionation (Section 6.4). Under these assumptions, we may rewrite ξ_i independent of i as,

$$\xi = \frac{1}{1 + (k_i k_t [I])^{\frac{1}{2}}/k_p [M]} \tag{7.6}$$

where k_i, k_p and k_t represent the initiation, propagation and termination rate constants, respectively. The molecular mass distribution of the polymer produced in a single phase reaction may therefore be represented by a "most probable distribution", following Flory (1953), i.e.,

$$w_x^v = x\xi^{x-1}(1-\xi)^2 \tag{7.7}$$

In Table 7.4 we showed ξ values obtained by fitting Eq(7.7) to data from the single phase polymerizations in an SCF. It was observed that ξ values were small (~0.5) under these conditions, much smaller than in conventional liquid phase solvents (where ξ is frequently greater than 0.99). The anomalous properties of dilute components in a supercritical mixture reduces the absolute value of k_p relative to the corresponding values in a liquid solvent and explain the unusually small value of ξ (Section 6.4). Accordingly, the rates of propagation of radicals relative to termination in an SCF are smaller than in conventional, liquid-phase systems and polymers of relatively small average molecular mass, i.e., small values of the kinetic chain length, ν_{cl} are obtained. Consequently, the polydispersity of the product polymer,

$$M_w/M_n = 1+\xi \tag{7.5c}$$

is smaller in SCF solvents than for polymers produced in liquid phase polymerizations. Polymers produced in SCF are therefore, of a smaller average molecular mass and have narrower molecular mass distributions than

polymers synthesized in liquid phase reactions.

As pressure is increased the character of a SCF solvent becomes more liquid-like, and hence the polymers synthesized at higher pressures (still in a single phase polymerization) have polydispersities approaching the liquid-like value (ideally, 2.0).

8.2 SCF PRECIPITATION POLYMERIZATION: RESULTS

8.2.1 Experimental Results

SCF Polymerization reactions conducted with styrene (above a minimum concentration, *ca.* 3.33 wt% at 17 MPa and 333K) in ethane demonstrate the presence of a *precipitate* polymer phase, with a composition distinct from the polymer in the SCF phase. Analysis of these two, different polymer samples show that the dominant components even after reaction times of 48 h, in both the SCF and coacervate phases are monomer and initiator, verifying that conversions are low, even at relatively large reaction times. This is an independent check of the low value of probabilities of propagation, as deduced from the single phase polymerization experiments.

From the precipitation polymerization experiments, we may deduce apparent "partition coefficients" for the different chain length oligomers between the SCF phase and the solid phase. These partition coefficients, defined as,

$$K_i = \frac{w_i^v}{w_i^s} \tag{8.2a}$$

$$= \frac{\text{Weight fraction of chain i in SCF phase}}{\text{Weight fraction of chain i in SCF-free precipitate phase}} \tag{8.2b}$$

were then compared to corresponding partition coefficients for the respective

chains as measured in solubility experiments under the same conditions of pressure and temperature. For polystyrene chains above a molecular mass of 400, the partition coefficients deduced from the two experiments were identical, within experimental error. *The governing mechanism in a precipitation polymerization reaction therefore, is a dynamic equilibrium of polymer chains across the two phases. For molecular masses greater than ~400 the equilibrium partition coefficients, as measured in the solubility experiments govern this fractionation*, while below this molecular mass the equilibrium is influenced due to the presence of dissolved initiator (either due to the presence of solution non-idealities, or the influence of initiator-fragments present at the end of each chain).

A problem frequently encountered in liquid phase precipitation polymerizations is an enhanced reaction rate in the precipitate phase (as compared to the liquid phase) due to the increased concentrations of unterminated radicals in the precipitate. This phenomenon, known as the Tromsdorff effect, is undesired due to the resultant broadening of the molecular mass distribution of the precipitate polymer. In contrast, the time evolution of precipitation polymerization reactions of styrene in ethane described in Section 7.2.3.1 suggests that there is no significant reaction in the precipitate-phase, since the precipitate molecular mass distributions do not broaden as one proceeds to larger reaction times. Two arguments can be made for this lack of Tromsdorff effect in SCF polymerizations:

- Small values of kinetic chain lengths, ν_{cl}, are encountered at the monomer concentrations employed in the experiments. The majority of chains in the precipitate phase may thus be terminated, and it is therefore unlikely that further reactions occur in the precipitated polymer.
- Also, Flory (1953) has suggested that the presence of a Tromsdorff effect requires a minimum amount of plasticization of the polymer-phase. It is speculated that the poor solvent quality of the SCF coupled with the fact that the polymer is close to its glass transition temperature (T_g) ensure that the coacervate is not plasticized at the operating conditions considered.

It is for these reasons that we observe no reaction in the precipitate phase although it contains *ca.* 30 wt% of monomer and also contains *ca.* 10 wt% initiator. No quantitative data exist to substantiate these claims, and we suggest two possible routes for the resolution of this problem:

- Macroscopic quantities of polymer must be synthesised and analyzed for unterminated radicals, say by ESR.
- Experiments must be designed so that a SCF precipitation polymerization may be conducted under conditions where the kinetic chain length, ν_{cl}, is larger than the peak molecular mass in the precipitate. In this case, a larger fraction of polymer chains in the precipitate will be unterminated, allowing us, in principle, to observe a Tromsdorff effect.

The sensitivity of the precipitate polymer compositions to changes in operating conditions (*viz.*, pressure, temperature, monomer concentration and initiator concentration) were also studied, and we summarize below the results of these investigations:

a. Pressure: The pressure of operation determines the fractionating behaviour of the SCF solvent. As one proceeds to higher pressures, the solvent-character of an SCF moves from gas-like (low solubility, "strong" fractionation) to liquid-like (high solubility, "poor" fractionating power). At higher pressures, therefore, it is expected that the precipitate obtained will be of a broader molecular mass distribution, since the solvent now is less discriminating with respect to the fractionation of chains on the basis of molecular mass, between an SCF-rich phase and a polymer-rich phase.

Experimental results presented in Section 7.2.3.1 for three operating pressures (12, 17 and 25 MPa) show that, indeed, as one proceeds to higher pressures, the product polymers are of a broader molecular mass distribution. Also, the average molecular mass of the precipitate polymer increases with increasing pressure.

From the experimental results at the three pressures, it was also deduced that the partition coefficients for polystyrene chains of molecular masses greater than ~400 as measured in the reaction experiments are identical to corresponding results obtained from the solubility experiments. For lower molecular mass chains, however, the partition coefficients as measured in the polymerization experiments are smaller than those from the solubility results.

Also, in all experiments conducted to examine the effect of pressure (all conducted at 3.33 wt% styrene in ethane, at 333K with 5.84×10^{-5} gm AIBN/gm ethane), there was no observable broadening of the precipitate molecular mass distribution with increasing reaction time implying that the Tromsdorff effect does not manifest itself at the examined pressures.

b. Monomer Concentration: Initial monomer concentration is an important variable due to two reasons. First, since the kinetic chain length, ν_{cl}, increases linearly with [M], it is expected that longer chain polymers may be produced in the SCF phase at higher monomer concentrations. Also, since polystyrene chains are completely soluble in styrene, an increase in monomer concentration is expected to make the fractionation character of the SCF phase more liquid-like. The implication of both these statements is that the average molecular mass of the precipitated polymer should increase as [M] increases.

SCF precipitation polymerizations were conducted at three monomer concentrations (3.33 wt%, 5.0 wt% and 6.66 wt% styrene in ethane at 17 MPa and 333K). Results at the three conditions illustrate that the average molecular mass of the precipitate polymer does increase; however, their polydispersities, M_w/M_n, are essentially independent of [M]. Also, at these conditions, there is no observed broadening of the precipitate molecular mass distribution at all reaction times, implying that no autoacceleration effects are experienced.

An interesting point concerns itself with the relative insensitivity of

the position and composition of the peak in the molecular mass distribution of the precipitate phase to changes in operating conditions. We have presented arguments to show that this peak represents the point where the SCF-phase polymer compositions change from kinetic control to precipitation control, i.e., below this molecular mass the molecular mass distribution of the SCF polymer is determined by the rates of propagation of radicals, while above this molecular mass the rate of precipitation determines the SCF-phase composition. The lack of sensitivity of the peak molecular mass to variations in operating conditions, therefore, implies that this change in control, from kinetic to precipitation, is essentially independent of the operating conditions employed in a SCF polymerization.

c. Other Variables Examined: Variations of precipitate compositions to changes in temperature and initiator concentration were also examined. It was found that initiator concentration ($0<[I]\leq 5.84\times10^{-5}$ gm/gm ethane) and temperature (333K-343K) did not affect the composition of either the SCF or the precipitate phase. However, it was observed that higher values of both variables resulted in higher conversions of monomer to product polymer. The rationale for this is provided in sections 7.2.3.4 and 7.2.3.5 respectively.

8.2.2 Modelling Results

In Chapter 6, we have presented two models to correlate experimental data obtained from SCF precipitation polymerizations.

8.2.2.1 The Transient Model: The fundamental assumption in the formulation of the transient model is that concentrations of both radicals and precipitated polymer chains are time dependent. The time evolution of a precipitation polymerization in this framework may be pictured to occur in three, distinct stages:

a. Initially, the reaction mixture of SCF, monomer and initiator is a *single-phase, homogenous* solution. Reaction begins through the

decomposition of initiator to form free-radicals which then add monomer to form longer chain-radicals in a propagation step. The reaction maybe terminated by a bimolecular addition or by disproportionation [Eq.(2.9)-(2.13)].

b. As the reaction proceeds in time, the concentrations of polymer chains, terminated and unterminated, increase and, at some point, they nucleate to form a second, solid phase.

c. Subsequent to this precipitation step, polymers of all chain-lengths equilibrate between the two phases following the partition law as discussed in Section 8.2.1 for the distribution of polymer chains between a coacervate-phase and a SCF-phase. Reaction continues to occur in the SCF phase but not in the precipitate-phase.

Each of these steps have been formulated into a mathematical model. A salient feature of the model, within the scope of this work, is its lack of sensitivity to the assumed nucleation model (step b). We have observed in our use of the model that the final compositions of the two equilibrium phases are essentially governed by the reaction rate constants, *viz.* k_i, k_p and k_t, and the underlying equilibria of polymer chains between the SCF and coacervate-phases. In the implementation of the model, therefore, a simple nucleation model has been employed to capture qualitatively the essential features of the phase separation phenomenon. This involved the delineation of the first chain length that reached its binodal concentration in the gas-phase. The binodal concentration of a chain was determined from the partition law,

$$\log_{10}(K_x) = \log_{10}(w_x^v/w_x^s) = C_0 - C_1 X_x \qquad (4.4)$$

by setting w_x^s equal to unity. The qualitative nature of this model, in predicting nucleation time, must be emphasised in this context, and if more detailed information such as particle sizes, or volume to surface area ratios of the particles formed, is desired, then a more exact theory of nucleation, as outlined in Section 6.1 must be employed.

A question related to the implementation of this model to correlate SCF

polymerizations is to obtain an order of magnitude estimate of the reaction rate constants, k_i, k_p and k_t (both by addition and disproportionation) in SCF solvents, relative to corresponding values of these constants in liquid-phase polymerizations. To interpret the effect of SCF solvents on reaction rate constants, it must be realized that dilute components dissolved in a supercritical fluid frequently have large, negative partial molar volumes. On examining the relevant reactions in a polymerization process,

$$I \longrightarrow 2R^{\bullet} \qquad \text{(Initiation)} \qquad (2.9)$$

$$RM_x^{\bullet} + M \longrightarrow RM_{x+1}^{\bullet} \qquad \text{(Propagation)} \qquad (2.12)$$

$$RM_x^{\bullet} + RM_y^{\bullet} \longrightarrow P_{x+y+2} \qquad \text{(Addition)} \qquad (2.13a)$$

$$\longrightarrow P_{x+1} + P_{y+1} \qquad \text{(Disproportionation)} \qquad (2.13b)$$

in the context of the LeChatelier principle, it is immediately clear that the rate constant for termination by disproportionation will not be affected dramatically by the large negative partial molar volumes of the reactants and products. In contrast, a bimolecular reaction which yields a single product molecule, such as the propagation or the termination by addition, are unfavourable under these conditions. The overall manifestation of this effect is a reduction in the propagation (or termination by addition) rate constant. By extension, an opposite behaviour may be observed in the initiation reaction, where the initiator dissociates to form two free radicals.

By employing typical values for SCF solvents, through the use of the Activated States theory, we have shown that the propagation and termination by addition steps will have rate constants that are typically 1-2 orders of magnitude smaller than in liquid solvents. Also the initiation and the disproportionation steps are essentially unaffected. The consequence of these anomalous kinetic rate constants are:

1. The rate of polymerization in SCF relative to liquid phase solvents

is small at the lowest pressures. However, as pressure is increased the polymerization rate will increase and approach the "liquid-like" value.

2. Polymers of a low average molecular mass and narrow molecular mass distributions will be produced. In the past, special chemistry was needed to synthesize low molecular mass polymer standards. SCF, thus are convenient media for the synthesis of such low volume, high value-added products.

The transient model for SCF polymerization reactions has been used to correlate successfully precipitate polymer compositions and also to reproduce qualitatively the molecular mass distribution of the polymers in the SCF phase at several pressures. Kinetic parameters obtained by fitting the model to experiment follow the trends expected for these constants relative to corresponding numbers in liquid solvents. However, the model predictions for different monomer concentrations are not as satisfactory (see Section 7.3.2).

8.2.2.2 The Steady-State Model: In the past it has been common practice to model free-radical polymerization processes as reactions in which rates of the formation and loss of radicals are at a steady state (see Section 6.2.4). It was our aim to explore the feasibility of using a steady-state model for our reaction system due to the inherent simplicity of dealing with the algebraic equations rather than differential equations.

We chose to employ the steady-state approximations only in cases where there were two phases at equilibrium, *viz*. this model was used only subsequent to precipitation due to the fact that all experimental data for SCF precipitation polymerizations were available only at long times.

The important assumption in this formulation was, therefore, that subsequent to precipitation all concentrations (except monomer and initiator), in both phases are constant, as suggested by experimental findings. The only change with time then, corresponds to an increase in mass of the solid due to precipitation. On solving the algebraic equation set obtained by setting

the time derivatives in the transient model equations [Eq.(6.17)-(6.21)] to zero, we obtain the time-invariant compositions of the radicals and terminated polymer chains in both the SCF and the precipitate phases.

We employed this model to correlate the experimental data for a variety of conditions using essentially the same parameters as employed in the transient model. The fits obtained to the SCF phase compositions on a first three mer-free basis were satisfactory, but the coacervate-phase compositions were not well predicted. The reason for this is speculated to be the effect on the partitioning behaviour of polymers present in small quantities in the coacervate phase, that may be dominated by the effects of diffusion of polymer chains in this phase. These chains may thus not be in a true, thermodynamic equilibrium between the SCF and the precipitate phases under reaction conditions. It is our anticipation that model predictions will be more consistent if this feature of diffusion limitations were incorporated in the formulation.

At this time, therefore, the steady-state model is not adequate to represent the phenomena occurring in a SCF precipitation polymerization.

CHAPTER 9

CONCLUSIONS AND RECOMMENDATIONS FOR FUTURE WORK

9.1 CONCLUSIONS

There are four important conclusions that may be drawn from the results of the work.

We have shown that supercritical fluids (SCF) are powerful fractionating media for polymers and that this fractionating power may be modified from gas-like to liquid-like with relatively small changes in pressure, or by the addition of small amounts of liquids as co-solvents.

Data obtained for the solubility of polystyrene in SCF have been correlated with a statistical-mechanics based lattice model equation of state which was developed to model mixtures of molecules of disparate sizes. The lattice EOS reproduced all experimentally observed trends for the polystyrene-ethane system across variations in pressure, temperature and polymer chain length with a single apparently constant value of a binary interaction parameter, δ_{12}, in most cases.

Precipitation polymerization reactions have been conducted in SCF to demonstrate the viability of this novel synthesis scheme to produce polymers of a low average molecular mass and a relatively narrow molecular mass distribution. In the analysis of data from these reaction experiments we also verified that polymer chains in these experiments partition themselves across the reacting SCF phase and the precipitate phase following the same partition law as measured in the solubility experiments (This result is invalid for the smallest chain lengths). Also no reactions occur in the precipitate phase suggesting the absence of a Tromsdorff effect in the coacervate. As one proceeded to higher pressures or monomer concentrations,

the average molecular weight of the precipitate increased suggesting the approach to liquid-like behaviour of the SCF solvent.

Data from the precipitation polymerizations have been quantitatively correlated with a transient model developed for this purpose. On fitting this model to experiment, and independently from activated state theories, we have shown that SCF solvents selectively modify the reaction rate constants for specific kinetic steps in the reaction mechanism thus allowing for the synthesis of polymers of molecular weight distributions significantly different from polymers produced in liquid-phase systems.

9.2 RECOMMENDATIONS FOR FUTURE WORK

There are several aspects of the examined work that need to be clarified or explored in greater detail. Below are listed some of the areas which potentially may help in understanding the unresolved aspects of SCF precipitation polymerizations:

- Pure polystyrene and ethane were employed in the solubility measurements. However, in the precipitation experiments we have suggested that the fractionation power of the SCF solvent may change as one uses larger quantities of monomer. Solubility experiments with SCF mixtures of ethane and styrene must be performed to delineate the effect of changing monomer concentration on the partitioning ability of SCF.

- In Chapter 7 we have suggested that the addition of AIBN to a mixture of styrene-polystyrene-ethane may result in solution non-idealities that cause the short polymer chains to have smaller partition coefficients as compared to a case where no AIBN is present. Solubility measurements for polystyrene mixed with AIBN will help clarify this issue.

- Also, in Chapter 7 we proposed that the lower partition coefficients

for the small chain length oligomers may be due to the presence of an AIBN end group on each chain. Fractionation experiments must be conducted with polystyrene samples produced in the precipitation polymerization reactions to explore this possibility. A related question then is to understand the effect of diffusion on the solubility of the long chain polymers (that are present in weight fractions less than *ca.* 10^{-3}) into the SCF phase.

- In all our studies with the polystyrene-ethane system we have demonstrated the presence of a log-linear dependence for K_i on X_i. In the existing literature it has been shown for liquid solvents that this log-linear behaviour tends to break down as one proceeds to higher molecular weight polymers. It would be relevant to examine the solubility of higher molecular weight polymers in SCF to probe if the linearity at low molecular weights does extend to the longer chain length polymers.

- In the modelling of solubility data using the lattice EOS we assumed that the polystyrene phase is always at thermodynamic equilibrium state. The implication of this statement is that the polymer phase is above its glass-transition temperature. To date, however, few data exist that illustrate the effect of polymer chain length, solvent SCF concentrations, pressure or temperature on the T_g of such polymers. A potentially interesting problem is the measurement and the subsequent modelling of the glass transition temperatures of polymers as a function of these operating variables.

- Also, in the modelling we assumed that the multicomponent polymer-SCF equilibrium could be treated by a linear combination of n-mer-SCF quasi-binaries. Although this assumption is satisfactory above a polymer molecular weight of ~800 g $mole^{-1}$, below this molecular weight end effects become dominant. A possible remedy for this issue is to model the polymer-SCF system as a multicomponent system, possibly by using concepts of continuous thermodynamics. Also, end effects should be accounted for in the determination of the pure

component parameters of the various chain length polymers.

- An interesting observation made in the precipitation experiments regards the lack of a Tromsdorff effect in the coacervate phase. We have suggested that the reason for this phenomenon is due to the inherently small kinetic chain lengths encountered in SCF precipitation polymerizations which ensure that most precipitated chains are terminated.

  a. Convincing arguments for the absence of reaction in the precipitate phase may be provided only if macroscopic quantities of polymer are synthesised and analyzed for unterminated radicals, say by ESR.

  b. Another possible route to study the lack of a Tromsdorff effect would be to increase the monomer concentration. It must, however, be remembered that the addition of monomer to ethane will have the same effect on the fractionating ability of the SCF as was achieved by the addition of propane to ethane in the solubility experiments, as reported in Chapter 4. While the need for careful design of experiments is crucial, it is nevertheless significant to analyze experiments under higher [M] since there are only two possible outcomes:

  - A Tromsdorff effect may be observed.
  - If there is no [M] effect, then we can obtain higher precipitation rates. If the presence of a large number of unterminated radicals is discovered in the coacervate phase in any of these experiments, then this precipitate may be employed to form block copolymers with small average degrees of polymerization with other monomers, again in an SCF solvent.

- We have inferred from our experimental data and modelling that the kinetic rate of propagation in an SCF is much smaller than in liquid solvents. However, a direct independent technique for the measurement of reaction rate constants must be devised to substantiate this claim.

- A steady-state model was formulated to correlate experimental data

from the precipitation polymerizations. However, we have shown that this model does not accurately fit the experimental trends. The reason for the failure of the steady-state model is not clear at this juncture, and further study of this lack of agreement may help improve our understanding of the complex mechanism of SCF precipitation polymerizations.

NOTATION

ENGLISH

a	Attractive parameter in the van der Waals EOS (Jm^3mole^{-2})
a	Activity of component [Eq(3.NN)]
$\underline{A}$	Total Helmholtz energy of system (J)
A(T),B(T)	Constants, [Eq(4.3)]
[AH]	Concentration of chain transfer agent [Eq(2.14)]
A_λ	Absorbance [Eq(2.2)]
b	Volume parameter in the van der Waals EOS (m^3mole^{-1})
B	Generalized property [Eq(0.2)]
B_λ	Molar absorbance
c	Solute concentration in SCF phase [$mole\ m^{-3}$; Eq(2.1)]
C_p	Specific heat ($J\ mole^{-1}\ K^{-1}$)
C_0, C_1	Constants [Eq(4.4)]
$D, \mathcal{D}$	Diffusivity ($m^2\ s^{-1}$)
d_λ	Optical length of sample cell (m)
E	Potential energy of the system of molecules
f	Fugacity of a component (MPa)
g	Combinatorial term in Canonical Partition function
h	Planck's constant
ΔH_{sub}	Enthalpy of sublimation ($J\ mole^{-1}$)
I	Light intensity [Eq(2.2)]
[I]	Initiator concentration ($mole\ \ell^{-1}$)
k_B	Boltzmann's constant ($J\ mole^{-1}\ K^{-1}$)
k_i	Initiation rate constant (s^{-1})
K_i	Partition coefficient of polymer of chain length i
K_i^{old}	Partition coefficient of polymer of chain length i as defined in the existing literature [Eq (4.2)]
K	Reaction rate constants [Chapter 6]
k_p	Propagation rate constant ($\ell\ mole^{-1}\ s^{-1}$)
k_t	Termination rate constant ($\ell\ mole^{-1}\ s^{-1}$)
k_r	Rate constant of a bimolecular reaction ($\ell\ mole^{-1}\ s^{-1}$)
m_s	Mass of precipitate per gm of SCF (gm./ gm. SCF)
[M]	Monomer concentration ($mole\ \ell^{-1}$)
$[M]_0$	Initial monomer concentration ($mole\ \ell^{-1}$)
M	Molecular weight ($g\ mole^{-1}$)
M_n	Number averaged molecular weight ($g\ mole^{-1}$)
M_w	Weight averaged molecular weight ($g\ mole^{-1}$)
$(MW)_i$	Molecular weight of polymer of chain length i ($g\ mole^{-1}$)
$(MW)_I$	Molecular weight of initiator ($g\ mole^{-1}$)
n_{pol}	Number of segemnts per polymer molecule (Notation of Flory, 1953)
n_i	Concentration of polymer of chain length i ($mole\ \ell^{-1}$)
N	Number of moles
N	Number of mixture components [Chapter 3]

P	Pressure (Nm^{-2})
P_{osm}	Osmotic pressure (Nm^{-2})
$[P_x]$	Concentration of polymer of chain length i (mole ℓ^{-1})
q	Effective chain length of a chain molecule, accounting for the connectivities of the segments
r	Radial position [Eqs(4.15), (4.16)]
r	Number of segments per molecule
r_p	Rate of polymerization (mole ℓ^{-1} s^{-1})
R	Universal gas constant (J $mole^{-1}$ K^{-1})
R	Radius of sphere [Eqs(4.16), (4.17)]
$R^{\bullet}$	Radical formed by dissociation of initiator
$[RM_x^{\bullet}]$	Concentration of radical with x monomeric unit (mole ℓ^{-1})
Sc	Schmitt number ($\equiv \nu/D$)
t	Time (s)
t	Logarithm of absorbance [Eq (2.3)]
Δt	Time step in integration [Eq(6.37)]
$t_{\frac{1}{2}}$	Half life (s)
t_D	Characteristic diffusion time (s)
t_{rxn}	Reaction time (s)
T	Temperature (K)
T_g	Glass Transition Temperature (K)
u, w	Constants in cubic EOS [Eq(3.3)]
v	Phase molar volume (m^3 $mole^{-1}$)
v_H	Lattice unit cell size (m^3 $mole^{-1}$)
v_s	Molar volume of solvent (m^3 $mole^{-1}$; Notation of Flory, 1953).
v^*	Hard core volume (m^3 $mole^{-1}$)
$\underline{V}$	Total volume of system (m^3)
v_H	Lattice unit cell volume (m^3 $mole^{-1}$)
w_i	Weight fraction of chain length i (gm mer/gm of phase)
x_i	Mole fraction
X_i	Chain length of polymer
$y^{(n)}$	n^{th} Legendre Transform
y_i	Mole fraction of species i
z	Lattice coordination number
zq	Number of external contacts per molecule
Z	Compressibility (Pv/RT) (dimensionless)

GREEK

α_0, α_1	Constants [Eq(4.6)]
β	Thermodynamic temperature ($\equiv 1/k_B T$)
$\gamma(T)$	Term in chemical potential accounting for internal degrees of freedom of a chain molecule
Γ	Non-randomness correction [Eq(3.46)]
δ_{ij}	Binary interaction parameter in EOS [Eq(3.52)]
δ', δ''	Reference state chemica potentials [Eqs(3.63), (3.64)]
$\Delta\epsilon_{ij}$	$\equiv 2\epsilon_{ij} - \epsilon_{ii} - \epsilon_{jj}$
ϵ	Interaction energy between molecule segments (J $mole^{-1}$)
ζ	$\equiv \epsilon_{11}/RT$
η_1, η_2	Constants [Eq(2.5)]
η', η''	Reference state chemical potentials [Eqs(3.65), (3.66)]

ϑ	Surface area fractions of molecules
κ_T	Isothermal compressibility (bar^{-1})
λ	Wavelength [m; Eq(2.2)]
λ	Function accounting for the number of internal degrees of freedom of a chain molecule
$[\lambda_i]$	Concentration of all species of chain length i (mole ℓ^{-1})
μ	Chemical potential
ν	Kinematic viscosity ($m^2\ s^{-1}$)
ν_i	Stoichiometric coefficient [Eq(6.5)]
ν_{cl}	Kinetic chain length in a polymerization reaction
ξ	Constant [Eq(2.6)]
ξ_0, ξ_1	Constants [Eq(4.8)]
ξ_{ij}	Term in the quasi-chemical equation [Eq.(28a)]
ξ	Probabilty of propagation [Chapter 7 and 8]
π	= 3.14152654
ρ	Density (mole m^{-3})
ρ_{SCF}	SCF density (kg m^{-3})
σ	Separation factor [Eq(2.6)]
σ	Derivative taken on saturation curve [Eq(4.13)]
σ_∞	Separation factor for infinite chain length polymer
τ_1, τ_2, τ_3	Functional equation representation [Eqs(3.23), (3.24)]
Ω	Canonical Partition Function
Ω_c	Configurational contribution to the canonical partition function
χ	Flory-Huggins parameter
ϕ	Fugacity coefficient
ϕ_i	Volume fraction of species i
Φ	Weight fraction of SCF in polymer [Eq(4.7b)]
ψ_i	Transformed mole fractions for Newton-Raphson search [Eq(3.60)]

SUPERSCRIPTS

'	Phase dilute in polymer
''	Phase concentrated in polymer
~	Reduced quantity
*	Reducing quantity
-	Surface area fractions on a hole-free basis
‡	Activated State
^	Property in a mixture
0	Random configuration of molecule segments and holes
liq	Property in liquid solvent
s	Condensed phase property
s,t	Phase identity [Eq (3.59)]
SCF	Property in SCF solvent
v	Gas phase property

SUBSCRIPTS

0	Species 0, holes
1	Species number 1
11	Contacts between segments of two molecules of species 1
a	Attractive property [Eq.(17)]

c	Critical property
c	Concentration based equilibrium constant [Chapter 6]
eq	Equilibrium property
f	Equilibrium constant based on fugacities [Chapter 6]
i	Species i
ij	Contacts between segments of an i molecule and a j molecule
j	Species j
ke	Kinetic energy contribution
L	Liquid phase property
liq	Liquid phase property
M	Mixture property
NR	Non-random configuration of molecule segments
osm	Osmotic term
pol	Polymer property
R	Random configuration of molecule segments
R	Repulsive contribution [Eqs.(3.31), (3.32)]
s	Solvent property (Flory-Huggins formulation)
sol	Solvent property
SCF	Property of supercritical fluid
V	Vapour phase property
x	Polymer chain length (used interchangably with i)
ϕ	Reaction rate constant based on fugacity coefficients

REFERENCES

Abraham K.P., Ehrlich P., "Partial Molar Volume of a Polymer in Supercritical Solutions", *Macromolecules*, 8(6),944(1975).

Abrams D.S., Prausnitz J.M., "Statistical Thermodynamics of Liquid Mixtures: A New Expression for the Excess Gibbs Energy of Partly or Completely Miscible Systems", *AIChE J*, 21(1), 116(1975).

Abuselme J.A., Vera J.H., "A Generalized Solution Method for the Quasi-Chemical Local Composition Equations", Submitted for publication to *J. Chem. Eng.*, 1986.

Angus S., Armstrong B., deReuck K.M., *International Thermodynamic Tables of the Fluid State of Carbon Dioxide*, Pergamon Press, Oxford, 1976.

Bamford C.H., Jenkins A.D., "Acrylonitrile: The Behaviour of Free Radicals in Heterogeneous Systems", *Proc. Roy. Soc. London*,A216,515(1953).

Bamford C.H., Jenkins A.D., "The Occlusion of Free Radicals: Physical Factors Determining the Concentration and Behaviour of Trapped Radicals", *Proc. Roy. Soc. London*, A278,220(1955).

Bamford C.H., Ledwith A., Sen Gupta P.K., "Particulate Precipitation Polymerization: A Convenient Procedure For the Synthesis of Crosslinked Polymers useful as Polymeric Supports", *J.Appl.Polym. Sci.*, 25, 2559(1980).

Barrett K.E.J., Thomas H.R., "Kinetics and Mechanism of Dispersion Polymerization", Dispersion polymerization in organic media, Ed. Barrett K.E.J., John Wiley and Sons, New York, 1975.

Bovey F.A., Winslow F.H., *Macromolecules: An Introduction to Polymer Science*, Academic Press, New York, 1979.

Brandup J., Immergut E.H., *Polymer Handbook*, Second Edition, John Wiley and Sons., New York,1975.

Breitenbach V.J.W., Wolf B.A., "Untersuchen von Phasengleichgewichten an Polymeroesungen mittels Saulenfraktionierung", *Die Makromol. Chemie*, 108, 263(1967).

Carnahan N.F., Starling K.E., "Intermolecular Forces and the Equation of State for Fluids", *AIChEJ*, 18(6),1184(1972).

Chatelain J., "Two Stage Bulk Polymerisation Process of Vinyl Chloride", *Br. Polym. J.*, 5, 457(1973).

Chrastil J., "Solubility of Solids and Liquids in Supercritical Gases", *J. Phys. Chem.*, 86, 3016(1982).

Debenedetti P.G., "*Diffusion in Supercritical Fluids*", PhD Thesis, Massachusetts Institute of Technology, 1984.

Debenedetti P.G. and Kumar S.K. "Infinite Dilution Fugacity Coefficients and the General Behavior of Dilute Binary Systems", *AIChE J*, 32(8), 1253(1986a).

Debenedetti P.G. and Kumar S.K. "Dilute Binary Mixtures: Thermodynamics and Fluctuation-theory Based Statistical Mechanics", *Presented at the AIChE meeting, Miami Beach*, November 1986b.

Diepen G.A.M., Scheffer F.E.C., " The Solubility of Naphthalene in Supercritical Ethylene II", *J. Phys. Chem.*, 57,575(1953).

Diepen G.A.M., Scheffer F.E.C., "The Solubility of Naphthalene in Supercritical Ethylene", *J. Am. Chem. Soc.*, 70,4085(1948).

Dieters U.K., "A New Semi Empirical Equation of State for Fluids I", *Chem. Eng. Sci.*, 36,1139(1981).

Donohue M.D., Prausnitz J.M., "Perturbed Hard Chain Theory for Fluid Mixtures : Thermodynamic Properties for Mixtures in Natural Gas and Petroleum Technology", *AIChEJ*, 24(5), 850(1975).

Eckert C.A., "High Pressure Kinetics in Solution", *Ann. Rev. Phys. Chem.*, 23, 2548(1972).

Ehrlich P., "Partial Molar Volume Anamoly in Supercritical Mixtures and the Free Radical Polymerization of Ethylene", *J. Macromol. Sci. Chem.*, A5(8),1259(1971).

Ehrlich P., Mortimer G.A., "Fundamentals of the Free-Radical Polymerization of Ethylene", *Adv. Polymer Sci.*, 7, 386(1970).

Erickson J.E., "*Selectivity of enzyme reactions using Supercritical Fluids*", Ph.D. Thesis, Massachusetts Institute of Technology, 1987.

Fitch R.M., Tsai C.H., "Particle formation in polymer colloids III: Prediction of the number of particles by a homogenous nucleation theory", *Polymer Colloids, Proc. ACS Symp.*, Chicago, Illinois, Sept 13-18,1970, Plenum,1970.

Flory P.J., "Thermodynamics of High Polymer Solutions", *J. Chem. Phys*, 9, 660(1941).

Flory P.J., "Thermodynamics of High Polymer Solutions", *J. Chem. Phys.*, 10, 51(1942).

Flory P.J., "*Principles of Polymer Chemistry*",Cornell University Press, Ithaca, 1953.

Flory P.J., "Thermodynamics of Polymer Solutions", *Trans. Faraday Soc.*, 49, 7(1970).

Friedrich J.P., "Supercritical CO_2 Extraction of Lipids from Lipid-containing Materials", *U.S. Patent 4,493,854*(1985).

Froment G.F., Bischoff K.B., *Chemical Reactor Analysis and Design*, John Wiley and Sons, New York, N.Y.,1979.

Gearhart J.A., Garwin L., "ROSE Process improves Resid Feed", *Hydrocarbon Proc.*, 55, 5(1976).

Gilbert S.W., Eckert C.A., "A Decorated Lattice-Gas Model of Supercritical Fluid Solubilities and Parital Molar Volumes", *Flu. Phase Equil.*, 30, 41(1986).

Goodwin R.D., Roder H.M., Straty G.C., *Thermophysical Properties of Ethane from 90 to 600K at Pressures to 700 Bar*, NBS, Boulder, Colorado, 1976.

Gubbins K.E., Shing K.S., Street W.B., "Fluid Phase Equilibria: Experiment, Computer simulation and Theory", *J. Phys. Chem.*,87,4573(1983).

Guggenheim E.A., *Mixtures*, Clarendon Press, Oxford, 1954.

Gutowski T.G., Suh N.P., Cangialose C., Berube G.M., " A Low Energy Solvent Separation Method", *Polymn. Eng. and Sci.*, 23(4), 230(1983).

Hannay J.B., Hogarth J., "On the Solubility of Solids in Gases", *Proc. Roy Soc. London.*, 29,324(1879).

Hannay J.B., "On the Solubility of Solids in Gases II", *Proc.Roy. Soc. London.*, 30,484(1880).

Haward R.N., "Polymerization of Methyl Isopropenyl Ketone in Cyclohexane", *J. Polym. Sci.*, 3, 10(1948).

Helling R.K., "*Oxidation Kinetics of Simple Compounds in Supercritical Water: Carbon monoxide, Ammonia and Ethanol*", Ph.D. Thesis, Massachusetts Institute of Technology, 1986.

Hirschfelder J.O., Curtiss C.O., Bird R.B., *Molecular Theory of Gases and Liquids*, John Wiley and Sons, N.Y., 1954.

Hoffman M., "Teilchenbildung und Abbruchsreaktion bei der Fallungspolymerisation von Styrol in Methanol", *Makromol. Chem.*,177,1021(1976).

Huang K., *Statistical Mechanics*, John Wiley and Sons, New York, 1963.

Huggins M.L., "Solutions of Long Chain Compounds", *J. Chem. Phys.*,9,440(1941).

Huggins M.L., "Some Properties of Solutions of Long-Chain Compounds", *J. Phys. Chem.*,46,151(1942).

Jain R.K., Simha R., "On the Equation of state of argon and organic liquids", *J. Chem. Phys*, 72(9), 4909(1980).

Jenkins A.D., "Occlusion Phenomena in the Polymerization of Acrylonitrile and Other Monomers", Chapter 6, Vinyl Polymerization, Vol.1, Part I, Ed.G. E.Ham, Marcel Dekker, New York,1967.

Joffe J., Schroeder G.M., Zudkevitch D., "Vapor-liquid Equilibria with the Redlich-Kwong Equation of State", *AIChE J*, 48, 261(1970).

Joshi D.K., Prausnitz J.M., "Supercritical Fluid Extraction with Mixed Solvents",*AIChEJ*, 1984.

Juba M.R., Personal Communication, 1984.

Juba M.R., "A Review of Mechanistic Considerations and Process Design Parameters for Precipitation Polymerization ", *ACS Symp.Ser.*, 104,1979.

Katayama T., Oghaki K., Maekawa G., Goto M., Nagano T., "Isothermal vapor-liquid Equilibria of Acetone-Carbon dioxide and Methanol-Carbon Dioxide Systems at High Pressures", *J. Chem Eng. Jpn*, 8, 89(1975).

Katz S.N., "Method for Decaffeinating Coffee", *U.S. Patent 4,276,315*(1981).

Kennedy G.C., "A Portion of the System Silica-Water", *Econ. Geol.*, 45(629),1950

Klesper E., "Chromatography with Supercritical Fluids", *Angew.Chem. Int. Ed.*, 17, 738(1978).

Kleintjens L.A., Koningsveld R., Stockmayer W.H., "Liquid-Liquid Phase Separation in Multicomponent Polymer Solutions XIV. Dilute and Concentrated Polymer Solutions in Equilibrium (continued)", *Br. Polym. J.*, 8,144(1976).

Kleintjens L.A., "Mean-Field Lattice Gas Description of Vapour-Liquid and Supercritical Equilibria", *Fluid. Ph. Equil.*, 10, 183(1983).

Klientjens L.A., Koningsveld R., "Mean field Lattice Gas Description of the System CO_2/H_2O", *Sepn.Sci.and Tech.*, 17(1),215(1982).

Koningsveld R., Stockmayer W.H., Kennedy J.W., Kleintjens L.A., "Liquid-Liquid Phase Separation in Multicomponent Polymer Systems. XI. Dilute and Concentrated Polymer Solutions in Equilibrium", *Macromolecules*, 7(1),73(1974).

Krukonis V.J., "Supercritical Fluid Nucleation of Difficult-to-Comminute Solids", *Paper presented at the AIChE Annual Meeting, San Francisco*, 1984.

Krukonis V.J., "Processing of Polymers with Supercritical Fluids", *Polym. News.*, 11, 7-16(1985).

Kumar S.K. and Reid R.C. "Derivation of the Relationships Between Partial Derivatives of Legendre Transforms", *AIChE J*, 32(7),1224(1986).

Kurnik R.T., *"Supercritical Fluid Extraction: A Study of Binary and Multicomponent Solid-Fluid Equilibria"*, Sc.D. Thesis, Massachusetts Institute of Technology, 1981.

Kurata M., *Thermodynamics of Polymer Solutions*, Ch. 2, Harwood Academic Publishers, New York, 1982.

Landau L.D., Lifshitz E.M., *Statistical Physics*, Pergamon Press, New York, 3rd Ed., 1980.

Laws D.R.J., Bath N.A., Ennis C.S., Wheldon A.G., "Hop Extraction with Carbon dioxide", *U.S. Patent 4,218,491*(1980).

McHugh M.A., Guckes T.L., "Separating Polymer Solutions with Supercritical Fluids", *Macromolecules*, 18,674(1985).

McHugh M.A., Krukonis V.J., *"Supercritical Fluid Extraction: Principles and Practice"*, Butterworth, Stoneham,MA, 1986.

Mickeleit M., Lacmann R., "Statistical Mechanics and Thermodynamic Properties of Liquid Multicomponent Mixtures. Part I. The Taylor Series for Quasichemical Equilibrium of Ternary Mixtures", *Fluid Ph. Equil.*, 12,201(1983).

Modell M., Reid R.C., *Thermodynamics and its Applications*,2 ed., Prentice Hall, 1983.

Moore P.W., Clouston J.G., Chaplin R.P., "Gamma Radiation Initiated Polymerization of Styrene at High Pressures", *J. Polymn. Sci.*, 19, 1659(1981).

Moore, Pearson, *Kinetics and Mechanism*, John Wiley & Sons,1981.

Ng H-J., Kalra H., Robinson D.B., Kubota H., "Equilibrium phase properties of the toluene-hydrogen sulfide and n-heptane-hydrogen sulfide binary systems", *J. Chem. Eng. Data.*, 25, 51(1983).

Nielsen A.E., *Kinetics of Precipitation*, Pergamon press,New York,1964.

Nitsche J.M., Teletzke G.F., Scriven L.E., Davis H.T., "Phase and Tension Behavior of Water, Carbon dioxide and Decane: Comparison of a Lattice Gas Model and the Peng-Robinson Equation", *Flu. Phase Equil.*, 14, 203(1983).

Norris R.G.W, Smith R.R., "Catalysed Polymerization of Methyl Methacrylate in the Liquid Phase", *Nature*, 150,336(1942).

Norris R.G.W., Brookman E.F., *Proc. Roy. Soc. London*, 171A,147(1939).

Odian G., *Principles of Polymerization*, 2nd Ed., John Wiley & Sons, New York, 1985.

Okada M., Nose T., "Quasi-Chemical Treatment of the Hole Theory for r-mers I. Pure Liquids", *Polymn. J.*, 13(4), 399(1981a).

Okada M., Nose T., "Quasi-Chemical Treatment of the Hole Theory for r-Mers. II. Mixtures", *Polymn. J.*, 13(6), 591(1981b).

Panagiotopoulos A.Z., "*High Pressure Phase Equilibrium: Experimental and Monte Carlo Studies*", PhD Thesis, Massachusetts Institute of Technology, 1986.

Panagiotopoulos A.Z., Kumar S.K., "A Generalized Technique to Obtain the Pure Component Parameters for Two-Parameter Equations of State", *Fluid Ph. Equil.*, 22,77(1985).

Panayiotou C., Vera J.H., "Local Compositions and Local Surface Area Fractions: A Theoretical Discussion", *Can. J. Chem. Eng.*, 59, 501(1981).

Panayiotou C., Vera J.H., "Statistical thermodynamics of r-mer fluids and their mixtures", *Polym. J*, 14(9),681(1982).

Patterson D., Delmas G. "Critical State in Chain-Molecule Mixtures", *Trans Faraday Soc.*, 65,708(1969).

Paul P.F.M., Wise W.S., *Principles of Gas Extraction*, Mills and Boon, London, 1971.

Paulaitis M.E., Krukonis V.J., Kurnik R.T., Reid R.C., "Supercritical Fluid Extraction", *Rev. Chem. Eng.*, 1(2),179(1983).

Pemberton R.C., Mash C.J., "Thermodynamic properties of aqueous nonelectrolyte mixtures II. Vapour pressures and excess Gibbs energies for water + ethanol at 303.15 K to 363.15 K determined by an accurate static method"., *J. Chem. Therm.*, 10, 867(1978).

Peng D.Y., Robinson D.R., "A New Two Constant Equation of State", *Ind. Eng Chem. Fundam.*, 15(1),59(1976).

Peter S., Brunner G., "Process for decaffeinating coffee", *U.S. Patent 4,322,255*(1982).

Prigogine I., *The Molecular Theory of Solutions*, North Holland Publishing Co., Amsterdam, 1957.

Randall L.G., "The Present Status of Dense Supercritical Gas Extraction and Dense Gas Chromatography: Impetus for DGC/MS Development", *Sepn. Sci. and Tech.*, 17(1),1(1982).

Ray W.H., Jain S.K., "On the Modelling of Bulk poly(vinyl chloride) Reactors", *J. Appl. Polymn. Sci.*, 19,1297(1975).

Redlich O., Kwong J.N.S., "On the Thermodynamics of Solutions V", *Chem. Rev.*, 44,233(1949).

Reid R.C., Prausnitz J.M., Sherwood T.K., *The Properties of Gases and Liquids*, 3rd Ed., McGraw Hill, 1977.

Rößling G.L., Franck .U., "Solubility of Anthracene in Dense Gases and Liquids to 200°C and 2000 bar", *Ber. Bunsenges. Phys. Chem.*, 87, 882(1983).

Rowlinson J.S., Swinton F.L., *Liquids and liquid mixtures* ,3rd Ed., Butterworths, London, 1982.

Sanchez I.C., Lacombe R.H., "An Elementary Molecular Theory of Classical Fluids. Pure Fluids", *J. Phys. Chem.*, 80(21),2352(1976).

Sanchez I.C., Lacombe R.H., "An Elementary Equation of State for Polymer Liquids", *J. Poly. Sci., Polymn. Lett. Ed.*, 15,71(1977).

Sandler S.I., Lee K-H, "A Proper Theoretical Basis for Local Composition Mixing Rules and a New Class of Activity Coefficient Models", *Flu. Phase Equil.*, 30, 135(1986).

Schmitt W.J., *"The Solubility of Monofunctional Organic Compounds in Chemically Diverse Supercritical Fluids"*, Ph.D Thesis, Massachusetts Institute of Technology, 1984.

Schmitz F.P., Klesper E., "Polystyrene Separation by Supercritical Chromatography", *Polymn. Commn.*, 24,142(1983).

Schmitz F.P., Klesper E., "Supercritical Fluid Chromatography of Oligostyrenes by means of Eluent Gradients", *Makromol. Chem., Rapid. Commun.*, 2,735(1981).

Schröder E., Arndt K-F., "Löslichkeitverhalten von Makromolekülen in Komprimierter Gasen", *Faserforschung und Textiltechnik*, 27(3), 135(1976a).

Schröder E., Arndt K-F., "Löslichkeitverhalten von Makromolekülen in Komprimierter Gasen", *Faserforschung und Textiltechnik*, 27(3), 141(1976b).

Schwab F.C., "Anionic Dispersion Polymerization of Styrene", *Polymer preprints*,25(1),150(1984).

Schulz G.V., "Die Verteilungsfunktionen Polymolekularer Stoffe und ihre Ermittelung durch Zerlegung in Fraktionen", *Z. Phys. Chem.*, B39,155(1941).

Schulz G.V., Jirgensons B., "Die Abhaengigkeit der Loeslichkeit von Molekulargewicht", *Z. Phys. Chem.*, B46, 105-136(1940).

Soave G., "Equilibrium Constants from a Modified Redlich-Kwong Equation of State", *Chem. Eng. Sci.*, 27,1197(1972).

Simha R., Somcynsky T., "On the Statistical Thermodynamics of Spherical and Chain Molecule Fluids", *Macromolecules*, 2(4), 342(1969).

Spahl R., Luft G., "Fraktionierungserscheinungen bei der Entmischung von Ethylen-Polyethylen-Gemischen", *Angewan. Makromole. Chem.*, 115, 87-102(1982).

Staverman A.J., "The Entropy of High Polymer Solutions", *Rec. Trav. Chim. Pays-bas*, 69, 163(1950).

Subramaniam B., McHugh M.A., "Reactions in Supercritical Fluids - A Review", *Ind. Eng. Chem. Proc. Des. Dev.*, 25,1(1986).

Swaid I., "*NIR-spektroskopische Untersuchungen zum Phasenverhalten von Decan + CO_2, Adamantan + CO_2 sowie Octacosan + CO_2 im Temperaturbereich 300-450 K unde bei Drucken bis 1 kbar*", Ph.D. Thesis, Ruhr-Universitat, Bochum, 1982.

Tong Z., Einaga Y., Fujita H., "Separation Factor Study of Model Polystyrene Mixtures in Cyclohexane", *Macromolecules*,18,2264(1985).

Tsekhanskaya Yu. V., Iomtev M.B., Muskina E.V., "Solubility of Naphthalene in Ethylene and Carbon dioxide under Pressure", *Russ. J. Phy. Chem.*, 38(9), 1173(1964).

Tsuyumoto M., Einaga Y., Fujita H., "Phase Equilibrium of the Ternary Systems Consisting of Two Monodisperse Polystyrenes and Cyclohexane", *Polymn. J.*, 16(3), 229(1984).

van der Waals J.D., Doctoral thesis, Leiden,1873.

Vimalchand, Donohue M.D., "Thermodynamics of Quadropolar Molecules: The Perturbed Anisotropic Chain Theory", *Ind. Eng. Chem. Fundam.*,24,849(1985).

Wang W.V., Kramer E.J., Sachse W.H., "Effects of High-Pressure CO_2 on the Glass Transition Temperature and Mechanical Properties of Polystyrene", *J. Polym. Sci. Polym. Phys. Ed.*,20,1371(1982).

Weisphart J., *Thermodynamic equilibria of boiling mixtures*, Springer-Verlag, Berlin,1975.

Willson R.C., "*Fermentation Product Recovery by Supercritical Fluid Extraction: Microbiological and Phase Equilibrium Aspects*", PhD Thesis, Massachusetts Institute of Technology, Cambridge, MA, 1987.

Zeman L., Patterson D., "Pressure Effects in Polymer Solution Phase Equilibria. II. Systems Showing Upper and Lower Critical Solution Temperatures", *J. Phys. Chem.*,76,1214(1972).

Zosel K., "Separation with Supercritical Gases: Practical Applications", *Angew. Chem Int. Ed. Engl.*,17,702(1978).

Zosel K., "Process for the Direct Decaffeination of Aqueous Coffee Extract Solutions", *U.S. Patent 4,348,422*(1982).

APPENDIX I

CALIBRATION OF THE SIZE EXCLUSION CHROMATOGRAPH

AI.1 Introduction

Size exclusion chromatography was performed on a high-performance liquid chromatograph (a Hewlett Packard 1090A with a 254 nm UV detector, and a refractive index detector) installed with ultrastyragel columns (Waters, THF loaded # 10570, 10571 and 10572) and equipped with an autosampler. Data from the chromatograph was collected on an IBM-XT computer with an A/D board (DT2805, 12 bit) using ASYST software. The data collection was triggered externally by the chromatograph, and could be set up so as to collect data at any desired rate (a standard rate of 2 Hz per channel was found to be adequate). The computer program for the collection and storage of data is shown in Section AI.3. The raw chromatographic data was subsequently analyzed by a program written in FORTRAN 77 (presented in Section AI.3) for peak areas, peak elution times and other relevant variables.

AI.2 Calibration of SEC

The first set of calibrations performed on the SEC relates to the determination of the elution times of polymers of different molecular weights. For this purpose various polystyrene standards from M_n ~ 700 to 600,000 were employed (Scientific Polymer Products, Polymer calibration kit). Using the elution times for the various peaks a standard ℓn M vs elution time relationship was deduced. In Figure AI.1 we show these data, along with a orthogonal polynomial of order 3 fitted to the elution time data for peak molecular masses of < 13,000. It is seen that for molecular weights of < 5000 the graph displays a linear regime. It is in this regime that molecular weights of unknown samples may be determined unequivocally. At larger molecular weights, the curve is no longer linear suggesting that

we are approaching the limit of resolution the columns employed.

A related calibration involves the correlation of the mass of polymer injected, to the area under the chromatograms. We used dilute solutions (< 0.7 wt%) of two different polystyrene standards (M_n~ 700, M_w/M_n ~ 1.2, Scientific Polymer Products; M_n~ 2060, M_w/M_n~ 1.1, Pressure Chemicals) which were injected into the SEC in various amounts ranging 2×10^{-6}-6×10^{-5} gm of polymer. The area under the UV Detector signal curve, plotted against elution time, between the base lines (in units of [mV×min/100]) was then correlated to the mass of polymer injected. In Figure A1.2 we demonstrate the quality of this correlation. As can be seen the calibration curve in this regime is always linear, and independent of the mass and the molecular weight of the polymer sample. This curve thus represents a universal mass calibration for polystyrene in our SEC apparatus.

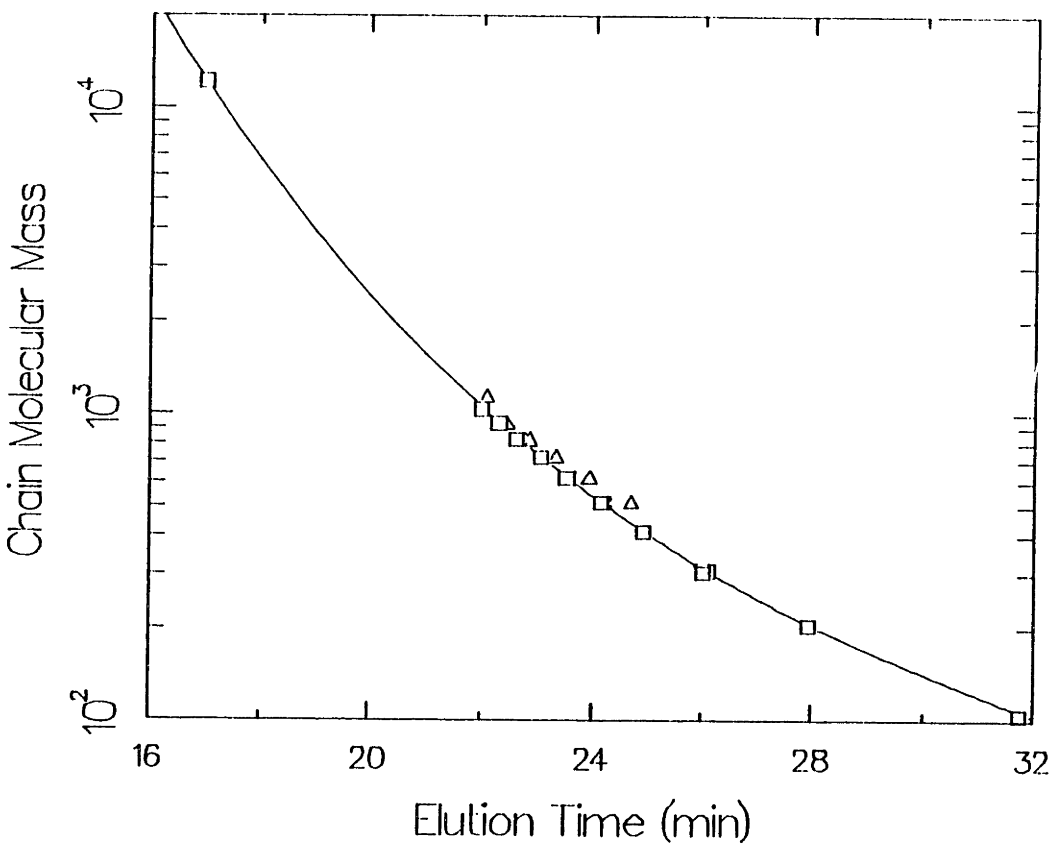

Figure AI.1: UV Detector calibration curve for the determination of the molecular mass of polymer chains as a function of elution time.

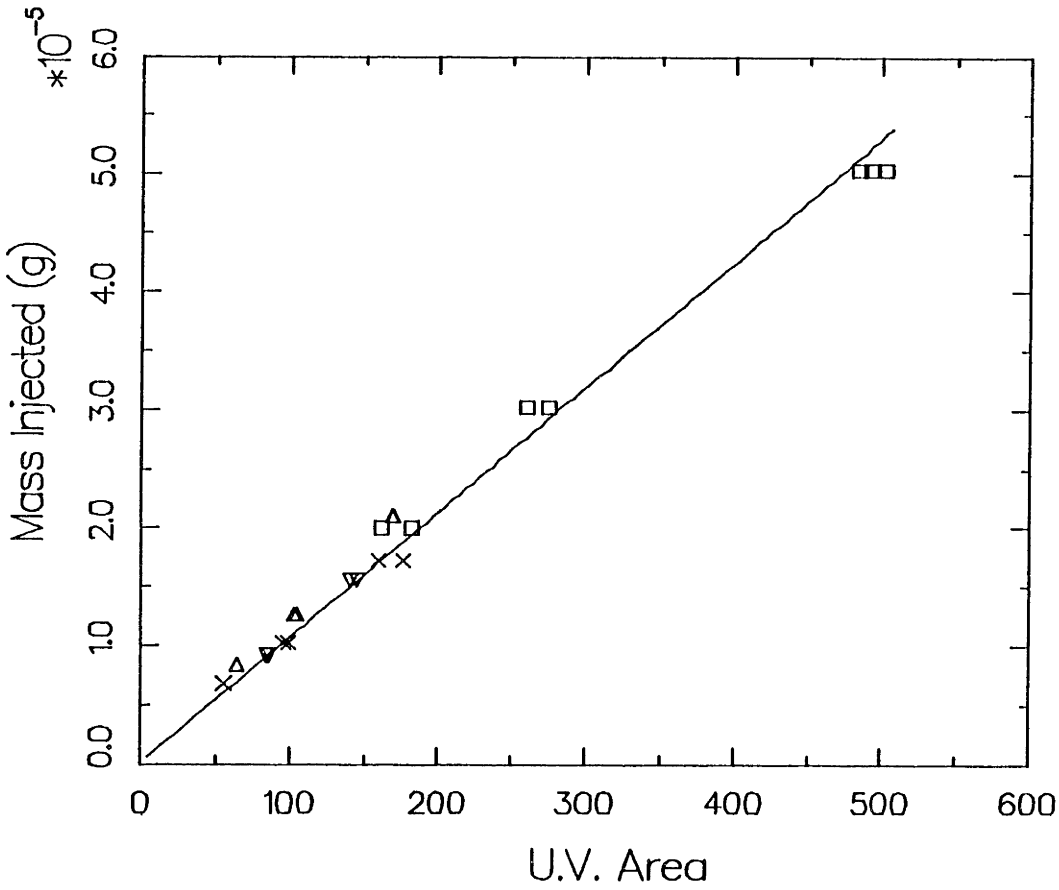

Figure AI.2: UV Detector calibration curve for the determination of the quantity of polymer injected by the measurement of the area under the chromatographic curve.

AI.3 Program used in ASYST software for data collection

```
INTEGER SCALAR NRUN
INTEGER SCALAR NCOUNT
INTEGER SCALAR NPTS
INTEGER SCALAR NSUBFILES
INTEGER SCALAR NBEGIN
INTEGER SCALAR NEND
INTEGER SCALAR NFILE.COUNT
INTEGER SCALAR NSYNC.PERIOD
INTEGER SCALAR NRUN.COUNT
INTEGER SCALAR BEGIN.CHAN
INTEGER SCALAR END.CHAN

INTEGER DIM[ 20 ] ARRAY N/SEC
INTEGER DIM[ 120 ] ARRAY DATA
INTEGER DIM[ 40 ] ARRAY CHAN
INTEGER DIM[ 20 ] ARRAY GAIN
INTEGER DIM[ 20 ] ARRAY NCHAN
INTEGER DIM[ 1 ] ARRAY DUMMY

REAL DIM[ 20 ] ARRAY TIME
REAL DIM[ 120 ] ARRAY XAXIS

REAL SCALAR SYNC
REAL SCALAR ELAPS.TIME
REAL SCALAR TIME.INCREMENT

DIM[ 20 , 20 ] STRING.ARRAY FILE.NAME

DT2800
0 1 A/D.TEMPLATE DATA.CHNL
0 0 A/D.TEMPLATE DUMMY.CHNL


: INPUT

 0 NRUN :=
 0 NCOUNT :=
 0 TIME :=
 0 N/SEC :=
 0 CHAN :=
 0 NCHAN :=

 CR ." # of runs to be run ?" #INPUT
 NRUN :=

 BEGIN
     NCOUNT 1 + NCOUNT :=

     CR ." Enter file name"  "INPUT
```

```
      FILE.NAME "[ NCOUNT ] ":=

      CR ." Enter time in minutes for run" #INPUT
      TIME [ NCOUNT ] :=

      CR ." Enter # of samples/sec " #INPUT
      N/SEC [ NCOUNT ] :=

      CR ." Enter begin channel " #INPUT
      CHAN [ NCOUNT 2 * 1 - ] :=

      CR ." Enter end channel " #INPUT
      CHAN [ NCOUNT  2 * ] :=

      CR ." Enter A/D board gain " #INPUT
      GAIN [ NCOUNT ] :=

      CR ." Enter # of a/d channels " #INPUT
      NCHAN [ NCOUNT ] :=

      NCOUNT NRUN >=
      UNTIL
;

: FILEOPEN

      FILE.TEMPLATE
      8 COMMENTS
      TIME [ NRUN.COUNT ] 60. * N/SEC [ NRUN.COUNT ] *  NPTS :=
      NPTS NCHAN [ NRUN.COUNT ] * NPTS :=

      NPTS 120 /  NSUBFILES :=

      INTEGER DIM[ 120 ] SUBFILE
      NSUBFILES TIMES
      END

FILE.NAME "[ NRUN.COUNT ] DEFER> FILE.CREATE
FILE.NAME "[ NRUN.COUNT ] DEFER> FILE.OPEN
;

: PLOT
     XAXIS []RAMP
     XAXIS 1. - XAXIS :=

     XAXIS 127 / TIME [ NRUN.COUNT ] * XAXIS :=
     VERTICAL GRID.OFF
     HORIZONTAL GRID.OFF

     1000 DATA :=
     4100 DATA [ 2 ] :=
```

```
    XAXIS DATA XY.AUTO.PLOT
;


: DATA.ACQ

    0 DATA :=
    0 ELAPS.TIME :=
    1000. N/SEC [ NRUN.COUNT ] / 50. / SYNC :=

    CLEAR.TASKS

    1 NFILE.COUNT :=
    NRUN.COUNT 2 * 1 - NBEGIN :=
    NRUN.COUNT 2 * NEND :=
    CHAN [ NBEGIN ] 1 * BEGIN.CHAN :=
    CHAN [ NEND ] 1 * END.CHAN :=
    DATA.CHNL BEGIN.CHAN END.CHAN RESET.A/D.CHNLS
    DATA.CHNL GAIN [ NRUN.COUNT ] A/D.GAIN
    DATA.CHNL
    DATA CYCLIC TEMPLATE.BUFFER

    DATA.CHNL A/D.INIT

    DUMMY.CHNL
    DUMMY TEMPLATE.BUFFER
    DUMMY.CHNL EXT.TRIG
    DUMMY.CHNL A/D.INIT
    DUMMY.CHNL A/D.IN>ARRAY

    DATA.CHNL 1 TASK A/D.IN>ARRAY
    50 TASK.PERIOD
    SYNC 1 TASK.MODULO
    PRIME.TASKS

    TRIGGER.TASKS

    BEGIN
    NFILE.COUNT NSUBFILES >=

        BEGIN
        ?BUFFER.SWITCH
        UNTIL


    NFILE.COUNT SUBFILE
    DATA ARRAY>FILE

    NFILE.COUNT 1 + NFILE.COUNT :=
    UNTIL
    STOP.TASKS
```

```
    FILE.CLOSE
;


: MAIN

  0 NRUN.COUNT :=
  INPUT

  BEGIN
      NRUN.COUNT 1 + NRUN.COUNT :=
      NRUN.COUNT NRUN >=
      FILEOPEN
      PLOT
      DATA.ACQ
  UNTIL
;
```

AI.4 Program for the integration of SEC data

```
c*****************************************
c
c December/30/1985 11:08pm
c
c*****************************************


      implicit real(a-h,o-z)

      real time(3600),inrism(3600),inuvsm(3600),time1(360)
      real inri(3600), inuv(3600),diffuv(360),diffri(360),rmwuv(3600)
      real rmwri(3600), diff2uv(360),diff2ri(360),uvcalib(10),ricalib
     1(10),abase(20),bbase(20),peakstart(20),peakend(20),uvwtcal(20),
     lriwtcal(20)
      integer beginloc(20),endloc(20),istart(20),iend(20)
      character*20 file1

c*****************************
c
c     Files are opened here
c
c*****************************

      write (*,*) 'Enter input filename'
      read  (*,'(a)') file1
      open (1,file=file1)
      open (2, file='calibin')
      open (3, file='slicesri')
      open (4, file='out')
      open (7, file='slicesuv')
      open (11, file='diff')
      open (12, file='uvpeaks')
      open (13,file='ripeaks')


c*******************************
c
c     inputs
c
c*******************************

      write (*,*) ' initial time ?'
      read  (*,*) timeinit
10    read (1,*) t,p1,p2
      if (t.ge.timeinit) then
      read (1,*) (time(i),inuv(i),inri(i),i=1,2000)
      go to 11
      else
      go to 10
```

```
      endif
11    read (2,*) cutupuv,cutupri
      read (2,*) cutdnri,cutdnuv

c*************************************************
c     Calibration curves are read as coefficients for orthogonal polynomials.
c     nuvpoints represents the uv polynomial order, i.e., nuvpoints= order+1
c     similar ideas for the ri curve
c*****************************************

      read (2,*) nuvpts
      read (2,*) (uvcalib(i),i=1,nuvpts)
      read (2,*) nripts
      read (2,*) (ricalib(i),i=1,nripts)
      read (2,*) nuvwtpt
      read (2,*) (uvwtcal(i),i=1,nuvwtpt)
      read (2,*) nriwtpt
      read (2,*) (riwtcal(i),i=1,nriwtpt)


c*********************************
c
c     Data smoothing
c     data is smoothed by block averaging
c     9 successive elements in each block
c
c***********************************

      j=1
      do 100 i=5,1995,9
      inrism(j)=(inri(i-4)+inri(i-3)+inri(i-2)+inri(i-1)+
     1inri(i)+inri(i+1)+inri(i+2)+inri(i+3)+inri(i+4))/9
      inuvsm(j)=(inuv(i-4)+inuv(i-3)+inuv(i-2)+inuv(i-1)+
     1inuv(i)+inuv(i+1)+inuv(i+2)+inuv(i+3)+inuv(i+4))/9
      timel(j)=time(i)
      write(11,*) timel(j),inuvsm(j),inrism(j)
      j=j+1
100   continue

c*******************************
c
c     differentiation of smoothed data
c
c*******************************

      ncount=j-1
      do 101 i =1,ncount-1
      diffuv(i)=(inuvsm(i+1)-inuvsm(i))/(timel(i+1)-timel(i))
      diffri(i)=(inrism(i+1)-inrism(i))/(timel(i+1)-timel(i))
101   continue
```

```
      do 102 i=1,ncount-1
      diff2uv(i)=(diffuv(i+1)-diffuv(i))/(time1(i+1)-time1(i))
      diff2ri(i)=(diffri(i+1)-diffri(i))/(time1(i+1)-time1(i))
102   continue

c*******************************
c
c     uv detector: identification of peaks
c     and peak base points.
c
c*******************************

      write (4,*) ' U.V. Detector '
      write (4,*) ' --------------'
      write (4,*) '  '
      ipcoun=0
      nbegin=1
103   do 104 i =nbegin,ncount-1
      if (abs(diffuv(i)).ge.cutupuv) then
      ipcoun=ipcoun+1
      peakstart(ipcoun)=time1(i-1)
      beginloc(ipcoun)=i-1
      write (4,*) ' peak ',ipcoun, 'starts at ',peakstart(ipcoun)
      goto 105
      else
      go to 104
      endif
104   continue
      if (beginloc(ipcoun).lt.nbegin) go to 108


105   endloc(ipcoun)=0
      do 106 i=beginloc(ipcoun)+1,ncount-1
      if (abs(diffuv(i)).le.cutdnuv.and.inuvsm(i).le.4090.0) then
      if (abs(diffuv(i-2)).le.cutdnuv.and.abs(diffuv(i-1)).le.cutdnuv.
     land.abs(diffuv(i+1)).le.cutdnuv.and.abs(diffuv(i+2)).le.cutdnuv)
     1then
      peakend(ipcoun)=time1(i)
      endloc(ipcoun)=i
      write (4,*) ' peak ends at ',peakend(ipcoun)
      go to 107
      else
      go to 106
      endif
      else
      go to 106
      endif
106   continue

107   if (endloc(ipcoun).eq.0) then
      endloc(ipcoun)=ncount
      peakend(ipcoun)=time1(ncount)
```

```
      endif
      if (endloc(ipcoun).lt.(ncount-10)) then
      nbegin=endloc(ipcoun)+5
      go to 103
      endif

108   do 109 k=1,ipcoun
      do 109 i=1,2000
      if (time(i).eq.peakstart(k)) istart(k)=i
      if (time(i).eq.peakend(k))   iend(k)=i
109   continue


c************************
c
c     uv baseline determination
c
c************************

      write (4,*) '  '
      write (4,*) ' Base line parameters'
      write (4,*) '----------------------'
      write (4,*) '       a(slope)      b(intercept)  '
      do 110 k=1,ipcoun
      abase(k)=(inuv(istart(k))-inuv(iend(k)))/(time(istart(k))-time(ien
     1d(k)))
      bbase(k)=(inuv(istart(k))-abase(k)*time(istart(k)))
      write (4,*) k,abase(k),bbase(k)
      write (*,*) abase(k),bbase(k)
110   continue


c************************
c
c     integration and reporting results
c
c************************

      zmom=0.
      fmom=0.
      thmom=0.

      do 114 k=1,ipcoun
      do 112 i=istart(k),iend(k)
      inuv(i)=inuv(i)-bbase(k)-abase(k)*time(i)
      arg=0.0
      term=1.0
      do 111 j=1,nuvpts
            arg=arg+uvcalib(j)*term
            term=term*time(i)
111   continue
```

```
      rmwuv(i)=10**arg
      if (rmwuv(i).le.104.0) rmwuv(i)=104.0
      if (inuv(i).le.0.0)then
      inuv(i)=0.
      endif
112   continue


      do 113 i=istart(k)+1,iend(k)
      arg=(inuv(i)+inuv(i-1))*0.5*(time(i)-time(i-1))
      zmom=zmom+(arg/(rmwuv(i)+rmwuv(i-1))*2.)
      fmom=fmom+arg
      thmom=thmom+arg*(rmwuv(i)+rmwuv(i-1))/2.0
113   continue
114   continue

      smn=fmom/zmom
      smw=thmom/fmom
      fpoly=smw/smn
      write(4,201) zmom,fmom,thmom
201   format (/,10x, 'zeroth momemt of distribution',e15.6,/10x,'first
     1momemt of distribution  ',e15.6,/10x,'second momemt of distrib
     lution   ',e15.6)
      write (4,202) smn,smw,fpoly
202   format (/10x,' number average molecular weight   ',f10.3,
     1/10x, ' weight average molecular weight   ', f10.3
     1/10x, ' polydispersity                    ',f10.3)

      wtinj=0.
      term=1.0
      do 1141 i=1,nuvwtpt
              wtinj=wtinj+term*uvwtcal(i)
              term=term*fmom
1141  continue

      write (4,203) wtinj
203   format (/,10x,' Weight injected in sample, uv detector',e15.7,'gm
     1')

      do 116 j=1,80
           cutmw=j*104.0
           cutmwlow=cutmw-52.
           cutmwhig=cutmw+52.
           sum=0.
           do 115 k=1,ipcoun
           do 115 i=istart(k)+1,iend(k)
           if (rmwuv(i).lt.cutmwhig.and.rmwuv(i).ge.cutmwlow) then
           sum=sum+((inuv(i)+inuv(i-1))/2.*(time(i)-time(i-1)))
           endif
115        continue
      write (7,*) cutmw,sum/fmom
116   continue
```

```
c*******************************
c
c  uv peak determination
c
c*******************************

      local=-9
      do 120 k=1,ipcoun
      istart(k)=beginloc(k)+1
      do 120 i=istart(k),endloc(k)
      cpeak1=diffuv(i)*diffuv(i-1)
      cpeak2=sqrt(abs(cpeak1))
      if (cpeak1.lt.0.0.and.cpeak2.ge.20.0.and.diff2uv(i).lt.-10) then
      timepeak=time1(i)
      istart(k)=i+10

      do 117 j=local+10,2000
            if (time(j).eq.timepeak) then
            local=j
            go to 118
            endif
117   continue

118   maxsig=0.
      maxpt=1
      do 119 j=local-20,local+20
            if (inuv(j).ge.maxsig) then
            maxsig=inuv(j)
            maxpt=j
            endif
119   continue

      write (12,*) time(maxpt),rmwuv(maxpt)
      endif
120   continue



c*******************************
c
c     ri detector peak detection
c     and determination of base-points
c
c*******************************

      write (4,*) ' '
      write (4,*) ' ri detector  '
      write (4,*) ' ----------- '
      ipcoun=0
      nbegin=1
121   do 122 i=nbegin,ncount-1
```

```
      if (abs(diffri(i)).ge.cutupri) then
      ipcoun=ipcoun+1
      peakstart(ipcoun)=time1(i-1)
      beginloc(ipcoun)=i-1
      write (4,*) 'peak', k, '   starts at ', peakstart(ipcoun)
      go to 123
      else
      go to 122
      endif
122   continue
      if (beginloc(ipcoun).lt.nbegin) go to 126

123   endloc(ipcoun)=0
      do 124 i=beginloc(ipcoun)+1,ncount-1
      if (abs(diffri(i)).le.cutupri.and.inrism(i).le.4090.0) then
      if (abs(diffri(i-2)).le.cutdnri.and.abs(diffri(i-1)).le.cutdnri.
     1and.abs(diffri(i+1)).le.cutdnri.and.abs(diffri(i+2)).le.cutdnri)
     1then
      peakend(ipcoun)=time1(i)
      endloc(ipcoun)=i
      write (4,*) 'peak ends at  ',peakend(ipcoun)
      go to 125
      else
      go to 124
      endif
      else
      go to 124
      endif
124   continue

125   if (endloc(ipcoun).eq.0) then
      endloc(ipcoun)=ncount
      peakend(ipcoun)=time1(ncount)
      endif

      if (endloc(ipcoun).lt.(ncount-10)) then
      nbegin=endloc(ipcoun)+5
      go to 121
      endif


126   do 127 k=1,ipcoun
      do 127 i=1,2000
      if (time(i).eq.peakstart(k)) istart(k)=i
      if (time(i).eq.peakend(k))   iend(k)=i
127   continue

c*************************
c
c     ri baseline determination
c
c*************************
```

```
      do 128 k=1,ipcoun
      abase(k)=(inri(istart(k))-inri(iend(k)))/(time(istart(k))-time(ie
     lnd(k)))
      bbase(k)=(inri(istart(k))-abase(k)*time(istart(k)))

      write (4,*) abase(k),bbase(k)
128   continue


c**************************8
c
c     ri integration and reporting results
c
c*************************

      zmom=0.
      fmom=0.
      thmom=0.

      do 132 k=1,ipcoun
      do 130 i= istart(k),iend(k)
      inri(i)=inri(i)-bbase(k)-abase(k)*time(i)

      arg=0.0
      term=1.0
      do 129 j=1,nripts
            arg=arg+ricalib(j)*term
            term=term*time(i)
129   continue

      rmwri(i)=10**arg
      if(rmwri(i).le.104.) rmwri(i)=104.0
      if (inri(i).le.0.0) inri(i)=0.0
130   continue

      do 131 i=istart(k)+1,iend(k)
      arg=(inri(i)+inri(i-1))*0.5*(time(i)-time(i-1))
      zmom=zmom+(arg/(rmwri(i)+rmwri(i-1)))*2.0
      fmom=fmom+arg
      thmom=thmom+arg*(rmwri(i)+rmwri(i-1))/2.0
131   continue
132   continue

      smn=fmom/zmom
      smw=thmom/fmom
      fpoly=smw/smn
      write (4,201) zmom,fmom,thmom
      write (4,202) smn,smw,fpoly

      wtinj=0.
      term=1.0
```

```
      do 1321 j=1,nriwtpt
              wtinj=wtinj+riwtcal(j)*term
              term=term*fmom
1321  continue

      write (4,204) wtinj
204   format (//,10x,' Wt. injected R.I. detector  ',e15.7,'  gms')

      do 134 j=1,40
      cutmw=j*104.0
      cutmlow=cutmw-52.0
      cutmhig=cutmw+52.0
      sum=0.0
          do 133 k=1,ipcoun
          do 133 i=istart(k)+1,iend(k)
          if (rmwri(i).lt.cutmhig.and.rmwri(i).ge.cutmlow) then
          sum=sum+((inri(i)+inri(i-1))/2.0*(time(i)-time(i-1)))
          endif
133       continue
      write (3,*) cutmw,sum/fmom
134   continue

c************************
c
c     ri peak determination
c
c************************

      local=-9
      do 138 k=1,ipcoun
      istart(k)=beginloc(k)+1
      do 138 i=istart(k),endloc(k)
      cpeak1=diffri(i)*diffri(i-1)
      cpeak2=sqrt(abs(cpeak1))
      if (cpeak1.lt.0.0.and.cpeak2.ge.50.0.and.diff2ri(i).lt.-10.) then
      timepeak=time1(i)
      istart(k)=i+10


      do 135 j=local+10,2000
           if (time(j).eq.timepeak)then
           local=j
           go to 136
           endif
135   continue

136   maxsig=0.
      maxpt=1
      do 137 j=local-20,local+20
             if (inri(j).ge.maxsig) then
             maxsig=inri(j)
             maxpt=j
```

```
            endif
137   continue
      write (13,*) time(maxpt),rmwri(maxpt)
      write (13,*) time(maxpt)
      write(4,*) time(maxpt)
      endif

138   continue

      end
```

APPENDIX II

SOLUBILITY RESULTS: RAW EXPERIMENTAL DATA

In this appendix we present the measured values of partition coefficients for the different styrene oligomers in various gases at all pressures, temperatures and solvent gases examined. In each table there is a run number provided: runs which have a prefix of 800 were data obtained from the polystyrene standard of $M_n \sim$ 800 g $mole^{-1}$, while a prefix of 200 is data obtained from a polymer of $M_n \sim$ 2060 g $mole^{-1}$. Reported partition coefficients are defined as in Eq(4.1).

Table AII.1: Partition coefficients for polystyrene chains in ethane at 333K and 8.5 MPa.

Run # Chain Mol. Wt	80037	80040	80042	80043
312	1.44E-02	7.38E-03	1.14E-02	1.03E-02
416	4.19E-03			
520	9.90E-04			
624	4.28E-04	1.74E-04	1.95E-04	2.84E-04
728	2.32E-04	2.28E-05	8.76E-05	1.44E-04
832	1.15E-04	2.21E-05	1.21E-04	
936	3.38E-05	7.10E-06		

Table AII.2: Partition coefficients for polystyrene chains in ethane at 333K and 10 MPa.

Run # Chain Mol. Wt	80017	80018	80019	80020	80021
312	2.92E-02	3.87E-02	2.28E-02	2.70E-02	1.91E-02
416	1.30E-02	1.85E-02	1.41E-02	2.06E-02	1.65E-02
520	4.60E-03	6.30E-03	4.64E-03	7.96E-03	5.62E-03
624	1.79E-03	2.22E-03	1.52E-03	3.19E-03	2.06E-03
728	7.57E-04	8.83E-04	5.35E-04	1.24E-03	7.65E-04
832	3.00E-04	3.27E-04	1.64E-04	4.53E-04	2.58E-04
936	1.01E-04	1.11E-04		1.50E-04	
1040	2.13E-05	2.10E-05		4.14E-05	

Table AII.3: Partition coefficients for polystyrene chains in ethane at 333K and 15 MPa.

Run # Chain Mol. Wt	2001	20084	80024	80025	80026
312		5.07E-02	1.33E-02	2.19E-02	1.51E-02
416		3.58E-02	3.25E-02	4.05E-02	4.32E-02
520		1.74E-02	1.77E-02	2.42E-02	2.69E-02
624		1.01E-02	9.15E-03	1.58E-02	1.64E-02
728		5.55E-03	4.92E-03	8.77E-03	8.53E-03
832		9.48E-04	2.60E-03	4.41E-03	4.27E-03
936	1.07E-03		1.42E-03	2.14E-03	2.06E-03
1040	5.61E-04		8.16E-04	1.05E-03	9.91E-04
1144	3.08E-04		4.82E-04	5.46E-04	4.55E-04
1248	1.55E-04		3.84E-04	3.99E-04	2.67E-04
1352	7.99E-05		1.56E-04	1.41E-04	4.17E-05
1456	3.60E-05		2.21E-05	9.51E-05	
1560	1.40E-05				

Table AII.3 (continued)

Run # Chain Mol. Wt	80027	80028	80029	80048	80049
312	7.14E-02	7.56E-02	2.91E-02	9.65E-02	6.24E-02
416	7.34E-02	9.69E-02	5.16E-02	5.15E-02	4.53E-02
520	4.17E-02	5.16E-02	2.68E-02	2.33E-02	2.80E-02
624	2.15E-02	2.59E-02	1.34E-02	1.09E-02	1.54E-02
728	1.16E-02	1.39E-02	7.10E-03	5.41E-03	8.81E-03
832	6.09E-03	7.39E-03	3.67E-03	2.71E-03	4.78E-03
936	3.09E-03	3.93E-03	1.84E-03	1.30E-03	2.74E-03
1040	1.51E-03	2.13E-03	9.08E-04	5.94E-04	1.33E-03
1144	6.89E-04	1.13E-03	3.66E-04	2.42E-04	6.32E-04
1248	2.43E-04	4.70E-04		4.63E-05	2.58E-04
1352				3.14E-05	

Table AII.4: Partition coefficients for polystyrene chains in ethane at 333K and 25 MPa.

Run # / Chain Mol. Wt	2003	20011	20034	20035	20046
312	3.55E-02				1.54E-02
416	3.76E-02				1.86E-02
520	2.12E-02				1.42E-02
624	1.57E-02				1.33E-02
728	1.38E-02				1.42E-02
832	9.62E-03	5.15E-03	4.40E-03	5.70E-03	1.16E-02
936	6.01E-03	4.34E-03	4.29E-03	5.03E-03	7.84E-03
1040	3.85E-03	3.46E-03	3.74E-03	4.01E-03	5.04E-03
1144	2.64E-03	2.73E-03	3.24E-03	3.12E-03	3.38E-03
1248	1.67E-03	1.93E-03	2.42E-03	2.26E-03	2.11E-03
1352	1.09E-03	1.32E-03	1.72E-03	1.54E-03	1.34E-03
1456	6.85E-04	8.58E-04	1.15E-03	1.04E-03	8.61E-04
1560	4.35E-04	5.41E-04	7.73E-04	6.76E-04	5.56E-04
1664	2.81E-04	3.54E-04	5.00E-04	4.18E-04	3.48E-04
1768	1.72E-04	2.13E-04	3.07E-04	2.42E-04	2.24E-04
1872	1.01E-04	1.33E-04	1.85E-04	1.34E-04	1.45E-04
1976	6.30E-05	8.04E-05	1.14E-04	6.09E-05	9.76E-05
2080	3.33E-05	4.12E-05	6.60E-05	1.46E-05	6.18E-05
2184	2.24E-05	2.20E-05	1.96E-05		4.85E-05
2288	1.15E-05	1.19E-05	2.47E-06		3.06E-05
2392	1.14E-06	3.98E-06			2.05E-05
2496					1.96E-05
2600					1.10E-05

Table AII.4 (continued)

Run # / Chain Mol. Wt	8001	8002	8003	8004	8006
312	2.97E-02	5.73E-02	8.12E-02	4.21E-02	2.76E-02
416	1.87E-02	4.97E-02	9.15E-02	6.54E-02	4.34E-02
520	1.28E-02	2.56E-02	5.19E-02	4.52E-02	3.07E-02
624	8.26E-03	1.28E-02	3.05E-02	3.04E-02	2.08E-02
728	6.72E-03	7.16E-03	1.93E-02	2.03E-02	1.40E-02
832	5.96E-03	4.37E-03	1.23E-02	1.30E-02	9.14E-03
936	5.89E-03	2.72E-03	8.25E-03	8.24E-03	5.87E-03
1040			5.99E-03	5.29E-03	3.77E-03
1144				3.45E-03	2.38E-03
1248				2.36E-03	1.48E-03
1352				1.66E-03	1.03E-03
1456				1.37E-03	3.52E-04
1560				1.13E-03	

Table AII.5: Partition coefficients for polystyrene chains in ethane at 333K and 34.5 MPa.

Run # / Chain Mol. Wt	2009	20053	20057	20058	20091
312					
416					
520					
624					
728					
832					
936			6.62E-03	8.73E-03	9.48E-03
1040	6.49E-03	1.23E-02	6.32E-03	8.25E-03	7.88E-03
1144	5.62E-03	1.09E-02	6.27E-03	7.98E-03	6.79E-03
1248	4.36E-03	8.61E-03	5.09E-03	6.99E-03	5.20E-03
1352	3.33E-03	6.82E-03	4.28E-03	6.03E-03	3.94E-03
1456	2.43E-03	5.21E-03	3.43E-03	4.93E-03	2.87E-03
1560	1.75E-03	3.89E-03	2.70E-03	3.92E-03	2.06E-03
1664	1.22E-03	2.86E-03	2.08E-03	3.04E-03	1.48E-03
1768	8.49E-04	2.09E-03	1.57E-03	2.30E-03	1.04E-03
1872	6.02E-04	1.53E-03	1.18E-03	1.74E-03	7.49E-04
1976	4.11E-04	1.11E-03	8.64E-04	1.28E-03	5.24E-04
2080	2.82E-04	7.99E-04	6.34E-04	9.45E-04	3.75E-04
2184	2.01E-04	5.85E-04	4.69E-04	7.01E-04	2.65E-04
2288	1.41E-04	4.29E-04	3.46E-04	5.15E-04	1.91E-04
2392	9.97E-05	3.08E-04	2.50E-04	3.81E-04	1.38E-04
2496	7.01E-05	2.29E-04	1.88E-04	2.83E-04	9.95E-05
2600	5.01E-05	1.71E-04	1.44E-04	2.11E-04	7.43E-05
2704	3.62E-05	1.28E-04	1.09E-04	1.58E-04	5.32E-05
2808	2.57E-05	9.82E-05	8.30E-05	1.21E-04	4.03E-05
2912	1.80E-05	7.41E-05	6.25E-05	9.21E-05	2.81E-05
3016	1.45E-05	5.72E-05	4.65E-05	6.64E-05	2.63E-05
3120	8.64E-06	4.41E-05	3.45E-05	5.05E-05	1.85E-05
3224	4.70E-06	3.40E-05	2.66E-05	4.07E-05	1.01E-05
3328	4.16E-06	2.84E-05	1.88E-05	3.00E-05	3.59E-06
3432	2.41E-06	2.37E-05	1.53E-05	2.08E-05	
3536		1.60E-05	8.59E-06	1.54E-05	
3640		7.88E-06	3.48E-06	1.16E-05	
3744				9.84E-06	
3848				2.95E-06	
3952				2.77E-06	
4056				7.64E-07	

Table AII.5 (continued)

Run # Chain Mol. Wt	20092	80031	80056	80057	80058
312		3.75E-02	2.08E-01		1.12E-01
416		1.80E-01	2.19E-01	1.71E-01	1.08E-01
520		1.61E-01	1.61E-01	1.61E-01	9.49E-02
624		1.22E-01	1.21E-01	1.35E-01	7.84E-02
728		9.10E-02	9.47E-02	1.06E-01	6.17E-02
832		6.52E-02	7.13E-02	7.98E-02	4.61E-02
936	7.23E-03	4.67E-02	5.39E-02	5.88E-02	3.30E-02
1040	6.12E-03	3.42E-02	3.94E-02	4.23E-02	2.31E-02
1144	5.40E-03	2.55E-02	2.91E-02	3.06E-02	1.61E-02
1248	4.27E-03	1.94E-02	2.12E-02	2.19E-02	1.11E-02
1352	3.34E-03	1.48E-02	1.56E-02	1.56E-02	7.28E-03
1456	2.48E-03	1.33E-02	1.15E-02	1.11E-02	4.54E-03
1560	1.83E-03	1.08E-02	8.64E-03	7.35E-03	2.18E-03
1664	1.31E-03	9.35E-03	6.33E-03	4.23E-03	
1768	9.46E-04		4.24E-03		
1872	6.81E-04		2.44E-03		
1976	4.78E-04				
2080	3.32E-04				
2184	2.41E-04				
2288	1.72E-04				
2392	1.23E-04				
2496	8.78E-05				
2600	6.37E-05				
2704	4.78E-05				
2808	3.33E-05				
2912	2.51E-05				
3016	2.03E-05				
3120	1.56E-05				
3224	1.04E-05				
3328	1.03E-05				
3432	9.81E-06				
3536	7.50E-06				
3640	3.94E-06				
3744	4.74E-07				
3848					
3952					
4056					

Table AII.6: Partition coefficients for polystyrene chains in ethane at 313K and 25 MPa.

Run # Chain Mol. Wt	80072	80073	80074	80075
416	1.64E-01	1.22E-01	9.72E-02	9.29E-02
520	1.14E-01	9.69E-02	9.47E-02	1.08E-01
624	7.40E-02	6.50E-02	6.90E-02	8.38E-02
728	4.91E-02	4.27E-02	4.64E-02	5.75E-02
832	3.28E-02	2.83E-02	3.06E-02	3.76E-02
936	2.15E-02	1.85E-02	1.98E-02	2.40E-02
1040	1.38E-02	1.19E-02	1.27E-02	1.53E-02
1144	9.01E-03	7.54E-03	8.16E-03	9.77E-03
1248	5.74E-03	4.60E-03	5.18E-03	6.05E-03
1352	3.34E-03		3.21E-03	3.42E-03
1456	1.88E-03		1.78E-03	1.64E-03

Table AII.6 (continued)

Run # Chain Mol. Wt	20063	20065	2066
1144	5.33E-03	4.72E-03	5.39E-03
1248	3.80E-03	3.49E-03	4.06E-03
1352	2.71E-03	2.61E-03	3.11E-03
1456	1.93E-03	1.90E-03	2.26E-03
1560	1.34E-03	1.35E-03	1.64E-03
1664	9.08E-04	9.22E-04	1.17E-03
1768	6.09E-04	6.31E-04	8.08E-04
1872	4.14E-04	4.49E-04	5.64E-04
1976	2.65E-04	2.91E-04	3.83E-04
2080	1.62E-04	1.88E-04	2.59E-04
2184	9.98E-05	1.28E-04	1.82E-04
2288	5.51E-05	8.20E-05	1.25E-04
2392		5.27E-05	8.56E-05
2496		3.39E-05	5.53E-05
2600		1.80E-05	3.24E-05
2704			2.20E-05
2808			1.29E-05

Table AII.7: Partition coefficients for polystyrene chains in ethane at 323K and 25 MPa.

Run # / Chain Mol. Wt	80060	80062	80063	80064	80065
312		1.71E-01	1.32E-01	9.23E-02	
416		1.43E-01	1.30E-01	1.05E-01	7.70E-02
520		1.01E-01	9.86E-02	8.52E-02	7.00E-02
624		7.07E-02	7.10E-02	6.25E-02	5.51E-02
728	2.76E-02	5.03E-02	5.05E-02	4.40E-02	3.99E-02
832	2.72E-02	3.52E-02	3.49E-02	2.99E-02	2.74E-02
936	2.24E-02	2.38E-02	2.34E-02	1.97E-02	1.80E-02
1040	1.52E-02	1.54E-02	1.54E-02	1.28E-02	1.17E-02
1144	8.86E-03	9.87E-03	1.03E-02	8.43E-03	7.76E-03
1248	4.85E-03	6.22E-03	6.93E-03	5.55E-03	5.15E-03
1352	2.64E-03	3.84E-03	4.53E-03	3.54E-03	3.41E-03
1456	1.48E-03	2.32E-03	2.93E-03	2.20E-03	2.26E-03
1560	8.70E-04	1.22E-03	1.59E-03	1.20E-03	1.46E-03
1664	5.42E-04				1.04E-03
1768					5.30E-04
1872					1.95E-04

Table AII.7 (continued)

Run # / Chain Mol. Wt	20068	20070
1456	1.18E-03	8.85E-04
1560	8.58E-04	6.54E-04
1664	6.02E-04	4.82E-04
1768	4.10E-04	3.32E-04
1872	2.82E-04	2.34E-04
1976	1.96E-04	1.70E-04
2080	1.25E-04	1.14E-04
2184	8.60E-05	8.58E-05
2288	5.82E-05	6.43E-05
2392	3.75E-05	4.42E-05
2496	2.36E-05	3.49E-05
2600	1.61E-05	
2704	1.02E-05	

Table AII.8: Partition coefficients for polystyrene chains in CO_2 at 333K and 25 MPa.

Run # Chain Mol. Wt	COO8003	COO8004	COO8005
312	1.31E-02		
416	1.85E-02	1.13E-02	1.14E-02
520	1.03E-02	6.91E-03	7.94E-03
624	5.44E-03	3.80E-03	4.50E-03
728	2.93E-03	2.09E-03	2.47E-03
832	1.48E-03	1.07E-03	1.26E-03
936	7.06E-04	5.22E-04	6.09E-04
1040	3.04E-04	2.49E-04	2.67E-04
1144	1.31E-04	1.18E-04	9.11E-05

Table AII.9: Partition coefficients for polystyrene chains in a mixture of ethane and propane (ca. 87:13 by mole) at 333K and 25 MPa.

Run # Chain Mol. Wt	M108003	M108004	M108005
416	9.53E-02	6.77E-02	5.43E-02
520	8.46E-02	6.76E-02	5.97E-02
624	7.00E-02	5.99E-02	5.71E-02
728	5.56E-02	5.01E-02	4.98E-02
832	4.11E-02	3.81E-02	3.89E-02
936	2.93E-02	2.73E-02	2.84E-02
1040	2.12E-02	1.95E-02	2.04E-02
1144	1.56E-02	1.42E-02	1.50E-02
1248	1.17E-02	1.03E-02	1.13E-02
1352	8.84E-03	7.31E-03	8.77E-03
1456	7.25E-03	5.52E-03	7.57E-03
1560	5.83E-03	3.45E-03	6.34E-03
1664	4.98E-03	9.19E-04	7.17E-03
1768	1.59E-03		8.24E-03

APPENDIX III

COMPUTER PROGRAMS FOR LATTICE EOS

For the implementation of the lattice EOS for the modelling of mixtures of molecules of disparate sizes we need separate programs for the determination of pure component parameters, and for phase equilibrium calculations. A modular approach was adopted so as to use a maximum number of subroutines commonly in both calculations. These subroutines, along with an abbreviated description of their purpose are listed in Tables AIII.1- AIII.3.

The programs are all written in common FORTRAN 77 and can run under IBM Professional Fortran on an IBM-XT or AT microcomputer (with a 8087/80287 coprocessor.) The programs have also been run, with minor modifications, on a Data General MV4000 system. A fact complicating the implementation of the lattice EOS is that it does not have a cubic functionality in volume. Special care was therefore taken to ensure that a robust algorithm was employed so that convergence is assured in most, commonly encountered situations.

Copies of all programs can be obtained either from the author, or from Professors R.C.Reid or U.W.Suter at MIT.

Table AIII.1: Common Subroutines with a brief description of their function.

Name	Description
FNEWT	Newton-Raphson Solver for a set of non-linear algebraic equations, for outer loop.
SNEWT	Newton Solver for inner loop.
LU	Lower-Upper decomposition of Jacobian matrix for NEWTON.
BACK	Solution of algebraic equations by back-substitution.
FUNCT1	Function that provides residues for outer loop.
FUNCT2	Function residues for inner loop.
EOS	Equation of state subroutine. Accepts temperature and volume and outputs pressure.

Table AIII.2: Subroutines for calculation of ϵ_{11} and v^* for subcritical pure components.

Name	Function
ABCAL	Calculates the pure component properties. Inputs include vapour pressure, temperature, saturated liquid densities and molecular weight for the relevant compound. Also initial estimates for ϵ_{11} and v^* are required. Can also compute parameters at different temperatures with relevant P,T, liquid density inputs using a zeroth order continuation scheme.
NU	Calculates the fugacity of the component in the relevant phase.

Table AIII.3: Subroutines for computation of phase equilibria for binary mixtures.

Name	Function
EQUILO	Calculates equilibrium phase compositions and densities. Inputs include T,P, and the pure component parameters for both the mixture components. Employs zeroth order continuation for extension to different pressures.
MIXCAL	Calculates mixture parameters, ϵ_M, v_M^*, q_M and r_M.
THETA	Computes the surface area fractions of each molecular species and also the total surface area fraction of molecules on the lattice.
FUG	Calculates the fugacity of each component in the relevant phase.
STAB	Computes the elements of the stability matrix to ensure that calculated results follow the Gibbs Duhem relationship, and also represent stable equilibrium states.

APPENDIX IV

PRECIPITATION POLYMERIZATION REACTIONS: RAW EXPERIMENTAL DATA

In this appendix we present experimental data obtained when styrene was polymerized in supercritical ethane in a precipitation mode. In each table a run number is provided for each column of data; a suffix "ppt" or "ext" to this number implies that the corresponding numbers are precipitate phase or SCF phase compositions, respectively. SCF phase compositions are reported in units of g mer/ g SCF, while precipitate phase compositions are in units of g mer/ g *SCF-free* solid. Also, the times for which each reaction was conducted is shown in the appropriate tables. All reported experimental data have been obtained when the polymerization was conducted with an AIBN concentration of 5.84×10^{-5} g/g SCF.

Table AIV.1: Compositions of the precipitate phase and SCF phase polystyrenes synthesised in ethane at 333K, 12 MPa and 3.33 wt% monomer.

Run #	91.ppt	91.ext	92.ppt	92.ext	93.ppt	93.ext
Time (h)	23	23	20	20	20	20
Mol. Wt						
104	3.08E-01	2.10E-02	5.99E-01	1.66E-02	5.59E-01	1.80E-02
208	2.98E-01	1.23E-02	1.86E-01	9.62E-03	2.24E-01	1.15E-02
312	7.33E-02	1.71E-03	3.54E-02	1.71E-03	4.20E-02	2.57E-03
416	1.61E-02	3.31E-04	1.17E-02	3.49E-04	1.52E-02	1.56E-03
520	2.31E-02	1.52E-04	1.06E-02	1.23E-04	1.43E-02	9.67E-04
624	2.97E-02	7.94E-05	1.08E-02	3.78E-05	1.46E-02	4.60E-04
728	3.15E-02	1.95E-05	1.10E-02	1.21E-05	1.41E-02	2.52E-04
832	3.71E-02	2.94E-06	1.50E-02	7.46E-06	1.72E-02	1.63E-04
936	3.80E-02		1.75E-02		1.75E-02	7.53E-05
1040	3.05E-02		1.70E-02		1.54E-02	2.98E-05
1144	2.67E-02		1.73E-02		1.43E-02	1.19E-05
1248	2.11E-02		1.51E-02		1.17E-02	8.57E-07
1352	1.60E-02		1.25E-02		9.24E-03	
1456	1.24E-02		1.02E-02		7.40E-03	
1560	9.40E-03		7.86E-03		5.68E-03	
1664	7.40E-03		6.25E-03		4.59E-03	
1768	5.73E-03		4.78E-03		3.57E-03	
1872	4.10E-03		3.39E-03		2.56E-03	
1976	3.32E-03		2.70E-03		2.09E-03	
2080	2.31E-03		1.85E-03		1.45E-03	
2184	1.86E-03		1.43E-03		1.17E-03	
2288	1.33E-03		9.64E-04		8.39E-04	
2392	1.06E-03		6.77E-04		6.69E-04	
2496	7.15E-04		4.42E-04		4.28E-04	
2600	5.38E-04		3.10E-04		2.82E-04	
2704	3.89E-04		1.87E-04		2.26E-04	
2808	2.92E-04		7.06E-05		1.54E-04	
2912	2.54E-04		2.97E-05		1.11E-04	
3016	1.58E-04				9.96E-05	
3120	8.53E-05				4.19E-05	
3224	4.06E-05				1.04E-05	
3328	1.39E-05				2.37E-06	

Table AIV.1 (continued)

Run #	96.ppt	96.ext
Time (h) Mol. Wt	46	46
104	3.03E-01	1.87E-02
208	2.98E-01	1.27E-02
312	5.71E-02	1.50E-03
416	2.34E-02	7.30E-04
520	2.93E-02	4.68E-04
624	3.09E-02	1.97E-04
728	3.07E-02	1.14E-04
832	3.62E-02	7.54E-05
936	3.47E-02	4.62E-05
1040	3.00E-02	
1144	2.73E-02	
1248	2.22E-02	
1352	1.76E-02	
1456	1.40E-02	
1560	1.08E-02	
1664	8.63E-03	
1768	6.75E-03	
1872	4.87E-03	
1976	3.99E-03	
2080	2.83E-03	
2184	2.27E-03	
2288	1.62E-03	
2392	1.25E-03	
2496	8.51E-04	
2600	5.46E-04	
2704	3.85E-04	
2808	2.17E-04	
2912	1.16E-04	
3016	4.63E-05	
3120	5.80E-08	

Table AIV.2a: Compositions of the precipitate phase and SCF phase polystyrenes synthesised in ethane at 333K, 17 MPa and 3.33 wt% monomer.

Run #	80.ext	80.ppt	82.ext	82.ppt	85.ext	85.ppt
Time (h)	44	44	30	30	16	16
Mol. Wt						
104	1.65E-02	3.72E-01	1.43E-02	3.17E-01	1.29E-02	3.85E-01
208	1.13E-02	2.89E-01	8.37E-03	2.28E-01	1.16E-02	2.42E-01
312	3.83E-03	1.15E-01	4.13E-03	7.65E-02	4.39E-03	5.83E-02
416	2.72E-04	3.40E-02	1.58E-03	3.58E-02	1.11E-03	1.59E-02
520	7.14E-05	3.67E-02	1.35E-03	4.41E-02	8.44E-04	2.47E-02
624	7.15E-06	3.00E-02	8.97E-04	3.90E-02	4.69E-04	2.20E-02
728	1.95E-06	2.26E-02	6.90E-04	3.16E-02	4.64E-04	2.08E-02
832	1.67E-06	2.11E-02	3.35E-04	3.25E-02	1.10E-04	2.53E-02
936	1.72E-06	1.70E-02	1.86E-04	3.04E-02	5.58E-05	2.56E-02
1040	6.95E-07	1.23E-02	8.09E-05	2.64E-02	1.94E-05	2.57E-02
1144		1.05E-02	3.68E-05	2.55E-02	2.72E-06	2.69E-02
1248		8.22E-03	1.36E-05	2.18E-02		2.45E-02
1352		6.48E-03	3.68E-06	1.80E-02		2.12E-02
1456		5.27E-03	7.67E-07	1.49E-02		1.79E-02
1560		4.17E-03		1.19E-02		1.44E-02
1664		3.44E-03		9.78E-03		1.17E-02
1768		2.79E-03		7.91E-03		9.32E-03
1872		2.09E-03		5.96E-03		6.86E-03
1976		1.75E-03		4.99E-03		5.63E-03
2080		1.26E-03		3.64E-03		4.03E-03
2184		1.04E-03		3.04E-03		3.21E-03
2288		7.86E-04		2.34E-03		2.35E-03
2392		6.20E-04		1.95E-03		1.80E-03
2496		4.55E-04		1.47E-03		1.33E-03
2600		3.28E-04		1.12E-03		9.15E-04
2704		2.66E-04		9.52E-04		7.28E-04
2808		1.93E-04		7.14E-04		5.07E-04
2912		1.57E-04		6.01E-04		3.91E-04
3016		1.27E-04		4.87E-04		2.55E-04
3120		8.58E-05		3.82E-04		1.83E-04
3224		6.62E-05		3.16E-04		1.47E-04
3328		3.71E-05		2.53E-04		8.05E-05
3432		3.51E-05		1.98E-04		1.49E-05
3536		1.60E-05		1.57E-04		
3640		9.88E-06		1.37E-04		
3744		2.55E-06		1.27E-04		
3848				8.91E-05		
3952				8.00E-05		
4056				6.24E-05		
4160				4.64E-05		

Table AIV.2a (continued)

Run #	88.ext	88.ppt
Time (h) Mol. Wt	16.5	16.5
104	1.70E-02	4.36E-01
208	1.13E-02	2.02E-01
312	2.30E-03	6.01E-02
416	4.54E-04	3.21E-02
520	2.23E-04	3.53E-02
624	3.39E-04	3.35E-02
728	2.28E-04	2.34E-02
832	7.11E-05	2.04E-02
936	3.60E-05	1.95E-02
1040	1.11E-05	1.74E-02
1144	2.54E-06	1.79E-02
1248		1.73E-02
1352		1.53E-02
1456		1.35E-02
1560		1.13E-02
1664		9.55E-03
1768		7.93E-03
1872		6.01E-03
1976		5.09E-03
2080		3.71E-03
2184		3.10E-03
2288		2.34E-03
2392		1.88E-03
2496		1.42E-03
2600		1.01E-03
2704		8.37E-04
2808		5.83E-04
2912		4.75E-04
3016		4.04E-04
3120		2.95E-04
3224		2.14E-04
3328		1.46E-04
3432		1.24E-04
3536		9.75E-05
3640		4.69E-05
3744		1.03E-05
3848		8.10E-06

Table AIV.2b: Compositions of the precipitate phase and SCF phase polystyrenes synthesised in ethane at 333K, 17 MPa and 5.0 wt% monomer.

Run #	79.ppt	79.ext	99.ppt	99.ext	101.ppt	101.ext
Time (h)	20	20	7.5	7.5	23	23
Mol. Wt						
104	2.53E-02	4.33E-01	2.63E-02	5.40E-01	2.25E-02	4.61E-01
208	1.36E-02	2.12E-01	1.44E-02	2.54E-01	1.47E-02	1.85E-01
312	4.00E-03	5.30E-02	2.79E-03	4.28E-02	3.90E-03	3.92E-02
416	1.71E-03	2.26E-02	1.77E-03	1.67E-02	1.66E-03	9.75E-03
520	1.60E-03	2.11E-02	1.25E-03	3.19E-02	1.67E-03	1.23E-02
624	9.29E-04	1.95E-02	4.82E-04	4.82E-03	1.27E-03	1.74E-02
728	4.64E-04	1.79E-02	3.31E-04	5.33E-03	8.93E-04	2.05E-02
832	2.80E-04	2.17E-02	2.65E-04	7.02E-03	7.40E-04	2.67E-02
936	9.94E-05	2.42E-02	1.68E-04	7.60E-03	3.88E-04	3.08E-02
1040	3.60E-05	2.34E-02	9.63E-05	8.58E-03	1.64E-04	2.87E-02
1144	1.17E-05	2.39E-02	5.74E-05	9.72E-03	5.41E-05	2.77E-02
1248	1.24E-06	2.16E-02	2.92E-05	9.59E-03	1.31E-06	2.44E-02
1352	1.86E-02		1.52E-05	9.21E-03	2.01E-02	
1456	1.59E-02		7.66E-06	8.42E-03	1.68E-02	
1560	1.31E-02		4.07E-06	7.35E-03	1.36E-02	
1664	1.12E-02		3.02E-06	6.59E-03	1.15E-02	
1768	9.42E-03		8.22E-07	5.71E-03	9.64E-03	
1872	7.28E-03		4.60E-03		7.44E-03	
1976	6.32E-03		4.13E-03		6.52E-03	
2080	4.72E-03		3.18E-03		4.91E-03	
2184	4.04E-03		2.79E-03		4.30E-03	
2288	3.19E-03		2.24E-03		3.48E-03	
2392	2.69E-03		1.92E-03		2.98E-03	
2496	2.07E-03		1.49E-03		2.37E-03	
2600	1.60E-03		1.15E-03		1.81E-03	
2704	1.34E-03		9.68E-04		1.62E-03	
2808	1.02E-03		6.74E-04		1.27E-03	
2912	8.51E-04		5.19E-04		1.11E-03	
3016	7.01E-04		4.22E-04		9.84E-04	
3120	5.22E-04		2.86E-04		7.94E-04	
3224	4.30E-04		1.99E-04		6.63E-04	
3328	3.57E-04		1.36E-04		5.91E-04	
3432	2.65E-04		8.45E-05		4.41E-04	
3536	2.08E-04		4.01E-05		3.88E-04	
3640	1.60E-04		8.34E-06		3.26E-04	
3744	1.31E-04				3.05E-04	
3848	7.84E-05				2.32E-04	
3952	6.43E-05				1.92E-04	
4056	3.98E-05				1.54E-04	
4160	2.96E-05				1.41E-04	

Table AIV.2c: Compositions of the precipitate phase and SCF phase polystyrenes synthesised in ethane at 333K, 17 MPa and 6.66 wt% monomer.

Run #	105.ppt	105.ext	106.ppt	106.ext
Time (h)	22	22	18	18
Mol. Wt				
104	4.65E-01	4.59E-02	3.65E-01	5.00E-02
208	2.69E-01	1.65E-02	2.96E-01	1.37E-02
312	3.86E-02	6.44E-04	4.13E-02	1.60E-04
416	9.53E-03	2.67E-04	6.75E-03	1.49E-06
520	9.70E-03	1.78E-04	7.49E-03	7.81E-06
624	1.11E-02	1.25E-04	9.91E-03	3.39E-05
728	1.33E-02	1.27E-04	1.28E-02	2.36E-05
832	1.68E-02	1.00E-04	1.88E-02	3.02E-05
936	1.68E-02	5.95E-05	2.16E-02	7.38E-06
1040	1.64E-02	3.44E-05	2.24E-02	3.34E-07
1144	1.63E-02	1.80E-05	2.35E-02	
1248	1.49E-02	6.35E-06	2.19E-02	
1352	1.34E-02	5.42E-06	1.98E-02	
1456	1.20E-02	5.60E-06	1.78E-02	
1560	1.04E-02	3.81E-06	1.56E-02	
1664	9.46E-03	5.13E-06	1.40E-02	
1768	8.41E-03	5.91E-06	1.24E-02	
1872	6.94E-03	3.20E-06	1.02E-02	
1976	6.42E-03	2.31E-06	9.44E-03	
2080	5.08E-03	2.57E-06	7.50E-03	
2184	4.63E-03	1.46E-06	6.83E-03	
2288	3.88E-03		5.73E-03	
2392	3.49E-03		5.16E-03	
2496	2.84E-03		4.26E-03	
2600	2.32E-03		3.45E-03	
2704	2.07E-03		3.10E-03	
2808	1.66E-03		2.48E-03	
2912	1.48E-03		2.24E-03	
3016	1.30E-03		1.99E-03	
3120	1.04E-03		1.57E-03	
3224	9.18E-04		1.39E-03	
3328	8.06E-04		1.22E-03	
3432	6.23E-04		9.30E-04	
3536	5.44E-04		8.22E-04	
3640	4.88E-04		7.32E-04	
3744	4.09E-04		6.41E-04	
3848	3.03E-04		4.89E-04	
3952	2.64E-04		4.46E-04	
4056	2.51E-04		3.89E-04	
4160	2.30E-04		3.41E-04	
4264	1.82E-04		3.00E-04	

Table AIV.2c (continued).

Run #	105.ppt	105.ext	106.ppt	106.ext
Time (h)	22	22	18	18
Mol. Wt				
4368	1.58E-04		2.55E-04	
4472	1.21E-04		1.91E-04	
4576	9.40E-05		1.71E-04	
4680			1.52E-04	
4784			1.40E-04	
4888			1.15E-04	
4992			9.77E-05	

Table AIV.3: Compositions of the precipitate phase and SCF phase polystyrenes synthesised in ethane at 333K, 25 MPa and 3.33 wt% monomer.

Run #	98.ppt	98.ext	103.ppt	103.ext
Time (h)	23	23	18	18
Mol. Wt				
104	5.38E-01	1.87E-02	3.98E-01	3.24E-02
208	1.63E-01	1.55E-02	2.55E-01	1.43E-02
312	3.34E-02	4.10E-03	5.12E-02	9.33E-04
416	1.14E-02	1.51E-03	1.72E-02	
520	1.37E-02	1.03E-03	1.93E-02	
624	1.22E-02	6.25E-04	1.80E-02	3.66E-05
728	1.03E-02	5.42E-04	1.73E-02	5.17E-05
832	1.16E-02	3.61E-04	2.15E-02	9.09E-05
936	1.28E-02	2.38E-04	2.25E-02	5.47E-05
1040	1.46E-02	1.59E-04	2.27E-02	4.85E-05
1144	1.79E-02	1.06E-04	2.35E-02	3.32E-05
1248	1.93E-02	6.35E-05	2.15E-02	2.03E-05
1352	1.96E-02	3.46E-05	1.89E-02	1.41E-05
1456	1.89E-02	1.67E-05	1.62E-02	5.48E-06
1560	1.72E-02	7.71E-06	1.35E-02	1.15E-06
1664	1.58E-02	3.04E-06	1.15E-02	8.05E-08
1768	1.37E-02	3.47E-07	9.69E-03	
1872	1.09E-02		7.56E-03	
1976	9.62E-03		6.63E-03	
2080	7.27E-03		5.03E-03	
2184	6.24E-03		4.36E-03	
2288	4.92E-03		3.49E-03	
2392	4.18E-03		3.01E-03	
2496	3.20E-03		2.34E-03	
2600	2.35E-03		1.85E-03	
2704	2.04E-03		1.55E-03	
2808	1.54E-03		1.20E-03	
2912	1.29E-03		1.03E-03	
3016	1.03E-03		8.73E-04	
3120	7.30E-04		6.71E-04	
3224	6.08E-04		5.63E-04	
3328	4.22E-04		4.57E-04	
3432	3.11E-04		3.72E-04	
3536	2.47E-04		3.18E-04	
3640	1.58E-04		2.57E-04	
3744	9.23E-05		2.22E-04	
3848	1.77E-05		1.68E-04	
3952			1.53E-04	
4056			1.37E-04	
4160			1.07E-04	
4264			8.14E-05	
4368			7.41E-05	
4472			3.94E-05	

Table AIV.4: Compositions of the precipitate phase polystyrenes synthesised in ethane at 343K and 17 MPa.[†]

Run #	pol701.ppt	pol702.ppt	plo703.ppt
Time (h)	23	20	26
Mol. Wt			
104	2.19E-01	1.45E-01	1.52E-01
208	3.09E-01	3.09E-01	3.24E-01
312	8.98E-02	1.38E-01	1.17E-01
416	3.39E-02	5.11E-02	4.76E-02
520	3.21E-02	5.58E-02	4.96E-02
624	3.34E-02	6.40E-02	4.57E-02
728	3.62E-02	5.17E-02	4.33E-02
832	3.92E-02	4.58E-02	4.23E-02
936	3.69E-02	3.47E-02	3.63E-02
1040	3.27E-02	2.48E-02	2.91E-02
1144	2.89E-02	1.99E-02	2.41E-02
1248	2.35E-02	1.50E-02	1.89E-02
1352	1.88E-02	1.12E-02	1.46E-02
1456	1.49E-02	8.56E-03	1.15E-02
1560	1.15E-02	6.38E-03	8.88E-03
1664	9.09E-03	4.96E-03	7.17E-03
1768	7.03E-03	3.78E-03	5.74E-03
1872	5.08E-03	2.69E-03	4.30E-03
1976	4.19E-03	2.15E-03	3.64E-03
2080	3.01E-03	1.48E-03	2.70E-03
2184	2.46E-03	1.20E-03	2.28E-03
2288	1.85E-03	8.67E-04	1.80E-03
2392	1.55E-03	6.78E-04	1.52E-03
2496	1.15E-03	5.10E-04	1.18E-03
2600	8.64E-04	3.68E-04	9.14E-04
2704	7.15E-04	2.76E-04	8.02E-04
2808	5.36E-04	2.08E-04	6.28E-04
2912	4.41E-04	1.69E-04	5.27E-04
3016	3.66E-04	1.17E-04	4.62E-04
3120	2.62E-04	9.10E-05	3.54E-04
3224	2.63E-04	6.75E-05	3.06E-04
3328	2.11E-04	4.55E-05	2.78E-04
3432	1.35E-04	3.49E-05	2.10E-04
3536	9.16E-05	2.92E-05	1.84E-04
3640	5.39E-05	1.34E-05	1.78E-04
3744	5.07E-05	1.29E-05	1.52E-04
3848	3.02E-05	4.99E-06	1.13E-04
3952	1.09E-05	2.97E-06	8.64E-05
4056	5.92E-06	1.49E-06	9.14E-05
4160	5.09E-06		7.19E-05

[†] In these experiments the SCF-phase compositions were not measured.